Fluorescent Labels for Reduction Sensitive Polycationic Gene Carriers

Constantin Zoltán Hózsa

2019

Fluorescent Labels for Reduction Sensitive Polycationic Gene Carriers

Dissertation zur Erlangung des Doktorgrades der Naturwissenschaften (Dr. rer. nat.) der Fakultät für Chemie und Pharmazie der Universität Regensburg

vorgelegt von

Constantin Zoltán Hózsa

aus Halle (Saale)

2019

Promotionsgesuch eingereicht am:	9. Dezember 2019
Die Arbeit wurde angeleitet von:	Prof. Dr. Achim Göpferich
Prüfungsausschuss:	Prof. Dr. Sigurd Elz (Vorsitzender) Prof. Dr. Achim Göpferich (Erstgutachter) apl. Prof. Dr. Miriam Breunig (Zweitgutachterin) Prof. Dr. Joachim Wegener (Driffprüfer)

"If you hide your ignorance, no one will hit you, and you'll never learn."
Ray Bradbury, "Fahrenheit 451"

"It does not matter how slowly you go as long as you do not stop."
Confucius

Contents

1 Introduction and goals of the thesis

1.1 Gene therapy

Gene therapy is the delivery of therapeutic nucleic acids into a patient's cells in order to prevent or treat genetic disorders or acquired diseases. This technology holds the potential to provide lasting therapies or even cures for medical conditions that are currently untreatable or for which only temporary and suboptimal conventional treatments exist.[1] Even though the basic therapeutic principle was conceptualized in as early as the 1970s,[2] the first gene therapies have reached regulatory approval only very recently.[3] The first commercial product, Gendicine, an adenoviral vector-based therapy for head and neck squamous cell carcinoma was approved in China in 2003. The first therapy approved in Western world is Alipogene tiparvovec or Glybera, an adeno-associated viral vector-based therapy developed by UniQure for the treatment of lipoprotein lipase deficiency, a rare inherited disorder.[4] It was launched in Europe in 2012 and was originally planned for approval in the United States. In 2017, however, UniQure decided against the renewal of the market authorization due to the lack of commercial success.[5] With an initial price of $1.6 million per treatment Glybera was the most expensive medicine in the world at the time[6] and with only one dose sold probably one of the most unsuccessful ones, too[7]. Despite this commercial failure and the lackluster sales of the second EMA approved gene therapy, Strimvelis[7], the global gene therapy market is growing rapidly. The last three years alone saw the introduction of three new therapies (Yescarta (Gilead), Kymriah (Novartis), and Luxturna (Spark Therapeutics))[8] and nearly 150 gene therapies are presently in development[9], or as a recent article in *Science* put it: "Gene therapy comes of age"[2].

1.2 Therapeutic strategies

Today the most advanced gene therapies are based on "gene addition", i.e., an additional gene is introduced into the host cell genome in order to express a therapeutic protein.[2] Several ex vivo and in vivo therapies based on this approach are already on the market or in advanced clinical trials.[10]

In ex vivo therapies patient cells are isolated and transfected in vitro. The genetically modified

cells are then selected, expanded in cell culture, and transplanted back into the patient. Ex vivo therapies are used to treat monogenic blood disorders that manifest in mature hematopoietic cells by modifying hematopoietic stem cells (HSCs).[10] In contrast to a conventional allogeneic bone marrow transplantation, this approach requires no histocompatible donor, there is no risk of a graft-versus-host reaction, and the lifelong administration of immune suppressants is avoided.[2] It has been used to treat primary immunodeficiencies (e.g., X-linked severe combined immunodeficiency and Wiskott-Aldrich syndrome), hemoglobin disorders (e.g., β-thalassemia major), and neurodegenerative storage disorders (e.g., adrenoleukodystrophy and metachromatic leukodystrophy).[10] Ex vivo gene therapies have also been used in cancer immunotherapy, more specifically in chimeric antigen receptor T cell therapy (CAR-T). The idea here is to boost the adaptive immune response against cancer by transducing autologous (and allogenic), harvested T cells in order to express an exogenous chimeric T cell antigen receptor (CAR). The receptor consists of an antigen-binding domain against cancer-associated antigens fused with an intracellular signal domain that mediates activation and co-stimulation of T cells.[2] In principle, T cells can be engineered to target virtually any tumor associated antigen, but the two currently available therapies, Yescarta and Kymriah, focus on the B lymphocyte antigen CD19 to treat B cell malignancies. CAR T-cell therapies for solid tumors and chronic infections are in development.[1]

Ex vivo therapies face considerable practical and regulatory obstacles, arising from the need to culture, manipulate, and transplant collected cells. For that reason, in vivo approaches that target specific organs are a very attractive alternative. They face, however, their own unique challenges, including the necessity of tissue-specific targeting and target cell specific gene expression, and the concern of unintentional germline modifications and immune responses.[2] The liver has long been an attractive target for in vivo gene therapy, especially as far as protein replacement therapies are concerned as it possesses several advantageous features that allow for a transfection with relative ease. Its abundant blood supply combined with the presence of sinusoids with their highly permeable open pore endothelial structure facilitates the access of blood-borne transfection agents, for example. More importantly, hepatocytes are robust, long-lived, and efficiently secrete proteins, which makes them ideal “factories” for therapeutic proteins.[10] Currently, liver-directed gene therapy is focused on the treatment of hemophilia B where the coagulation factor IX is absent or defective and the results of several clinical trials have been quite promising.[1, 2, 11] There are also ongoing efforts to adapt this approach for the treatment of hemophilia A, but they have not yet reached the same level of success, as the expression and secretion of the factor VIII molecule is more challenging.[1] The eye is another attractive therapeutic target. Its immune privilege lowers the risk of adverse immune reactions as a result of the treatment.[1] Recently, voretigene neparvovec (Luxturna) was approved by the FDA for the treatment of Leber's congenital amaurosis type 2[9] and gene therapies for

several other inherited retinal diseases are in development[2].

The achievements outlined above can easily hide the fact that "gene addition" approaches have very limited applications. In order for these approaches to work, the disease has to be caused by the absence of a functional protein, thus diseases rooted in dominant negative mutations cannot be treated.[1, 2] Moreover, the newly added genes are not regulated by endogenous promoters, resulting in less physiological and appropriate expression profiles.[2] Gene therapy could reach a wider application by incorporating novel gene editing approaches that enable precise in situ corrections and alterations of the genome. In gene editing, artificially modified DNA endonucleases bind to specific DNA sequences and induce double-strand breaks (DSB). The nuclease-induced DNA-damage is then corrected by different highly efficient repair mechanisms that mammalian cells possess. Depending on the presence or absence of a homologous sequence to guide the repair, genes can be deleted from or introduced into the genome. In absence of a guide sequence, a non-homologous end joining (NHEJ) is performed and results in either a variable-length insertion or deletion, both of which generally inactivate the affected gene. If a donor template is provided, a new gene sequence is inserted via a homology directed repair (HDR). This either corrects a mutation or introduces a new therapeutic gene.[1, 2] A number of different endonuclease classes have been engineered for the purpose of gene editing, including zinc finger nucleases (ZFN)s, transcription activator-like effector nucleases (TALENs), and clustered regularly interspaced short palindromic repeats CRISPR associated protein 9 systems (CRISPR/Cas9).[3] CRISPR/Cas9 has gained considerable attention in recent years due to the ease of altering its targeting specificity. Retargeting is simply achieved by replacing a short guide-RNA instead of having to alter the enzyme's amino acid sequence as in the case of ZFNs and TALENs.[10] The therapeutic use of CRISPR/Cas9 is still in its infancy and faces several feasibility and safety hurdles,[2] concerning off-target effects and the risk of triggering immune responses due to the prokaryotic origin of the enzymes[10], yet gene editing will undoubtedly find its niche in medicine.

"Classic" gene therapy, as well as gene editing, usually introduces permanent, irreversible changes into the host genome and the price and risk associated with such therapies may not be warranted in all cases. In some instances oligonucleotide based therapies are regarded as alternatives, but they are also therapy forms in their own right. They are not considered to be gene therapies in the strictest sense since they target the processes downstream of the gene transcription. A variety of therapeutic oligonucleotide classes have evolved, including but not limited to messenger RNAs (mRNAs), antisense oligonucleotides (AONs), micro RNAs (miRNA), and small interfering RNAs (siRNAs).[4] Each class has its own unique mechanism of action. mRNAs, for example, have emerged as promising tool for the development of genetic vaccines. They allow for the transient expression of protein antigens to trigger protective immunological

responses. mRNA vaccines could rival conventional vaccines as they combine high potency and safety with the capability for rapid development and potentially low manufacturing costs.[12] Other oligonucleotides, such as siRNA and the closely related miRNA are used to inhibit gene expression through RNA interference (RNAi). RNAi is an umbrella term for several cellular mechanisms, where the presence of short (usually 20 to 24 bp) double-stranded RNAs results in the repression of selected genes.[13, 14] The mechanism studied best involves the RNA-induced silencing complex (RISC), a multiprotein complex for which the oligonucleotides act as guide to direct it to complementary mRNAs. In case of a perfect or near perfect base pairing (usually in the coding region) between RNA guide and mRNA, the Argonaute 2 endonuclease within RISC degrades the target mRNA. This mechanism is mediated by siRNA and several siRNAs are currently being evaluated in clinical trials for treatment of, among other things, eye-related disorders, viral infections, and cancer.[15] The first siRNA based drug, Patisiran (Alnylam Pharmaceuticals) has recently been approved by the FDA and the European Commission for the treatment of hereditary transthyretin-mediated amyloidosis.[16, 17] miRNAs are only partially complementary to the target mRNA and typically bind in the 3'-untranslated regions. As a result, translation is arrested and followed by the mRNA's eventual degradation.[14] A single miRNA can influence the translation of multiple mRNAs, i.e., alter the expression of a whole set of genes.[14] miRNAs are an integral component of the cellular gene regulation and are usually not used as therapeutic agents per se. Their expression profiles, however, are a valuable tool for the diagnosis of a variety of disorders.

1.3 Delivery systems and vectors

The success of a gene therapy does not only depend on the therapeutic strategy and target, but also depends on the choice of the nucleic acid delivery system. In fact, drug development is often hampered by the lack of an efficient delivery system. Currently, therapeutic nucleic acids are typically delivered in the form of a nanosized vehicle. While some therapies have been developed that do not use any form of vehicle, this is not that common yet and often restricted to few select cases.[14] The need for a delivery vehicle arises from the fact that "naked" nucleic acids face many biological barriers on their way to the target cells and their cellular uptake is impeded by their negative charge and significant size. Even if the nucleic acid is taken up successfully, therapeutic success is not guaranteed since there are plenty intracellular obstacles as well (see Sections 2.1 and 5.1).

The gene therapies currently on the market are almost exclusively based on viral vectors. Viruses, with their long evolutionary history as cellular parasites, are highly efficient transfection agents. Two major virus classes have shown the most clinical promise: Retroviruses and

adeno-associated viruses (AAVs).[2] Retroviral vectors, which include γ-retroviruses and lentiviruses, are capable of reverse transcription and DNA integration. They are mainly used for the ex vivo transduction of HSCs and T-cells for CAR therapy.[3] In recent years, the focus of research has shifted from γ-retroviral to lentiviral vectors, partly due to their ability to deliver genes in non-dividing cells and carry larger, more complex gene cassettes.[2] More importantly, in contrast to γ-retroviral vectors, lentiviral vectors preferentially integrate into coding gene regions, which considerably lowers the risk of potentially oncogenic insertional mutageneses. AAVs are per se predominantly non-integrating. While this is again beneficial in terms of integration related adverse effects, it also limits long-term gene expression in long-lived post-mitotic cells. AAV vectors have proven to be effective in therapies that target the liver and the eye.[2]

The risk of an oncogenic insertional mutagenesis is not the only issue associated with viral vectors. Viral vectors have a limited transgene carrying capacity and that reduces their usefulness in certain therapeutic approaches like gene editing. An AAV capsid, for instance, has a typical size of approximately 20 nm and only offers room for about 4.5 to 5 kb of genetic material. In principle, this capacity is sufficient for the delivery of the 4.2 kb required for the complete CRISPR/Cas9 gene editing machinery (Cas9 endonuclease and guide RNA), but so close to the maximum carrier capacity consistent nucleic acid packaging is challenging. The inclusion of additional elements, such as reporters or DNA templates for the homology directed repair, in a single AAV particle is thus almost impossible. While methods have been developed to mitigate this problem, they considerably increase the technical complexity of the system.[18] Besides, viral vectors in general may not be ideal for gene editing therapies. Gene editing is a “hit-and-run” approach where the target DNA has to be modified only once. A permanent expression of the editing machinery is neither necessary nor desired. In fact, the long-term expression of CRISPR/Cas9, for example, increases the risk of inducing cellular toxicity and immune responses.[10] Even when used for therapeutic strategies other than gene editing, the relative complexity of viral vectors is an important hurdle in their early stage development that drives the high development costs. The creation of new virus variants by modifying the capsid, e.g., for organ specific targeting, is both time-consuming and expensive as it involves sophisticated biochemical and biotechnological techniques and know-how.[3, 19] Moreover, since viruses are biopharmaceuticals, their manufacturing costs are high compared to conventional chemical syntheses.[4] Problems with the scale-up of the production[20] and the required very rigorous in-process and quality controls further add to the costs.[19] One of the primary concerns with viral vectors is, however, their immunogenicity.[4] Immune responses against the viral vector, as well as the transduced cells, have been reported in many clinical studies and frequently render the therapy ineffective after one or a few administrations.[1, 2] This is particularly the case with AAVs, against which neutralizing antibodies are naturally found in most of the human popula-

tion. There are ongoing efforts to ensure the therapeutic success by developing less immunogenic capsid variants[3], excluding patients with a pre-existing immunity[2], and applying immunosuppressants before, during, and after the actual administration of the viral vector[4]. Still, a successful therapeutic outcome is not guaranteed.

In the light of these disadvantages, non-viral delivery strategies have more and more become a viable alternative and a dramatic increase in their use in clinical trials has been seen in recent years.[21] Admittedly, compared to their viral counterparts, many non-viral systems are still in relative early clinical development stages, but the results are encouraging, nonetheless, and have sparked interest of big pharmaceutical companies.[4]

A variety of different physical and chemical gene delivery methods have been developed, including electroporation, heat shock treatment, and biolistic particle delivery systems ("gene guns"), but in vivo use is normally restricted to vehicular, nanoparticulate systems based on lipids, (bio)polymers, and inorganic materials. In addition to their mostly non-immunogenic nature, which enables repeated in vivo application, these non-viral carriers have several decisive advantages over viral vectors. First of all, they are chemically synthesized, thus their manufacturing is comparatively cost-effective and can be scaled up with relative ease. The chemical synthesis also provides an enormous flexibility in vector design and permits to customize the system to the specifics of a given delivery challenge.[4] This customization includes the attachment of targeting ligands, modifications to improve biocompatibility, and the introduction of functionalities that enhance nucleic acid encapsulation or release. Non-viral systems also offer a higher flexibility as far as their nucleic acid freight is concerned. A large therapeutic load such as a 9.8 kbp plasmid DNA can be delivered by the very same non-viral carrier as a small 21 bp siRNA.[22] In addition, in most cases each carrier particle carries and delivers more than one single nucleic acid molecule. Particles based on branched 25 kDa polyethylenimine (bPEI 25), for instance, have been shown to contain around 90 individual plasmids.[23]

Despite these advantages, non-viral vectors are still far from ideal gene carriers. One of their biggest weaknesses is their poor delivery efficiency compared to viral vectors. Although tremendous improvements have already been made, the currently available systems are still not effective and specific enough for a wider clinical application and need further refinement in terms of function and structure.[4, 21] A non-viral vehicular delivery system must meet three basic requirements in order to be successful: Efficient nucleic acid condensation and packaging, the ability to overcome physiological barriers en route to target cells, and efficient cellular uptake and processing (see Sections 2.1 and 5.1.2).[4] The most promising systems today are based on nucleic acid complexing agents. The common characteristic of these agents is their cationic charge. It enables them to bind to the negatively charged nucleic acid phosphate backbone. The resulting charge neutralization causes the nucleic acid to condense into small,

highly ordered particles embedded in a matrix provided by the cationic agent (see Section 4.1).[4]

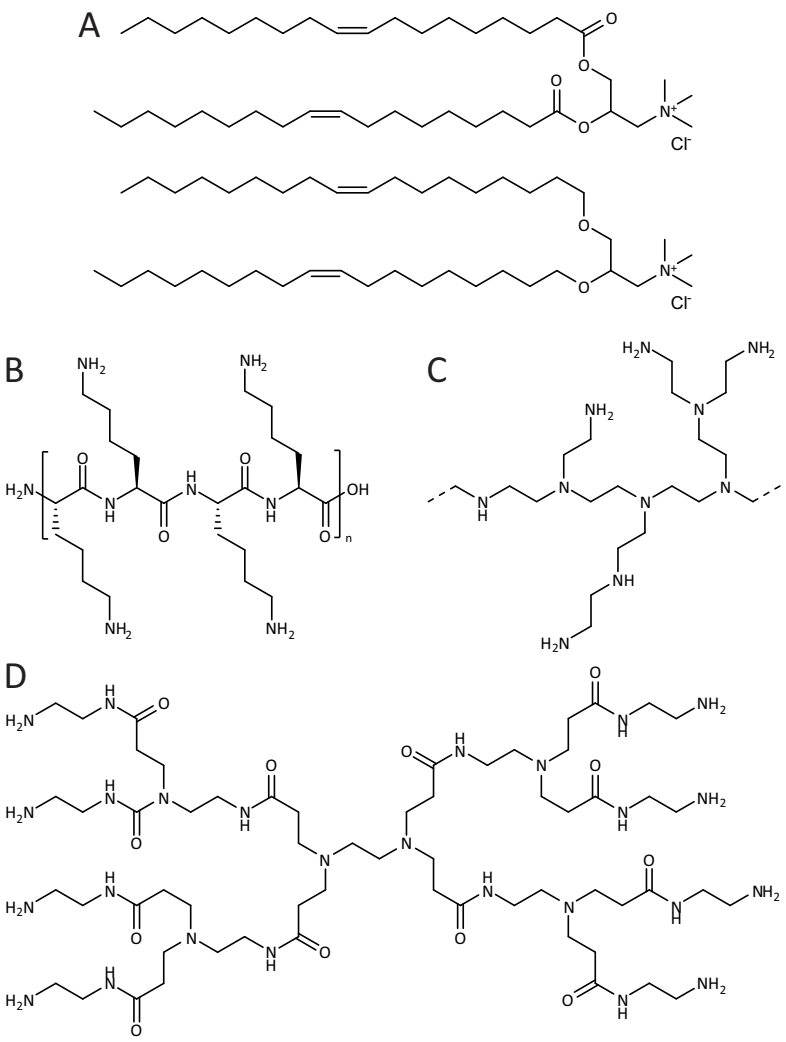

Figure 1.1: Typical non-viral gene carriers

Cationic lipids (A) like DOTAP (1,2-dioleoyl-3-trimethylammonium propane) and DOTMA (1,2-di-O-octadecenyl-3-trimethylammonium propane) form complexes called lipoplexes with nucleic acids. Nucleic acid complexes with cationic polymers are termed polyplexes. A large variety of polycations have been developed for gene delivery, including (B) poly(L-lysine) (PLL), (C) branched polyethylenimine (PEI), and (D) poly(amidoamine) (PAMAM) dendrimers.

Cationic phospholipids and lipid derivatives are among the oldest class of complexing agents (Figure 1.1A). They are used alone or in combination with neutral helper lipids and cholesterol. They form stable nanosized complexes (lipoplexes) of varying morphology[24] with nucleic acids through a thermodynamically directed self-assembly process.[4] Initially, permanently charged lipids like 1,2-dioleoyl-3-trimethylammonium propane (DOTAP) and 1,2-di-O-octadecenyl-3-trimethylammonium propane (DOTMA) were used, but the positive surface charge of the resulting lipoplexes not only severely limited the system's circulation time[21] due to interactions with serum components but also increased cytotoxicity. Later on PEGylated lipids were intro-

duced to mask the particle charge[21] ("stealth liposomes") and more recently lipid nanoparticles (LNPs) were developed. LNPs are based on novel, pH-sensitive lipids and represent the currently most advanced lipidic delivery system. They are structurally distinct from lipoplexes and have been used for siRNA, mRNA, and pDNA delivery.[25] At the moment, LNPs are under intense investigation in clinical trials.[25, 26]

Polymeric materials, especially polycations (Figure 1.1B, C, D), represent a further class of gene carriers that are currently the subject of intense research, partly due to their chemical diversity, shelf stability, and diverse architecture (e.g., linear, branched, dendritic, and combinations thereof).[19] Polycations are typically synthesized from cationic monomers containing primary, secondary, and tertiary amines. Similar to lipid carriers, they electrostatically interact with nucleic acids to form compact nanoparticulate complexes (polyplexes).[19] Among the many different polycation classes that have been evaluated for their transfection ability, including the naturally occurring polysaccharide chitosan, poly(*N*,*N*-diethylamino-2-ethylmethacrylate) (PDEAEMA), poly(amidoamine) (PAMAM) dendrimers, and poly(L-lysine) (PLL), polyethylenimine (PEI) – particularly branched 25 kDa PEI (bPEI 25) – is often considered to be the gold standard for in vitro and in vivo gene transfer[21, 27]. PEI's exceptional efficiency is attributed to a combination of several favorable properties. The high density of cationic charges allows for the formation of small, positively charged complexes that not only protect the nucleic acid against nucleases but also promote cellular uptake.[27] One of the most crucial factors responsible for PEI's high transfection efficiency could, however, be its ability to facilitate endosomal escape. The endosomal compartment is considered to be one of the most challenging barriers in non-viral gene delivery.[4] Several different escape mechanisms have been postulated with the "proton sponge hypothesis"[28, 29] being the most widely accepted one. In short, the buffering capacity of PEI's secondary and tertiary amines counteracts lysosomal acidification and promotes the organelle's rupture (see Section 5.1.2). In general, PEI's transfection efficiency, as well as cytotoxicity, increases with molecular weight.[27] bPEI 25[30] offers a good compromise between those two properties and often serves as reference standard in transfection studies. Its still significant cytotoxicity, however, limits its use particularly in in vivo applications. In an attempt to find PEI variants with better efficiency/cytotoxicity profiles, linear PEIs (lPEI) have come into focus. lPEIs form weaker and bigger complexes with DNA than bPEIs of comparable molecular weight, especially in solutions of high ionic strength (see Chapter 4).[27, 31] While larger particles demonstrate higher transgene expressions in vitro, the opposite is true for in vivo applications.[31] Several strategies have been developed to address the shortcomings of both PEI variants. Many of them involve cross-linking less toxic, low molecular weight linear PEIs to higher molecular weight branched PEIs with increased transfection efficiency.[30, 32] Ideally, the cross-links are not only biodegradable but also bioresponsive, i.e., the carrier integrity is maintained unless the vehicle is exposed to a certain very specific biological envi-

ronment.[33] Combined with additional functionalities like targeting ligands, carriers based on these modified polymers would be able to mimic some functions of viral vectors, arguably increasing the delivery success. In most cases biodegradability is achieved with the help of hydrolysable or reduction sensitive cross-linkers.[27, 33] Hydrolysable cross-linkers have the disadvantage that their exact degradation rate is difficult to control, which can result in the carrier's premature degradation and untimely cargo release (see Section 2.1). Reduction sensitive cross-linkers are based on disulfides. They exploit the large redox gradient between extra- and intracellular space,[34] i.e., they are exceptionally stable in the oxidizing extracellular space but are readily cleaved in the reducing intracellular environment (see Section 5.1.1).[35] Numerous studies have demonstrated that the presence of disulfides in polycationic carriers has a favorable influence on many aspects of the gene delivery process.[36] In some cases, however, the presence of disulfides has been shown to have the opposite effect and it is often not well understood why.[35] In fact, many aspects of the delivery are not well understood, yet. Even the seemingly simple question of where and when the linkers are cleaved during delivery is surprisingly difficult to answer and still subject to ongoing debate (see Section 5.1.2). It is easy to see that this lack of knowledge impedes the development of better stimuli-responsive delivery systems.

1.4 Overview and goals of the thesis

In order to develop better reduction sensitive polycationic gene carriers, a more thorough understanding of the factors contributing to the delivery success is necessary. It is already known that the balance between carrier stability and cargo release is pivotal and significantly depends on the polycation-nucleic acid interaction. The factors contributing to this interaction are, however, not sufficiently understood. Ideally, a structure-activity relationship encompassing the properties of both components would help to predict polyplex stability in the biological environment. Another, perhaps even more important success factor is the carrier's interaction with target cells. Although countless studies have been devoted to this very subject, surprisingly little of the delivery process is fully understood (see Section 4.1). Thus, it is evident that better analytical tools are needed to address these issues.

The main goal of this thesis is the development and characterization of new fluorescence-based analytical tools that allow for new insights into the interaction between polycations and nucleic acids, as well as cellular uptake, trafficking, and processing of reduction sensitive polyplexes. A particular focus of this work is placed on disulfide cross-linked derivatives of low molecular weight linear PEI due to their favorable transfection properties. It has already been established that the transfection efficiency of polyplexes based on these derivatives positively

correlates with the linker content under certain conditions.[31, 37] However, the transfection efficiency cannot be increased indefinitely by simply increasing the linker content, since insoluble gels are formed at higher cross-linking ratios, even though the bulk of the polymer strands generally remains unmodified. For that reason, it was first investigated how an existing synthesis method for cross-linking lPEIs with L-cystine can be optimized to allow for significantly higher cross-linking ratios than previously thought possible (Chapter 2). It was additionally investigated if this method could also be used for the synthesis of cross-linked PLLs. The cross-linked polycations were then compared with their respective unmodified counterparts with regard to their ability to deliver siRNA and pDNA into CHO-K1 model cells. Since these first tests were not able provide more detailed insights into the polycation/nucleic acid interaction, polymer cleavage, and cellular processing, the polymers were further modified with fluorescent dyes (Chapter 3). Fluorescent probes have countless applications in life sciences and can be used to investigate the immediate environment of biomolecules, which can, for instance, help to identify protein binding partners. They are usually supplied in a preactivated form, i.e., they are equipped with reactive groups like *N*-hydroxysuccinimide (NHS) esters that enable them to react with specific functional groups on (bio)molecules. Unfortunately, not all dyes are provided with a reactive group suitable for a particular labeling application, or due to the often inherent chemical instability of the reactive group, the preactivated probe is prohibitively expensive for larger scale experiments. Since the cross-linking method combines the activation of a carboxyl group and the reaction with a polymer amine in a simple one-pot reaction without the need for specialized equipment or work-up procedures, it was evaluated how it can be adapted for the labeling of polyamines with readily available, inexpensive, non-preactivated fluorophores in any regular biochemical lab. In order to establish suitable synthesis parameters, various linear, branched, and cross-linked PEIs were labeled with fluorescein (FAM) and tetramethylrhodamine (TAMRA), as two representative members of the widely popular class of xanthene dyes. Since one of the goals of this thesis is to study the cleavage of reduction sensitive polycations, the polymers were also labeled with the boron-dipyrromethene derived, reduction sensitive probe BODIPY FL L-cystine (BP_2) and its redox-inert counterpart BODIPY FL (BP). BP_2 was specifically chosen because of its structural similarity to the L-cystine cross-linker in order to ensure that the cleavage rates of probe and cross-linker match closely. Detailed investigations of the photophysical properties of fluorescent labels located on polycationic gene carriers are surprisingly scarce, although the proximity and high density of charged amines can have a significant impact on the fluorophores. Thus, the polymer derivatives were characterized with absorption and static emission spectroscopy. In addition, several chemical properties, including the BP_2 probe's cleavage at a physiological glutathione concentration were investigated as well. These experiments were the basis for more detailed investigations concerning the interaction between polycations and nucleic ac-

ids, as well as polymer cleavage (Chapter 4). In most studies that explore polycation/nucleic acid interactions with the help of fluorescence-based methods, either both polyplex components carry a probe (e.g., Förster resonance energy transfer (FRET) assays) or only the nucleic acid is labeled (e.g., ethidium bromide displacement assays). Unfortunately, it is often forgotten that any of those methods can only illuminate certain specific aspects of the interactions within polyplexes. FRET assays, for example, rely on relatively long-range fluorophore interactions, but they are "blind" towards very short ranged interactions as one would expected to find in tightly bound complexes. Another often overlooked aspect is the sensitivity of many fluorophores towards environmental changes and polyplex formation undoubtedly represents a significant environmental change for both the nucleic acid and the polymer. So in order to close this gap in knowledge, DNA and siRNA polyplexes based on labeled model PEIs were characterized with the help of steady-state and time-resolved fluorescence quenching assays, and confocal laser scanning microscopy (CLSM). The results of these experiments and their implications on the general experimental design of studies with fluorescently labeled polyplexes are also discussed. Furthermore, a sensitive new method for investigating very short-ranged interactions between polycations and nucleic acids was developed. It based on the photoinduced electron transfer (PET) from nucleobases to a fluorescent label on the polymer. The cleavage of BP_2 was investigated, too. Here it was of particular interest how the cleavage rate correlates with the molecular weights of the polyplex constituents and what implications that may have on the intracellular cargo release. This work's final experimental chapter (Chapter 5) is devoted to the question of how labeled polycations can be used for studying cellular uptake, trafficking, and processing of polyplexes with the help of techniques like flow cytometry, CLSM, and fluorescence spectroscopy. Again, CHO-K1 cells were used as model because of their widespread use in gene delivery studies. The general experimental parameters were established with the help of redox-insensitive TAMRA-PEI. This PEI-derivative was also used to explore the differences between the free polymer and the polymer in complex with DNA. Possible differences in the processing of redox-sensitive and insensitive polymers were examined with the help of TAMRA labeled disulfide cross-linked PEI. The cellular processing of reduction sensitive polyplexes was studied using BP_2 labeled PEIs. The first experiments served to verify that BP_2 is indeed cleaved during delivery and that the cleavage was dependent on cellular thiols. Later experiments examined the impact of internalized disulfides on the cellular redox homeostasis. Furthermore, the possible time point at which the polyplexes are exposed to reducing conditions during intracellular processing was investigated. Finally, differences in the uptake and trafficking of siRNA/lPEI and pDNA/lPEI polyplexes were identified.

2 Cross-linking of polycations with L-cystine

2.1 Introduction

The delivery efficacy and efficiency of gene delivery systems depend on the carrier's ability to overcome a multitude of biological barriers on its way to the intracellular target site. First, there is the high risk that the nucleic acid cargo is enzymatically degraded by nucleases present in the intravascular and intercellular environment.[36] Polycationic gene carriers are able to protect their sensitive payload by encapsulating it into impenetrable nanosized complexes. Ideally, this complexation also increases circulation times by reducing unspecific interactions with blood components and by preventing ion exchange reactions in the high ionic strength extracellular medium.[36, 38-41] Second, naked nucleic acids are not readily taken up by cells due to their negative charge and, especially in case of DNA, excessive size.[38, 42] A significant cellular uptake can only be achieved if the carrier is able to mask the nucleic acid's charge and by inducing the condensation of large nucleic acids.[38] Third, following the uptake, the delivery system usually reaches the endolysosomal pathway, a well-known bottleneck[43] for intracytosolic drug delivery. Unprotected nucleic acids are rapidly degraded during the maturation of early endosomes to acidic late endosomes and their subsequent fusion with lysosomes.[36] The carrier must limit its cargo's exposure to this aggressive environment by facilitating endolysosomal escape. After having reached the cytosol, nucleic acids are in some cases still associated with the carrier polymer.[38] While the best time point for cargo release is not fully understood[36], it is known that vector unpacking substantially contributes to the delivery success. The optimal release stage appears to vary with the type of nucleic acid. Free plasmid DNA, for instance, is essentially immobile within the cytosol and thus quickly degraded.[44] High gene expression levels have been demonstrated in cases where the DNA remained associated with a cationic carrier within the cytosol and beyond. It has been speculated that this is the result of a nuclear-localizing effect of the vector[42] or simply due to an increased cytosolic mobility of the condensed plasmid[44]. Regardless of the means by which the DNA reaches the nucleus, substantial expression levels require efficient DNA unpacking at some point.[38, 45] There is some evidence that nuclear DNA unpacking, in contrast to the cytosolic unpacking of mRNA, is indeed relatively efficient.[46] In other words, vector disassembly is a more significant barrier

for the delivery of mRNAs than for DNAs.[46] The significance of vector unpacking for the delivery of siRNA is less clear. Since siRNA is a relatively small polyanion compared to mRNA or plasmid DNA its interaction with polycations is weaker[38], which probably makes vector unpacking a lesser concern.[38, 47]

The relationship between the molecular weight of the carrier polymer and the transfection efficiency have extensively been investigated for polyethylenimine[48, 49] and other polycations[42]. Typically these properties are positively correlated.[42] Colloidal stability of the polycation/nucleic acid complexes, for instance, increases with molecular weight presumably due to the increased number of electrostatic interactions.[32] The molecular weight also controls polyplex size.[38] While the optimal polyplex size is a matter of debate[42], it is generally accepted that the polyplex diameter should be lower than 150 nm, the size limit for non-specific cellular uptake[38]. In case of PEI, a higher molecular weight decreases polyplex size by promoting DNA condensation and indirectly leads to higher transfection efficiencies.[50, 51] For PLL-carriers the correlation between molecular weight and polyplex size is not unambiguous. In one instance the use of 54 kDa PLL resulted in smaller (25 nm) polyplexes than with 10 kDa PLL (40 nm).[52] Then again 4 kDa PLL-DNA complexes had a diameter of 20-30 nm, while the diameter of 224 kDa PLL-DNA complexes ranged from 100 to 300 nm.[42]

Unfortunately, high molecular weight polycations in general are substantially more cytotoxic than their low molecular weight counterparts[32, 53] or in other words, high transfection efficiency comes at the price of high toxicity. In recent years, however, numerous non-viral carriers have been developed that try to unite the advantages of both polymer variants.[32] One of the most appealing strategies is to cross-link low molecular weight polycations with biodegradable linkers. In many cases the resulting high molecular weight products have lower toxicities and comparable or even higher transfection efficiencies than similarly sized non-cross-linked derivatives.[32, 52] Biodegradable linkers or biodegradable chemical bonds in general can also be used to provide gene carriers with additional functionalities (e.g., targeting moieties, steric shielding). The idea is to create more “intelligent” delivery systems that are designed to mimic viral responses to biological stimuli (e.g., changes in pH and redox potential, and the presence of certain enzymes)[32, 54]. Such stimuli-responsive systems would be able to perform specific tasks, such as cargo release or shedding of the coating polymer, at the optimal spatiotemporal point of the delivery process.[40]

Many, if not most biodegradable linkers used for the purposes outlined above contain hydrolysable bonds like amides, esters, ortho-esters, and imines.[30, 32] The use of acid-labile linkers (esp. esters) can be problematic as their degradation profiles are sensitive to subtle structural variations[36, 55]. This makes it difficult to construct carriers with high extracellular and low intracellular stability. The amino group in poly(amino esters), for example, is known to increase

the ester's hydrolysis rate, leading to premature carrier degradation.[36] Similarly, the amino functions in DNA carriers based on amine-modified graft polyesters act as catalyst for the hydrolysis of the PLGA side-chains.[56] Even if the hydrolysable carrier remains intact until it is taken up by target cells, there is the risk that it will finally be degraded in the highly acidic endolysosomal compartment. Since this compartment also houses the highest enzymatic activity of DNase I, a large proportion of the DNA will be lost.[31]

In contrast, disulfide bonds are exceptionally stable under the oxidizing conditions of the extracellular space, but are readily cleaved inside reducing cellular compartments like the cytosol.[36, 40, 57] They are particularly useful when carrier functions such as a steric shielding have to be switched on or off quickly after cellular uptake. Steric shielding, for instance, improves the colloidal stability of polyplexes but usually decreases their transfection efficiency.[36, 58] Bauhuber et al. have assessed the role of PEG-shields on the transfection rates of linear PEIs. Polyplexes based on PEIs where the steric shielding was attached through a non-degradable thioether bond had a significantly lower transfection efficiency than unshielded polyplexes. That was not the case when the thioether was replaced with a disulfide bond. It was concluded that the non-detachable PEG-shield may have interfered with intracellular polyplex processing, i.e., endosomal escape or cargo release. The removable PEG-shield allowed the carrier to regain its endosomolytic properties and to become more susceptible to cargo displacement in ion exchange reactions.[58]

Disulfides have also been used to temporarily increase the polymer's molecular weight in order to create less toxic carriers with improved transfection efficiencies. [40, 52] Oupický et al. have demonstrated the validity of this approach by creating laterally stabilized DNA complexes with linear 45 kDa and 187 kDa L-cystine cross-linked polylysines.[59] Lateral stabilization was achieved by coating the complexes with a reactive copolymer of N-(2-hydroxypropyl) methacrylamide and methacryloylglycylglycine 4-nitrophenyl ester (PHPMA). Compared to similar non-reduction sensitive 205 kDa PLL/DNA complexes, the transfection with the 187 kDa derivative resulted in a particularly high transgene expression in human retinoblast 911 cells. Similar results have been reported for other carrier polymers as well and there is growing evidence that the enhanced transfection properties are at least in part related to an improved intracellular nucleic acid release as consequence of the carrier's degradation.[36, 40, 52] Lin and Engbersen, and Kim et al., for example, have investigated the intracellular distribution of reduction sensitive and insensitive DNA-polyplexes.[36, 60] With the degradable carrier both the DNA and polymer were evenly dispersed in the cytoplasm, which was interpreted as complete cargo release. In contrast, micro-sized aggregated clumps were observed for the non-cleavable systems. Incidentally, the transfection efficiency of the degradable system was 20-fold higher.[36] Similar observations have been made for other polycations and nucleic acids. Breunig et al. have followed the intracellular fate of fluorescently labeled siRNA in complex with bPEI 25 kDa, lPEI

5 kDa, and sslPEI (lPEI 2.6 kDa cross-linked with 3 % DSP).[61] Their data indicate that siRNA is released from sslPEI to a much higher degree than from the other polymers. In a closely related study a disulfide cross-linked lPEI and a similarly sized non-cleavable lPEI were compared.[30] The degradable polycation proved to be two times more efficient in transfecting CHO-K1 cells with DNA.

When reduction sensitive high molecular weight polycations are constructed out low molecular weight components, disulfides are usually introduced with the help of linkers. The use of linkers requires fewer synthesis steps and results in higher yields[40] than directly converting preexisting functional groups to thiols and subsequently oxidizing them to disulfides. In order to obtain products with the desired properties, several aspects concerning the linker's structure have to be considered. In a biological environment disulfides are cleaved in thiol-disulfide exchange reactions with relatively bulky cellular reductants like glutathione or redox active enzymes (see Section 5.1). Thus, the cleavage rate strongly depends on the accessibility of the disulfide bond. This relationship can be exploited to alter the release characteristics of the delivery system. A carrier containing disulfides with a sterically demanding substituent has been demonstrated to release its load about one hundred times slower than a carrier with better accessible disulfides.[62] The linker structure also influences the carrier-nucleic acid interaction by altering the polycation's charge density. Amine reactive linkers with a structure comparable to Lomant's reagent (Figure 2.1) lower the polymer's charge density as two polymer amines are converted to amides during the cross-linking reaction. Sometimes this is a desired side effect since the lowered charge density facilitates nucleic acid release. In other cases linkers that contain protected additional amines such as N^{α},$N^{\alpha'}$-di-Boc-L-cystine (Boc-Cys-OH)$_2$ (Figure 2.1) have to be used.

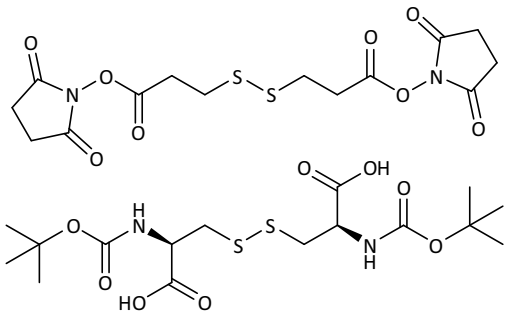

Figure 2.1: Chemical structures of two common disulfide containing cross-linkers

Above: Lomant's reagent (DTSP or Dithiobis(succinimidyl propionate)), below: N^{α},$N^{\alpha'}$-di-Boc-L-cystine ((Boc-Cys-OH)$_2$).

The cross-linking ratio, i.e., the amount of linker in relation to the amount of reactive groups on the polymer, is another significant factor that impacts the carrier's transfection properties. Systems with low cross-linking ratios possess a lower resistance towards nucleic acid cargo dis-

placement by competing anions. On the other hand, high cross-linking degrees can result in overstabilized polyplexes with insufficient cargo release within the required time frame.[45, 63] Lungwitz et al. have assessed the influence of the cross-linking ratio, linker type, and the polymer's molecular weight on the stability and transfection efficiency of reduction sensitive lPEI/DNA-polyplexes.[31] They observed that, regardless of the linker type, cross-linking reduces the amount of polymer necessary to achieve the maximum transfection efficiency. In addition, at least at low polymer/DNA ratios, the transfection efficiency increases with increasing linker content. Compared to lPEI 25 and bPEI 25/DNA polyplexes, the transfection efficiency and cell compatibility increased several fold, though polymers prepared with Lomant's reagent were more toxic than those with L-cystine. Despite these promising results, this work also highlights a limitation associated with the use of homobifunctional linkers to cross-link polyamines: It is not feasible to achieve substitution degrees beyond a certain limit or water-insoluble gel-like products are formed. Even close to that limit, the vast majority of the polymer remains unmodified. Higher substitution degrees and a larger percentage of modified polymer strands could arguably further improve carrier properties.

For these reasons, the aim of the work presented in this chapter was to further improve the $(Boc\text{-}Cys\text{-}OH)_2$/DMTMM based cross-linking procedure for lPEIs established by Lungwitz et al.[31] L-cystine was chosen over Lomant's reagent because of its superior toxicity profile and close structural resemblance to BODIPY FL L-cystine, a fluorescent label later used to monitor polymer degradation (Section 3.5.3). The resulting reduction sensitive product (S_2-lPEI) was analyzed with gel filtration chromatography and it was confirmed that by varying the synthesis parameters, it is indeed possible to obtain a higher cross-linking degree and modify a higher proportion of polymer strands. S_2-lPEI/DNA and siRNA polyplexes were more efficacious in transfecting CHO-K1 cells than polyplexes made from the parent polymer. The maximum transfection efficacy was shifted to a lower N/P value (ratio of polymer amines to nucleic acid backbone phosphates; see Section 2.2.3). Compared to redox inert carriers, the reduction sensitive polyplexes were moreover able to deliver significantly higher amounts of nucleic acid per cell, though the data might also be interpreted as evidence for enhanced cargo release. The synthesis method was also used to cross-link linear poly(L-lysine), but that had no positive effect on the transfection efficacy or cytotoxicity.

Fluorescently labeled S_2-lPEI and S_2-PLL (see Chapter 3) were used in subsequent experiments to investigate the (intracellular) processing of reduction sensitive polyplexes (Chapters 4 and 5).

2.2 Materials and methods

2.2.1 Cross-linking of PLL and lPEI

Materials

Low molecular weight linear poly(ethyleneimine) was synthesized by Uta Lungwitz by ring-opening polymerization of 2-ethyl-2-oxazoline (Sigma-Aldrich, Munich, Germany) followed by an acid hydrolysis of the resultant poly(2-ethyl-2-oxazoline) ($M_{n(GPC)}$ = 13.8 kDa, $M_{w(GPC)}$ = 16.8 kDa, PDI_{GPC} = 1.22, ω(N) = 0.1762).[31] lPEI was dried in vacuo at 95 °C before use. Linear poly(L-lysine hydrobromide) was obtained from Alamanda Polymers (Huntsville, Alabama, USA; cat. no. $PLKB_{25}$, lot no. 000-KB025-101, M = 5.2 kDa, $M_{n(NMR)}$ = 5.9 kDa, PDI_{GPC} = 1.02, DP_n = 28) and used without further purification. 4-(4,6-Dimethoxy-1,3,5-triazin-2-yl)-4-methylmorpholinium chloride (DMTMM), N^{α},$N^{\alpha'}$-di-Boc-L-cystine ($(Boc\text{-}Cys\text{-}OH)_2$) and all other chemicals were purchased from Sigma-Aldrich (Munich, Germany) in analytical grade. Millipore (Schwalbach, Germany) supplied a Milli-Q water purification system for the production of ultra-pure water (ρ = 18 MΩ·cm) and Amicon Ultra-15 centrifugal filter units ($MWCO$ = 3 kDa). Centrifugations were performed in a Beckman Coulter Avanti J-E centrifuge (Kreefeld, Germany) using Corning PP Centrifuge Tubes (Wiesbaden, Germany).

Cross-linking procedure

All syntheses were performed in 4 mL silanized glass vials containing a 5 mm magnetic stir bar. Linear PEI and PLL were dissolved in methanol and in a mixture of methanol and water, respectively (specific amounts are listed in Table 2.1). A methanolic $(Boc\text{-}Cys\text{-}OH)_2$ solution was added, followed by a methanolic solution of DMTMM after several minutes. After closing the reaction vessel, the clear solution was stirred at room temperature overnight. The solvent was evaporated under reduced pressure. For the removal of the BOC protecting group, 1 M HCl (approx. 2 mL) was added to the colorless, gel like or waxen crude product and the solution was stirred for one hour at room temperature.

S_2-lPEI was precipitated in a saturated sodium hydroxide solution and then washed with ice-cold water by centrifugation (15,000 g, 4 °C) until the supernatant became neutral. The white gel-like product was dissolved in 1 M HCl and purified three times by ultrafiltration in the same solvent.

S_2-PLL was immediately ultrafiltrated after synthesis with the following series of solvent mixtures (about three repeats each): 1 M HCl/DMSO (ϕ = 10 %), H_2O/DMSO (ϕ = 10 %), 0.1 M

NaOH, H_2O (until filtrate became neutral) and 10 mM HCl.

Finally, both cross-linked polycations were filtered through a 0.2 µm syringe filter (regenerated cellulose) and freeze dried overnight in silanized glass vials. The end products were yellowish or colorless brittle foams. Yields by mass: S_2-PEI – 40-70 %, S_2-PLL – 20-35 %.

Table 2.1: Reaction conditions for polycation cross-linking

Amounts of substances, molar ratios and solvent volumes used in the syntheses of cystine cross-linked lPEI and PLL

	amount of substance n/µmol			molar ratios		solvent volumes V/µL	
product	linear polymer	DMTMM	$(Boc\text{-}Cys\text{-}OH)_2$	$n((Boc\text{-}Cys\text{-}OH)_2)$/ n(lin. polymer)	n(DMTMM)/ $n((Boc\text{-}Cys\text{-}OH)_2)$	total	H_2O
S_2-lPEI_a	12.5	726.4	195.6	15.6	3.7	2160	-
S_2-lPEI_b	12.6	375.3	98.7	7.8	3.8	2160	-
S_2-PLL_a	6.1	137.0	36.1	5.9	3.8	590	200
S_2-PLL_b	11.9	580.7	161.4	13.6	3.6	960	200

2.2.2 Gel filtration chromatography

A Shimadzu HPLC system (Duisburg, Germany) with the following components was used for the polymer characterization and the degradation studies: SIL-10ADvp auto injector, LC-10ATvp liquid chromatograph, DGU 14A degasser, CTO-ASvp column oven and a SCL-10Avp system controller. The polymers were detected with a RID-10A refractive index detector ($t_{\text{flow cell}}$ = 40 °C) and a SPD-10Av UV-Vis Detector (λ = 247 nm). The chromatograms were exported from Class VP 6.12 and converted with the custom made software HPLC Data Converter for Shimadzu Files. The polycation hydrochlorides were dissolved in Dulbecco's phosphate buffered saline (γ = 1.43 to 5 g/L) and centrifuged at 16,000 g for 5 min to sediment particles and dust. Fifteen microliters of the supernatant were injected in each run. During the degradation studies, a 50 mM GSH stock solution was added to the samples to obtain a final GSH concentration of 5 mM. A Novema 3000 Å (PEI) or a Novema 300 Å (PLL) SEC column (10 µm, 8 x 300 mm, Polymer Standard Service, Mainz, Germany) was thermostated at 40 °C and run at a flow rate of 1 mL/min with 0.15 M NaCl + TFA (ϕ = 0.1 %). M_n, M_w and *PDI* were calculated relative to the retention time of dextran standards (M_w = 180 to 410,000 Da, Polymer Standard Service, Mainz) using the software GPC for Class VP 1.00. For calibration $\log M_p$(dextran) vs retention time was fitted with a third degree polynomial.

2.2.3 Cellular uptake of polyplexes

Plasmid isolation

Gene transfection efficiency was measured by the expression of the enhanced green fluorescent protein (EGFP). Cellular uptake efficacy and the amount of internalized polyplexes were measured with the help of a YOYO-1 labeled firefly luciferase expressing plasmid (pGL3-Enhancer). Both the EGFP encoding plasmid pEGFP-N1 (4733 bp, 2.92 MDa; Clontech, Saint-Germain-en-Laye, France) and the pGL3-Enhancer plasmid (5064 bp, 3.13 MDa; Promega GmbH, Mannheim, Germany) were amplified in *E. coli* JM109 grown in LB medium supplemented with kanamycin or ampicillin, respectively. For DNA isolation, a QIAGEN Plasmid Maxi Kit (Hilden, Germany) was used according to the manufacturer's instructions; the yield was determined by UV-Vis at 260 nm. The final aqueous DNA stock solution were kept at -20 °C.

Nucleic acid labeling

The cellular uptake efficacy and the estimated amount of internalized polyplexes were determined with the help of fluorescently labeled nucleic acids. Thirty minutes prior to the polyplex formation pDNA was stained with YOYO-1 ($\lambda_{abs\,max}$ = 491 nm, $\lambda_{em\,max}$ = 509 nm; Life Technologies GmbH, Darmstadt, Germany) at room temperature and protected from light. 6-FAM labeled siRNA, siGLO Green ($\lambda_{abs\,max}$ = 494 nm, $\lambda_{em\,max}$ = 520 nm), was purchased from Fisher Scientific Germany GmbH (Schwerte, Germany). Before use, the siRNA was resuspended in RNase-free water (γ = 0.25 g/L).

Polyplex formation

For the preparation of polyplexes 2 µg DNA were diluted in 50 µL 150 mM NaCl. The appropriate amount of polycation dissolved in the same volume of 150 mM NaCl was added and the solution was vortexed intensively for about 20 s. The polyplexes were allowed to mature for 15 min before use.

The amount of polycation in relation to the amount of nucleic acid is given by the N/P value. It is defined as the ratio of positively charged polymer amines to the negatively charged nucleic acid backbone phosphates (see appendix). Cell viability and transfection efficacy, were determined at N/P values ranging from 6 to 30. Cellular uptake efficacy and the estimated amount of internalized polyplexes were determined at an N/P of 8.

Cell culture and flow cytometry

The in vitro transfection efficacy and cell viability were determined according to a method described earlier[64] by using flow cytometry. For that, Chinese hamster ovary cells (CHO-K1; ATCC No. CCL-61) were seeded in 24-well polystyrene tissue-culture treated plates (Corning, Wiesbaden, Germany) at an initial density of 38,000 cells/well (n = 3) in Ham's F-12 supplemented with 10 % fetal calf serum (Biochrom AG, Berlin, Germany). The cells were grown for 18 h (37 °C, 5 % CO_2) and then washed with DPBS (w/o Ca^{2+}, Mg^{2+}, and phenol red; Invitrogen, Darmstadt, Germany). Thereafter, 900 µL serum-free cell culture medium and 100 µL polyplex solution were added (blanks: 150 mM NaCl). Four hours later the polyplex incubation medium was replaced with 1 mL Ham's F-12/10 % FCS and the cells were incubated for another 24 h. Adherent cells were trypsinized and combined with non-adherent cells. PLL and S_2-PLL treated cells could not be trypsinized completely so they were scraped off carefully from the bottom of the wells. All samples were washed once (200 g, 4 °C) with ice-cold DPBS and resuspended in 350 µL of the same buffer. To evaluate cell viability, 0.25 µL propidium iodide (γ(PI) = 1 g/L) was added immediately before each measurement.

The flow cytometry measurements were carried out on a BD FACSCalibur flow cytometer (Heidelberg, Germany) controlled by the software BD CellQuest Pro. In order to measure the EGFP and PI emission (λ_{ex} = 488 nm), the corresponding spectral regions were singled out using a 530/30 nm band-pass and a 670 nm longpass filter, respectively. Ten thousand events were collected for each sample and the data analysis was performed with WinMDI 2.9 (J. Trotter, The Scripps Research Institute, La Jolla, CA, USA). First of all, the sideward scattering intensity was plotted against the forward scattering intensity and a gate was set on the events representing intact cells. The EGFP and PI fluorescence intensity of those cells were plotted against each other. The plot was divided into quadrants, using non-transfected and PI negative cells as reference for cellular autofluorescence. Events with an EGFP and PI fluorescence intensity above the respective autofluorescence level were considered as transfected, non-viable cells. In contrast, events where only the EGFP emission was increased corresponded to transfected, viable cells; non-viable, non-transfected cells had only an increased PI fluorescence. The number of events in each quadrant was counted and the results were exported to MS Excel via MDI StatCon 2.6.

The cellular uptake efficacy and the approximate amount of internalized polyplexes were also determined with flow cytometry. For that, the procedure outlined above was modified in several aspects: Before the addition of the polyplexes, the cells were washed with DPBS and 200 µL of serum-free medium was added to each well. Then, 40 µL of the polyplex solution was added (1 µg pDNA or 1.07 µg siRNA per well, N/P = 8; blanks: DPBS) and the cells were

incubated for one or four hours. Immediately thereafter, the cells were prepared for flow cytometry. The emission of the labeled nuclei acids (λ_{ex} = 488 nm) was detected in the EGFP channel. The fluorescence intensity was plotted against the forward scattering intensity. Cells with an emission intensity above the autofluorescence of untreated cells were considered to be “transfected”. Again, the data were exported for further processing with MDI StatCon 2.6. The cellular uptake efficacy was defined as the number of transfected cells divided by the number of all detected cells expressed in percent. The amount of internalized polyplexes was estimated based on the geometric mean fluorescence intensity of transfected cells. Note: Due to the very different nature of the fluorophores used for pDNA and siRNA labeling, the corresponding intensity values are not directly comparable.

2.3 Results and discussion

Cross-linking of lPEI and PLL

The reaction of a polymer with a cross-linking agent normally results in a mixture of inter- and intramolecularly cross-linked products. If predominantly intermolecularly cross-linked products are formed, the restricted mobility of the growing polymer strands increases the viscosity of the system until gelation occurs, eventually.[65] Intramolecular cross-linking on the other hand, leads to a volume contraction of the polymer coils, resulting in a reduced viscosity.[65] The ratio between intra- and intermolecularly cross-linked species is governed by the reaction conditions (e.g., molar ratio of polymer and cross-linking agent, educt concentrations, and reaction temperature).[66] Dilute conditions limit the amount of intermolecular cross-linking[65] and this fact has been exploited for the synthesis of acid-labile gene carriers based on 1.8 kDa bPEI and glutaraldehyde as cross-linker.[66] Lungwitz et al. have used a similar approach to cross-link linear PEIs with (Boc-Cys-OH)$_2$.[31] They observed that the maximum cross-linking degree before gelation occurs decreases with the molecular weight of the lPEI. With 2.6 kDa and 4.6 kDa lPEI, the highest attainable cross-linking ratio was 8 % (BC8-lPEI2.6) and 1.5 % (BC1.5-lPEI4.6), respectively. Interestingly, their GFC data proved that most of the polymer actually remains unmodified even at the highest linker/lPEI ratios tested. In addition, according to the considerable fronting seen in the respective chromatograms, the products had a broad molecular weight distribution, i.e., high dispersity.

One of the aims of this work was to create L-cystine cross-linked lPEIs with narrower size distributions and lower ratios of unmodified polymer chains. For the reasons outlined above, it was hypothesized that this could be achieved by promoting intermolecular cross-linking and the simplest way to do that was to increase the reactant concentrations.

In a first attempt to synthesize a S_2-lPEI (S_2-lPEI_a, see Table 2.1) with a cross-linking ratio (*n*(L-cystine CO_2H)/*n*(ethyleneimine units)) of 8 %, the concentration of ethyleneimine units and (Boc-Cys-OH)$_2$ was increased more than two-fold compared to the synthesis of a similar derivative (BC8-lPEI2.6)[31] from Lungwitz et al. While no gelation was observed for BC8-lPEI2.6, S_2-lPEI_a precipitated in aqueous solvents (1 mM and 200 mM HCl, pure water, 50 mM borate buffer (pH = 9), and 0.2 M NaOH) unless 2-mercaptoethanol was added (data not shown). However, when a cross-linking ratio of 4 % was used in combination with a ten-fold higher reactant concentration (compared to the synthesis of BC4-lPEI2.6), a well soluble product (S_2-lPEI_b) was obtained. Based on the previous experiments with 4.6 kDa lPEI[31] and considering the 13.8 kDa lPEI used here, the maximum cross-linking degree achievable with the original synthesis method should have been less than 1.5 %. Thus, the modified synthesis protocol indeed allowed for significantly higher cross-linking degrees.

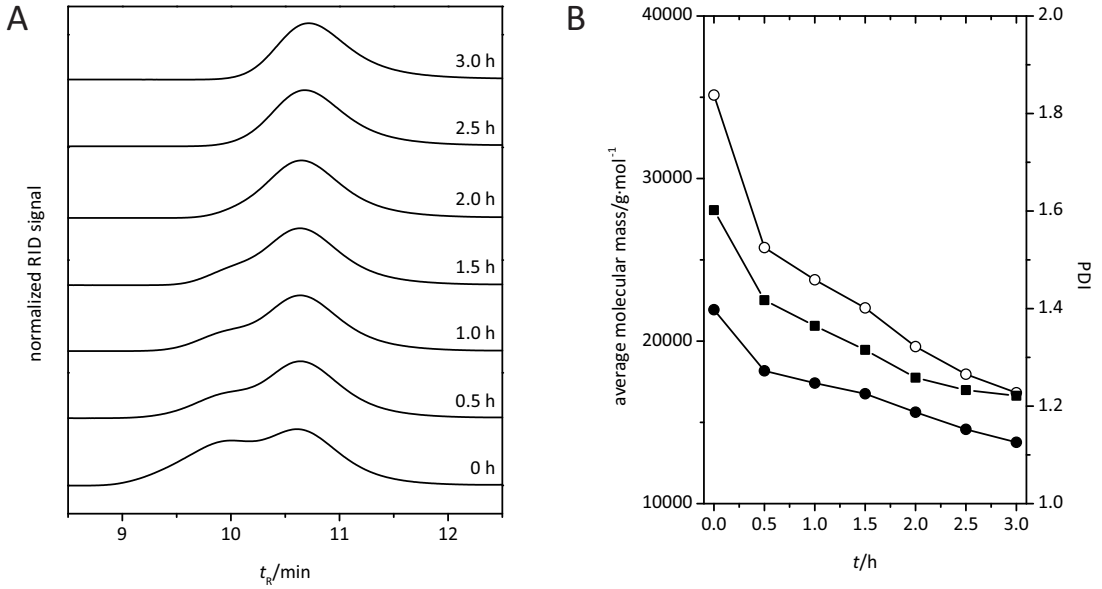

Figure 2.2: Cleavage of S_2-lPEI_b in the presence of GSH

A: GSH (c_{final} = 5 mM) was added to a sample of S_2-lPEI_b (γ_{final} = 5 g/L in PBS) and the polymer's cleavage was followed with gel filtration chromatography over the course of three hours (normalized RID traces of the relevant retention time t_R window shown). B: Time course of the corresponding number (M_n: ●) and mass (M_w: ○) average molecular mass, and the *PDI* (■). (Experimental details Section 2.2.2)

The molecular weight and molecular weight distribution of S_2-lPEI_b were analyzed with gel filtration chromatography and the chromatograms (Figure 2.2A) revealed several differences to those of BC4-lPEI2.6 (see Lungwitz et al.[31]). In case of the latter, the higher molecular weight species appear as 4 min long fronting to the signal of the non-cross-linked species, while with S_2-lPEI_b the cross-linked species appear as distinct peak with a width of about 1 min (Figure 2.2A, 0 h). The main species (60 %) is still the linear polymer (M_n = 15 kDa, M_w = 18 kDa, *PDI* = 1.18), but a significant proportion of the parent polymer is cross-linked (M_n = 49 kDa, M_w = 57 kDa, *PDI* = 1.15). More specifically, about two-thirds of the initial linear polymer was cross-

linked at least twice to form a higher molecular weight species, with a narrower size distribution than the PEI with the highest cross-linker content (BC8-lPEI2.6) produced according to the previous synthesis method.

To test whether S_2-lPEI_b is efficiently cleaved under near physiological thiol concentrations, it was treated with 5 mM GSH. According to the observed steady decrease of the molecular weight (Figure 2.2A and B), S_2-lPEI_b is completely cleaved within the investigated time frame. Moreover, there is no evidence for the presence of an overstabilized species.

For the preparation of S_2-PLLs, the same synthesis method was used as for S_2-lPEIs, but the end products were purified with ultrafiltration instead of precipitation under strongly basic conditions in order to avoid amide hydrolysis.

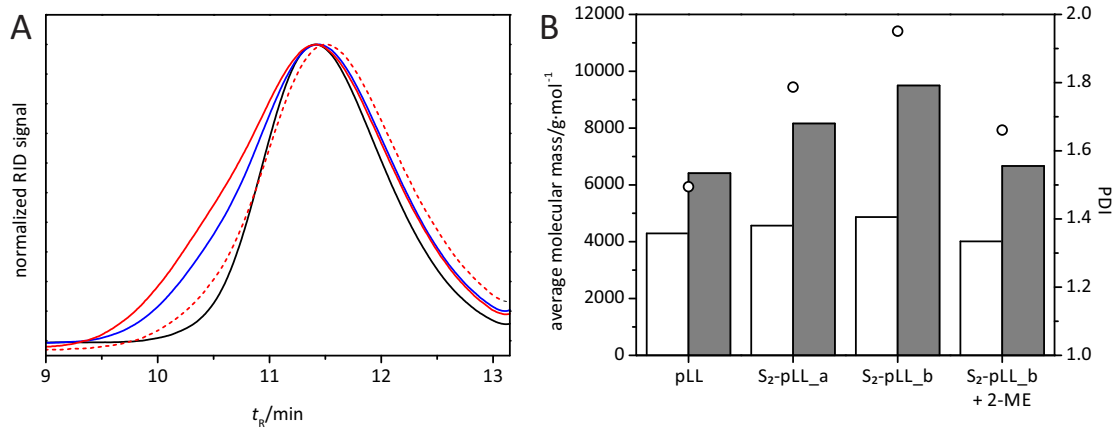

Figure 2.3: Results of the gel filtration chromatography of PLL, S_2-PLL_a, and S_2-PLL_b

A: PLL (black), S_2-PLL_a (blue), and S_2-PLL_b (red) were dissolved in PBS (γ_{final} = 1.43 g/L) and followed with gel filtration chromatography (normalized RID traces of the relevant retention time t_R window shown). A similarly concentrated sample of S_2-PLL_b in the presence of 100 mM 2-ME (red, dashed) was also examined. B: Corresponding number (M_n: white bars) and mass (M_w: gray bars) average molecular masses, and *PDI*s (○). (Experimental details Section 2.2.2)

Although S_2-PLL_a and S_2-PLL_b were synthesized at approximately the same cross-linker/linear polymer ratios used for S_2-lPEI_b and S_2-lPEI_a, respectively, neither a gelation nor a comparable molecular weight increase was seen (Figure 2.3A and B). Even at the highest cross-linking ratio, the size increase was modest at best (PLL: M_n = 4.3 kDa, M_w = 6.4 kDa, *PDI* = 1.49 vs S_2-PLL_b: M_n = 4.9 kDa, M_w = 9.5 kDa, *PDI* = 1.95). The absence of any meaningful higher molecular weight fraction indicates that PLL was predominantly cross-linked intramolecularly. In fact, intramolecular cross-linking must have been excessive, since some fraction of S_2-PLL_b is apparently not even cleaved in the presence of 100 mM 2-ME (Figure 2.3A red, dashed; $t_R \approx$ 10.4 min). The species belonging to that fraction are probably so compact, that the reductant is unable to fully penetrate the entangled polymer strands.

This excessive intramolecular cross-linking compared to S_2-lPEIs is very likely related to structural differences between the polymer classes. PLLs possess a high density of sterically unhin-

dered and highly mobile primary amines[67] and this may strongly increase the chances that both activated carboxylic group in (Boc-Cys-OH)$_2$ react with neighboring amines of the same polymer strand. Mädler et al. have used short model peptides to study the effects of neighboring amino acids on the reactivity of homobifunctional NHS esters.[68] They observed increased reactivities of the amino acid side chains towards NHS esters and the formation of intramolecular cross-links when two modifiable amino acids were in close proximity. They hypothesized that such cross-links are favored due to entropic effects and due to the high local concentration of the cross-linker. With peptides containing two lysines the tendency for the formation of intramolecular cross-links increased with increasing pH and reached 100 % at pH = 9.1.

Transfection efficacy, cell viability, and uptake quantity

Next, it was assessed if the differences in the polymers' structure and molecular weight distributions to the polymers from Lungwitz et al. were also reflected in the transfection properties. For that, the transfection efficacy, i.e., the percentage of cells with transgene expression, and cell viability were determined for DNA polyplexes based on the polyamines with the highest cross-linking ratio (S$_2$-lPEI_b and S$_2$-PLL_b) and their respective parent polymers (lPEI and PLL).

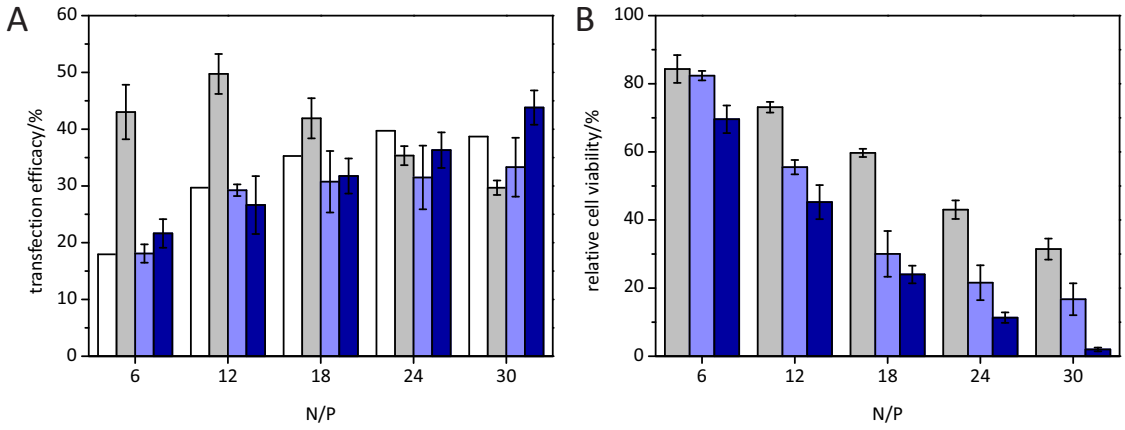

Figure 2.4: Transfection efficacy and relative cell viability for lPEI, S$_2$-lPEI_b, PLL and S$_2$-PLL_b / DNA polyplexes
CHO were incubated for four hours with polyplexes based on lPEI (white bars), S$_2$-lPEI (gray), PLL (light blue), and S$_2$-PLL (dark blue) and the EGFP encoding plasmid pEGFP-N1 (2 µg DNA per 38,000 cells, *n* = 3). After 24 h the percentage of EGFP positive cells served as measure for the transfection efficacy. Non-viable cells were identified through their PI uptake; the percentage of viable cells was a measure for the relative cell viability (B). Note the transfection efficacy of lPEI/DNA-polyplexes had been measured in an earlier, independent experiment and, therefore, no information on the standard deviation is available.[31] (Mean values ± sample standard deviation; experimental details Section 2.2.3)

Cross-linking lPEI to S$_2$-lPEI_b led to significantly increased transfection efficacies at low N/P ratios (Figure 2.4A, white and gray bars; N/P = 6 … 18). At N/P = 6, for instance, the biode-

gradable derivative demonstrated a 2.4-times higher efficacy than lPEI. The maximum transfection efficacy also increased and was shifted to lower N/P ratios (lPEI: N/P = 24, 40 % vs S_2-lPEI_b: N/P = 12, 50 %). This cannot be attributed to size differences between lPEI and S_2-lPEI_b polyplexes, as both polyamines formed polyplexes of approximately the same diameter with DNA under the conditions tested (see Chapter 4). Above N/P = 18 the transfection efficacy of the redox sensitive polyplexes dropped below that of lPEI-polyplexes and declined further. In contrast, the efficacy of lPEI-polyplexes plateaued at N/P = 24. A decreasing transfection efficacy at high N/P values has been ascribed to a metabolic inhibition by unbound polymer.[69]

S_2-lPEI_b's maximum transfection efficacy is significantly higher than those of bPEI 25 and lPEI 25 and, more importantly, S_2-lPEI_b is almost as efficacious as BC8-lPEI2.6 (about 58 % at N/P = 12), the derivative with the highest cross-linking ratio (8 %) from Lungwitz et al. This relatively high transfection efficacy, despite S_2-lPEI_b's lower cross-linking ratio, is in part certainly related to the relatively high molecular weight of the parent lPEI. The transfection efficacy of linear PEIs is known to increase with molecular weight.[58] Another factor adding to the transfection efficacy is the cross-linked polymer's size and size distribution. Lungwitz et al., for instance, were able to raise the transfection efficacy of BC8-lPEI2.6 from about 22 % to 37 % at low N/P ratios by using a higher molecular weight polymer fraction gained from size exclusion chromatography. At higher N/P ratios the effect was partially inversed. With S_2-lPEI_b on the other hand, no fractionation was required to obtain an efficacy of 43 %, likely due to its already higher percentage of cross-linked polymer strands and narrower molecular weight distribution.

S_2-lPEI_b turned out to be considerably more cytotoxic (Figure 2.4B, gray bars) than any of the cystine cross-linked lPEIs from Lungwitz et al. Cell viability decreased linearly from 84 % (N/P = 6) to 31 % (N/P = 30) making the polymer almost as toxic as bPEI 25 and lPEI 25. This rise in toxicity compared to the lPEI2.6 derivatives is probably related to the relatively high molecular weight of the parent polymer. Breunig et al. have demonstrated decreasing cell viability with increasing molecular weight for lPEIs larger than 4.6 kDa.[53]

Cross-linking PLL had no advantageous effect on the transfection efficacy, except at the highest N/P ratio (Figure 2.4A, light and dark blue bars). This lack of improvement is understandable when comparing PEI and PLL based carriers. Endolysosomal escape of the carrier is a major bottleneck for a successful transfection. Polycations like PEI possess a high buffering capacity at the acidic conditions found within the endolysosomal compartment which results in the osmotic rupture of vesicular membranes via the proton sponge mechanism (Section 5.1.2)[70]. In contrast, the ϵ-amino groups (pK_a = 9-10[71]) of polylysines are already completely protonated at neutral pH, thus these carriers have no efficient means for endosomal escape. Cross-

linking does not change the polymer's buffering range since the cystine cross-linker's pK_a lies is in a similar range.

Cross-linking further increased PLL's already substantial cytotoxicity (Figure 2.4B, light and dark blue bars). At the highest N/P ratio tested, essentially no viable cells remained. No similar increase was seen for S_2-lPEI_b (data not shown) and other cystine cross-linked lPEIs[31], where the toxicity was independent of the linker ratio.[31] The exact reason for the toxicity increase in S_2-PLL_b could not be deduced from the available data. It can be speculated, however, that it is related to different physicochemical characteristics of PLL and S_2-PLL_b/DNA polyplexes. In general, polycation cytotoxicity is the result of an interaction of charged polymer amines with cellular membranes.[72] High molecular weight PLL/DNA complexes are known to aggregate depending on the ionic strength of the surrounding medium.[42] When these aggregates reach the cell surface or endolysosomal vesicles, the very high local polyamine concentration may likely be significantly more damaging to cells than being in contact with regular polyplexes. In addition, the endolysosomal pathway where S_2-PLL_b likely accumulates, arguably contains no reductive capability (at least in the cell line tested here), so the polymer cannot be broken down into less harmful fragments.

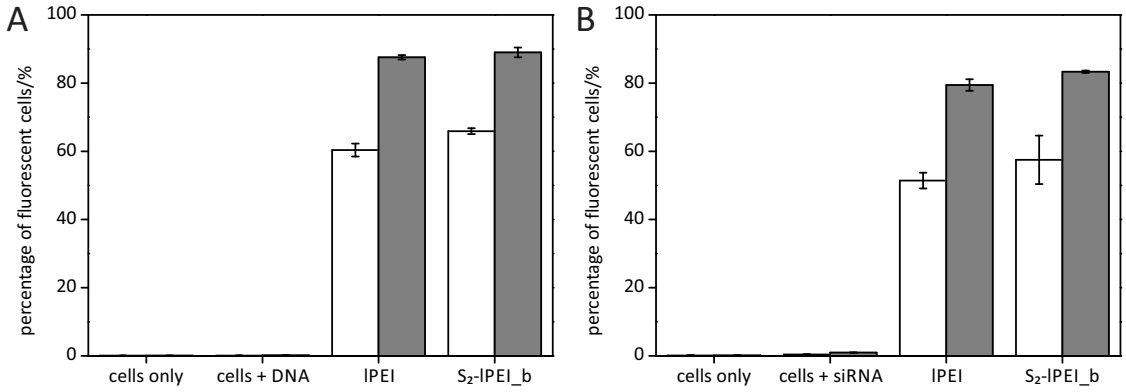

Figure 2.5: Cellular uptake efficacy of polyplexes based on linear and disulfide cross-linked PEI

CHO cells were incubated for one (white bars) or four hours (gray bars) with polyplexes based on YOYO-1 labeled pDNA (A) or fluorescent siGLO Green siRNA (B) and lPEI or S_2-lPEI_b (N/P = 8). The cellular fluorescence intensity was determined with flow cytometry (*n* = 3); living cells possessing an emission intensity above a threshold value set by the blank samples were considered as "transfected". The amount of transfected cells was normalized against the amount of all living cells (mean values ± corrected sample standard deviation). See also Figure 2.6. (Experimental details Section 2.2.3)

Due to their favorable transfection characteristics lPEI and S_2-lPEI_b based polyplexes were characterized in more detail regarding their cellular uptake efficacy, i.e., the percentage of cells with nucleic acid uptake. To this end, cells were incubated for one or four hours with polyplexes containing fluorescently labeled DNA (Figure 2.5A) or siRNA (Figure 2.5B). According to the data, the uptake efficacy depended on the type of delivered nucleic acid. A higher percentage of cells were transfected with DNA than with siRNA (e.g., S_2-lPEI_b polyplexes after

1 h: 66 % vs 57 %) but overall the differences were moderate, especially after four hours of incubation (89 % vs 83 %). The polymer structure had no noticeable effect on the transfection efficacy or the uptake rate. The differences between the linear and the cross-linked derivative were usually within the margin of error, regardless of the incubation time.

The delivery success cannot be evaluated from the uptake efficacy alone without considering the amount of internalized DNA or siRNA and the degree of endosomal escape, in fact, the latter appears to be rate-limiting for many nucleic acid delivery strategies.[73] For that reason, the extent of nucleic acid uptake was estimated based on the mean cellular fluorescence of transfected cells. The fluorescence intensity of lPEI/DNA and S_2-lPEI_b/DNA treated cells was almost identical; cross-linking apparently did not promote DNA delivery (Figure 2.6A). In contrast, S_2-lPEI_b/siRNA treated cells exhibited an emission intensity twice as high as cells treated with non-reduction sensitive polyplexes after four hours of incubation (Figure 2.6B, gray bars).

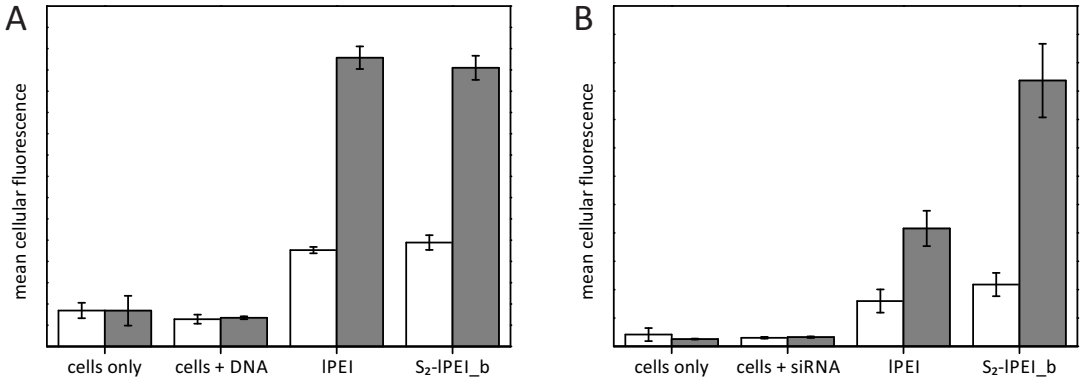

Figure 2.6: Estimation of the amount of internalized polyplexes based on linear and disulfide cross-linked PEI

CHO cells were incubated for one (white bars) or four hours (gray bars) with polyplexes based on YOYO-1 labeled pDNA (A) or fluorescent siGLO Green siRNA (B) and lPEI or S_2-lPEI_b (N/P = 8). The cellular fluorescence intensity was determined with flow cytometry (*n* = 3); living cells possessing an emission intensity above a threshold value set by the blank samples were considered as "transfected". The mean cellular fluorescence intensity of transfected cells (shown in the Figures) is an indirect measure for the amount of internalized polyplexes (geometric mean values ± corrected sample standard deviation). Note, the intensity values for the transfection with pDNA and siRNA are not comparable due to the different fluorescent dyes used. See also Figure 2.5. (Experimental details Section 2.2.3)

The most obvious explanation for this behavior, which has also been suggested by Breunig et al. for similar disulfide cross-linked PEIs[61], is an increased cellular uptake of S_2-lPEI_b/siRNA polyplexes. This begs the question, however, why the ratio between the internalized amount of lPEI/DNA and S_2-lPEI_b/DNA increases over the incubation period. At different but constant uptake rates (e.g., 10 unit/time vs 20 unit/time), the ratio would not change over time. Thus, either the uptake rates vary over time, which is unlikely or additional effects come into play. Seeing that S_2-lPEI_b apparently forms tighter complexes with siRNA than lPEI (Figure 4.3) and a fluorophore's emission if often quenched in the confinement of a polyplex (see Chapter 4), it

seems likely that the siRNA label is quenched to a greater extent in S_2-lPEI_b than in lPEI based complexes. Consequently, the siRNA amount delivered with S_2-lPEI_b is initially underestimated. After four hours, when the S_2-lPEI_b/siRNA polyplexes presumably have been unpacked, the fluorescence is restored and the mean cellular fluorescence intensity rises much faster than that of lPEI/siRNA treated cells. In principle, the validity of this hypothesis can be tested using static and time-resolved fluorescence techniques. An increased quenching of the fluorophores in S_2-lPEI_b/siRNA polyplexes would be apparent in a lower fluorescence lifetime τ and characteristic changes in the absorption and emission spectra (see Chapter 3 and 4). Unfortunately, the required measurements could not be carried out due to practical limitations. Judged alone from the properties of 5(6)-carboxyfluorescein (FAM; Section 3.3), the dye used for the siRNA labeling, quenching actually may not be that significant. Quenching is often the result of dye aggregation, which is driven by the hydrophobicity of the fluorophore. This is the reason why the relatively hydrophobic rhodamines are frequently prone to aggregate. In contrast, fluorescein derivatives are generally much more hydrophilic.

Differences in trafficking of both siRNA polyplexes could instead account for the observed differences in the fluorescence intensities. In contrast to the YOYO-1 dye used for DNA labeling, FAM is quite pH-sensitive and its emission intensity decreases substantially under acidic conditions (see Section 3.3 and Figure 3.14). There is also evidence that PEI is not capable of fully preventing endosomal acidification[74], so once the siRNA polyplexes reach the acidic endolysosomal compartment one would expect to see a decrease in the emission intensity. Again, the amount of internalized material is initially underestimated, but once the carrier reaches the slightly basic environment of the cytosol, probe fluorescence is restored. The different emission intensity time courses for lPEI/siRNA and S_2-lPEI_b/siRNA would then be the result of different endosomal escape rates. The polyplex variant with the highest escape rate would demonstrate the highest relative intensity increase. It has been suggested that longer PEI chains promote endosomal escape[75] and S_2-lPEI_b/siRNA indeed demonstrated the highest intensity increase here. It was also attempted to measure the escape rates of both polyplex variants more directly with flow cytometry but the data were inconclusive (see Chapter 5; data not shown). If S_2-lPEI_b/siRNA polyplexes indeed demonstrated a higher propensity for endosomal escape, this could be the result of an increased vesicular PEI accumulation or a higher buffering capacity in the presence of the disulfide cross-linker's relatively acidic amine group, which itself is the result of the disulfide's electron-withdrawing effect[36]. If and how the observed differences to lPEI/siRNA complexes are reflected in the gene silencing effect was not investigated. It must also be mentioned, that the DNA polyplexes tested could also experience different endosomal escape rates, but due to YOYO-1's pH-insensitivity this would not result in different intensity increases.

2.4 Conclusions

A previous attempt to cross-link lPEIs using a (Boc-Cys-OH)$_2$/DMTMM-based method resulted in products with a relatively broad molecular weight distribution and a low percentage of modified polymer strands.[31] Attempts to modify a larger proportion of the polymer resulted in the formation of insoluble gels.

Here it was demonstrated, however, that by carefully optimizing the synthesis parameters it is possible to attain products with a significantly narrower molecular weight distribution. Furthermore, significantly higher substation degrees could be achieved without the formation of gels even for parent lPEIs of relatively high molecular weight. In principle the new method can also be used for cross-linking other polyamines, but as demonstrated with PLL, the reduction sensitive products are not necessarily better suited for gene delivery. The cleavable PLL derivative was too inefficient and too toxic to be used as gene delivery agent. The lack of improved delivery properties seems to be related to the presence of highly mobile amines in the linear parent polymer.

The S_2-lPEI synthesized here, possesses a higher transfection efficacy at the lowest N/P ratio and at least a similar efficacy at higher N/P ratios than comparable cross-linked lPEIs[31], synthesized with the non-optimized procedure. Interestingly, the uptake efficacy for the delivery of siRNA and pDNA did not improve noticeable. The parent lPEI apparently already is relatively efficacious. Differences between the linear and cross-linked polymer were, however, seen in the amount of internalized nucleic acids. Cross-linking improved siRNA, but not pDNA internalization, which seems to confirm earlier reports that cellular uptake is only limiting for siRNA delivery.[30, 61] Upon closer inspection, the data can also be interpreted as evidence that S_2-lPEIs improve endosomal escape and may offer an additional explanation for the reportedly[61] superior gene silencing efficiency of reduction sensitive lPEIs.

3 Labeling of polycations

3.1 Fluorescence in bioanalytical applications

Fluorescence spectroscopy and time-resolved fluorescence techniques are considered to be among the most versatile tools in life sciences and neighboring fields of research. Methods like fluorescence microscopy, flow cytometry, or DNA microarrays are routinely used for diagnostic and research purposes in laboratories world-wide.[76, 77]

Fluorescence-based methods have largely replaced radioactive assays in the last three decades due to their many advantages. Fluorophores, i.e., organic molecules with high fluorescence efficiency, are much easier and safer to handle than radioactive tracers[76] and can be detected with very high sensitivity (up to single molecules[78]). Different fluorophores are easily detected simultaneously.[76, 77] Fluorescent probes can also provide information on the local environment of the (bio-)molecules of interest.[77] Fluorescence quenching[79] (see Chapter 4) or Förster resonance energy transfer (FRET)[80, 81], for example, help to elucidate the interaction between ligands and receptors. Yet, in light of the multitude of possible assays it is often forgotten that the introduction of fluorescent probes ("labeling") must be performed with care as it can alter the function of the labeled species or the fluorophore itself.

One frequently encountered problem is the concentration dependent change of the fluorophore's nature.[82] High local dye concentrations can lead to the formation of aggregates with altered absorption and emission characteristics. In such cases the relation between absorption intensity and dye concentration no longer obeys Beer's law (positive and negative deviations are known).[82-84] In addition, the presence of aggregates also interferes with methods like FRET, which rely on the well-defined spectral overlap of two fluorescent species. In fact, fluorescence intensity changes or changes of the fluorescence lifetime cannot be interpreted reliably without knowledge of the corresponding emission spectra.[84]

3.2 Basic principles of photoluminescence

Molecules and atoms are excited to higher energy states through the interaction with electromagnetic fields, i.e., photons. The excitation energy is afterwards released in a nonradiative

process or through photoluminescence. The mechanism of luminescence depends on the nature of the excited electronic state. Light is emitted either through fluorescence or phosphorescence (Figure 3.5). Prerequisite for both is the presence of a chromophore, i.e., a moiety capable of absorbing electromagnetic radiation of a specific wavelength range. For organic chromophores, the lower wavelength limit of absorption lies around 200 nm. Below that, the photon energy exceeds the dissociation energy of most chemical bonds, leading to photochemical decomposition. The upper wavelength limit lies in the near-infrared region ($\lambda_{abs\ max}$ = 1.0-1.2 µm).[85] The chemical stability of molecules absorbing at wavelengths beyond that limit is reduced, as low lying excited triplet states drastically increase the probability for the formation of highly reactive biradicals.

3.2.1 Light absorption of dyes

Molecular structure

The interaction between organic compounds and light (mostly) depends on the electronic structure of the molecule and the excitation wavelength. Stronger chemical bonds require higher photon energies to be excited.

In saturated compounds all bonds are formed by σ-electrons. Their wave function has a rotational symmetry in respect to the bond direction. This creates a significant orbital overlap, making σ-bonds relatively strong. The electronic excitation of σ-bonds requires photon energies above 7.8 eV (λ_{ex} < 160 nm)[86], which is high enough to ionize the molecule. Unsaturated compounds additionally contain π-bonds, whose wave functions are characterized by nodes located at the nuclei (Figure 3.1). The presence of these nodes reduces the orbital overlap, thus, π-bonds are weaker than σ-bonds. In molecules where π-electrons are delocalized in a system of alternating double bonds, bond strength is reduced even further. Such molecules are able to absorb light at wavelengths above 200 nm, where only the lowest energy transitions (n → π*, π → π*) are possible.[86]

Light absorption

In molecules with conjugated double bonds, the symmetry axes of the π-orbitals are arranged in parallel, ensuring maximal orbital overlap; the π-electrons form a “cloud” above and below the chain of atoms. The rotation around σ-bonds is restricted, giving the molecule a more rigid and planar structure. The quantum-mechanical background of light absorption can be described on a semiquantitative basis by the free electron gas model.[87, 88] This highly simplified

model ("particle in a box") assumes that π-electrons are non-interacting and move freely along a chain of alternating double bonds. The potential energy within the system is constant, but rises to infinity at both chain ends (potential well). Each electron's wave function is found by solving the Schrödinger equation for this system. The eigenfunctions ψ_n (further referred to as orbitals) are the wave functions allowed inside the imaginary box. Their corresponding eigenvalues E_n show that the electrons can only have certain discrete energies:[89]

$$\psi_n = \left(\frac{2}{L}\right)^{\frac{1}{2}} \sin\left(\frac{n\pi x}{L}\right) \text{ for } 0 \leq x \leq L \tag{3.1}$$

$$E_n = \frac{n^2 h^2}{8mL^2} \tag{3.2}$$

Where n is the quantum number, which numbers the allowed electron states of the system (i.e., number of antinodes of the eigenfunction), L is the length of the conjugated electron chain, extending about one bond length beyond each chain end, m is the electron mass, h is Planck's constant and x is the electron's position along the molecular backbone.

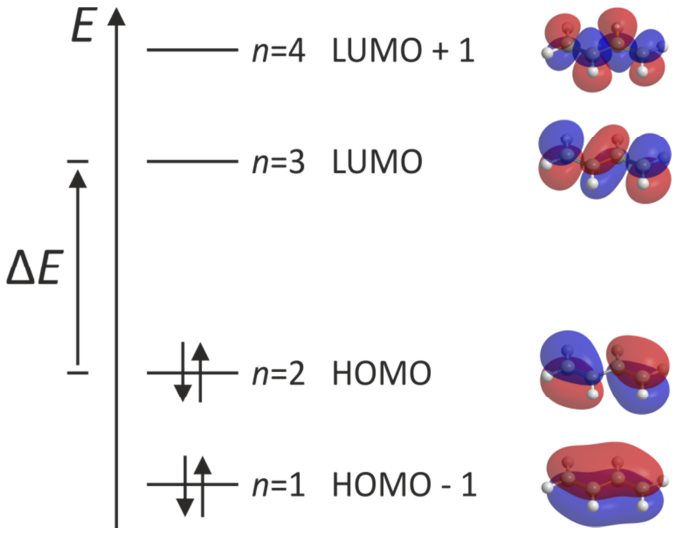

Figure 3.1: Energy level diagram of the π molecular orbitals of *s-trans* 1,3-butadiene

Each molecular orbital has an energy proportional to its quantum number and can be populated by two electrons with opposite spins (Pauli exclusion principle). In the ground state only the lowest two orbitals are filled (n = 1, 2). Light absorption can promote an electron from the highest occupied molecular orbital (HOMO, π) to the lowest (or higher) unoccupied molecular orbital (LUMO, π*). The photon's energy corresponds to the "energy gap" ΔE between HOMO and LUMO. The wave function for each orbital is shown on the right hand side.

According to Pauli's exclusion principle, each molecular orbital or energy level is populated by at most two electrons that differ in their spin quantum number ("spin up or down"). Thus, in the ground state of a four π-electron (N = 4) system like 1,3-butadiene, the two lowest energy levels (n = 2) are occupied. All other states are empty (Figure 3.1). The energy difference ΔE

between the highest occupied molecular orbital (HOMO) and the lowest unoccupied molecular orbital (LUMO; n = 3) is given by the following expression:

$$\Delta E = E_{\mathrm{LUMO}} - E_{\mathrm{HOMO}} = \frac{h^2}{8mL^2}(N+1) \tag{3.3}$$

To allow for an electronic transition from the HOMO to the first excited state, the molecule has to absorb a photon of corresponding energy ($\Delta E = E_{h\cdot\nu}$). The wavelength λ of the absorbed photon (3.5) is given by the previous equation in combination with the Planck relation (3.4):

$$E_{h\nu} = h\nu = \frac{hc_0}{\lambda} \tag{3.4}$$

$$\lambda = \frac{8mc_0}{h} \cdot \frac{L^2}{N+1} \tag{3.5}$$

Where c_0 is the speed of light in vacuum, ν is the frequency of the absorbed photon.

This very simple model allows to approximate the location of the intense main absorption band, especially in case of symmetric, linear dyes like cyanines, with relatively high accuracy.[85] Generally, the absorption intensity depends on the probability or transition strength for a particular transition. In the classical model, a molecule is an arrangement of positive and negative charges acting as oscillating dipole. The dipole interacts with radiation of a given frequency ν_i when it at least temporarily oscillates at similar frequency.[90] The interaction intensity is known as oscillator strength f_i and is related to the absorption intensity. In fully allowed transitions f_i is exactly one:

$$f = 4.32 \times 10^{-9} \int_{\text{absorption band}} \varepsilon(\tilde{\nu})\,\mathrm{d}\,\tilde{\nu} \tag{3.6}$$

Where $\tilde{\nu}$ is the wave number and ε is the molar absorption coefficient.[85]

From a quantum mechanical perspective a molecule undergoes a transition between the initial (ground) state G and the final (excited) state E through coupling of the electromagnetic field to the transition dipole moment μ_{GE}:

$$\mu_{\mathrm{GE}} = \int \psi_{\mathrm{E}}^{*} \hat{\mu} \psi_{\mathrm{G}}\,\mathrm{d}\tau \tag{3.7}$$

Where ψ_{E}* and ψ_{G} are the wave functions for the excited and ground state, $\hat{\mu}$ is the dipole moment operator and τ represents the volume element.[90]

Transitions are allowed if μ_{GE} is nonzero, which is the case when ground and excited state have different symmetries. For most transitions, the transition dipole moment's vector components

are unequal and, therefore, the electronic transition has a defined orientation or polarization. The oscillator strength is proportional to the absolute value of μ_{GE} squared.

Electronic energy levels

In contrast to atomic spectra, organic compounds have very broad absorbance and emission bands, ranging over several tens of nanometers, as many individual transitions with slightly different transition probabilities and energies are superimposed. This is mostly due to the coupling of electronic to vibrational transitions (Figure 3.2, right). Organic fluorophores often consist of dozens of atoms, allowing a multitude of vibrations over the molecular skeleton. In solution these vibrational sublevels are broadened through collisions and electrostatic perturbations caused by solvent molecules. An additional broadening is attributed to the coupling to extremely broad rotational transitions. Consequently, the spectrum's vibrational fine structure (Figure 3.2, left) is lost in the quasicontinuum of overlapping states and cannot be resolved, except in gas phase measurements or when dyes are dispersed in organic glass at very low temperatures.[85]

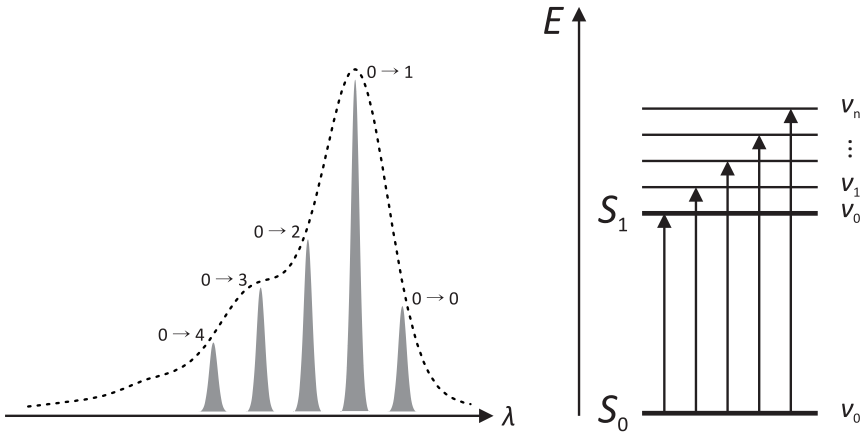

Figure 3.2: Electronic and vibrational energy levels of an organic dye molecule

Right: At room temperature an organic dye absorbs light in its electronic (S_0) and vibrational (v_0) ground state (vibrational levels of S_0 not shown) and reaches one of the vibrational sublevels (v_i) of the first excited electronic state (S_1). Each of those sublevels is shifted to higher or lower energies through the interaction with solvent molecules; molecular rotations further broaden these energy levels (not shown for the sake of clarity). Left: As consequence, individual transitions (black absorption lines) are no longer discernible in the quasicontinuum of overlapping states (dashed: typical absorption spectrum of an organic dye in solution) except under special measurement conditions. The numbers refer to the vibrational energy levels.

At room temperature, the thermal energy kT corresponds to 207 cm^{-1}, which is far too low to populate higher electronic or vibrational states. Thus, transitions to higher excited electronic states start from an excited rotational level of the electronic and vibrational ground state (S_0v_0). To reach an excited electronic or vibrational state from the ground state, typically ener-

gies in the range of 10^4 cm^{-1} or 500–4000 cm^{-1}, respectively, are required. In contrast, reaching rotational sublevels only requires 1–100 cm^{-1}.

Franck–Condon principle

The shape of an absorption (and emission) spectrum is determined by the intensity of the individual vibrational transitions (Figure 3.2), i.e., how likely a particular vibronic transition is. To predict a specific transition probability, the potential energy of a molecule has to be considered as a function of the internuclear distance (Figure 3.3). An anharmonic potential like a Morse potential gives a good approximation for a molecule's vibrational structure. Generally, excited electronic states possess a spatially more extended and diffuse electron distribution, here indicated by a broader potential curve (S_1). Each electronic state contains a finite number of bound vibrational energy levels (v_i … v_{max}). The energetic distance between neighboring vibrational energy levels decreases with the potential energy approaching the dissociation energy. The potential barrier defines the turning points for the nuclei's oscillation. Upon absorption, an electron is promoted from S_0v_0 to one of the higher vibrational sublevels of the first or one of the higher excited electronic states (S_nv_n).

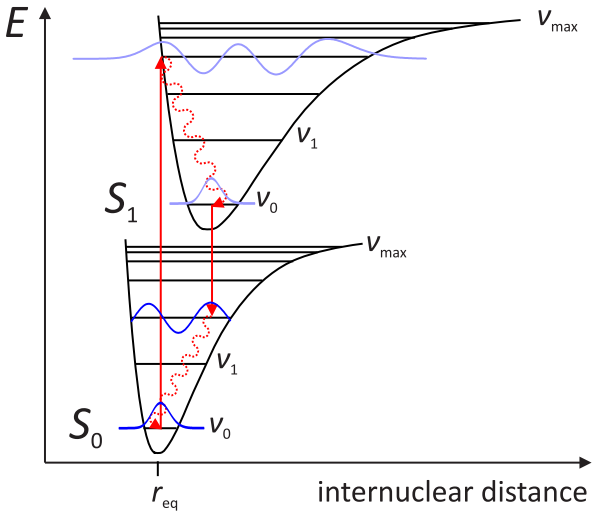

Figure 3.3: Franck-Condon principle

The potential energy of a molecule is best described by an anharmonic potential that is different for each electronic energy level (here: S_0, S_1; higher electronic states are not depicted). There is a finite number of excited vibrational states above the vibrational ground level (v_0 … v_{max}). During absorption (red upward arrow) the most likely transition (vertical transition) is the one where both vibrational wave functions involved (dark and light blue) have the highest overlap (S_0v_0 → S_1v_n). The molecule is now in a short-lived, nonequilibrium state (Franck-Condon state). At that point, the nuclei did not yet have time to adapt to the change in the local electrostatic potential (Born–Oppenheimer approximation). After losing their excess vibrational energy through collisions with surrounding solvent molecules (red wavy arrow) the molecule is in the vibrational ground state of the first excited electronic state (S_1v_0). In most cases fluorescence will take place from this state (Kasha's rule; red downward arrow) and one of the higher vibrational states of the electronic ground level is reached. Eventually the molecule returns to S_0v_0.

This transition changes the local electron density, i.e., electrostatic potential, and forces the nuclei to assume new positions, eventually. However, since nuclei are several magnitudes heavier than electrons, they essentially remain fixed in their prior equilibrium configuration during the timescale of the transition (Born–Oppenheimer approximation).[91] According to the Franck-Condon principle, the most likely transition (vertical transition) is the one in which the nuclei change their positions least (Figure 3.3, red upward arrow).[92, 93] More precisely, the transition probability (intensity) is proportional to the square of the overlap of both vibrational wave functions involved.

After the transition, the molecule is in a very short-lived nonequilibrium, Franck-Condon state. In a process called solvent or vibrational relaxation, the molecule releases its excess vibrational energy within the order of 10^{-12} s through collisions with surrounding solvent molecules (Figure 3.3, wavy arrows) and reaches the thermal equilibrium at the lowest vibrational level of an excited electronic state ($S_n v_0$). From that level the molecule very quickly relaxes further to the lowest vibrational level of the first excited electronic state ($S_1 v_0$).

3.2.2 Light emission

Since the process of fluorescence (10^{-8} s) takes far longer than the relaxation processes outlined above, the molecule is in the thermal equilibrium of the first excited state before it is able to return to the ground state under the emission of light (Figure 3.3, red downward arrow). That means that even if the molecule was excited to higher excited electronic states, fluorescence with appreciable yield will only take place from $S_1 v_0$ (Kasha's rule).[94] This also means that the emission wavelength is independent from the excitation wavelength.

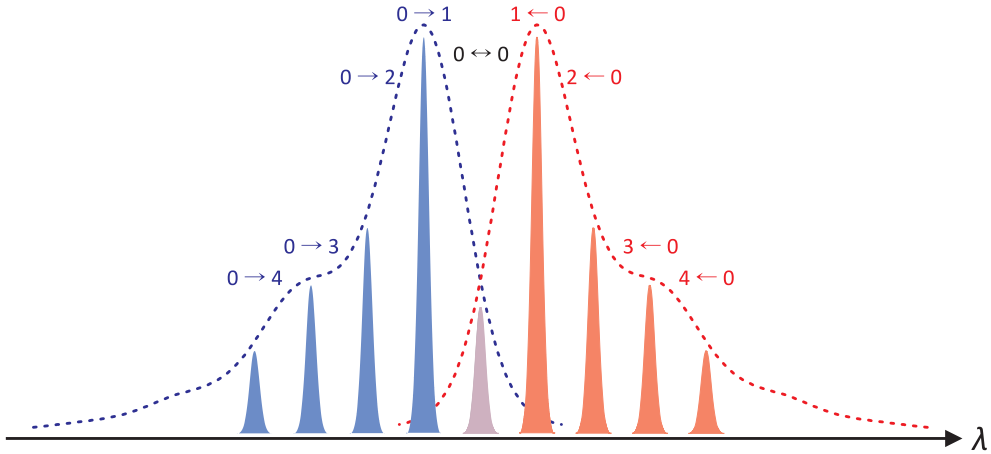

Figure 3.4: Vibrational structure of the absorption and fluorescence spectrum of a typical organic dye

The $S_0 \rightarrow S_1$ absorption spectrum is typically a mirror image of the fluorescence spectrum. This is due to the fact that the spacing of the vibrational energy levels is similar in S_0 and S_1. The wavelength of the emission maximum is red-shifted compared to the corresponding absorption band (Stokes shift) due to the loss of vibrational energy. The numbers designate the vibrational energy level of S_0 and S_1.

A fluorescence spectrum is generally the bathochromically shifted (Stokes shift) mirror image of the corresponding $S_0 \rightarrow S_1$ transition. This is another consequence of the Franck-Condon principle: Since nuclear geometries are hardly altered during electronic transitions, the spacing between vibrational sublevels, in other words the spectrum's vibrational structure or shape, is preserved from the ground state (Figure 3.4).[76] The Stokes shift is mainly the result of energy dissipation through solvent relaxation. In certain cases, solvent effects and energy transfers etc. further increase the bathochromic shift.

Deactivation of excited states

Besides the absorption and emission processes outlined above, a molecule can undergo a number of other transitions. A Jablonski diagram (Figure 3.5) summarizes possible energy states and the transitions between them. A molecule in an excited singlet state S_n (antiparallel electron spins: $\uparrow\downarrow$) can interact with additional photons and be promoted to higher singlet states (e.g., $S_1 \rightarrow S_2$). Those states are short-lived and are quickly relaxed and depopulated through nonradiative processes (internal conversion, vibrational relaxation). The vibrational ground state of the first excited electronic state itself is depopulated either through radiation (fluorescence) or internal conversion, followed by vibrational relaxation back to S_0v_0. As a general rule, the more flexible and mobile (vibration, rotation) a molecular skeleton is, the less excitation energy is released as radiation. In addition to molecular flexibility, coupling to hydrogen vibrations and reversible charge transfers between electron donating and electron withdrawing groups can further increase the rate for internal conversion.

A molecule can also exist in other electronic states than singlet states. For each singlet state there is a corresponding triplet state of lower energy. Triplet states are reached through intersystem crossing (ISC). ISC very inefficient in most organic molecules, as it involves the classically forbidden spin reversal of an electron.[88] Heavy atom substituents can increase the ISC rate through spin-orbit coupling. The molecule returns from triplet states to the ground state, either through a radiative (phosphorescence) or nonradiative process. As both mechanisms involve another forbidden singlet-triplet transition, triplet states possess considerably longer lifetimes than singlet states (usually microseconds to seconds). The long lifetimes, combined with the fact that molecules in excited states are more reactive than in the ground state, increase the probability for intermolecular reactions that lead to the destruction of fluorophores (photobleaching).

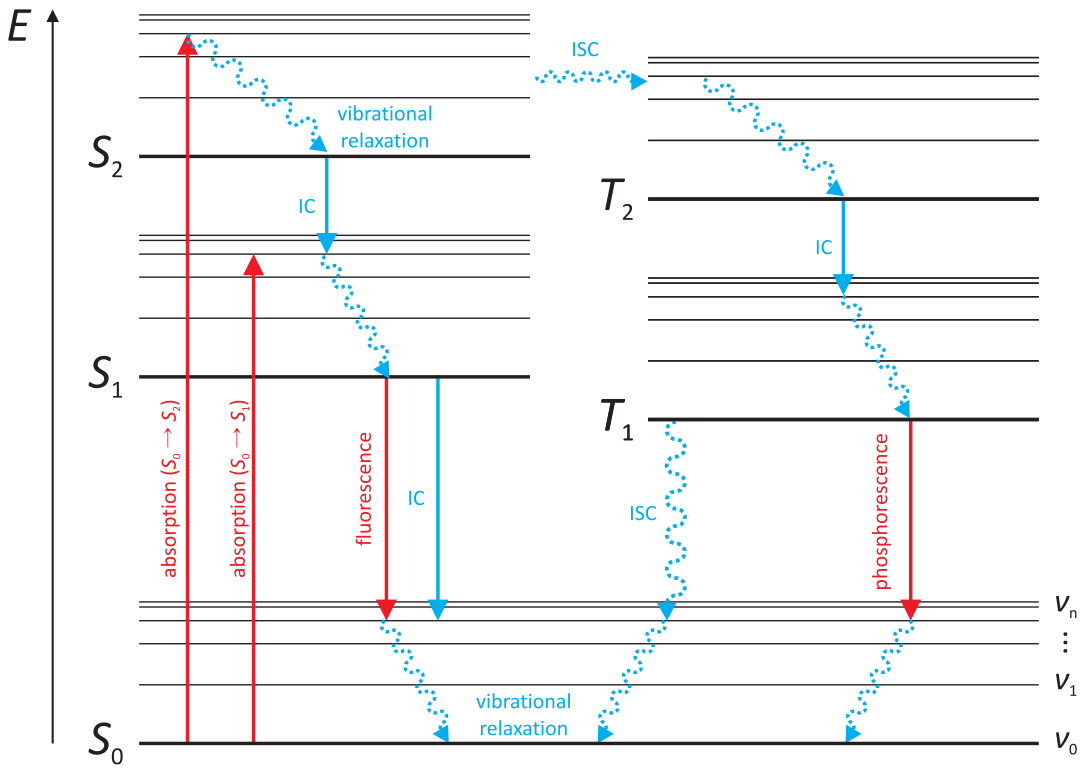

Figure 3.5: Jablonski diagram

A Jablonski diagram offers a simplified overview over the electronic and vibrational transitions of a molecule: Radiative and nonradiative transitions are colored red and blue, respectively. Thick lines: Vibrational ground states (v_0),. Thinner lines: higher vibrational levels (v_{0+n}). S_n: singlet state, T_n: triplet state. IC: internal conversion, ISC: intersystem crossing. Typical lifetimes are: $S_1 \rightarrow S_0$ 1-10 ns, $T_1 \rightarrow S_0$ milliseconds to seconds, IC 1 ps. Effects like singlet-singlet and triplet-triplet absorptions are omitted for clarity.

Quantum yield and lifetime

Fluorescence quantum yield and lifetime are the most important characteristics of fluorophores. The quantum yield Φ_f is defined as the ratio between the number of absorbed and emitted photons. From a quantum mechanical perspective there is always a finite probability for light absorption and emission, so Φ_f can never exactly be equal to zero. Likewise, Φ_f cannot be equal to exactly one.[88] The value of Φ_f depends on the rate constants for the radiative transition (k_r) and all other competing, nonradiative transitions (k_{nr}):

$$\Phi_f = \frac{k_r}{k_r + k_{nr}} \tag{3.8}$$

k_{nr} includes all nonradiative processes:

$$k_{nr} = k_{IC} + k_{ISC} + k_Q \tag{3.9}$$

Where k_{IC}, k_{ISC} and, k_Q are the rate constants for internal conversion, intersystem crossing, and quenching (see Chapter 4), respectively.

The constants k_r and k_{nr} are related to the measured lifetime τ, the average time a molecule stays in the excited state:

$$\tau = \frac{1}{k_r + k_{nr}} \tag{3.10}$$

The natural lifetime τ_n is the lifetime in absence of nonradiative deactivation processes (k_{nr} = 0). It can be derived from the absorption spectrum, extinction coefficient, and emission spectrum.[95]

$$\tau_n = \frac{1}{k_r} \tag{3.11}$$

Absolute quantum yields are difficult to determine experimentally. Instead, they are often calculated in relation to τ and τ_n:

$$\Phi_f = \frac{\tau}{\tau_n} \tag{3.12}$$

Most commercial fluorescence dyes used for bioanalytical applications have quantum yields close to one and lifetimes in the range of several nanoseconds.

Fluorophore dimers

Changes in fluorescence quantum yields often originate from the reversible formation of fluorophore dimers or higher aggregates. The spectroscopic properties of such aggregates are described by the molecular exciton model,[96] which applies to cases where the electron overlap of the constituent molecules is small, i.e., the chromophores retain their individuality. The excited states of fluorophores in aggregates are no longer degenerate since the interaction of their transition dipoles leads to exciton splitting. The extent of the exciton splitting can be calculated as follows:

Two fluorophores in close proximity of each other experience the van der Waals interaction energy E_{vdW}. It slightly lowers the ground state energy level E_G compared to that of non-interacting fluorophores. E_G is the sum of the ground state energies (E_{M1} and E_{M2}) of the isolated monomers and E_{vdW} (Figure 3.6):[96]

$$E_G = E_{M1} + E_{M2} + E_{vdW} \tag{3.13}$$

The dimer's excited state energy E_E is derived similarly. For cases where two identical monomers are involved in the dimer formation, two solutions exist:

$$E_E = E_M + E_M^* + E_{vdW}^* \pm \mathcal{E} \tag{3.14}$$

Where the asterisk refers to the excited state and $\mathcal{E}$ is the exciton splitting term. The latter represents the interaction energy from the exchange of excitation energy between the monomers.

The energy difference between ground and excited state gives the characteristic form of the transition energy in aggregates:[96]

$$\Delta E_{EG} = \Delta E_M + \Delta E_{vdW} \pm \mathcal{E} \tag{3.15}$$

The dimer's excited singlet state energy level is split into two non-degenerate energy levels, $S_{1'}$ and $S_{1''}$. The energy difference $\Delta\mathcal{E}$ between the two new energy levels depends on the transition moment μ_{EG} for the (singlet-singlet) monomer transition and on geometric considerations. For a dimer with coplanar inclined transition dipoles (Figure 3.6) $\Delta\mathcal{E}$ is calculated according to:[96]

$$\Delta\mathcal{E} = \frac{2|\mu_{EG}|^2}{r_{M1M2}^3}(1 + 3\cos^2\vartheta) \tag{3.16}$$

Where r^3_{M1M2} is the center to center distance and ϑ is the angle between the polarization axes of the monomers.

Depending on ϑ, dimers are classified as J- ($0° \leq \vartheta < 54.7°$) or H-aggregates ($54.7° < \vartheta \leq 90°$). Maximum resonance splitting occurs at an angle of 0° and 90°; at 54.7° (arcos 1/√3) $\Delta\mathcal{E}$ is zero and there is no intermonomeric dipol-dipol interaction. Forbidden (singlet-triplet) transitions have a negligible resonance splitting due to their small oscillation strengths. The transition moments for allowed transitions to the upper and the lower excitonic level are calculated according to:

$$\mu_{S_{1'}G} = \sqrt{2\mu_{EG}\cos\vartheta} \text{ and } \mu_{S_{1''}G} = \sqrt{2\mu_{EG}\sin\vartheta} \tag{3.17}$$

The corresponding oscillation strengths are given by (see 3.2.1):

$$f_{S_{1'}G} = \left|\mu_{S_{1'}G}\right|^2 = \left|\sqrt{2\mu_{EG}\cos\vartheta}\right|^2 \text{ and } f_{S_{1''}G} = \left|\mu_{S_{1''}G}\right|^2 = \left|\sqrt{2\mu_{EG}\sin\vartheta}\right|^2 \tag{3.18}$$

J-aggregates, or Scheibe-type aggregates, have independently been discovered by G. Scheibe and E. E. Jelley in the 1930s.[97-99] In ideal J-dimers, the monomers have a head-to-tail arrangement with in-line transition dipoles ($\vartheta = 0°$; Figure 3.6). Accordingly, the transition to the

higher exciton state is forbidden ($f_{S1''G}$ = 0), while the population (and depopulation) of the lower state is strongly allowed ($f_{S1'G} = 2 \cdot f_M$). For that reason, the quantum yields of J-aggregates often surpass those of their parent monomers.[86] J-dimers can be identified through their strong red-shifted absorption band, next to the monomer transition.

In contrast, H-aggregates ($\vartheta = 90°$) are characterized by very low fluorescence intensities and hypsochromically shifted absorption bands, because only the transition to the higher exciton state is allowed. The lower exciton state is populated through internal conversion from the upper exciton level almost immediately after excitation. Since the radiative transition from there to the ground state is forbidden, the molecule remains in an excited state for a significant amount of time, which makes it highly susceptible to nonradiative relaxation processes such as quenching and intersystem crossing.

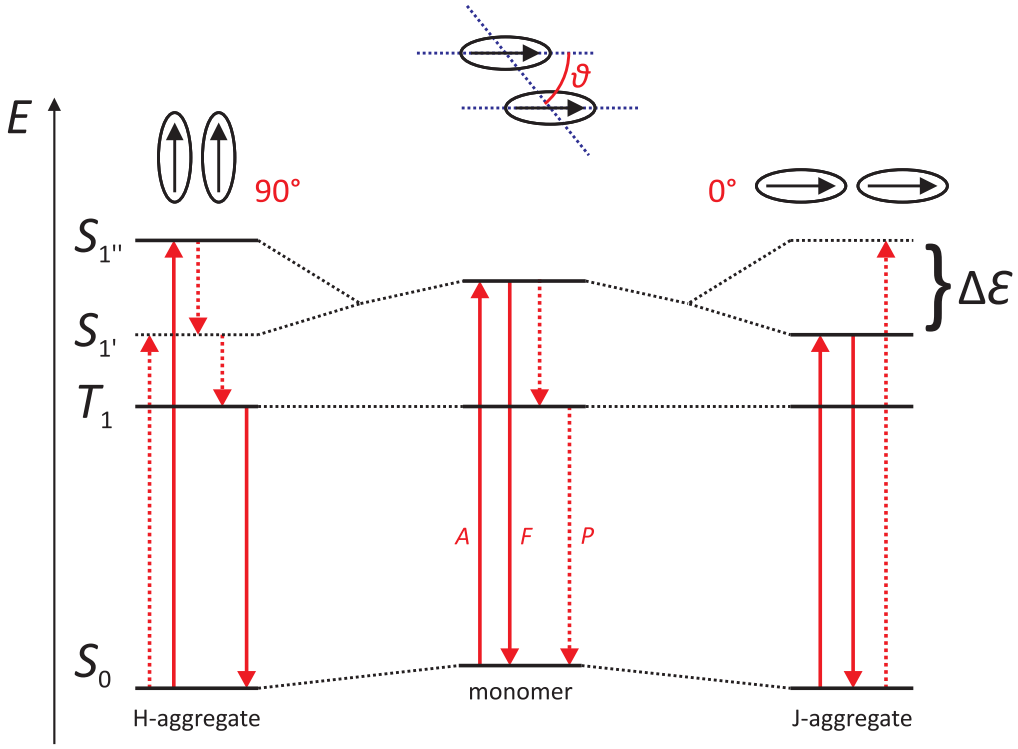

Figure 3.6: Electronic transitions in monomers and dimers with coplanar inclined transition dipoles

During dimer formation, the van der Waals interaction energy lowers the ground state energy level. The interaction of the transition dipoles causes an exciton splitting ($\Delta\varepsilon$) of the excited electronic states. Now two transitions (to and from $S_{1'}$ and $S_{1''}$) are possible. Their transition moments depend on the angle ϑ between the monomers' polarization axes. In J-aggregates only the lower exciton level is (efficiently) populated. Return to the ground state is strongly allowed and the dimers are highly fluorescent. H-aggregates often show very weak fluorescence as the triplet state is efficiently populated through intersystem crossing. Dashed arrows indicate internal conversion and forbidden processes.

The dimerization process is an interplay between dispersion forces, that tend to bring the monomers together in a position where the interaction energy is highest, and the repulsive Coulomb force if the molecules are charged.[85] The tendency to dimerize increases in solvents

with high dielectric constants (e.g., water) where the Coulomb repulsion is efficiently lowered. In many cases dimerization is dominated by hydrophobic interactions, i.e., the formation of a shell of polar solvent molecules around nonpolar residues. With decreasing dye polarity, the aggregation tendency increases in polar solvents.[88]

Dye aggregation, especially H-aggregation, can be a serious issue in applications where the use of water as solvent would be beneficial (e.g., as lasing medium[88]) or cannot be avoided (e.g., in cell biology). This particularly applies to many popular rhodamine derivatives[100]: An aqueous rhodamine 6G solution, for instance, cannot be used as lasing medium, as H-aggregation is observed at dye concentrations as low as 1 µM.[101] With increasing dye concentration, more and more aggregates form and efficiently prevent lasing at 100 µM.[88] There are other examples, however, where the aggregates' altered photophysical properties allowed the development of new analytical methods. Ogawa et al. have recently demonstrated the use of tetramethylrhodamine H-dimers for in vivo optical molecular imaging.[102] They attached tetramethylrhodamine (TAMRA) to the antibody trastuzumab and at sufficiently high labeling densities the dye's fluorescence was partly quenched. After uptake in cancer cells, the probe's fluorescence was restored probably as a result of the dimer destabilization following the antibody's denaturation in endosomes. The dye-antibody conjugate was used to visualize tumors in mice. Similar dequenching assays have been used to follow the cleavage of polypeptides by proteases.[103]

3.3 Fluorophores used for polycation labeling

To this day hundreds of different fluorescent probes have been developed and made commercially available. Great care must be taken to select the suitable dye for a particular experiment. In general, it is advisable to use dyes with well-defined spectra, high quantum yield, and high photostability. For in vitro and in vivo experiments, smaller fluorophores should be preferred to avoid interference with biological function. Moreover, the dye's excitation and emission wavelengths need to be greater than about 350 nm or the spectral overlap with aromatic amino acids, nucleobases or other intrinsic fluorophores, will lower the measurement sensitivity[104]. The available technical equipment (filter sets, light sources …) also needs to be taken into consideration. Depending on the particular analytical question, "passive" and "active" probes can be used. The spectral characteristics of passive probes are (largely) independent of the environment, while active probes respond to the presence of certain ions, enzymes, or changes in pH etc.

In the course of this work three representative fluorophores were chosen for the labeling and subsequent characterization of PEI and PLL derivatives and their respective complexes with nucleic acids. The xanthene dye fluorescein (FAM) served as model to establish the labeling procedure. Its well-known, partially pH-dependent, properties facilitated the characterization of the labeled product. Based on these first results, the polycations were labeled with tetramethylrhodamine (TAMRA). TAMRA possesses spectroscopic properties that are largely independent of pH and redox conditions. TAMRA-PEIs were meant as emission intensity reference in experiments with BP_2-labeled polymers. TAMRA-PEIs also helped to elucidate the interaction between polycations and nucleic acids in polyplexes (see Chapter 4). One of the main focuses of this work was to investigate the cleavage of reduction sensitive, disulfide containing polymers for gene delivery. To this end, various PEI and PLL derivatives were labeled with the reduction sensitive dye BODIPY® FL L-cystine (BP_2). BP_2 itself is non-fluorescent, but becomes highly fluorescent in the presence of thiols. This increase in fluorescence intensity permitted to study the intracellular processing of polyplexes, and the relationship between polymer cleavage and polyplex disintegration.

5(6)-Carboxyfluorescein

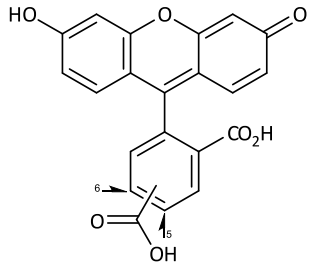

Figure 3.7: Structure of fluorescein derivative used
5(6)-carboxyfluorescein (FAM), *M* = 376.32 g/mol

Fluorescein is the first xanthene dye ever synthesized. It was discovered by Adolf Baeyer in 1871.[105] Today, fluoresceins are, in part due to economic reasons and because of their wide availability, among the most popular and most often used fluorescent dyes.[106] The amine reactive derivative fluorescein isothiocyanate (FITC) is the most common reagent for covalent protein and peptide labeling, particularly for the preparation of immunoreagents. FITC-oligonucleotide conjugates routinely serve as hybridization probes.[77] Only very recently Dam et al. have reported on the use of the tumor-specific probe FITC-folate for intraoperative, real-time visualization of tumor tissue. In this first in-human proof-of-principle, they were able to identify and remove ovarian cancer deposits directly during surgery.[107]

Although numerous alternatives to fluorescein exist today, its persistent popularity originates from the combination of many advantageous properties (e.g., high ε and Φ_f under certain

conditions) at a relatively low price. The dye's fair water solubility is beneficial in bioanalytical applications and it can act as FRET-donor for TAMRA (R_0(FAM-TAMRA) = 55 Å).[77] Fluorescein's main disadvantages are its low photostability, specifically in the presence of oxygen, and its broad emission spectrum, which makes it less suitable for multicolor applications.[77]

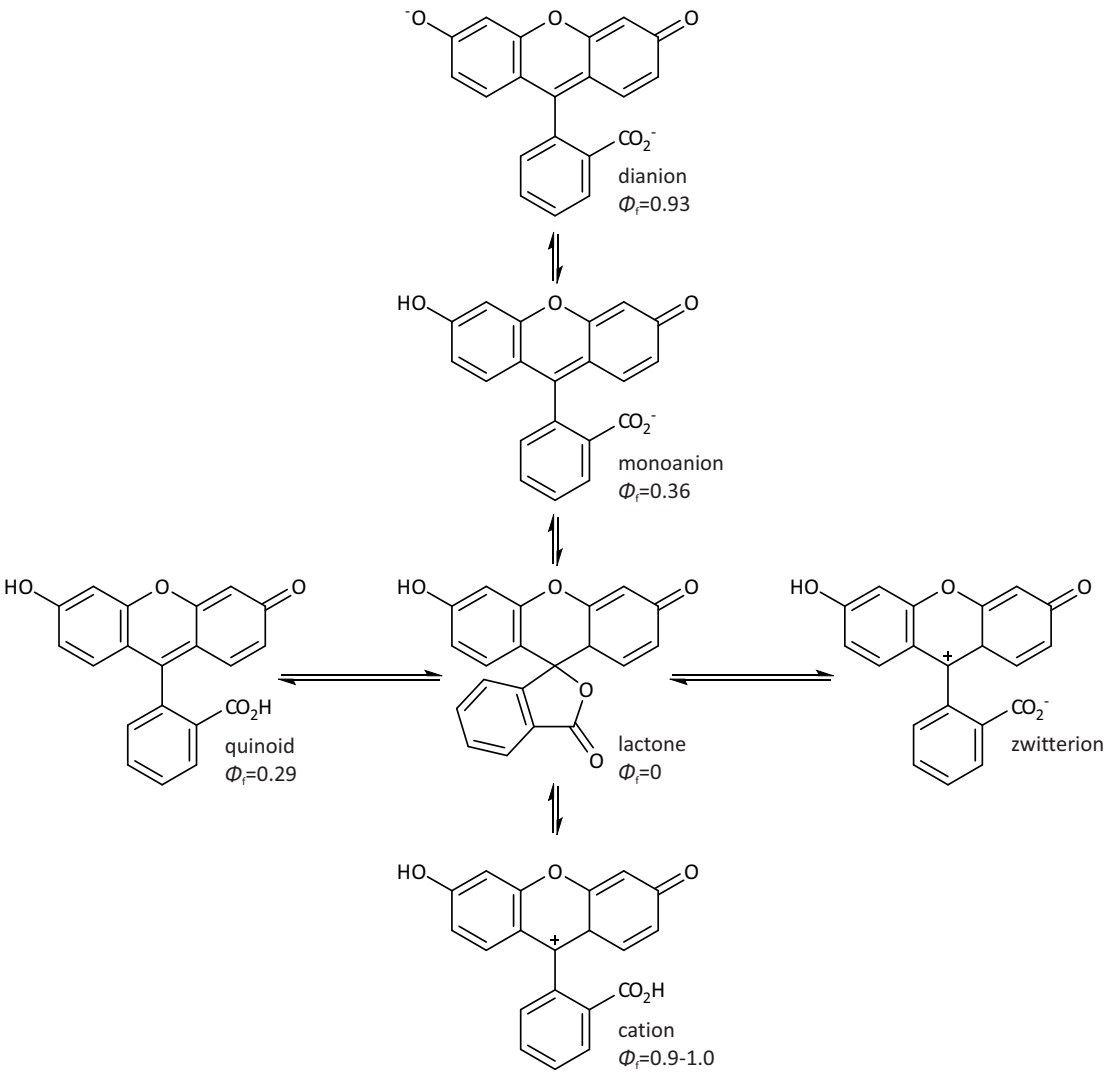

Figure 3.8: Simplified schema of fluorescein's prototropic forms in aqueous solution[108]

Fluorescein can exist in six (seven in non-aqueous media)[108] prototropic forms. The highly fluorescent dianion dominates in basic solution. Under physiologically relevant conditions, it is in equilibrium with the monoanion. With decreasing pH, first the neutral species (quinoid, lactone, and zwitterion), then the cation predominate.

Fluorescein's absorption and emission spectra are strongly pH-dependent.[109] This is based on the dye's complex acid-base equilibrium in solution. In aqueous media alone, six prototropic forms are known (Figure 3.8).[108] The highly fluorescent dianion (Φ_f = 0.92-0.95) and the significantly less fluorescent monoanion (Φ_f = 0.36-0.37) are the most abundant species (pK_a = 6.31-6.80; the exact value varies with the electrostatic environment around the fluorophore) at physiologically relevant conditions.[109] At lower pH a non-fluorescent lactone is

formed.[108] The pH-sensitivity of fluorescein derivatives permitted the development of ratiometric pH assays for the intracellular microenvironment.[110]

Boron-dipyrromethene derivatives

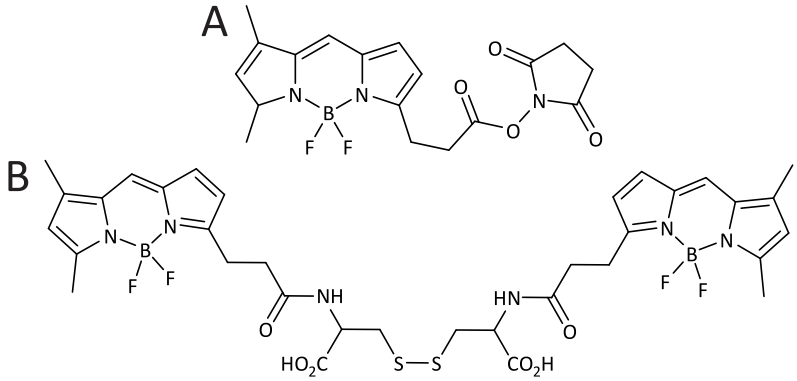

Figure 3.9: Structures of boron-dipyrromethene (BODIPY) dyes used

A: Amino reactive 4,4-difluoro-5,7-dimethyl-4-bora-3a,4a-diaza-s-indacene-3-propionic acid succinimidyl ester (BP SE or BODIPY® FL), *M* = 389.16 g/mol; B: Reduction sensitive BODIPY® FL L-cystine (BP_2), *M* = 788.44 g/mol

4,4-Difluoro-4-bora-3a,4a-diaza-*s*-indacene, or BODIPY-type dyes were first synthesized by Treibs and Kreuzer in 1968 through the reaction of di- and tripyrromethanes with boron trifluoride diethyl etherate in the presence of triethylamine.[111] BODIPYs can be considered as rigidized cyanine dyes.[104] Their spectroscopic properties can be altered with relative ease by modifying the core structure, and their low toxicity to cells[112] makes them valuable tools for protein or DNA labeling, and other bioanalytical applications.[113] One of the most commonly used boron-dipyrromethene derivatives is the unsymmetrically substituted BODIPY FL (Figure 3.9A). It can serve as pH-insensitive alternative to fluorescein in some applications.[77] The electronic dipole of BODIPY FL's strong $S_0 \rightarrow S_1$ transition (500 nm, $\varepsilon \approx 90000\ M^{-1}\ cm^{-1}$) is polarized along the long molecular axis. The weaker $S_0 \rightarrow S_2$ transition (375 nm, $\varepsilon \approx 4500\ M^{-1}\ cm^{-1}$) is probably a mixture of in-plane polarized transitions.[104] The emission maximum of BODIPY FL is located around 513 nm.

Boron-dipyrromethenes have some exceptional properties compared to other fluorophores. They have narrow absorption and emission bands, and their quantum yield for fluorescence is close to one even in water.[77] Their $S_0 \leftrightarrow S_1$ transitions are strongly overlapping (small Stokes shift), making this dye class useful for donor-donor energy migration experiments.[114, 115] One of their most remarkable features is their exceptionally weak solvatochromism.[113] This is the result of a perpendicular orientation of the permanent dipole moment to the electronic transition dipole moment,[114] which lowers the ground state dipole moment and the difference in the dipole moments between the electronic ground and excited state.

Many BODIPYs, especially those without sterically demanding substituents, have the tendency

to form H- and J-dimers at close orbital contact.[113, 116] The group around Johansson has investigated these dimers with the help of model aggregates on double-labeled proteins (H-dimers), labeled lipid vesicles[114], or labeled diaminocyclohexane (J-dimers).[115] BODIPY H-dimers tend form in aqueous solution over the course of several days.[117] They have an absorption maximum at 477 nm.[114] The molecular planes of the stacked fluorophores are 2.7 Å to 7.6 Å apart (Figure 3.10A). The $S_0 \rightarrow S_1$ transition dipoles are parallel, while the electric dipole moments are antiparallel for energetic reasons.[114, 115, 117] J-dimers have an absorption maximum at 570 nm and a broad emission centered around 630 nm. The monomers are oriented in a plane with collinear transition dipoles (Figure 3.10B). The angle between the long molecular axes is 55° and the center to center of mass distance is 3.8 Å.[115] It must be noted, that there is some dispute concerning the formation of BODIPY J-dimers. Based on experiments with BODIPY labeled membrane probes and cofacial BODIPY dimers on a xanthene scaffold,[112, 118, 119] some authors argue that the 630 nm emission originates from excimers instead of J-dimers.[112]

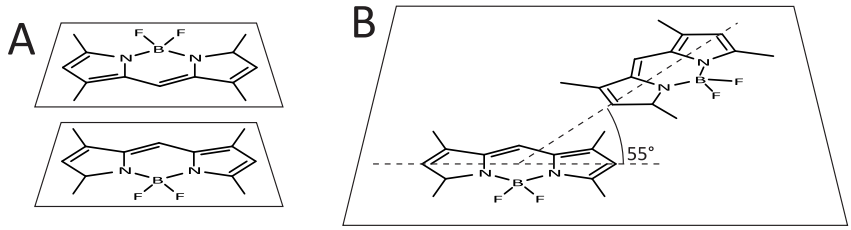

Figure 3.10: Proposed structures for BODIPY dimers

A: In H-dimers the monomers are stacked with parallel transition dipole moments and antiparallel electric dipole moments. The molecular planes are 2.7 Å[114] to 7.63 Å[117] apart. B: In J-dimers both monomers are located in the same plane at a distance of 3.8 Å.[115] The angle between the long molecular axes is 55°. Adapted from [115].

BODIPY aggregates have been used in experiments focusing on molecular disassembly or degradation. The dequenching of BODIPY H-dimers, for example, allowed to visualize the disassembly of the vesicular stomatitis virus in macrophages.[120] Another study has investigated how linear, disulfide cross-linked PEIs made for gene delivery are degraded in HeLa cells. Surprisingly, no data was gathered on the behavior of polyplexes.[55] J-dimers have been used to study cellular membrane microdomains.[121]

BODIPY FL L-cystine (BP_2) is a special BODIPY FL dimer created by Invitrogen by attaching two fluorophores to the amino groups of L-cystine (Figure 3.9B). BP_2 is virtually non-fluorescent until the bridging disulfide is cleaved in a thiol-disulfide exchange reaction. It was originally designed for the thiol specific labeling of proteins, cells and thiolated oligonucleotides.[77]

Tetramethylrhodamine derivatives

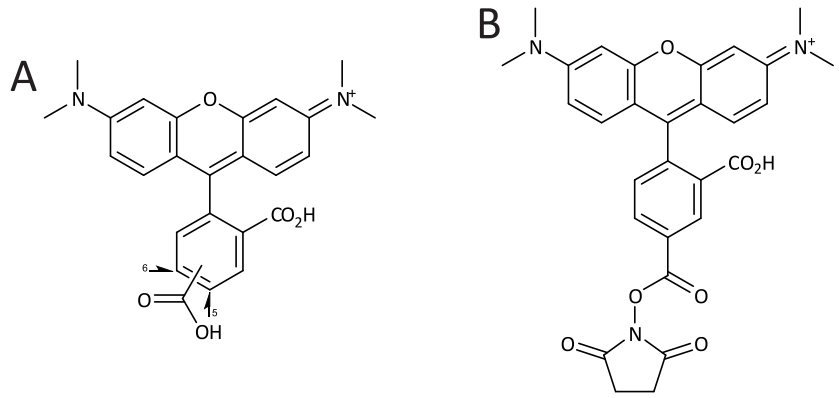

Figure 3.11: Structures of tetramethylrhodamine (TAMRA) dyes used

A: 5(6)-carboxytetramethylrhodamine (TAMRA), *M* = 466.92 g/mol; B: Amino reactive 5-carboxytetramethylrhodamine N-succinimidyl ester (TAMRA SE), *M* = 527.53 g/mol

Tetramethylrhodamine also belongs to the large class of xanthene dyes. Xanthenes are widely used in biochemical and chemical analyses, and rhodamines in particular are often used for protein labeling, especially for antibodies in immunohistochemistry, and for labeling oligonucleotides in sequencing applications.[77] With their high molar absorption coefficients, high quantum yields, and their low tendency for triplet formation, they are suitable for high sensitivity applications.[122, 123] Their photostability is higher than that of fluoresceins and their spectral properties are largely independent from the pH. However, rhodamines are usually very sensitive towards the polarity and the chemical nature of the solvent.[88] This seems to be related to the mobility of the amines at positions three and six of the xanthene core, but the exact mechanism is in dispute.[122] The carboxyphenyl substituent at position nine is not part of the chromophore and its presence has little effect on the dye's absorption and emission characteristics:[88] tetramethylrhodamine – $\lambda_{abs\ max}$ = 543 nm, $\lambda_{em\ max}$ = 570 nm and pyronine y – $\lambda_{abs\ max}$ = 547 nm, $\lambda_{em\ max}$ = 568 nm (in methanol).[124] It protects the xanthene core, however, from nucleophilic attacks from hydroxyl ions that eventually lead to the destruction of the dye in the presence of oxygen.[125, 126]

Xanthenes and BODIPYs are comparable in several photophysical aspects. Their $S_0 \rightarrow S_1$ transition moment is oriented in parallel to the long molecular axis and both dyes are prone to dimerization; rhodamine H- and J-dimers have been described in literature.[127] Christie et al., for instance, have synthesized a reduction sensitive probe similar to BODIPY FL L-cystine. To this end, two TAMRA molecules were cross-linked with cystamine to form a H-dimer.[128] Another feature common to both dye classes is their ability for photoinduced electron transfer (PET).[79, 129, 130] This mechanism is important in conjunction with the labeling of gene carriers and will be discussed in Chapter 4.

3.4 Materials and methods

3.4.1 Fluorescence labeling of polycations

Materials

The labeling and work-up procedure is similar to the cross-linking procedure (see 2.2.1) and was performed on lPEI, S_2-lPEI_b·HCl, PLL, S_2-PLL_b·HCl (see Chapter 1), branched poly(ethyleneimine) 25 kDa (bPEI 25, $M_{w(LS)}$ = 25 kDa, $M_{n(GPC)}$ = 10 kDa, ω(N) = 0.3056; Sigma-Aldrich, Munich, Germany), and 10 kDa (bPEI 10, M_w = 10 kDa (no method disclosed), ratio of primary, secondary, and tertiary amines approx. 0.25/0.5/0.25; Polysciences, Eppelheim, Germany). Additionally required chemicals and solvents were purchased from Sigma-Aldrich (Munich, Germany) in analytical grade. Fluorescent dyes were supplied from the following companies: 4,4-difluoro-5,7-dimethyl-4-bora-3a,4a-diaza-s-indacene-3-propionic acid succinimidyl ester (BP SE) and L-cystine cross-linked BODIPY (BP_2; Invitrogen, Darmstadt, Germany), 5(6)-carboxytetramethylrhodamine (TAMRA) and 5(6)-carboxyfluorescein (FAM; Merck, Darmstadt, Germany), and 5-carboxytetramethylrhodamine N-succinimidyl ester (TAMRA SE, Sigma-Aldrich, Munich, Germany).

Labeling with carboxyphenyl containing dyes

The polycations (free base) were dissolved in about 500 µL of a DMSO/methanol mixture (ϕ(DMSO) = 0.5). Polycation hydrochlorides were dissolved in about 400 µL water and 200 µL DMSO. More water was added if needed for a complete dissolution. An appropriate amount of dye, dissolved in DMSO ($\gamma \approx 10$ g/L), was added and the solution was stirred for several minutes. Finally, DMTMM (in methanol) was added. For the specific amounts of chemicals see Table 3.1 and Table 3.2. The reaction was stirred overnight at room temperature and protected from light. In most cases unbound dye was removed by ultrafiltration using the following sequence of solvents: 10 % DMSO, water, 50 mM borate buffer (pH = 9) for PEI or 0.1 M NaOH for PLL-derivatives, water, and 10 mM HCl. Each solvent was used until the permeate was free from unbound dye (thin layer chromatography: silica gel, eluent methanol). During pH-changes the crude product was washed repeatedly with water until the permeate became neutral.

In case of TAMRA-lPEI, the removal of unbound dye is a variation of the method described by Breunig et al.[53] In short, a saturated NaOH solution was added to the reaction mixture until the polymer precipitated. The precipitate was then washed with ice-cold water by centrifugation (15,000 g, 4 °C) until the supernatant became neutral. Free dye was discarded with the

supernatant. Afterwards the polymer was redissolved in 3 M HCl.

In all cases the purified product was filtered (0.2 µm RC) and then freeze dried overnight.

Table 3.1: Reaction conditions for the labeling of PEIs with carboxyphenyl containing dyes

Amounts of substances and molar ratios of the polymer, dye and activating reagent. The theoretical labeling density of the reaction is given by *r*(polymer).

			amount of substance *n*/µmol			molar ratios	
product	polymer type	dye	polymer	dye	DMTMM	*r*(polymer)	*r*(DMTMM)
BP_2-lPEI	lPEI	BP_2	2.70	1.27	10.15	2.13	8.01
TAMRA-lPEI_1	lPEI	TAMRA	3.00	1.42	5.24	2.12	3.70
TAMRA-lPEI_2	lPEI	TAMRA	3.18	10.22	37.69	0.31	3.69
FAM-lPEI	lPEI	FAM	6.01	66.43	332.47	0.09	5.00
TAMRA-S_2-lPEI	S_2-lPEI_b	TAMRA	0.64	2.51	10.01	0.26	3.99
BP_2-S_2-lPEI_1	S_2-lPEI_b	BP_2	1.60	0.27	2.43	6.01	9.13
BP_2-S_2-lPEI_2	S_2-lPEI_b	BP_2	0.95	0.38	4.77	2.50	12.54
BP_2-S_2-lPEI_3	S_2-lPEI_b	BP_2	0.86	0.38	3.65	2.25	9.59
BP_2-S_2-lPEI_4	S_2-lPEI_b	BP_2	0.94	0.04	0.76	24.64	19.94
BP_2-S_2-lPEI_5	S_2-lPEI_b	BP_2	1.12	0.03	0.03	44.05	1.14
TAMRA-bPEI 10_1	bPEI 10	TAMRA	5.91	18.58	74.34	0.32	4.00
TAMRA-bPEI 10_2	bPEI 10	TAMRA	5.67	16.17	17.78	0.35	1.10
BP_2-bPEI 25_1	bPEI 25	BP_2	1.93	1.27	10.15	1.52	8.01
BP_2-bPEI 25_2	bPEI 25	BP_2	1.92	0.10	0.77	20.00	8.02
BP_2-bPEI 25_3	bPEI 25	BP_2	1.22	0.38	3.04	3.19	7.98
BP_2-bPEI 25_4	bPEI 25	BP_2	1.24	0.13	0.51	9.75	3.99
BP_2-bPEI 25_5	bPEI 25	BP_2	1.24	0.13	0.13	9.75	1.00

Molar ratios are defined as follows: *r*(DMTMM) = *n*(DMTMM)/*n*(dye), *r*(polymer) = *n*(polymer)/*n*(dye); in case of labeled S_2-lPEI_b *n*(polymer) refers to the “parent monomer” lPEI.

Table 3.2: Reaction conditions for the labeling of PLLs with carboxyphenyl containing dyes

Amounts of substances and molar ratios of the polymer, dye and activating reagent. The theoretical labeling density of the reaction is given by *r*(polymer).

			amount of substance *n*/µmol			molar ratios	
product	polymer type	dye	polymer	dye	DMTMM	*r*(polymer)	*r*(DMTMM)
BP_2-PLL	PLL	BP_2	2.87	0.13	1.02	22.61	8.03
BP_2-S_2-PLL_1	S_2-PLL_b	BP_2	2.85	0.16	1.28	17.81	8.00
BP_2-S_2-PLL_2	S_2-PLL_b	BP_2	2.15	0.03	0.10	76.31	3.59
BP_2-S_2-PLL_3	S_2-PLL_b	BP_2	1.89	0.03	0.10	67.20	3.59

Molar ratios are defined as follows: *r*(DMTMM) = *n*(DMTMM)/*n*(dye), *r*(polymer) = *n*(polymer)/*n*(dye); in case of labeled S_2-PLL_b *n*(polymer) refers to the "parent monomer" PLL.

Labeling with *N*-succinimidyl ester activated dyes

All polymers (except S_2-lPEI_2·HCl) were dissolved in 0.4-1 mL dry chloroform. Two equivalents of triethylamine were added per dye molecule. S_2-lPEI_b·HCl was dissolved in 500 µL $NaHCO_3$ buffer (200 mM, pH = 8.33); the resulting pH drop was corrected with 1 M NaOH. Finally, the desired dye amount ($\gamma \approx 10$ g/L in DMSO; specific amounts listed in Table 3.3) was added. The reaction was then stirred overnight at room temperature and protected from light. Then the organic solvents were evaporated and the crude product was purified with ultrafiltration. The further work-up procedure is described in the previous section.

Table 3.3: Reaction conditions for the labeling of PEIs with *N*-succinimidyl ester activated dyes
Amounts of substances and molar ratios of the polymer and dye. The theoretical labeling density of the reaction is given by *r*(polymer).

			amount of substance *n*/µmol		molar ratio
product	polymer type	dye	polymer	dye	*r*(polymer)
BP-lPEI_1	lPEI	BP	1.47	2.44	0.60
BP-lPEI_2	lPEI	BP	1.80	1.73	1.04
BP-lPEI_3	lPEI	BP	1.54	0.41	3.75
BP-S_2-lPEI	S_2-lPEI_b	BP	0.95	0.26	3.71
BP-bPEI 10_1	bPEI 10	BP	3.18	0.77	4.12
BP-bPEI 10_2	bPEI 10	BP	4.46	0.45	9.98
TAMRA-SE-bPEI 10	bPEI 10	TAMRA	6.62	12.89	0.51
BP-bPEI 25_1	bPEI 25	BP	1.55	0.54	2.86
BP-bPEI 25_2	bPEI 25	BP	1.30	0.13	10.00
BP-bPEI 25_3	bPEI 25	BP	1.34	0.44	3.01
BP-bPEI 25_4	bPEI 25	BP	1.65	0.54	3.03
BP-bPEI 25_5	bPEI 25	BP	2.56	0.13	20.00
BP-bPEI 25_6	bPEI 25	BP	2.25	0.05	43.82
BP-bPEI 25_7	bPEI 25	BP	1.30	0.77	1.68
BP-bPEI 25_8	bPEI 25	BP	1.63	0.16	10.06

Molar ratios are defined as follows: *r*(DMTMM) = *n*(DMTMM)/*n*(dye), *r*(polymer) = *n*(polymer)/*n*(dye); in case of labeled S_2-lPEI_b *n*(polymer) refers to the "parent monomer" lPEI.

3.4.2 Spectroscopic characterizations

UV-Vis spectroscopy

UV-Vis absorption measurements were carried out on an Uvikon 941 spectrometer upgraded with a UVS900 light kit (Goebel Instrumentelle Analytik, Au in der Hallertau, Germany). Generally, the sample was dissolved in 500 µL DPBS (γ(polymer) = 1-10 g/L) and then measured in

semi-micro fused quartz cuvettes (path length: 10 mm) at a scan speed of 200 nm/min. Pure DPBS served as reference. Before each new measurement series a baseline run was performed.

The actual labeling densities (r(polymer) = n(polymer)/n(dye)) of the TAMRA-lPEI derivatives were determined with the help of Beer's law. For that, the instrument was calibrated against a TAMRA solution ($A_{550\,nm}$; γ(TAMRA) = 208 … 416 µg/L in DPBS). Then the absorbance of the labeled polymer ($A_{554\,nm}$; γ(TAMRA-lPEI) = 43.1 mg/L in DPBS) was measured. From that data and the known sample mass, m(dye) and m(polymer) were calculated and converted to the corresponding amounts of substance.

For the dye degradation experiments the TAMRA-PEI derivative was diluted from 3.5 g/L to 1.75 g/L with DPBS and immediately thereafter the time-course of the 564 nm absorbance was measured. One thousand data points were collected during 20 min. A monoexponential function was fitted to the data to calculate the decay half-lives ($t_{½}(A_{564\,nm})$).

Fluorescence spectroscopy

Fluorescence excitation and emission spectra were collected on a LS-55 fluorescence spectrometer (PerkinElmer, Rodgau, Germany) equipped with a R928 red sensitive photomultiplier (PMT). All measurements were either carried out with the standard single cell sample holder (PS semi-micro cuvettes, path length: 10x4 mm) or with the plate reader accessory (white Nunc PS F96 MicroWell Plates; Langenselbold, Germany). The standard solvent was DPBS. Sample absorbance was kept below 0.1 to avoid self-absorbance of the emission light. Each measurement series began by setting the desired excitation and emission wavelengths. Whenever possible an emission filter was used. Then, the bandpasses were adjusted (usually between 2.5 and 7.0 nm). Finally, the PMT-voltage was set. Care was taken to keep the maximum signal intensity well below the saturation limit of the PMT. Data was recorded at 500 nm/min at every 0.5 nm. Corrections for the PMT's spectral sensitivity and the spectrum of the light source were always applied. Each sample was measured four times. The data was exported from FL WinLab (PerkinElmer) via LS-55 Spektrenkonverter 1.1. Where indicated, data were normalized against the first time point.

In order to determine the fluorescence intensity increase (ratio between the I_F at the respective $\lambda_{em\,max}$ of the cleaved and uncleaved polymer) of BP_2 labeled polymers under reductive conditions, the samples' emission spectra (λ_{ex} = 488 nm; solvent: DPBS) were recorded in the absence and the presence of 100 mM 2-mercaptoethanol (2-ME). Additionally, the time course of the $I_F(\lambda_{em\,max})$ in the presence of 5 mM GSH was investigated. For that, the polymers were dissolved in a 50 mM phosphate buffer (pH = 7.11). Then GSH was added and the sample's emission intensity was measured in predefined time intervals (Δt = 0.5 … 10 min). The data

(n = 3) were collected at room temperature and normalized against the first time point. Unless indicated otherwise, the data were corrected for photobleaching by measuring samples without GSH in parallel. Finally, a monoexponential function was fitted to the data to determine $t_{½}(I_{F\,\lambda em\,max})$.

The pK_a value of FAM attached to lPEI was estimated by measuring the polymer's fluorescence intensity (λ_{ex} = 495 nm, λ_{em} = 523 nm, γ(PEI) = 10 mg/L) at different pH-values: pH = 1.05 (0.1 M HCl), 4.01 (50 mM potassium hydrogen phtalate), 7.4 (DPBS), 8.5 (10 mM borate buffer), 9.00 (H_3BO_3/KCl/NaOH) and 12.95 (0.1 M NaOH). After plotting the emission intensity against the pH a sigmoidal function (see Appendix) was fitted to the data. The position of the infliction point corresponds to the pK_a.

The influence of the pH on the emission properties of TAMRA-lPEI_2 was evaluated by measuring the fluorescence intensity at the following conditions: λ_{ex} = 554 nm, λ_{em} = 582 nm, γ(TAMRA-lPEI_2) = 25 mg/L; pH = 1.00 (0.1 M HCl), 4.15 (50 mM NaOAc/HOAc), 6.15 (50 mM MES), 7.05 (50 mM phosphate buffer), 7.95 (50 mM HEPES), 9.65 (100 mM borate buffer) and 13 (0.1 M NaOH).

3.5 Results and discussion

Polyplexes based on linear and branched PEIs of comparable molecular weight differ in their ability to transfect cells.[61, 131] A better understanding of what causes this difference could help to improve existing gene carriers. Regrettably, most studies so far have focused on the intracellular processing of the nucleic acid component, usually with the help of fluorescently labeled DNA or RNA.[61, 131] Much less attention has been devoted to the polymer component.[132] There seems to be only one study that has directly compared the cellular uptake and intracellular processing of a fluorescently labeled lPEI and bPEI.[132] However, the polymers were not in complex with nucleic acids, so it is unclear how the results of that study apply for the processing of polyplexes.

3.5.1 Labeling with DMTMM activated FAM

Fluorescence labeling of polycationic gene carriers is usually done with amine-reactive fluorophore derivatives. Many commercially available dyes are sold as pre-activated succinimidyl esters or isothiocyanates, which react to carboxamides or thioureas, respectively. Unfortunately, most of these ready-to-use products are sensitive to moisture and will deteriorate in stock solution over several months. This instability in combination with their significant price (FITC costs about thirty times more than FAM (2012)) can have a major impact on larger scale studies. Beyond that, not all amine reactive dyes are suitable for labeling secondary amines like in

lPEI.[106] Therefore, there is a need for a novel, inexpensive labeling method for polycations that is as simple as if using pre-activated fluorophores.

The condensing agent DMTMM showed its potential for preparing L-cystine cross-linked lPEIs[31] and PLLs (see Chapter 1) in a simple one-pot synthesis. This section evaluates if DMTMM may also serve as activating agent in the preparation of fluorescently labeled polycations. 5(6)-Carboxyfluorescein was chosen as model dye because of its close structural relationship to other xanthenes. FAM's carboxylic group at position 5(6) of the phenyl ring could potentially be suitable to form an amide with polycations. Moreover, FAM's distinct acid-base equilibrium could give an insight into the structure of the labeled product.

Labeling procedure

The labeling procedure is a simple one-pot reaction: lPEI and FAM were dissolved in a mixture of organic solvents (DMSO/methanol) and then a DMTMM solution was added. The DMSO in the mixture is known to lead to demethylation of DMTMM[133] with a reaction half-life of just over three hours, but its use was unavoidable because of the low solubility of the later used rhodamines (see Section 3.5.2) in pure methanol. In order to avoid the complete loss of the condensing agent before the amidation was completed, DMTMM was added in excess. Unbound dye could successfully be removed by ultrafiltration. The final product, a hydrochloride, was well soluble in aqueous media. This property facilitated in vitro testing as no potentially toxic organic cosolvents or surfactants were required for the preparation of stock solutions.

Spectroscopic investigations

The photophysical properties of FAM labeled lPEI were compared to those of pure FAM. Absorption and fluorescence spectroscopy revealed no changes to the overall shape of the spectra (Figure 3.12A and B), though both the absorbance and emission maxima were bathochromically shifted by about 10 nm and their peak widths had increased from 40 nm to 53 nm (emission maxima).

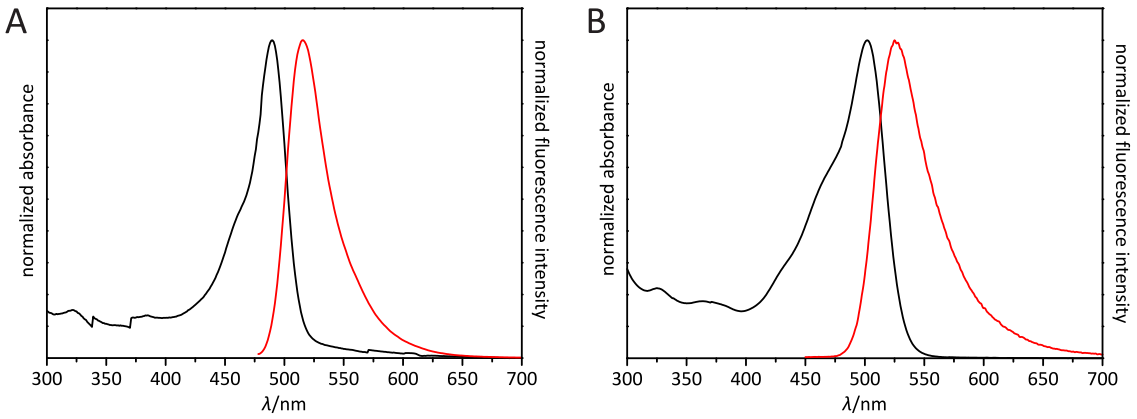

Figure 3.12: Normalized absorption (black) and emission (red) spectra of FAM and FAM-lPEI

A: FAM – $\lambda_{abs\ max}$ = 490 nm (DPBS, pH = 7.4), $\lambda_{em\ max}$ = 515 nm (10 mM TRIS, pH = 9.0; data from Torsten Mayr, Fluorophores.org). B: FAM-lPEI – $\lambda_{abs\ max}$ = 502 nm (γ = 0.43 g/L, DPBS, pH = 7.4), $\lambda_{em\ max}$ = 525 nm (γ = 0.11 g/L, H_3BO_3/KCl/NaOH, pH = 9.0, λ_{ex} = 420 nm). (Experimental details Section 3.4.2)

Similar spectral changes have been reported for other FITC labeled macromolecules like BSA[134] or dextran (data from Invitrogen.com not shown). They are related to the fact that fluorophores attached to macromolecules experience a different local electronic environment than unbound fluorophores. At higher labeling densities, interactions between neighboring fluorophores can also contribute to spectral changes.[134]

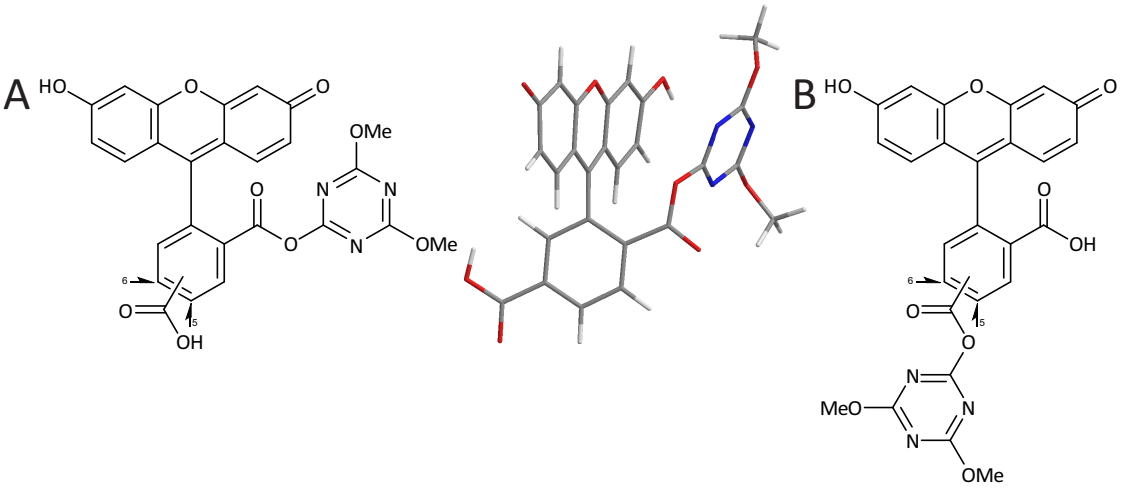

Figure 3.13: Possible structures of DMTMM activated FAM

During the activation process DMTMM can potentially react with the carboxylic acid in position 2 (A, left) or 5(6) (B) of FAM's carboxyphenyl substituent. If the activation takes place at position 2, the xanthene ring and the acyloxy-triazine pose a significant steric barrier for a subsequently attacking amine (A, right; geometric optimization).

FAM carries two carboxylic groups at its carboxyphenyl substituent (in position 2 (≡ $^{\prime}CO_2H$) and 5(6) (≡ $^{\prime\prime}CO_2H$)), which potentially can be used for amidation. In case of the closely related rhodamines, the position next to the xanthene ring ($^{\prime}CO_2H$) is said to be inaccessible for the covalent coupling of analytes due to steric hindrance.[135] Nonetheless, there are studies that prove otherwise.[136, 137] For FAM, the actual coupling site can be determined by investigating the pH-

dependent spectral properties of a labeled product. Any modification on $^{I}CO_2H$ would prevent the formation of the non-fluorescent lactone and the zwitterion (Figure 3.8) under acidic conditions,[108] and change the excitation spectrum compared to the unmodified dye. However, when the excitation of FAM-lPEI was examined at different pH-values, apart from minor bathochromic shifts, the spectra (Figure 3.14A) closely resembled those reported in literature for the unbound dye. At pH = 4 the spectrum is dominated by the emission of the neutral species (p-quinoid, lactone, and zwitterion), whereas at pH = 1.05 spectral features of the cation can be seen ($\lambda_{ex\ max}$ = 440 nm, literature: 437 nm).[108, 138] These data clearly indicate that only $^{II}CO_2H$ was able to react with the polymer and this may very well apply in general for other dyes of similar structure. Interestingly, $^{I}CO_2H$ remained unmodified, even though DMTMM is an efficient condensing agent even for the reaction of secondary, aliphatic amines with aromatic, sterically hindered carboxylic acids.[139] Thus, it can be assumed that $^{I}CO_2H$ is at least activated by DMTMM, but seems to fail to react with the amine. Since $^{I}CO_2H$ is in the vicinity of the xanthene ring and the activating agent is rather bulky (Figure 3.13A), the regioselectivity for the reaction with the polymer is probably kinetically controlled. In the absence of any large molecular entities that block the nucleophilic attack of the PEI amine from both sides (Figure 3.13B), $^{II}CO_2H$ is able to react at a much higher rate than $^{I}CO_2H$.

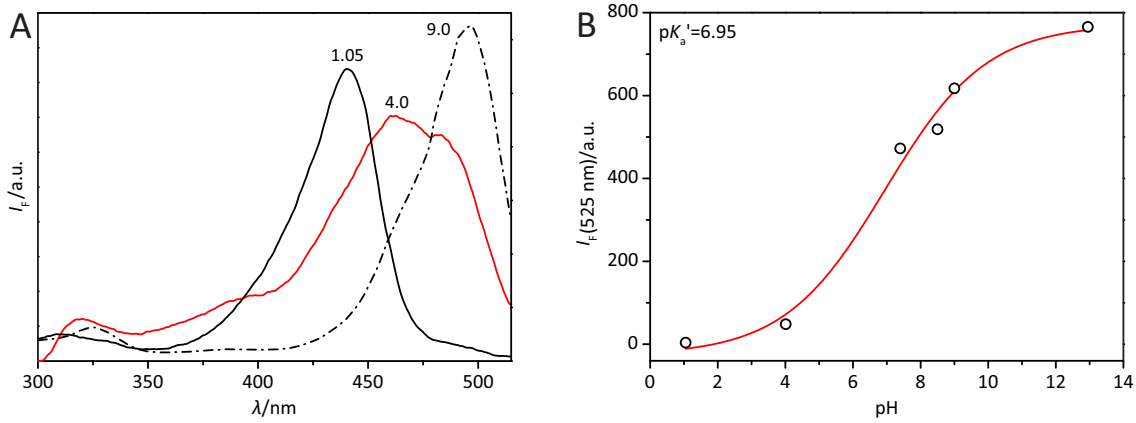

Figure 3.14: Excitation and emission properties of FAM-lPEI at different pH-values

FAM-lPEI was dissolved (γ = 10 mg/L) in solutions of different pH (1.05, 4.01, 7.4, 8.5, 9.00 and 12.95). A: Excitation spectra (λ_{em} = 525 nm) at pH = 1.05 (black), 4.0 (red), and 9.0 for comparison (---; not drawn to scale). B: Fluorescence intensities (circles, λ_{ex} = 495 nm, λ_{em} = 525 nm) as a function of pH. A Boltzmann function derived from the Henderson–Hasselbalch equation was fitted to the data (red curve; see Appendix) to estimate the apparent pK_a. (Experimental details Section 3.4.2)

FAM-lPEI was characterized further by determining the apparent pK_a (pK_a') of the acid-base equilibrium between its mono- and dianionic form by measuring the emission intensity at different pH values (Figure 3.14B). With a value of 6.95, the pK_a' is slightly higher than the value reported by Sjöback et al. for fluorescein (pK_a' = 6.41).[138] The pK_a' in general is sensitive to the immediate electrostatic environment around the fluorophore,[109] so it is conceivable that

the observed shift is caused by the probe's proximity to the polycation. Since the pK_a' is still in the physiologically relevant pH-range, FAM-lPEI could potentially be used to study pH-changes that internalized polyplexes might be subjected to (Section 5.1.2). It must also be mentioned that the pK_a' shift might also be a measurement artifact due to the limited data available.

3.5.2 Labeling with TAMRA derivatives

Next, it was evaluated whether the DMTMM based method could generally be used for labeling PEIs with xanthenes. For that, lPEI with a molecular weight of 16.8 kDa, a similarly sized branched PEI (bPEI 10, M_w = 10 kDa), and S_2-lPEI_b (see Section 2.2.1) were labeled with TAMRA. As lPEIs only contain secondary amines, while bPEIs additionally possess primary and tertiary amines, it was of particular interest to investigate the influence of the polymer's chemical structure on the labeling process and the properties of the labeled product. All polymers were labeled successfully and a simplified procedure to remove unbound dye was found. Interestingly, the polymer-dye conjugates' pH-stability was related to chemical nature of the polycation.

Labeling of lPEI and S_2-lPEI

The synthesis method for FAM-lPEI was modified in some aspects to account for the differences of the educts. During the labeling of S_2-lPEI, the methanol in the solvent mixture had to be replaced with water, as the polymer hydrochloride was insoluble in the presence of the alcohol. The replacement had no detrimental effect on the labeling procedure or the dye's solubility. The removal of unbound dye from labeled lPEI was based on a modified method published by Breunig et al.[53] In short, the crude product was precipitated with a concentrated NaOH solution and then washed with water until the pH was neutral. This method is faster than ultrafiltration and has fewer technical limitations. For instance, there is neither the risk for a membrane rupture nor are there any restrictions concerning the membrane's *MWCO* or solvent compatibility. There is, however, the risk that the strongly basic conditions negatively affect the dye. Thus, the spectra of the labeled products were examined closely, but did not reveal any adverse effects. Apart from minor bathochromic shifts and slightly increased Stokes shifts (TAMRA: 23 nm, TAMRA-PEIs: ≈ 27 nm), the absorption and excitation spectra were virtually identical to those of TAMRA (Figure 3.15); the largest red shift was observed for TAMRA-S_2-lPEI.

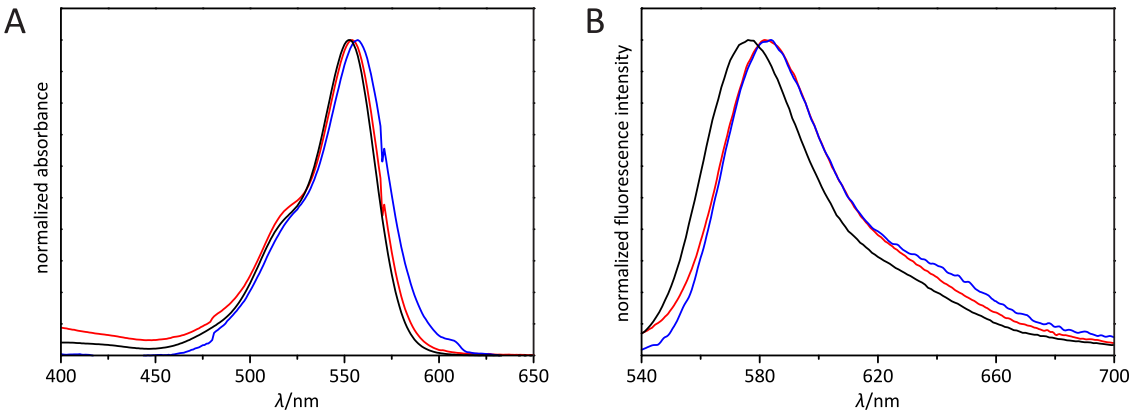

Figure 3.15: Normalized absorption (A) and emission (B) spectra of TAMRA and TAMRA-lPEI derivatives

TAMRA (black), TAMRA-lPEI_2 (red) and TAMRA-S_2-lPEI (blue) were dissolved in DPBS (pH = 7.4). The wavelengths of maximum absorbance ($\lambda_{abs\ max}$)/emission intensity ($\lambda_{em\ max}$ at λ_{ex} = 488 nm) are 553 nm/576 nm (data from Invitrogen.com, pH = 7), 554 nm/581 nm, and 557 nm/584 nm. Data for TAMRA-lPEI_1 not shown for the sake of clarity. (Experimental details Section 3.4.2)

Next, it was investigated how efficient the DMTMM based labeling actually is and how the efficiency is affected by the labeling ratios. For that, TAMRA-lPEI_1 and TAMRA-lPEI_2 were labeled under the very same conditions, but in case of the latter the dye amount was increased almost tenfold. The molar ratio between TAMRA and DMTMM was kept constant. The UV-Vis data showed that the labeling reaction is rather inefficient. Only 3 % and 10 % of the initially used dye was successfully attached to TAMRA-lPEI_1 and TAMRA-lPEI_2, respectively. A large excess of dye did not improve the labeling density significantly, suggesting that the reaction is controlled by the initial amount of DMTMM rather than the amount of dye. DMTMM is consumed in two competing processes during labeling: Dye activation and demethylation by DMSO. Assuming the latter is much faster than the activation, not enough DMTMM will be left to activate significant amounts of TAMRA, eventually. So to achieve higher labeling densities, the use of DMSO should be avoided or DMTMM must be used in greater excess.

The results from the previous section (Section 3.5.1) demonstrate that FAM retains its pH-sensitivity on lPEI, but in order to create a ratiometric pH assay for intracellular studies, a pH-insensitive reference is also needed. To test if TAMRA-lPEI might serve as reference, TAMRA-lPEI_2's fluorescence intensity (λ_{em} = 582 nm) was measured as a function of the pH (Figure 3.16). As expected for a rhodamine dye, its emission intensity was essentially constant within the physiologically relevant pH range[140], and decreased only under extremely acidic and basic conditions. Evidently, the labeling procedure does not negatively affect the dye's applicability as pH reference.

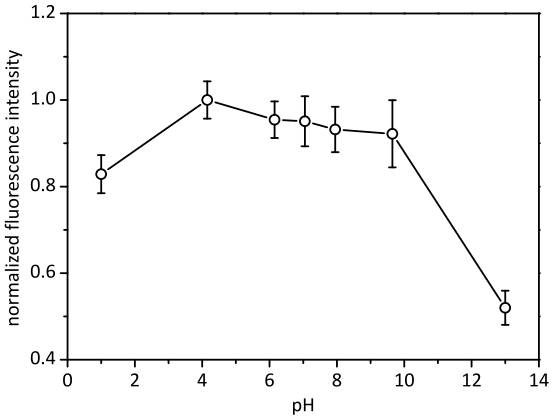

Figure 3.16: pH-dependent fluorescence of TAMRA-lPEI_2

The emission intensity (λ_{ex} = 554 nm, λ_{em} = 582 nm) of TAMRA-lPEI_2 was measured at different pH-values (γ(PEI) = 24.8 mg/L; pH = 1.0, 4.15, 6.15, 7.05, 7.95, 9.65, and 13.0). The data were normalized against the maximum intensity (pH = 4.15). (Experimental details Section 3.4.2)

Labeling of branched PEI 10 kDa

In order to compare the DMTMM based labeling method with the "conventional" labeling method based on a preactivated, commercially available dye, bPEI 10 was additionally labeled with TAMRA SE. For comparability, a similar polymer-dye ratio (r(polymer) ≈ 0.3) was used as for lPEI and S_2-lPEI. The reaction with TAMRA SE was performed in dry chloroform to minimize the hydrolysis of the active ester. In all cases, unbound dye was removed by ultrafiltration.

The main absorbance band of all TAMRA-bPEIs was significantly more red-shifted (563 nm; Figure 3.17A) than those of TAMRA-lPEI (554 nm) and TAMRA-S_2-lPEI (557 nm). The magnitude of the bathochromic shift seemed to increase with the degree of branching: TAMRA-bPEI 10, with 25 % tertiary amines (10 nm) > TAMRA-S_2-lPEI, with ≈ 1 % tertiary amides (4 nm) > TAMRA-lPEI (1 nm) > unbound TAMRA. Such bathochromic shifts are known for a large number of cationic dyes.[141] They are not necessarily related to dye-dye interactions, which are in turn dependent on the labeling density, but to changes in polarity and refractive index in the chromophore's environment.[142] In case of TAMRA-PEIs, the charge density (i.e., the number of charged amines per unit volume) around the chromophore increases with polymer compactness and that results in an increasing bathochromic shift. Conversely, the extent of the bathochromic shift could be an indirect measure for the polymer's charge density and degree of branching. Since both properties significantly influence cytotoxicity[50, 51] and uptake efficiency[61] of PEI-derived gene carriers, it might be fruitful to test this hypothesis in a further, more detailed study.

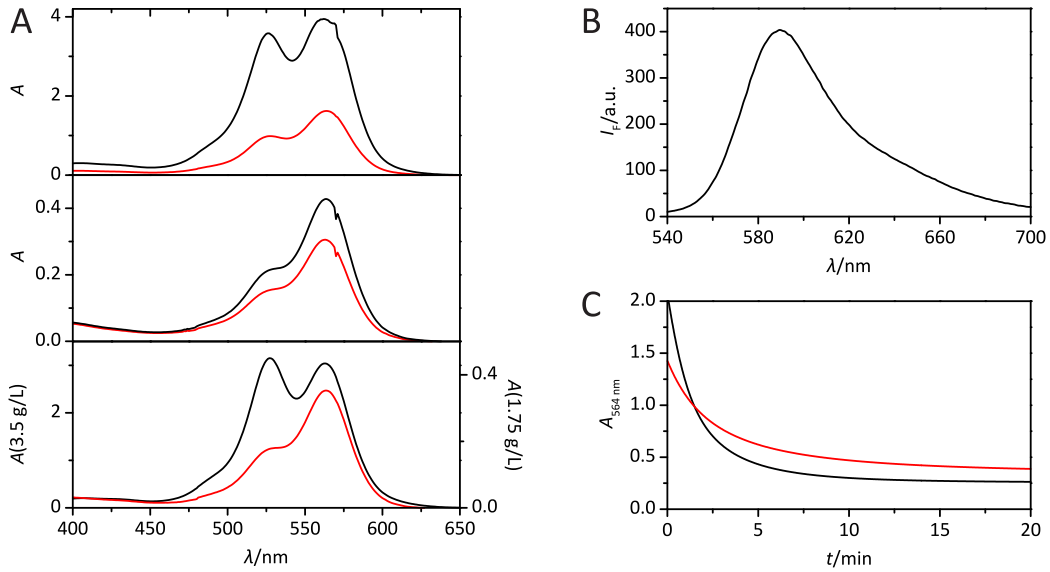

Figure 3.17: Absorption and emission characteristics of TAMRA-bPEI 10 derivatives

A: From the top down: TAMRA-bPEI 10_1 and TAMRA-bPEI 10_2 were diluted from 3.5 g/L to 1.75 g/L (in DPBS) and their absorption spectra were measured immediately (black) and at t = 6 min or 21 min (red), respectively. Bottom: Undiluted (3.5 g/L, t = 0 min (black)) and diluted TAMRA-SE-bPEI 10 (1.75 g/L, t = 40 min (red)) in DPBS. B: Fluorescence emission spectrum of TAMRA-SE bPEI 10, 40 min after dilution from 3.5 g/L to 1.75 g/L in DPBS (λ_{ex} = 488 nm, $\lambda_{em\ max}$ = 589.5 nm). C: TAMRA-bPEI 10_2 (black) and TAMRA-SE-bPEI 10 (red) were diluted from 3.5 g/L to 1.75 g/L (in DPBS) and the absorbance at 564 nm was measured over a period of 20 min. A monoexponential function was fitted to the data. The corresponding half-lives ($t_{½}$) are 1.7 and 3.3 min. (Experimental details Section 3.4.2)

A very prominent feature in TAMRA-bPEIs' absorption spectra (Figure 3.17A) was the appearance of a new blue-shifted band at 526-529 nm. The shape of the corresponding emission spectrum (Figure 3.17B) was unchanged. This phenomenon is well-known for rhodamines and indicates the presence of non-emitting H-dimers in addition to dye monomers.[85, 102, 143] In H-dimers, the transition dipoles of both chromophores are strongly coupled and the excitation energy is delocalized over the entire (homo)bichromophoric system.[144] The dimer behaves as a new single quantum system with unique spectral properties[144] and its absorption spectrum is no longer a linear combination of two independent monomer spectra. By applying the strong exciton coupling model of Simpson and Peterson,[145] H-dimers can be used as molecular rulers to measure very short intramolecular distances.[103, 144, 146] This method could be used to complement FRET-based techniques, since FRET measurements can only be used to measure relatively long distances where the dipolar coupling is weak. More specifically, FRET measurements should only be performed at distances greater than 50 % of the Förster radius R_0 for a given fluorophore pair (R_0(TAMRA-TAMRA) = 4.4 nm)[144]. It is obvious that disregarding the presence of non-fluorescent H-dimers can easily lead to the misinterpretation of fluorescence intensity data, so it is surprising that this aspect has not yet been taken into consideration in experiments with fluorescently labeled polyplexes. For that reason, the properties of the H-

dimers on TAMRA-bPEI 10 were investigated in more detail.

According to the Simpson-Peterson approximation the exciton coupling interaction energy U is related to the distance R between point dipoles:[144]

$$U = \frac{1}{4\pi\varepsilon_0} \cdot \frac{|\mu|^2}{n^2 R^3} |\kappa| \tag{3.19}$$

Where ε_0 is the vacuum permittivity, n is the solvent's refractive index ($n(H_2O)$ = 1.333), κ is the dipole orientation factor between the monomers (κ(H-dimers) = 1)[103], and μ^2 is the squared module of the transition dipole. It was not possible to determine a stable value for μ^2 experimentally, due to the changes in the absorption spectrum over time (see below). Instead, a literature value of $\mu^2 = 9.5 \times 10^{-58}$ C² m² was used for the calculations.[144] U is related to the spectral shift $\Delta\tilde{\nu}$ between the absorption maxima of dimer and monomer:[144]

$$U = hc_0\Delta\tilde{\nu} \tag{3.20}$$

For TAMRA-bPEI_10 ($\Delta\tilde{\nu}$ = 1217 cm^{-1}) U equaled 24.2 × 10^{-21} J and after substituting all values in Equation 3.19, R was calculated to be 0.58 nm. Similar values have previously been reported for TAMRA.[144, 146]

Beyond calculating the interchromophoric distance, the analysis of the absorption spectra also allowed to determine the aggregate's geometric properties. In H-dimers, the angle ϑ between the polarization axes of the monomers is 90° and since TAMRA's $S_0 \rightarrow S_1$ transition moment is oriented along the nitrogen-nitrogen axis[122], the fluorophores must either be stacked on each other (Figure 3.6) or aligned side-by-side.[103] Both configurations can be distinguished by the relative position of the $S_0 \rightarrow S_2$ transition located at around 357 nm. A bathochromic shift in respect to the monomer's transition suggests a side-by-side alignment. Conversely, a hypsochromic shift indicates stacked fluorophores[103] and this was the case for TAMRA-bPEI 10_1 (2-3 nm blue-shift; data not shown). This finding was somewhat unexpected. Fluorophore stacking is likely driven by hydrophobic forces, but those play a minor role in the formation of rhodamine dimers.[103] Therefore, a side-by-side arrangement would seem more likely. Evidently, the presence of the compact and highly charged polycation bPEI alters the complex interplay[83, 85] between attractive (e.g., hydrogen bonding, hydrophobic interactions, and van der Waals forces) and repulsive forces (e.g., electrostatic repulsion) during dimerization. It is unclear if bPEI generally promotes the formation of stacked TAMRA-H-dimers, as the short-wavelength transition could only be measured in one case.

Interestingly, TAMRA aggregated on bPEI 10, but not on lPEI or S_2-lPEI. In other words, only in case of TAMRA-bPEI 10 were the chromophores close enough together for an efficient interchromophoric interaction. In part, this is could be related to the labeling density. As demonstrated before, the labeling of lPEI/S_2-lPEI is inefficient. Statistically each PEI molecule carried

0.3 TAMRA molecules, at most. At such a low labeling density, dye aggregation seems improbable. Due to the structural and chemical differences between the different PEI variants, the labeling of bPEI 10, on the other hand, could be much more efficient (>1 dye per PEI), even though it was performed under similar conditions (esp. labeling ratio). The resulting higher labeling density would then promote aggregate formation. bPEI 10's highly compact polymer structure could also play a role in the aggregation process, by forcing individual dye molecules closer together.

The presence or absence of H-dimers was not the only difference between TAMRA-bPEI 10 and TAMRA-lPEI/S_2-lPEI. All TAMRA-bPEI 10 derivatives turned out to be exceptionally pH sensitive and lost their color and ability to fluoresce, under basic conditions. In contrast, TAMRA-lPEIs retained their color even when being precipitated with a saturated NaOH solution. The rate of discoloration increased with the pH: No changes were observed in acidic solution (0.16 M HCl or water; Figure 3.18). At slightly (DPBS; Figure 3.17A and C) or strongly (0.16 M NaOH; Figure 3.18) basic conditions the loss of color was gradual ($t_{½}(A_{564\ nm})$ = 1.7 … 3.3 min, Figure 3.17C) or instantaneous, respectively. This finding is in contrast to the generally low pH-sensitivity of rhodamines compared to other xanthenes. Unlike fluoresceins, rhodamines do not form non-fluorescent inner lactones in polar solvents.[88] It is, however, possible to create extremely pH-sensitive rhodamine based probes by amidating position two ($^{\prime}CO_2H$) of the carboxyphenyl substituent.[136, 137] At high pH these amides nucleophilically attack the partially positively charged C9 of the xanthene ring (opposite of the ring oxygen) to reversibly form non-fluorescent spirolactams (pK_a = 2.8-6.5; see Figure 3.19).[137] A wide range of amines can be used for this amidation, including tetraethylenepentamine[147], and bulky ones like 1-adamantylamine or 1-naphthylamine.[137]

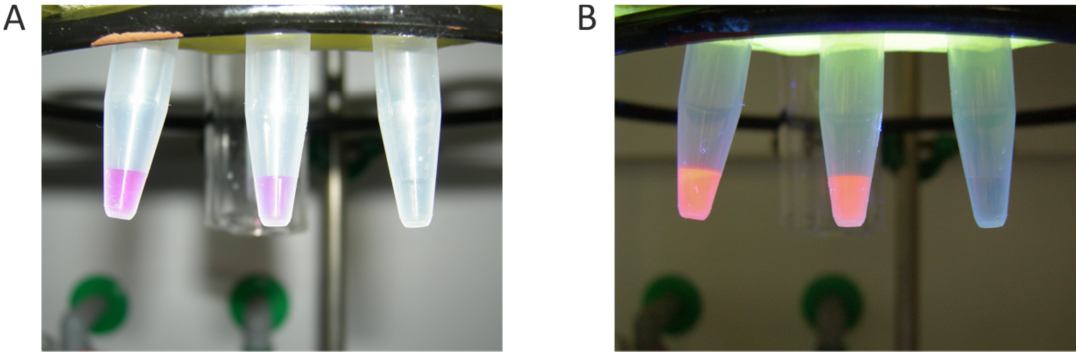

Figure 3.18: pH-dependent discoloration of TAMRA-bPEI 10

Samples from left to right: Eighty microliters of either 0.2 M HCl, Water or 0.2 M NaOH were added to twenty microliter samples of a TAMRA-bPEI 10_2·HCl solution (γ(PEI) = 3.5 g/L in DPBS). The results were observed under ambient (A) and UV-light (B, λ_{ex} = 355 nm).

For that reason, it is conceivable that bPEI's primary amines might have reacted with DMTMM activated TAMRA at $^{\prime}CO_2H$ to form a pH-sensitive amide (Figure 3.19). The results of several

observations, however, contradict this hypothesis. To begin with, the addition of an excess amount of HCl to a discolored TAMRA-bPEI solution did not restore the product's color (data not shown). The reaction was irreversible and this precludes the existence of a pH-dependent equilibrium between a ring-opened and a spirocyclic TAMRA-bPEI. Moreover, as demonstrated in the synthesis of FAM-lPEI, the DMTMM based labeling method is $^{II}CO_2H$ selective. $^{I}CO_2H$ is not modified so the labeled product per se is unable to form a spirolactam. Finally, the labeling was also performed with TAMRA SE, a dye where exclusively the $^{II}CO_2H$ is activated (Figure 3.11B). Still, the product was pH-sensitive.

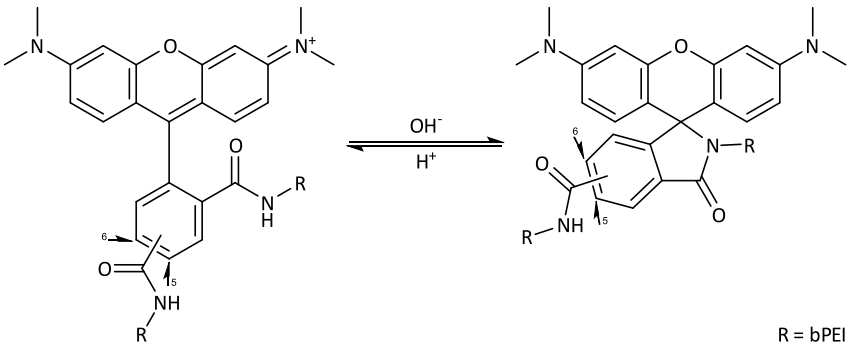

Figure 3.19: Hypothetical pH-dependent equilibrium between ring-opened and spirocyclic TAMRA-bPEI
During labeling (activating reagent DMTMM), branched PEI might be attached to both of TAMRA's carboxylic groups. The resulting fluorescent, ring-opened product would be in equilibrium with its non-fluorescent, spirolactam form. The latter would dominate under basic conditions.

Thus, another mechanism must be responsible for TAMRA-bPEI's pH-sensitivity and there is some indication that the carboxyphenyl substituent plays an important part in it. An irreversible color loss under basic conditions has been described for pyronine dyes. Pyronines are structurally similar to rhodamines, but lack the bulky carboxyphenyl which shields the xanthene C9 from nucleophilic attacks.[125] Therefore, pyronines quickly form a colorless xanthydrol in the presence of OH^-. This reaction is reversible unless the xanthydrol is subsequently oxidized to a xanthone by dissolved oxygen.[148] The C9 substituent in xanthenes evidently does not offer a complete protection against attacking nucleophiles, otherwise the reversible formation of rhodamine spirolactons, -lactams, and thiospirolactons[149], i.e., a reaction with "inner" nucleophiles, would not be possible. There are no obvious reasons why the chromophore should not be able to react with "external" nucleophiles, too. In the case at hand, the most plausible reaction would be the (irreversible) nucleophilic addition of a PEI amine. Considering TAMRA-lPEI's stability under basic conditions, the attacking species cannot be a secondary PEI amine (or a hydroxyl ion). A participation of tertiary PEI amines also seems unlikely due to steric restrictions, which leaves primary PEI amines as attacking species, though they are usually less nucleophilic than secondary amines. Given the very bulky and carboxyphenyl protected xanthene core, steric hindrance may in this case play a far greater role than nucleophilicity[150].

Without doubt, more data are necessary to establish the exact mechanism for TAMRA-bPEI's pH-sensitivity and its tendency to form H-aggregates. Until then, TAMRA and perhaps rhodamines in general cannot be considered as suitable fluorescent labels for branched PEI.

The mere fact that two so closely related molecules like TAMRA-lPEI and -bPEI unexpectedly behave so fundamentally different, demonstrates how important it is to perform detailed spectroscopic characterizations on new fluorescent probes. This is often neglected in literature, but not knowing the characteristics of the probe will lead to the misinterpretation of especially quantitative data. In the context of gene delivery vehicles, such data are used to assess uptake efficiency and polyplex integrity. To give one example: Kong et al. have used "rhodamine (Rho)" (exact dye type not disclosed) labeled bPEI 25 kDa as FRET acceptor for "Alexa 488 (FITC)" (*sic*) labeled pDNA in polyplexes.[151] Their method allowed them to simultaneously determine uptake efficiency (Rho fluorescence yield) and structural integrity (FRET efficiency: Alexa 488 → Rho) of polyplexes. Regrettably, the authors neither provided any absorption spectra nor investigated the effect of alkaline conditions on the PEI-rhodamine conjugate. Without these data and in view of the close similarity of their rhodamine bPEI 25 to TAMRA-bPEI 10, it is impossible to judge the validity of their conclusions.

3.5.3 Labeling with BODIPY FL L-cystine (BP_2) and BODIPY FL SE (BP SE)

For the development of specialized carriers for DNA and RNA a detailed knowledge about the intracellular processing of the delivery system is beneficial. As far as redox-sensitive polycation based gene carries are concerned, the most crucial issues are the exact spatiotemporal point of carrier cleavage and, not necessarily occurring simultaneously, the release of the cargo. Until now, not much attention has been devoted especially to the carrier cleavage and to some degree this is understandable. The complexity of intracellular disulfide processing makes it difficult to derive general rules from experiments with specific carriers or model compounds.[40]

One attempt to gain a better insight into the degradation of a S_2-lPEI derivative has been made by Lee et al.[55] Their BODIPY FL labeled polymer was non-fluorescent (probe-probe self-quenching) until it was cleaved in the presence of GSH. It allowed them to visualize the polymer's degradation in HeLa cells, but they did not attribute this process to any particular cellular compartment. Also, they did not investigate polyplexes based on their polymer. It is important to note that the fluorescence increase they had observed is not directly the result of polymer degradation. Strictly speaking, dequenching occurs when individual polymer fragments move apart from each other, i.e., the probe-probe distance increases. Consequently, their method would not allow differentiating intact polymer strands from polymer fragments

still in tight complex with nucleic acids (see Chapter 4). In order to investigate carrier cleavage and polyplex dissociation separately, additional probes like BP_2 are required. Depending on the exact nature of the polymer bound BP_2, polymer cleavage could be detected by the release of highly fluorescent BODIPY FL moieties, whose fluorescence is independent from the polymer's complexation state.

For the present work, a representative selection of linear (lPEI, PLL), branched (bPEI 25, bPEI 10), and cross-linked (S_2-lPEI, S_2-PLL) polycations were labeled with BP_2 and BP SE. BP_2 is an almost ideal choice for investigating the degradation of S_2-lPEI and S_2-PLL. Due to its close structural relationship to the L-cystine cross-linker, it can be assumed that both are cleaved under the same conditions. All labeled polymers were subjected to photophysical characterizations in the absence and presence of reductive conditions. It was found that polymer bound fluorophores tended to form aggregates under most conditions. The aggregation was strongly influenced by the polymer structure and, to a lesser degree, the fluorophore class.
It was furthermore evaluated how suitable the DMTMM based strategy was for labeling with non-xanthene fluorophores.

General properties of BP_2

Uncleaved BP_2 has a very low emission intensity due to an efficient probe-probe quenching. The shapes of its absorption and emission spectra, and the positions of its characteristic transition bands (Figure 3.20B; $S_0 \rightarrow S_1$: 504 nm, $S_0 \leftarrow S_1$: 511 nm, $S_0 \rightarrow S_2$: 350 nm (broad)) in MeOH were nearly identical to those of its monomeric counterpart BODIPY FL (Figure 3.20B; data partially not shown). In a more polar environment (DPBS; Figure 3.20A, dashed) this was only the case for cleaved BP_2 (BP-SH). The dimeric form possessed an additional absorption band located at 478 nm (Figure 3.20A, solid); the $S_0 \rightarrow S_2$ transition was unaltered. This new band was non-emitting as the fluorescence spectrum was always identical to that of BODIPY FL, regardless of which absorption band was excited (data not shown). In accordance with this conclusion, the excitation spectrum (λ_{em} = 515 nm; data not shown) provided no evidence for the presence of a new, weakly emitting species. All these observations indicate that H-dimers are partially formed. Normally, this process is very slow and has been shown to take over 24 h for a relatively hydrophobic BODIPY derivative and required a dye concentration of at least 3 µM.[117] In case of the less hydrophobic BP_2, a dimerization was observed at a concentration as low as 2.54 µM (corresponding monomer concentration: 5.1 µM). In contrast, no dimerization occurred in a monomer solution of the same concentration (Figure 3.20A, dashed). Apparently, the proximity of the fluorophores in BP_2 promotes a rapid intramolecular H-

dimerization even under conditions where the corresponding monomers would fail to do so due to their higher solubility.

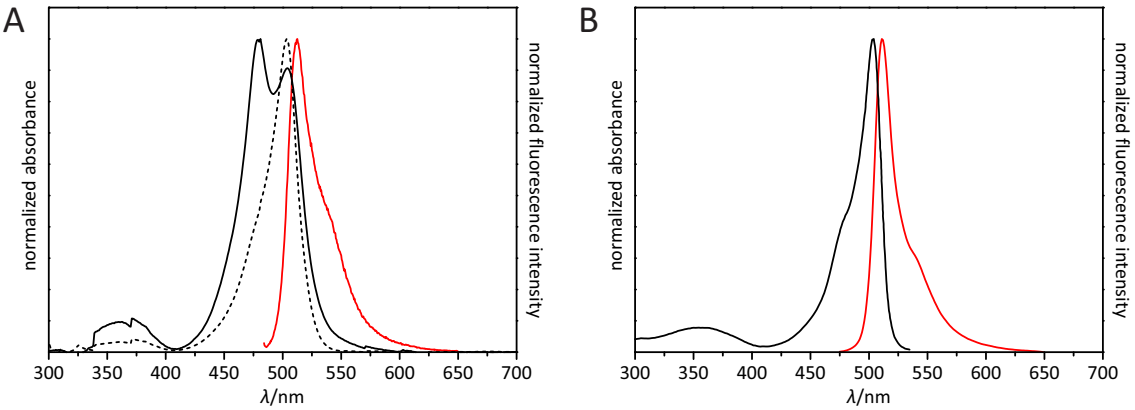

Figure 3.20: Normalized absorption (black) and emission (red) spectra of BODIPY derivatives

A: BODIPY FL L-cystine in DPBS – Absorption spectra ($\gamma(BP_2)$ = 2 mg/L) in the absence (solid; $\lambda_{abs\ max}$ = 479 nm and 504 nm) and the presence (dashed; $\lambda_{abs\ max}$ = 503 nm) of 100 mM 2-mercaptoethanol. Emission spectrum (λ_{ex} = 479 nm, $\lambda_{em\ max}$ = 512 nm; $\gamma(BP_2)$ = 10 mg/L) in the absence of 2-mercaptoethanol. The absorption spectra were baseline corrected. B: Absorption and emission spectrum of uncleaved BODIPY FL L-cystine and BODIPY FL, respectively in MeOH ($\lambda_{abs\ max}$ = 504 nm, $\lambda_{em\ max}$ = 511 nm). Data provided by Invitrogen; dye concentrations and excitation wavelength were not disclosed. (Experimental details Section 3.4.2)

By assuming that BP_2 forms H-dimers of the usual geometry (Section 3.3) and by using a value for μ that was experimentally determined for Tetramethyl BODIPY (22.9×10^{-30} C m)[115], the Simpson-Peterson approximation was used to calculate the intra-fluorophoric distance R between the BP moieties to be 0.51 nm. A comparable value (R = 0.49 nm) has been obtained by Mikhalyov et al. for bis-BODIPY-FL-propionyl-1,2-*cis*-diaminocyclohexane (b-BACH)[115], a rigidized bichromophoric system whose structure is closely related to BP_2. They have also reported on a relatively long ranged (R_0 = 6.0 nm) donor-acceptor energy migration (DAEM) from excited monomers to H-dimers and on a donor-donor energy migration (DDEM) from excited to ground state monomers. Both mechanisms represent additional non-radiative relaxation paths. In view of the structural relationship between their system and BP_2, it is very likely that DAEM/DDEM also occurs on BP_2 labeled polymers and polyplexes. However, this work is not focused on investigating this phenomenon in detail.

General aspects of the labeling with BP_2

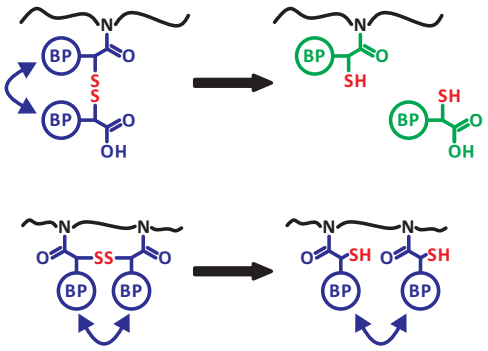

Figure 3.21: Possible BP_2 binding modes on PEI (BP_2-lPEI shown)

Simplified schema of the "dangling" (above) and "bridging" configuration (below) before and after disulfide cleavage. Probe-probe self-quenching (↔) still occurs after cleavage if the remaining BODIPY FL monomers are sufficiently close to each other.

In contrast to all other fluorophores used in this work, BP_2 possesses two equivalent carboxylic groups. If both carboxyls react with PEI then BP_2 is bound in a "bridging" configuration and acts as cross-linker (Figure 3.21). A reaction with one only carboxyl leads to a "dangling" configuration. The binding mode affects BP_2-PEI's fluorescence properties under reductive conditions: Upon cleavage of dangling BP_2, a dequenched, highly fluorescent BODIPY monomer is released and the concentration of polymer bound monomer is halved. The absorption and emission spectra will be dominated by the transitions of the unbound BODIPY monomer. When bridged BP_2 is cleaved, the labeling density does not change and the remaining fluorophores will still experience probe-probe quenching. The fluorescence increase will be relatively low and the absorption spectrum will still show features of aggregates.

Aggregation phenomena on BP_2- and BP-PEIs

All BP_2-polymer derivatives were synthesized according to the method used for the synthesis of FAM-lPEI. The work-up procedure, however, had to be modified to avoid HCl concentrations above 10 mM, otherwise the products slowly and irreversibly lost their color. For the same reason BP_2-S_2-lPEI was not synthesized by cross-linking BP_2-lPEI, as this would have involved a Boc-L-cystine deprotection step with HCl. Instead, the cross-linked polymer was directly labeled with BP_2. The cause for the color loss is unknown. It can be speculated that it involves an electrophilic H^+-attack on positions 2 and 6 of the dipyrromethene, where the least positive charge is located.[113] For the labeling with BP SE the same method was used as for the labeling with TAMRA SE.

Generally, aggregation phenomena were observed for almost all BP_2 and BP SE labeled polymers (with exception of S_2-lPEI; see next section). The absorption and emission spectra of the labeled polymers were exceptionally complex and bore little to no resemblance to unbound BP_2 and BODIPY FL. Since the spectra could be interpreted in a number of ways, the conclusions drawn here are to be considered qualitative rather than quantitative.

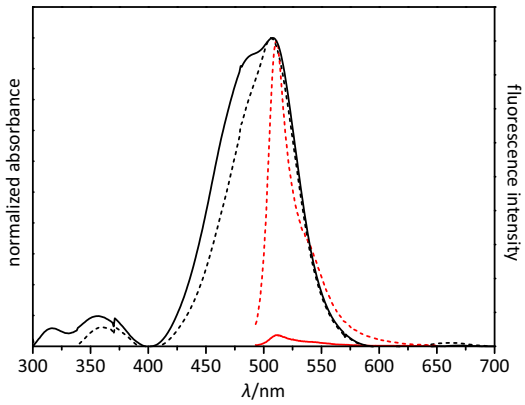

Figure 3.22: Absorption and emission characteristics of cleaved and uncleaved BP_2-lPEI

Baseline corrected absorption spectra (black) of BP_2-lPEI in DPBS in the absence (solid; $\gamma(BP_2\text{-lPEI}) = 2.5$ g/L, $\lambda_{abs\ max} = 490$ nm and 508 nm) and the presence (dashed; $\gamma(BP_2\text{-lPEI}) = 1.0$ g/L, $\lambda_{abs\ max} = 506$ nm) of 100 mM 2-mercaptoethanol. Emission spectra (red; $\lambda_{ex} = 488$ nm, $\gamma(BP_2\text{-lPEI}) = 1.0$ g/L in DPBS) in the absence (solid; $\lambda_{em\ max} = 512$ nm) and the presence (dashed; $\lambda_{em\ max} = 511$ nm) of 100 mM 2-mercaptoethanol. (Experimental details Section 3.4.2)

BP_2-lPEI was the PEI derivative whose spectral properties most closely resembled those of the reference. Similar to BP_2, its absorption spectrum featured an H-dimer band (Figure 3.22, black: solid) next to the monomer's transition ($\lambda_{abs\ max} = 508$ nm). However, this band did not disappear completely in the presence of 2-ME (Figure 3.22, black: dashed), but remained visible as shoulder on the main transition. At the same time, the emission intensity increased almost thirtyfold (Figure 3.22, red: solid and dashed; $\lambda_{em\ max} = 512$ nm) and the presence of unbound dye was verified with TLC (data not shown). Both observations indicate that a significant amount of BP_2 is bound in a dangling configuration. The H-dimer's incomplete disappearance was certainly not the consequence of an incomplete disulfide cleavage. 2-ME is a strong reductant and normally used when a complete disulfide reduction is desired.[152] More likely, the density of the remaining polymer bound BODIPY monomers remained high enough to allow for dye aggregation and in part lPEI might have promoted the aggregation by providing a polar microenvironment around the fluorophores[153]. Unfortunately, the labeling density (and the labeling efficiency) could not be determined spectroscopically due to the presence of aggregates. An exact calculation of the BODIPY-BODIPY distance within the H-dimer was also not possible, as the position of the corresponding absorption band could not be determined unequivocally. Assuming a peak center at 480 nm, R is equal to 0.49 nm. Judged from the fluorescence spectra, the labeling had no detrimental effects on the dye's emissive properties.

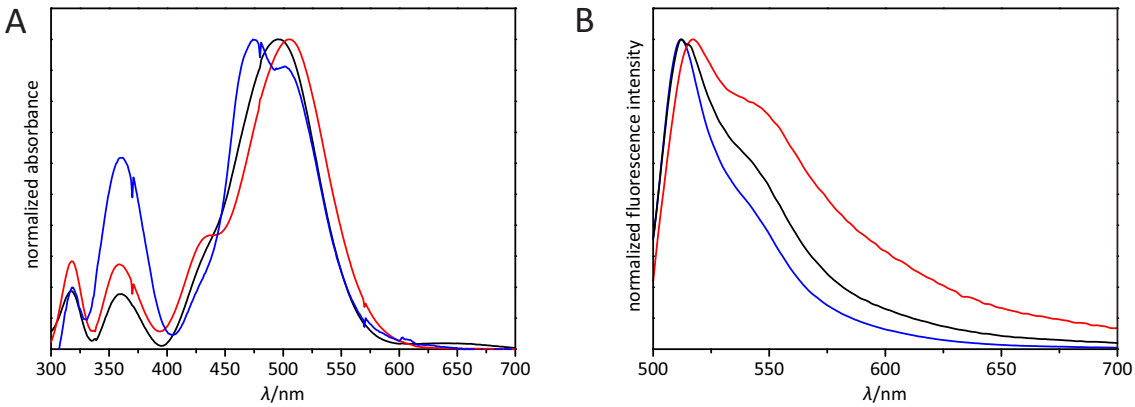

Figure 3.23: Absorption and emission characteristics of BP-lPEIs

A: Baseline corrected absorption spectra of BP-lPEI_1 (black; γ = 2 g/L, $\lambda_{abs\ max}$ = 496 nm), BP-lPEI_2 (red; γ = 2 g/L, $\lambda_{abs\ max}$ = 505 nm), and BP-lPEI_3 (blue; γ = 2 g/L, $\lambda_{abs\ max}$ = 474 nm) in DPBS. B: Corresponding emission spectra (λ_{ex} = 488 nm; $\lambda_{em\ max}$ = 512, 518, and 512 nm). (Experimental details Section 3.4.2)

Since BP-lPEI was to be used as the non-reduction-sensitive reference to BP_2-lPEI, both polymers were labeled at comparable theoretical labeling densities. Thus, it is reasonable to assume that both polymers would have very similar absorption and emission spectra. Surprisingly, that was not the case: The main absorption band off all BP-lPEIs (Figure 3.23A) was structureless with no discernible vibronic shoulder. There was no indication for the presence of H-dimers, expect in case of BP-lPEI_3 (λ_{abs} ≈ 470 nm, R_{est} = 0.47 nm), the derivative with the lowest labeling ratio. The absorption maximum of BP-lPEI_2 was slightly red-shifted in respect of those of the other BP-lPEIs. All polymers demonstrated a distinct transition centered around 430 nm at the short wavelength end of their main absorbance. The fluorescence spectra (Figure 3.23B) were also altered to varying degrees and exhibited what appears to be an increase in the intensity of the vibronic shoulder (λ_{em} ≈ 540-560 nm). The most pronounced changes were found for BP-lPEI_2; it was also the only derivate whose main fluorescence peak was bathochromically shifted ($\lambda_{em\ max}$ = 518 nm). None of these spectral peculiarities were correlated to the theoretical labeling density in any obvious way.

Many spectral features of BP-lPEIs were also found in BP_2-bPEIs (Figure 3.24). This included the presence of a short wavelength absorption band (λ_{abs} ≈ 436-445 nm) and an increased emission intensity around 540-550 nm. Again, H-dimerization occurred only once (BP_2-bPEI 25_1: λ_{abs} = 469 nm, R = 0.43 nm) and as with BP-lPEIs, there was no obvious connection between the labeling density and the shape and position of the absorbance and emission bands. The polymer's redox state had little influence on the emission spectrum, except in case of BP_2-bPEI 25_1, where the maximum shifted from 523 nm to 512 nm after cleavage and the peak width decreased slightly. Moreover, BP_2-bPEI 25_1 was the only derivative with a comparatively large (8.7-fold) intensity increase after total cleavage. Apparently, in that case the labeling conditions were suitable to produce significant amounts of dangling BP_2.

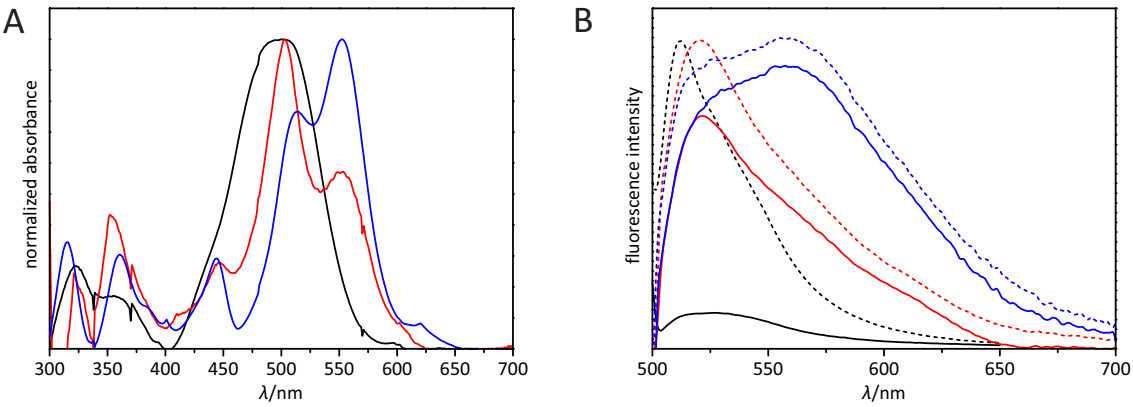

Figure 3.24: Absorption and emission spectra of different cleaved and uncleaved BP_2-bPEI 25 batches

A: Normalized absorption spectra of BP_2-bPEI 25_1 (black, γ = 1.89 g/L, $\lambda_{abs\ max} \approx$ 500 nm), BP_2-bPEI 25_4 (red, γ = 10 g/L, $\lambda_{abs\ max}$ = 447 nm, 503 nm, and 553 nm), and BP_2-bPEI 25_3 (blue, γ = 15.68 g/L, $\lambda_{abs\ max}$ = 444 nm, 514 nm, and 553 nm) in DPBS. The spectra were baseline corrected. B: Emission spectra of BP_2-bPEI 25_1 (γ = 0.33 g/L, $\lambda_{em\ max}$ = 523/512 nm), BP_2-bPEI 25_4 (γ = 0.2 g/L, $\lambda_{em\ max}$ = 522/520 nm), and BP_2-bPEI 25_3 (γ = 0.2 g/L, $\lambda_{em\ max}$ = 558/555 nm) in the absence (solid) and presence of 100 mM 2-mercaptoethanol (dashed). The respective emission intensity increases (λ_{ex} = 488 nm) were 8.7, 1.3, and 1.1-fold. (Experimental details Section 3.4.2)

Other features like an increased fluorescence near 580-590 nm (determined by deconvolution) were exclusively found in labeled bPEIs. The most prominent feature, however, was the low energy absorbance band at about 555 nm. It was present in all the spectra of BP_2-bPEI (except BP_2-bPEI 25_1) and also BP-bPEI (Figure 3.25A, $\lambda_{abs\ max}$ = 558 nm). In case of the latter it was significantly more intense than the monomer transition.

Due to its prominence, the 555 nm transition was examined in more detail. For that, BP-bPEI 25_4 was excited at 580 nm since the low energy transition is the only one with a significant spectral overlap with this excitation wavelength. Upon excitation, an emission at 626 nm was seen (Figure 3.25B, blue; λ_{ex} = 580 nm), which strongly suggests that the 555 nm species is emissive. When an excitation wavelength of 480 nm was used, the long wavelength emission was shifted to shorter wavelengths (Figure 3.25B, black; λ_{ex} = 480 nm, $\lambda_{em\ max}$ = 608 nm). This shift can be explained by the fact that at 580 nm only the red-emitting subpopulation of the absorbing species is excited. The presence of the 555 nm band as well as the absorbance bands located below the main absorbance peak, demonstrate the high susceptibility of most BODIPY labeled PEIs to dye aggregation. The complex spectra of those PEI derivatives made it difficult to characterize each aggregate species exhaustively. For that reason, some of the conclusions drawn here are based on what is known about BODIPY aggregates and fluorophore aggregates in general. One unexpected finding was the coexistence of different aggregate species on the very same dye-polymer system. The ratio between these species was not constant and changed depending on factors such as labeling density and, more importantly, steric effects from the polymer. The polymer's strong influence is reflected in the interchromophoric

distance of PEI-based H-dimers. Here, the BODIPY monomers were even closer (R = 0.43-0.49 nm) together than in BP_2 (R = 0.51 nm). Consistent with this observation was the presence of a high energy band (λ_{abs} ≈ 436-445 nm) next to the H-dimer transition. Such bands have been attributed to the formation of non-emitting H-trimers[96] or higher H-aggregates, which occurs when dyes are located in crowded, molecularly confined environments. Martínez et al., for instance, have demonstrated their formation for rhodamine 6G intercalated in solid thin Laponite clay films,[154, 155] but so far there are no reports on their existence on labeled polymers.

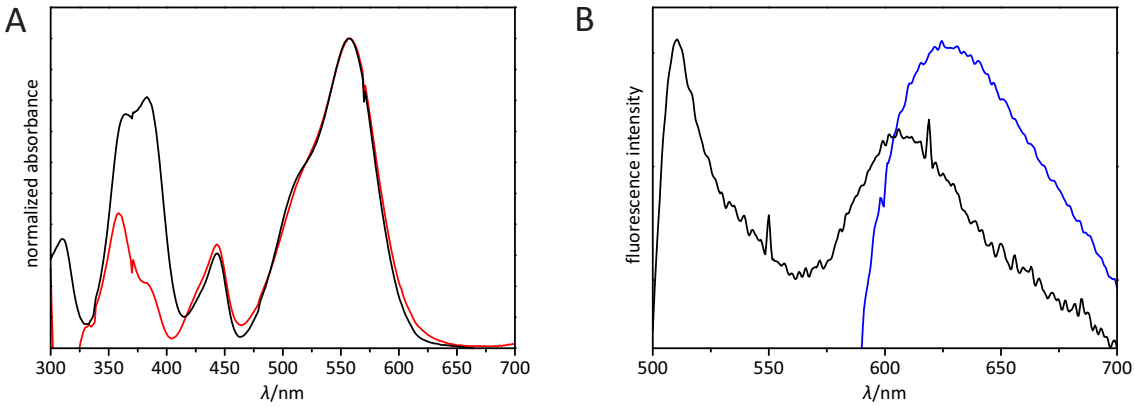

Figure 3.25: Absorption and emission spectra of BP-bPEIs

A: Baseline corrected absorption spectra of BP-bPEI 25_4 (black; $\lambda_{abs\ max}$ = 558 nm) and BP-bPEI 10_2 (red; $\lambda_{abs\ max}$ = 558 nm) in DPBS. B: Emission spectra of BP-bPEI 25_4 in DPBS, excited at 480 nm (black; $\lambda_{em\ max}$ = 511 and 608 nm) and 580 nm (blue; $\lambda_{em\ max}$ ≈ 626 nm). (Experimental details Section 3.4.2)

The nature of the 555 nm absorbing aggregate species is not directly evident. On the one hand, an additional longer wavelength absorption band in combination with a low energy emission typically characterizes J-dimers. On the other hand, the absorption and emission wavelengths of these aggregates clearly differ from BODIPY J-dimers found by other groups. According to the comprehensive photophysical analyses by Johansson and colleagues, BODIPY FL J-dimers absorb between 570 and 580 nm.[114, 115] The exact peak position was highly sensitive to small variations in the chromophore environment. Even with the two closely related BODIPY-lipid model systems examined in their studies, the absorption maxima differed by as much as 7 nm. The proximity to a highly charged polycation like PEI, could arguably have an even more significant impact on the dye's environment and account for the differences in the position of the absorbance band measured here to the literature data. Interestingly, Johansson's group did not find a similar environmental influence on the position of the emission maxima. The broad dimer emission was always centered at about 630 nm. This insensitivity towards environmental conditions was apparently a peculiarity of their experimental system. For BODIPY-PEIs, the deconvolution of the fluorescence spectra revealed a connection between polymer type and the emission wavelength. A fluorescence increase was found at 530-540 nm

and 565-575 nm for BP-lPEIs, at 540-550 nm and 580-590 nm for BP_2-bPEI 25s, and at 610-630 nm for BP-bPEIs. Intensity increases in the very same spectral ranges have been reported for other BODIPY derivatives as well. Makrigiorgos has described two emissions at 546 and 590 nm, when erythrocyte membranes were labeled with sufficiently high amounts of lipophilic C_{16}-BODIPY FL.[156] It must be noted, however, that despite the lack of conclusive absorption spectra, the fluorescence bands were attributed to excimers. Boldyrev et al. have investigated lipid monolayers containing a lipophilic probe designated Me_4-BODIPY-8 and observed bathochromically shifted absorption and emission maxima, as well as a broadening of the emission peak, under high surface pressure conditions (i.e., high dye surface concentrations).[157] The emission broadening was attributed to an increased fluorescence near 570 nm. The authors were unable to identify the definite cause for the low energy emission, but proposed the involvement of an excimer or fluorescent dimer.

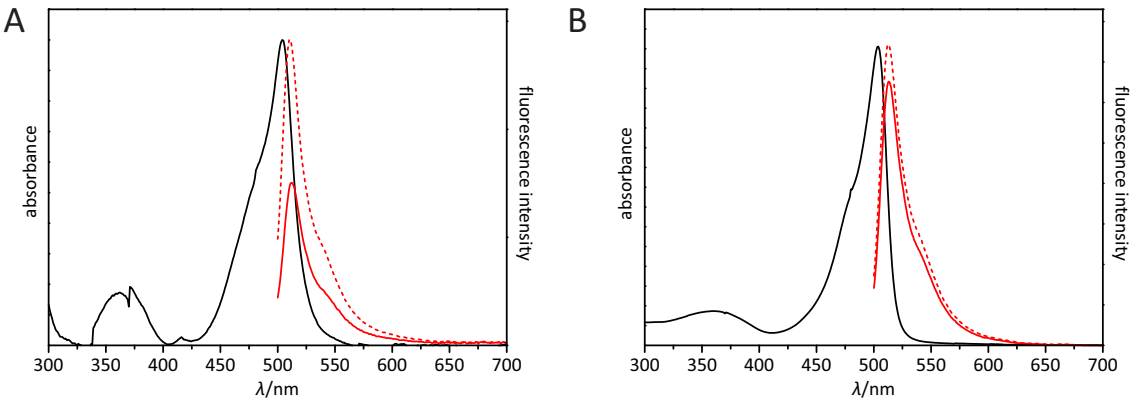

Figure 3.26: Absorption and emission characteristics of cleaved and uncleaved BP_2-S_2-lPEI_1 and BP-S_2-lPEI

A: Baseline corrected absorption spectrum (black) of BP_2-S_2-lPEI_1 in DPBS (γ = 10 g/L, $\lambda_{abs\ max}$ = 504 nm). Emission spectra (red; λ_{ex} = 488 nm, γ = 0.2 g/L in DPBS) in the absence (solid; $\lambda_{em\ max}$ = 512 nm) and the presence (dashed; $\lambda_{em\ max}$ = 511 nm) of 100 mM 2-mercaptoethanol. The emission intensity increase was 1.9-fold. B: Absorption spectrum (black) of BP-S_2-lPEI (γ = 3.1 g/L, $\lambda_{abs\ max}$ = 504 nm) in DPBS. Emission spectra (red; λ_{ex} = 488 nm, γ = 100 mg/L in DPBS) in the absence (solid) and presence of 100 mM 2-mercaptoethanol (dashed). The emission intensity increase (λ_{em} = 513 nm) was 1.14-fold. (Experimental details Section 3.4.2)

It is doubtful that all the different emission phenomena observed for BODIPY-PEIs and lipophilic BODIPY derivatives can be attributed to one single cause, like the formation of J-dimers. The apparent changes in the structure of BODIPY's vibronic shoulder ($\lambda_{em} \approx$ 530-560 nm), for instance, might originate from a "rigid medium" effect. This effect has been described for dyes in rigid and constrained environments.[154] Without doubt, compressed lipid films can be considered as rigid environments, but it is not clear if this similarly applies to BODIPY-PEIs. Even though the fluorescence spectra of the BODIPY-PEIs were examined closer, no clear evidence for a rigid medium effect was found due to the high complexity of the spectra. The spectra of TAMRA-lPEI and TAMRA-S_2-lPEI (Figure 3.15B) were more suitable for analysis and indeed the vibronic shoulder ($\lambda_{em} \approx$ 630-670 nm) of the cross-linked, arguably more rigid derivative, was

more intense. Admittedly, the effect was relatively small but still indicates that PEI bound BODIPYs may be affected, too. The more significant spectral changes, especially in the longer emission wavelength range, might result from the presence of structurally diverse emissive dye species. As far as BODIPY-PEIs are concerned, these species cannot be excimers as suggested by Makrigiorgos and Boldyrev et al., otherwise the corresponding absorption spectra would be identical to those of BODIPY monomers. More likely, BODIPY forms emissive ground state aggregates on PEI. In case of BP-bPEIs, the spectral similarities to Johansson's BODIPY-lipid systems suggest that these aggregates are J-dimers ($\vartheta \approx 55°$). The structure of the other BODIPY-PEI aggregates could not be resolved based on the available spectral data. Based on general photophysical considerations, some improbable structures, like J-dimers with $\vartheta < 55°$, can be ruled out. Such dimers would emit beyond 608-626 nm due to the increased exciton splitting, but there is no conclusive evidence for that in the fluorescence spectra.

It was also of interest to understand the reason behind the vastly different aggregation tendencies among the various fluorophore-PEI derivatives. BODIPY never aggregated on S_2-lPEI (Figure 3.26), regardless of the labeling density, or the probe's structure or binding mode. On bPEI or lPEI, however, it aggregated even at very low labeling densities. In case of TAMRA, aggregation was seen on bPEI, but not on lPEI and S_2-lPEI. These observations suggest that the polymer, i.e., the polymer's structure, plays the most important role in the aggregation process, although there is some contribution from the fluorophore itself, too. The polymer structure seems to determine whether an aggregation is promoted or prevented. Other factors like the labeling density rather determine which aggregate species form. It can be speculated how the polymer influences the complex interplay between attractive and repulsive forces during the aggregation process. On the one hand, the polycation PEI could force lipophilic fluorophores closer together by providing a polar microenvironment. On the other hand, steric hindrance from the polymer chains might prevent just that. The relative strength of these factors depends on so many variables (e.g., branching degree, polymer rigidity and size, or charge density) that it is difficult to predict the aggregation behavior for a given dye-polymer combination. In order to create an empirical model of this process, much more data would be needed. From a practical point of view, it is easier to simply test if the photophysical properties of a polymer/dye combination are suitable for the intended application. Many of the polymer-dye combinations investigated here, for instance, are less useful as fluorescent probes for studying gene delivery because of their strong aggregation tendencies. As far as BP_2 labeled S_2-PEIs are concerned, however, nothing in the photophysical data indicates that they cannot be used to investigate the thiol dependent polymer degradation. Caution should be exercised when using BP-PEIs as uncleavable reference. Their photophysical properties are not necessarily comparable to those of BP_2-PEIs.

Additional investigations and cleavage studies

The previous section revealed how important it is to consider dye aggregation when using fluorescent probes to investigate polycationic gene carriers. There are, however, even more things to consider. It is unclear, for instance, if the BP_2 probe attached to the polymer is still cleaved under physiological conditions like the free probe. It is also unclear if the findings made for PEIs also apply to other polycations. Furthermore, since BP turned out to be less suitable as fluorescence intensity standard, another more suitable dye must be found.
In order to shed light on those matters, it was tested if TAMRA-lPEI could serve as emission intensity reference for BP_2-PEIs. Moreover, BP_2 labeled PEI and PLL were exposed to a cytosolic GSH concentration and BP_2 labeled PLL derivatives were characterized photophysically.

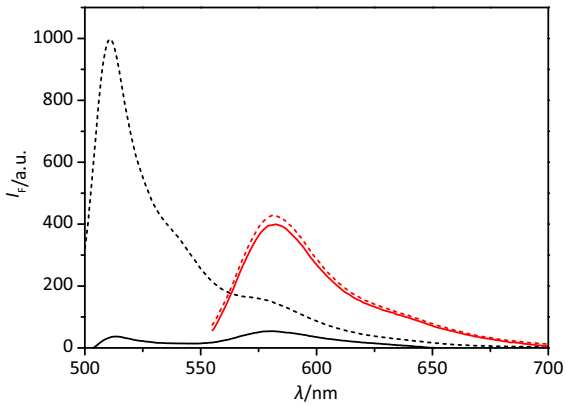

Figure 3.27: Emission spectra of a BP_2-lPEI/TAMRA-lPEI_2 mixture
A mixture of BP_2-lPEI (γ = 200 mg/L) and TAMRA-lPEI_2 (γ = 25 mg/L) in DPBS was excited at 488 nm (black) and 543 nm (red) in the absence (solid) and the presence (dashed) of 100 mM 2-mercaptoethanol. The emission intensity increase after disulfide cleavage was 27-fold for BP_2-lPEI (λ_{ex} = 488 nm, λ_{em} = 512 nm) and 1.1-fold for TAMRA-lPEI_2 (λ_{ex} = 543 nm, λ_{em} = 583 nm). (Experimental details Section 3.4.2)

BP is not an ideal choice as redox inert fluorescence standard mainly for two reasons: Its spectral overlap with BP_2 requires it to be measured in a separate sample and, more importantly, depending on the polymer it is attached to, its aggregation behavior significantly differs from that of BP_2. In many cases it makes more sense to use a reference dye less prone to aggregation and whose emission does not overlap with BODIPY's. Since TAMRA may meet those criteria, at least in part, a mixture of BP_2-lPEI and TAMRA-lPEI_2 was tested for its suitability in multicolor applications. For that, both polymers were mixed at a ratio where the emission maxima (Figure 3.27, solid; λ_{ex} = 488 nm, λ_{em} = 512 and 583 nm) of both dyes were equiintense. The sample was excited at wavelengths that match the emission lines of argon ion (488 nm) and helium neon (543 nm) lasers, which are frequently used in flow cytometry and CLSM. As expected, the BODIPY and TAMRA emissions were well separated. This was not completely the case after the addition of 2-ME (Figure 3.27, dashed; λ_{ex} = 488 nm), where the TAMRA emission appeared as shoulder on the BODIPY transition. This did not, however, con-

tribute to the emission in the wavelength range normally used for the detection of green-emitting fluorophores (λ_{em} ≈ 505-545 nm). Conversely, with an intensity increase of only 10 % (Figure 3.27, red; λ_{ex} = 543 nm) the fluorescence of cleaved BP_2-lPEI did not significantly add to that of TAMRA. According to these results, it is feasible to measure the BP_2- and TAMRA-PEI fluorescence independently in commonly used experimental setups and TAMRA-PEI can indeed be used as emission standard for the cleavage of BP_2-PEIs. The situation is surprisingly different when the labeled polymers are in complex with nucleic acids (Chapter 4). In that case the photophysical properties of the fluorophores are no longer independent.

The previous results have demonstrated that PEI attached BP_2 is readily cleaved under strongly reducing conditions (100 mM 2-ME). Since the cleavability of BP_2-PEIs under physiological conditions is an essential prerequisite for further studies concerning the in vitro degradation (Chapter 4) and intracellular processing of polyplexes (Chapter 5), the emission intensity of all BP_2 labeled polymers was also measured in the presence of 5 mM GSH, the most abundant cellular thiol.

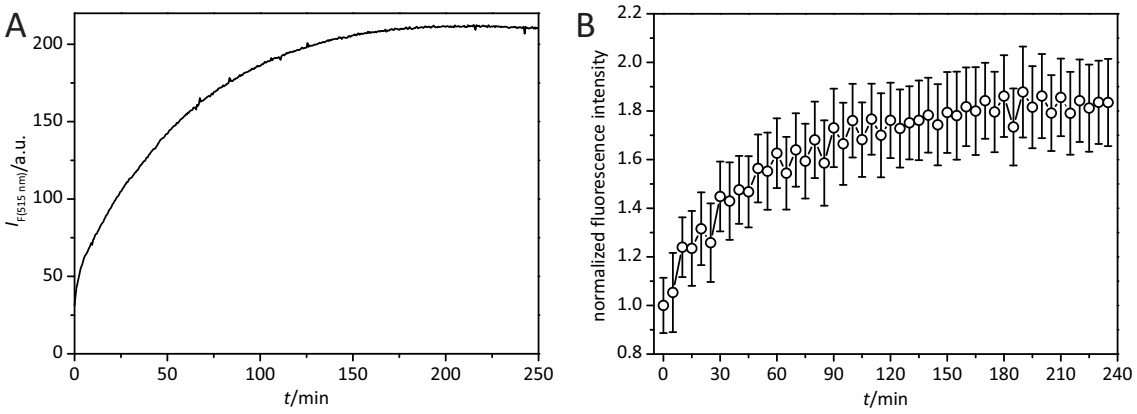

Figure 3.28: Time course of the emission intensity of BP_2-lPEI and BP_2-S_2-lPEI_1 in the presence of GSH

All samples were excited at 488 nm; *c*(GSH) = 5 mM. A: BP_2-lPEI (γ = 50 mg/L) in DPBS. The data (n = 2) were collected in 30 s intervals ($t_{½}(I_{F\ 515\ nm})$ = 57 min). The data were not corrected for photobleaching or normalized against the intensity at the first time point. B: BP_2-S_2-lPEI_1 (γ = 50 mg/L) in a 50 mM phosphate buffer (pH = 7.11). The data (n = 3) were collected in 5 min intervals ($t_{½}(I_{F\ 512\ nm})$ = 52 min); mean values ± sample standard deviation shown. (Experimental details Section 3.4.2)

Upon the GSH addition, the emission intensity of all BP_2-PEI samples steadily increased over time until it reached a plateau after about 150 min (Figure 3.28 and Figure 3.29). Although BP_2-PEIs were indeed cleaved under near physiological conditions, there were substantial differences to the cleavage with 2-ME. First of all, while the reaction with 2-ME was completed almost immediately, the reaction with GSH took far longer; the reaction half-lives $t_{½}$ were in the range of 45 to 60 min. Moreover, the cleavage with GSH resulted in much lower maximum intensity increases (e.g., BP_2-lPEI + GSH: ≈ 7×, + 2-ME: ≈ 30×), suggesting an incomplete probe cleavage. How can these differences be explained? The vastly different cleavage rates cannot

be attributed to a steric effect of the polymer, as the cleavage rate did not decrease with increasing polymer M_w or degree of branching. In fact, the highest rate was obtained for the cleavage of BP_2-bPEI_1. Apparently, the polymer does not impede the attack of the bulkier reductant GSH to a notable degree. More likely, the differences in the cleavage rates and maximum fluorescence intensity increases are indirectly related to the overall low GSH concentration. In principle, enough GSH would have been present at the beginning of the reaction to push the chemical equilibrium towards a complete reduction of all disulfides in the sample. On the other hand, the initial GSH excess may have been too low to allow for a high reaction rate, so competing reactions like GSH's gradual oxidation to GSSG by dissolved oxygen became significant. Eventually, the GSH concentration had decreased so much that the disulfide cleavage essentially stopped and fluorescence intensity remained constant.

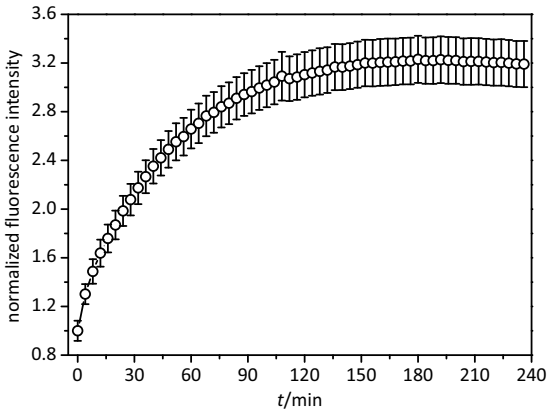

Figure 3.29: Time course of the normalized emission intensity of BP_2-bPEI 25_1 in the presence of GSH

BP_2-bPEI 25_1 (γ = 1 g/L) in 50 mM phosphate buffer (pH = 7.11) in the presence of 5 mM GSH (λ_{ex} = 488 nm, λ_{em} = 515 nm). The data (n = 3) were collected in 4 min intervals ($t_{½}(I_{F\ 515\ nm})$ = 44 min). (Mean values ± sample standard deviation; experimental details Section 3.4.2)

As demonstrated in the previous sections, the photophysical properties of BP_2 labeled PEIs are extremely sensitive to the "host" polymer structure. This raises the question if this is a peculiarity of PEIs or if other polycations are affected as well. To answer that, the photophysical properties of BP_2 labeled linear and disulfide cross-linked PLL were compared to those of their PEI counterparts.

BP_2-PLL's absorption and emission spectra (Figure 3.30A, black and blue) were, apart from minor shifts in the transition maxima ($\lambda_{abs\ max}$ = 501 nm, $\lambda_{em\ max}$ = 509 nm), identical to those of the cross-linked PEI derivatives BP_2-S_2-lPEI_1 and BP-S_2-lPEI, i.e., the BODIPY reference. There was no indication for the presence of H-dimers like with BP_2-lPEI. BP_2-S_2-PLL_1's absorption spectrum (Figure 3.30A, red), which was representative for all BP_2-S_2-PLL derivatives, entirely lacked, however, the transition of monomeric BODIPY. Instead, an almost featureless transition was present at 465 nm, with a very small vibronic shoulder at 445 nm. These spectral properties, together with the fact that it was impossible to obtain an emission spectrum, even in the

presence of 100 mM 2-ME, suggest complete H-aggregation. This conclusion was substantiated by the absorption spectrum's remarkable similarity to the calculated spectrum of a pure BODIPY H-dimer[117]. Complete H-aggregation is known to occur during the long-term storage of highly concentrated BODIPY solutions and, at a much faster rate, in case of BODIPY being embedded in a sol-gel derived glass.[117] So far there are no reports on a similar behavior of polymer bound BODIPY. This finding clearly suggests that the tendency to aggregate is a property that many fluorophores attached to polycations may share. It also again illustrates the problem of predicting dye aggregation based on the host polymer structure. BP_2 aggregated on cross-linked PLL, but not on linear PLL. For lPEI and S_2-lPEI the situation was exactly the other way round.

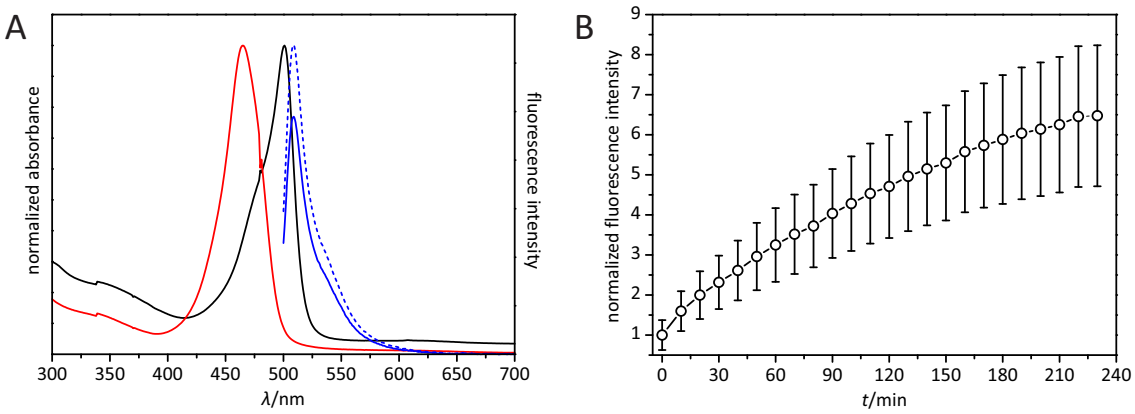

Figure 3.30: Absorption and emission characteristics of cleaved and uncleaved BP_2 labeled PLL derivatives

A: Normalized absorption spectra of BP_2-PLL (black; γ = 5 g/L, $\lambda_{abs\ max}$ = 501 nm) and BP_2-S_2-PLL_1 (red; γ = 2 g/L, $\lambda_{abs\ max}$ = 465 nm) in DPBS. Emission spectra of BP_2-PLL (blue; γ = 100 mg/L in DPS, $\lambda_{em\ max}$ = 509 nm) in the absence (solid) and presence of 100 mM 2-mercaptoethanol (dashed). The emission intensity increase (λ_{ex} = 488 nm) was 1.3-fold. BP_2-S_2-PLL_1 showed no measurable fluorescence. B: BP_2-PLL (γ = 100 mg/L) in 50 mM phosphate buffer (pH = 7.11) – Time course of the normalized emission intensity at 509 nm (λ_{ex} = 488 nm) in the presence of 5 mM GSH. The data (n = 3) were collected in 10 min intervals ($t_{½}(I_{F\ 509\ nm})$ = 165 min)); mean values ± sample standard deviation shown. (Experimental details Section 3.4.2)

Another interesting experimental result was the extraordinary stability of the H-dimers on S_2-PLL. The dimers neither dissociated in less polar solvents (80 % ethanol or pure methanol; data not shown) nor when 2-ME was added. The irreversible nature of the aggregation may be an indirect effect of the cross-linked polymer's structural compactness. In other words, PLL's n-butylamine side chains are close enough together to provide a (micro)environment of sufficient polarity and restricted molecular mobility to allow for H-dimerization in relatively nonpolar solvents. Another contributing factor to the aggregate stability might be steric hindrance of the side chains that blocks attacking thiols. Preventing the disulfide cleavage may prevent the dye monomers from moving away from each other. Unfortunately, the experimental data were ambiguous in that respect. BP_2-S_2-PLL's resistance to the degradation with 2-ME, and BP_2-PLL's very slow reaction with GSH (Figure 3.30B; $t_{½}$ = 165 min) compared to BP_2-PEIs argues for a

steric protection. Then again, cleavage with the bulkier reductant GSH resulted in a higher maximum intensity increase (BPs-PLL: GSH > 5-fold, 2-ME 1.3-fold) than with 2-ME. Obviously, there are additional, currently unknown factors that control the cleavage.

3.6 Conclusions

DMTMM is a useful condensing agent for labeling polycations with xanthene and boradiazaindacene dye derivatives. The fact that the complexity of the labeling and work-up procedure is comparable to the use of pre-activated dyes, but relies on considerably cheaper, readily available reagents overcompensates for the relatively low labeling efficiency. In case of xanthenes the labeling reaction is regioselective. Only the carboxylic group farthest away from the xanthene ring is susceptible to the amidation with a polymer amine. Thus, at least when linear and cross-linked PEIs are labeled, there are no changes in the dye's acid-base equilibrium. In many other cases, however, the reaction with the polymer leads to profound changes in the dye spectra and emission intensities. These changes are related to the formation of various aggregate species, including non-emissive H-dimers and emissive J-dimers. The dye aggregation is not directly a consequence of the DMTMM based labeling method, similar phenomena are observed when pre-activated dye are used, but arises from an interaction of the polycation with the attached dye. Until now, this polymer effect had not been investigated as most analytical methods for the characterization of gene delivery vehicles (e.g., uptake efficiency and polyplex integrity) quantify the emission intensity of fluorescently labeled nucleic acids. However, the development of more efficient gene delivery systems will arguably require a better knowledge about the polymer component's fate, too.

It was possible to identify the polymer structure (i.e., steric effects) and polymer chemistry (i.e., degree of amine substitution) as the decisive factors that govern the polymer-dye interaction. Other factors such as fluorophore type and labeling density also influence this interaction, but it was neither possible nor intended to identify and quantify all of them exhaustively. Therefore, the results obtained here should be regarded as a starting point for further, more detailed studies.

One of the intentions of this work was to create fluorescent probes that can be used to investigate the degradation of reduction sensitive PEIs. To this end, S_2-lPEI and the non-cleavable reference polymer lPEI were labeled with BP_2. The corresponding products possess favorable photophysical properties and are cleaved under near physiological redox conditions. Both qualities are important prerequisites for the experiments described in Chapters 4 and 5.

4 Polymer/nucleic acid interaction studies

4.1 Introduction

The interactions between polycation and nucleic acid play a crucial role in determining the delivery success of polyplexes. On the one hand, polyplexes have to remain stable until they reach their target site; on the other hand, they must have efficient means for on-target cargo release (see Section 2.1). It is not surprising that countless studies have been devoted to this subject and some trends concerning the optimal polymer structure for high transfection efficiency and low toxicity have emerged. Still the structure-activity relationship is often not well understood[67].

Most studies explore the polymer-nucleic acid interaction purely on a phenomenological basis, which is in part certainly related to the extraordinary complexity of this subject and the lack of sufficiently sensitive analytical methods[158]. The lack of knowledge is, for instance, reflected in the lack of published binding constants for PEI and PLL polyplexes.[67] Some studies try to shed light on the physicochemical principles underlying polyplex formation and dissociation with the help of thermodynamic and spectroscopic methods. It is understood that polyplex formation is a multi-step process, initiated by an unspecific, long-range electrostatic attraction between carrier polycation and polyanionic nucleic acid. The nucleic acid's charge density can be considered to be constant due to the complete deprotonation of the backbone phosphates under physiological pH. The polycation's charge varies with the polymer structure. For polyamines like PEI, protonation degrees between 10 and 50 % have been reported, depending on the ratio of primary, secondary, and tertiary amines.[159] The protonation state of the amines directly influences the mechanism of complex formation: Under acidic conditions the formation of PEI and PLL/DNA complexes is cooperative, meaning the binding of an amine promotes the binding of additional amines.[67] This is likely because the amine cation's charge is neutralized by the DNA phosphate, which increases the pK_a of neighboring ionizable secondary amines.[160] At pH = 7.4 and low N/P values polyplexes form via an independent binding mechanism. At higher N/P ratios, the binding also becomes cooperative. The pH-effect is less pronounced for PLL-polyplexes, as PLL's primary amines (pK_a = 9-10[71]) are completely protonated under phys-

iologically relevant conditions.[160] Two binding modes have been described for the actual binding of PEI on DNA.[158] In the first binding mode, PEI binds in the DNA groove and interacts with electronegative nitrogen and oxygen atoms of the DNA base[159] and is deprotonated[158]. This process is entropy driven by the release of strongly bound water molecules in the groove region, analogous to the DNA's interaction with certain proteins. The second binding mode, where PEI binds "externally" on the phosphate backbone, is more important in regard to polyplex formation, as the DNA's charge is here neutralized by the polyamine.[158] At 89-90 % charge neutralization, the DNA collapses into small, highly ordered particles with toroidal morphology.[161] The accompanying immense volume reduction in the range of a factor of 10,000 is prerequisite for encapsulating a large and extended molecule like plasmid DNA into a nanoparticulate carrier system. DNA condensation faces several significant energetic barriers, such as electrostatic repulsion of the backbone phosphates, loss of configurational entropy, and stiffness of the double helix. The net attractive force per base pair is very small, thus, condensation only occurs for DNA fragments longer than about 400 bp.[161] For that reason and for the fact that dsRNA is stiffer than dsDNA, 21 bp siRNAs are not likely to condense further with cationic agents. Instead, incomplete encapsulation and the formation of excessively large complexes occur.[38]

The individual contribution of the two binding modes depends on the N/P ratio. With increasing N/P PEI is redistributed from the groove to the backbone,[158] and the polyplex structure varies accordingly. At low N/P, i.e., below the critical ratio of about 2-2.5 for most polycations,[67, 160, 162-164] open particles form where DNA loops extend into the surrounding medium.[162] At the critical ratio, all phosphates are polymer bound, resulting in dense and condensed particles, that tend to aggregate due to their charge neutrality.[67] Above the critical ratio, excess polymer forms a protective shell structure around the polyplex core. The excess polymer is essential for polyplex stability and for the delivery success.[67, 162] However, free or weakly bound PEI also mediates toxicity, limiting in vivo use.[164]

The details of polyplex formation and nucleic acid condensation have been investigated with a variety of analytical methods. A commonly used method involves following the emission intensity of an intercalating dye, mostly ethidium bromide (EtBr), in DNA-polymer mixtures. With increasing polymer content a drop in the emission intensity is observed, which is usually interpreted as dye displacement due to DNA condensation.[160] Polyplex stability is also assessed by adding a polyanion competitor like heparin. In the presence of the competitor, the DNA is displaced from the complex, decondenses, and interacts with the intercalator. These assays have several shortcomings. First of all, it is implied that the dye's ability to interact with the nucleic acid is exclusively determined by the condensation state of the latter. This is an undue simplification. EtBr and similar intercalators have been demonstrated to be directly displaced by

(poly)cations,[163, 165] so the change in fluorescence intensity not only reflects the DNA's condensation state but also the dye's DNA affinity.[158] The polyanion competition assay has a similar limitation. Here, the apparent polymer-DNA interaction strength will vary with the polycation's affinity to the competitor, making it questionable to compare different polymer classes.[160] Last but not least, above the critical ratio information about the polyplex structure is not accessible with methods based on intercalators, as the dyes have already been released completely at the critical ratio.

Some disadvantages of dye displacement assays can be avoided by using a method based on the condensation dependent self-quenching of fluorophores covalently linked to the DNA backbone. Here, DNA is labeled with approximately one fluorophore per one hundred base pairs. At this labeling density no probe-probe self-quenching is observed, unless, DNA condensation brings the fluorescent moieties close enough together.[163, 165] As this method is insensitive to cation displacement, it detects DNA condensation in cases where the EtBr method fails. With the help of this assay it could be shown, for instance, that the presence of Ca^{2+} significantly lowers the amount of polycations required for complete condensation.[163]

Practically all the studies focus on the nucleic acid component of the polyplex. The polymer's fate is only assessed indirectly, if at all. There have been attempts to study carrier structure and integrity with the help of dual-labeled polyplexes.[166-168] The idea is, that FRET between a labeled polymer and a labeled nucleic acid is inefficient unless both components are in close proximity within an intact polyplex. Ko et al., for instance, have studied the interaction of a rhodamine labeled 2.7 and 25 kDa bPEI with a fluorescein labeled 20 bp oligodeoxynucleotide. They found evidence that the amines of the 2.7 kDa PEI have a better accessibility for the interaction with the nucleic acid than those of the higher molecular weight PEI, presumably due to a lower steric hindrance. In addition, they were able to quantify the amount of unbound polycation.[167] Despite the usefulness of FRET based methods to elucidate polyplex structure, it must not be forgotten that FRET measurements require considerable preparation and it can be hard to gain reliable data. Not only does the introduction of two extrinsic fluorophores require time and effort, but may also alter the physical properties of the molecules of interest. Moreover, the dye ratio for an optimal FRET efficiency is not necessarily one to one, necessitating additional optimization steps.[167, 168] The presence of local electric fields near highly charged molecules can also negatively impact FRET as it may restrict the alignment of the fluorophore dipole moments and change the orientation factor.[167]

One of the major focusses of this work is to obtain more information on the polymer's fate in nucleic acid complexes. In order to avoid the limitations of the fluorescence methods outline above, polycation/nucleic complexation, cleavage of reduction sensitive polyplexes, and nucle-

ic acid release were investigated with newly developed methods based on fluorescence quenching.

4.1.1 Quenching of fluorescence

Fluorescence quenching refers to any process that reduces the emission intensity of a sample. It usually depends on close molecular interactions, such as collisions with quenchers, the formation of ground state complexes (see Section 3.2.2), and excited state reactions and can serve as tool to study biochemical systems. As a matter of fact, one of the most frequently used bioanalytical procedures, the detection and quantification of DNA with the intercalating dye ethidium bromide relies on quenching. In aqueous solution, ethidium bromide is almost non-fluorescent due to an excited state reaction, i.e., a proton transfer to neighboring water molecules[169], and the interaction with dissolved oxygen, one of the best-known collisional quenchers[170]. When intercalated in double stranded DNA, however, the dye is efficiently shielded from solvent molecules and oxygen, leading to a several tenfold emission intensity increase.

Quenching processes resulting from collisions between quenchers and fluorophores are called collisional or dynamic quenching. In these cases, both molecules have to collide during the fluorophore's excited state lifetime and the fluorophore returns to the ground state without the emission of a photon. Mathematically this process is described by the Stern-Volmer equation. In the absence of a quencher, the fluorescence lifetime τ_0 depends on the rate constants for the radiative transition k_r and all nonradiative transitions excluding quenching k'_{nr} ($k'_{nr} = k_{nr} - k_q[Q]$; cf Section 3.2.2):

$$\tau_0 = \frac{1}{k_r + k'_{nr}} \tag{4.1}$$

In the presence of a given quencher concentration [Q] the excited state is additionally depopulated in a nonradiative processes k_q. The lifetime is then given by:

$$\tau = \frac{1}{k_r + k'_{nr} + k_q[Q]} \tag{4.2}$$

By using the usual definition for the fluorescence quantum yield Φ_f (3.8) and the definition for τ_0 (4.1), the ratio between the quantum yields in the presence (Φ) and absence (Φ_0) of quenching is given by:

$$\frac{\Phi_0}{\Phi} = 1 + k_q \tau_0 [Q] \tag{4.3}$$

As both the fluorescence intensity *F* and the lifetime τ are directly proportional to the respective quantum yields, the Stern-Volmer relationship can be written as

$$\frac{\Phi_0}{\Phi} = \frac{F_0}{F} = \frac{\tau_0}{\tau} = 1 + k_\mathrm{q}\tau_0[Q] = 1 + K_\mathrm{D}[Q] \tag{4.4}$$

where K_D is the Stern-Volmer quenching constant.
It is an important characteristic of dynamic quenching that it decreases the fluorescence intensity and lifetime, equally.

Quenching can also be the result of the formation of non-fluorescent ground state complexes between quencher and fluorophore (cf Section 3.2.2). In this process called static quenching the association constant K_S for the complex formation is given by

$$K_\mathrm{S} = \frac{[FQ]}{[F][Q]} \tag{4.5}$$

where [*FQ*], [*F*], and [*Q*] are the equilibrium concentrations of the complex, uncomplexed fluorophore, and uncomplexed quencher, respectively. The total fluorophore concentration $[F]_0$ is given by:

$$[F]_0 = [F] + [FQ] \tag{4.6}$$

Using this relation, the first equation can be rearranged to:

$$K_\mathrm{S} = \frac{[F]_0 - [F]}{[F][Q]} = \frac{[F]_0}{[F][Q]} - \frac{1}{[Q]} \tag{4.7}$$

As the fluorescence intensity *F* is directly proportional to the fluorophore concentration [*F*] this equation can be further rearranged to:

$$\frac{F_0}{F} = 1 + K_\mathrm{S}[Q] \tag{4.8}$$

Given the similarity to equation (4.4) it is evident that static and dynamic quenching cannot be distinguished based on intensity measurements alone, but require information on the fluorescence lifetime. In contrast to collisional quenching, static quenching does not alter τ, as the complexed fluorophores are non-fluorescent and only the uncomplexed, unperturbed species can be observed.
In many instances, both quenching mechanisms occur simultaneously and can be described with a modified Stern-Volmer equation:

$$\frac{F_0}{F} = (1 + K_D[Q])(1 + K_S[Q]) \quad (4.9)$$

These cases can easily be identified by an upward curvature of the Stern-Volmer plot.

Quenching vs Resonance Energy Transfer

Fluorescence quenching requires molecular contact at the van der Waals radii. At this distance the electron clouds of fluorophore and quencher interact and can exchange electrons. The rate constant k_E for the electron exchange interaction decreases exponentially with distance according to

$$k_E(r) = A\ \exp[-\beta(r - r_c)] \quad (4.10)$$

where A is a pre-exponential factor with a value near 10^{13} s^{-1} for orbital interactions, β is an empirical, donor-quencher pair dependent parameter with a typical value around 10 nm^{-1}, and r_c is the distance of closest approach (collisional radius). At distances greater than several tenths of nanometers the exchange interaction becomes insignificant. Hence, quenching is sensitive to factors that affect molecular contact.

In contrast, for RET the energy transfer rate k_T for the through-space interactions is described by

$$k_T(r) = \frac{1}{\tau_D}\left(\frac{R_0}{r}\right)^6 \quad (4.11)$$

where R_0 is the Förster distance, τ_D is the donor lifetime in absence of an acceptor, and r is the donor-acceptor center-to-center distance. The energy transfer rate remains high over several nanometers for typical fluorophore pairs, but is essentially zero in the range of strong coupling. RET based techniques have been used to investigate polycation-nucleic acid interactions on double labeled polyplexes.[166, 167] So far there are no detailed, comparable studies employing quenching techniques. This is surprising because, unlike RET, quenching is sensitive to electrostatic interactions and steric factors that arguably govern polyplex formation[167]. Thus, data from quenching assays could complement the information gained from RET measurements.

4.1.2 Photoinduced Electron Transfer (PET)

The fluorescence quenching assay developed in this work to investigate the interaction of various nucleic acid types with PEIs is partly based on a photoinduced electron transfer. In order

for PET to occur, an electron donor (D) and an electron acceptor (A) must collide to form an encounter complex (DA). In most cases, the PET donor is the quencher and the acceptor (A*) is the excited fluorophore. The excitation energy increases the fluorophore's ability to accept electrons and drives the charge separation. Once the electron has been transferred, the excited charge transfer complex ($[D^{\cdot+}A^{\cdot-}]^*$), a radical ion pair, relaxes to the ground state via charge recombination without the emission of a photon.

In the assay developed here, the electron is transferred from the nucleobase guanine to TAMRA attached to PEI. Due to its low oxidation potential compared to the other nucleobases, only guanine is an efficient quencher for numerous fluorophores.[79, 171] Using guanine as intrinsic quencher has an important advantage over assays that use two extrinsic fluorophores. Each additionally introduced probe increases the risk of altering intermolecular interactions and interfering with normal biological processes. Besides, the labeling process becomes cheaper and less time-intensive, if the molecules of interest contain suitable binding sites at all[172]. Amongst others, guanine based PET quenching has been used for the construction of molecular beacons[172] and in structural studies of RNA[79].

4.2 Materials and methods

4.2.1 Dequenching assay

The polyplex dequenching measurements were carried out according to the general procedure outlined in Section 3.4.2. In short, the data was collected with a LS 55 fluorescence spectrometer (PerkinElmer, Rodgau, Germany), equipped with a R928 PMT and the plate reader accessory in combination with white Nunc PS F96 MicroWell Plates (Thermo Fisher Scientific Inc., Waltham, MA., USA). The sample fluorescence was excited and detected at 488 nm and 512 nm, respectively.

Prior to the measurements, the polymer (2 g/L in PBS) and the nucleic acid (0.8-2.43 g/L in water) stock solutions were diluted with 50 mM phosphate buffer (pH = 7.11). For polyplex formation (N/P = 12), 20 µL of the polymer dilution was added to an equal volume of the nucleic acid dilution. After vortexing, the polyplexes were left to mature for at least 5 min. The samples contained either 1.62 µg pDNA or 1.67 µg siRNA, which corresponds to 5.25 nmol phosphate residues. The polyplex samples were then diluted to 100 µL with buffer or a mixture of buffer and GSH ($c(GSH)_{final}$ = 5 mM), transferred to 96-well microplates and measured immediately. Each sample was prepared in triplicate and was measured every 4 or 5 min over the period of 4 h. Samples containing no GSH served as reference to correct for photobleaching. Finally, the data were normalized against the emission intensity at the first time point.

4.2.2 Steady-state and time-resolved fluorescence quenching assays

In order to gain a better understanding of the quenching mechanisms of fluorescent labels in polyplexes, different nucleic acids complexes with TAMRA-lPEI_2 were investigated with steady-state and time-resolved fluorescence methods. Additionally, BP_2-lPEI based polyplexes were investigated with steady-state fluorescence spectroscopy. The nucleic acids used in the experiments comprise plasmid DNA (see Section 2.2.3), siRNA (13.4 kg/mol), and two custom-made DNA oligomers $p(dCdG)_{14}$ (8.60 kg/mol) and $p(dAdT)_{14}$ (8.58 kg/mol) from Eurofins Genomics GmbH (Ebersberg, Germany). Before use, the lyophilized single-stranded oligomers were resuspended in annealing buffer (10 mM TRIS, 1 mM EDTA, and 50 mM NaCl; pH = 7.5) to a final concentration of 1 g/L (116.4 µM) and then annealed in a thermal cycler (Mastercycler, Eppendorf AG, Hamburg, Germany) according to the following program: *V*(sample) = 100 µL; 98 °C for 15 min, controlled cooling down to 22 °C in four hours.

Steady-state fluorescence spectroscopy

The steady-state fluorescence intensity measurements were carried out according to the general procedure outlined in Section 3.4.2. In short, the data was collected with a LS 55 fluorescence spectrometer (PerkinElmer, Rodgau, Germany), equipped with a R928 PMT and the plate reader accessory in combination with white Nunc PS F96 MicroWell Plates (Thermo Fisher Scientific Inc., Waltham, MA., USA).

For polyplex formation, the polymer stock solution (γ(TAMRA-lPEI_2) = 0.345 g/L and γ(BP_2-lPEI) = 2 g/L in PBS) was diluted to 20 µL with 50 mM phosphate buffer (pH = 7.11). Depending on the nucleic acid type, either 2.98 µg (for pDNA and siRNA) or 3.12 µg (for DNA oligomers) of polymer was used per sample. Then, the appropriate amount of nucleic acid (N/P = 12, 8, 6, 4, 2), dissolved in the same volume and buffer, was added. After 5 min the polyplex solution was diluted with 60 µL buffer, transferred to the well plate and measured immediately (BP_2-lPEI: λ_{ex} = 488 nm/λ_{em} = 512 nm, TAMRA-lPEI_2: λ_{ex} = 554 nm/λ_{em} = 582 nm); each sample was prepared in triplicate.

Time-correlated single photon counting

The time-correlated single photon counting experiments (TCSPC) were performed at the University of Regensburg Institute of Physical and Theoretical Chemistry, department for Laser Spectroscopy and Photochemistry (Prof. Dr. Bernhard Dick) with assistance from Roger-Jan Kutta and Dr. Uwe Kensy.

Prior to the measurements, TAMRA-lPEI_2/DNA oligomer polyplexes were formed in 10 mM HEPES (pH = 7.4) by combining 170 µL polymer stock solution with 170 µL oligomer solution (N/P = 24, 12, 8, 4, 2); each sample contained 36.6 µg TAMRA-lPEI_2. After 5 min, the polyplexes were diluted with buffer to a final volume of 850 µL, transferred to a fluorescence micro cuvette (Quartz SUPRASIL, 500 µL, 10 × 2 mm; Hellma GmbH & Co. KG, Müllheim, Germany) and measured immediately.

A 370 nm emitting, pulsed LED (NanoLED; HORIBA Jobin Yvon GmbH, Unterhaching, Germany) with a temporal FWHM of 1.04 ns, operated at a measurement frequency of 500 kHz was used for sample excitation. The sample emission was detected at 582 nm and a 450 nm cutoff filter was used to prevent scattered excitation light from reaching the R928 PMT. The entrance slit to the PMT was carefully adjusted to attain between 0.0004 and 0.0009 photon counts per excitation pulse. Each sample was measured for 15 min at a data resolution of 12 bit. Finally, the instrument's response function was recorded and a time calibration was performed.

The data was deconvoluted and simultaneously fitted using a biexponential model with the help of the program MultExpFit (Prof. Dr. Bernhard Dick). The resulting fluorescence lifetimes were used for the Stern-Volmer plots.

4.2.3 Single polyplex dequenching microscopy

The effects of disulfide cleavage on single polyplexes or polyplex aggregates were studied with the help of a Zeiss Axiovert 200 M microscope (objective: Plan-Apochromat 63×/1.4 Oil) coupled to a Zeiss LSM 510 scanning device (Carl Zeiss Co. Ltd., Germany). BP_2-lPEI based polyplexes were excited at 488 nm (Ar^+-laser) and the emitted light was collected using a 505-530 nm bandpass filter ("green channel"). For the visualization of polyplexes additionally containing TAMRA-lPEI_2 the instrument was set to multitrack mode. The TAMRA label was excited at 543 nm (HeNe laser) and a 560-615 nm bandpass filter was used ("red channel").

Thirty minutes prior to the measurements the polyplexes (DNA: pEGFP-N1) were formed in a total volume of 25 µL of PBS according to the general procedure outlined in Section 2.2.3. An N/P ratio of 12 and 16 was used for BP_2-lPEI and BP_2-lPEI/TAMRA-lPEI_2 polyplexes, respectively. In case of the latter, a TAMRA-lPEI_2/BP_2-lPEI mass ratio of 0.125 was used to obtain comparable emission intensities at the dyes' respective emission maxima (determined with a LS-55 fluorescence spectrometer); the microscope's measurement settings were adjusted accordingly. To prevent the polyplexes' diffusion out of the confocal volume during the time frame of the image acquisition, the matured polyplexes were immobilized in 8 well Lab-Tek chambered cover glasses (Nunc GmbH & Co. KG, Germany) containing approximately 200 µl of a highly concentrated glucose solution (450 g/L in PBS). Between 2 and 3 µg of DNA were used per well. To investigate disulfide cleavage a 400 mM 2-ME solution was added to the wells. The

final 2-ME concentration was 114 mM. The image analysis was performed with ZEN 2012 (Carl Zeiss Microscopy GmbH, Jena, Germany); the fluorescence intensity profiles were created with ImageJ v1.49i (Wayne Rasband, National Institutes of Health, USA).

4.2.4 Polyplex size measurements

The hydrodynamic diameter of DNA and siRNA complexes with lPEI and S_2-lPEI_b in different dispersants was determined with dynamic light scattering using a Zetasizer Nano ZS particle characterization system (Malvern Instruments Ltd, Malvern (Worcestershire), UK) equipped with a 4 mW HeNe laser (632.8 nm). All measurements were performed at 22 °C (equilibration time 200 s) in disposable PS semi-micro cuvettes (path length: 10x4 mm). The measurement position and laser attenuation selection were set to automatic; the measurement angle was 173° (backscatter). Generally, each sample was measured one or three times in eleven runs. The dispersant properties (viscosity and refractive index) were calculated with the software provided by the instrument manufacturer (Zetasizer Software v6.01). For data analysis the general purpose model was used.

Polyplexes were formed by diluting 2.09 µg nucleic acid (in water) to a final volume of 42 µL with the corresponding buffer. The appropriate amount of polycation (stock solution: 2 g/L in PBS) to attain an N/P = 12 was diluted likewise. After combining both solutions and an incubation time of about five minutes, the polyplexes were diluted with the corresponding buffer or serum free HAM's F-12 tissue culture medium to a final measurement volume of 500 µL. The following buffers were used (all pH = 7.4): PBS, 10 mM HEPES, and 50 mM HEPES.

4.3 Results and discussion

4.3.1 BP_2-PEI dequenching assays

It was demonstrated in the previous chapter that the reduction sensitive BP_2 probe attached to PEI is still susceptible to disulfide cleavage under a physiological GSH concentration and can be used to monitor the degradation of cystine cross-linked S_2-lPEI. What had not been investigated is the influence of a nucleic acid complexation on the probe's cleavage. The experiments with free polymer also did not reveal the exact fluorescing species. In principle, there are three different possibilities: (1) If most BP_2 is bound in a dangling configuration (Figure 3.21), highly fluorescent BP-SH will be released upon cleavage. The remaining polymer bound BP-SH would probably still be self-quenched. (2) If most BP_2 is bound in a bridged configuration and the labeling density is low enough to prevent efficient self-quenching after cleavage, polymer

bound BP-SH will be the fluorescent species. (3) If the labeling density is low enough and most BP_2 is bound in a dangling configuration, polymer bound and released BP-SH will both be the fluorescent species. To know the identity of the fluorescent species is essential to correctly interpret the data (esp. from micrographs) for the intracellular distribution of the polyplexes. The distribution of the released and polymer bound probe may differ, but their fluorescence signals would be indistinguishable.

Since measurements with a spectrofluorometer are ensemble measurements, it is not possible to distinguish free and polymer bound BP-SH with that method. For that reason, the emission properties of individual BP_2-lPEI/DNA polyplexes and polyplex aggregates were assessed with confocal laser scanning microscopy. The polyplexes were immobilized in a medium of high viscosity to avoid their diffusion out of the confocal volume during the measurements. In accordance with the experiments done with uncomplexed BP_2-lPEI (Section 3.5.3), uncleaved polyplexes demonstrated a low level of BP fluorescence (Figure 4.1A, above and Figure 4.1B, black). Even in the sterically highly restricted environment within a polyplex, some portion of BP_2 is apparently still able to attain a conformation where quenching is incomplete. The addition of 2-ME led to a decrease of the fluorescence originating from the polyplex, while the fluorescence of the background increased significantly (Figure 4.1A, below and Figure 4.1B, red). Note: The increase of the background fluorescence was only visible with the naked eye, since it was too diffuse to be captured on CLSM micrographs.

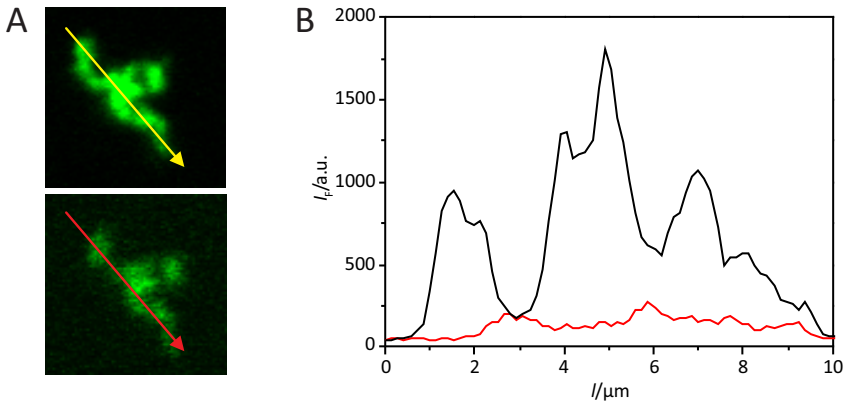

Figure 4.1: Emission intensity profile of BP_2-lPEI/DNA polyplexes before/after disulfide cleavage

A: Confocal micrographs of BP_2-lPEI/DNA polyplexes (N/P = 12) immobilized in a glucose solution before (above) and after (below) the addition of 2-ME. The arrows indicate the direction of the fluorescence intensity profile shown in B. Picture dimensions: 10.4 µm × 10.4 µm. B: Corresponding fluorescence intensity profiles before (black) and after (red) the disulfide cleavage. (Experimental details Section 4.2.3)

As the added reductant had been dissolved in a medium of lower viscosity, its addition might have provoked the polyplexes' movement out of the confocal volume. To compensate for any emission intensity changes unrelated to disulfide cleavage, the experiment was repeated with polyplexes that additionally contained TAMRA-lPEI_2 as reduction insensitive emission intensi-

ty reference. Hypothetically, this approach would also allow quantitative cleavage studies in living cells where polyplexes cannot be immobilized.

As far as the BP probe is concerned, no differences to polyplexes containing only BP_2-lPEI were observed (Figure 4.2A and B). All in all, the results are in line with the previous observations made for the cleavage of uncomplexed BP_2-lPEI (Section 3.5.3) and confirm that most BP_2 is bound in a dangling configuration. More importantly, released BP-SH is the only species contributing significantly to the fluorescence intensity rise after cleavage. Interestingly, the cleavage also led to a strong and unexpected emission intensity increase for TAMRA-lPEI_2 (Figure 4.2B), suggesting that TAMRA may not be a suitable reference dye after all.

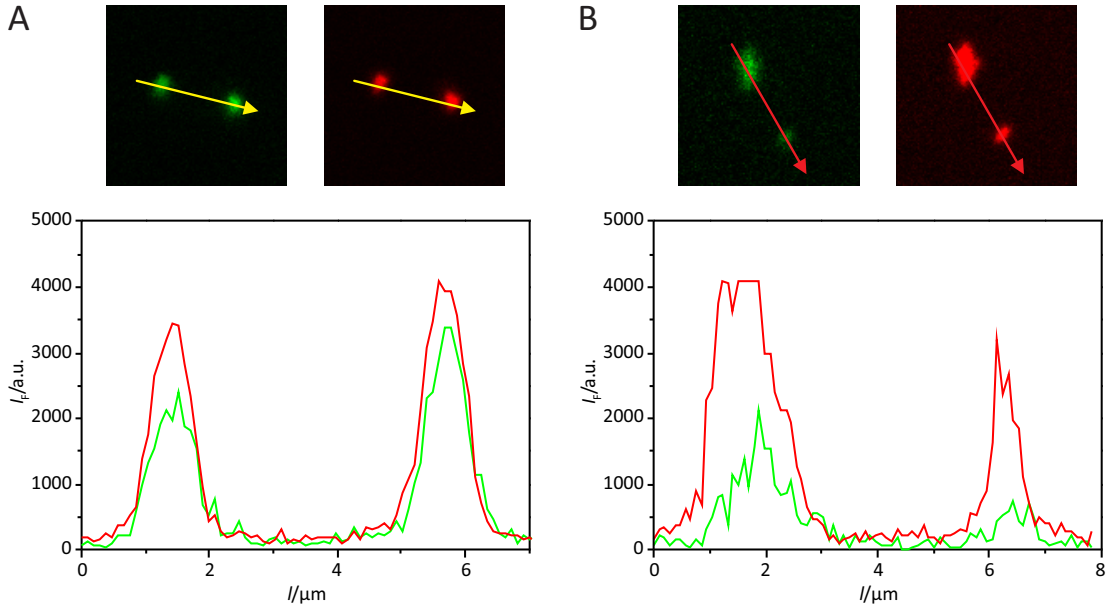

Figure 4.2: Emission intensity profile of BP_2-lPEI/TAMRA-lPEI_2/DNA polyplexes before/after disulfide cleavage

A: (above) Confocal micrographs of BP_2-lPEI/TAMRA-lPEI_2/DNA polyplexes (N/P = 16) immobilized in a glucose solution. Initially, the TAMRA-lPEI_2 and BP_2-lPEI emission intensities were similar. The arrows indicate the direction of the fluorescence intensity profile shown below. B: (above) Confocal micrographs of the same sample after the addition of 2-ME. Note the detector saturation in the red channel (at about 2 µm) shown in the fluorescence intensity profile below. Picture dimensions: 9.8 µm × 9.8 µm. (Experimental details Section 4.2.3)

It can be ruled out that this is the result of a RET from BP to TAMRA (e.g., sensitized emission), as the dyes' spectral overlap is too small for an efficient energy transfer. More importantly, the measurements were performed in multitrack mode where each dye is excited and measured individually. The dequenching of the TAMRA emission is probably related to the decreased density of polymer bound BP after cleavage. BP and TAMRA are both relatively hydrophobic dyes and may form non-fluorescent mixed aggregates in aqueous solution. Upon the addition of the reductant, BP is still able to form aggregates with neighboring BP-monomers. The less hydrophobic TAMRA,[173] however, will no longer be able to participate in the aggregate formation. The formation of mixed aggregates may additionally be disfavored due to the fact that BP and TAMRA are located on different polymer strands. The average distance between indi-

vidual BP-monomers on the very same polymer strand is likely lower than the average distance between BP and TAMRA molecules located on different polymer strands.

Although BP and TAMRA are not well suited as FRET pair, those results also have implications for FRET studies with polyplexes. Dye aggregation in general interferes with FRET and the data presented here and in the previous chapters suggest that fluorescence labeling of polycations and polyplex formation significantly increase the aggregation tendency. For that reason it seems advisable to avoid the use of relatively hydrophobic fluorescence probes for FRET studies.

In order to investigate the influence of the polymer structure and the nature of the nucleic acid on the polyplex cleavage, siRNA and DNA polyplexes based on non-cleavable (BP_2-lPEI) and cleavable (BP_2-S_2-lPEI) PEI were exposed to a physiological GSH concentration. The emission intensity increases over time (Figure 4.3) revealed distinct differences among the polyplex species. The fluorescence intensity of BP_2-lPEI/siRNA complexes increased almost as fast as the intensity of uncomplexed polymer (Figure 4.3A). In contrast, the intensity of BP_2-lPEI/DNA complexes rose much slower. In all cases no plateau was observed, indicating that cleavage had not been completed even after 4 h. In contrast, the time courses for the polyplexes based on the cleavable polymer (Figure 4.3B) reached a plateau within about 60 (DNA) to 120 min (siRNA). Again, the emission intensity increase of siRNA polyplexes was significantly higher than that of DNA polyplexes, but did not reach the intensity of the free polymer. Uncomplexed BP_2-PLL and BP_2-PLL in complex with siRNA and DNA were also tested. In that case, however, the polyplexes were cleaved as fast as the free polymer (data not shown).

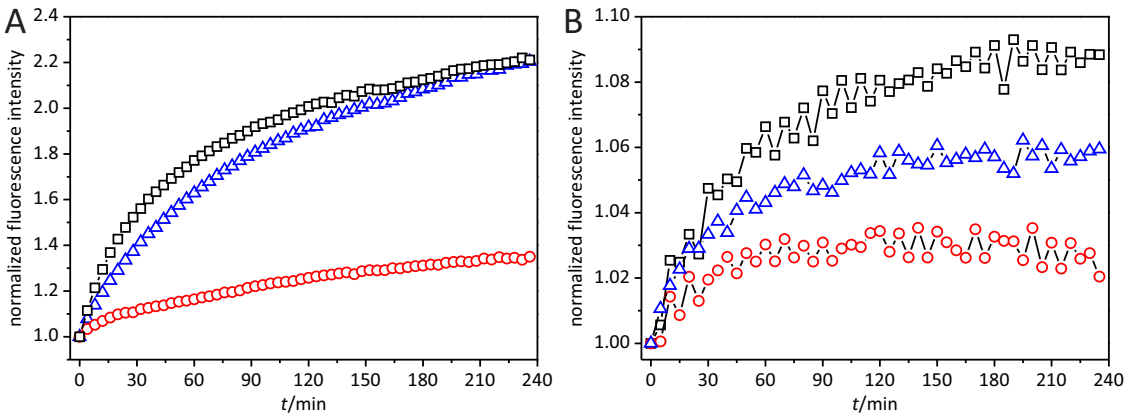

Figure 4.3: Time course of the emission intensity of BP_2-lPEI and BP_2-S_2-lPEI_1/polyplexes in the presence of GSH

GSH (c_{end} = 5 mM) was added to BP_2-lPEI (A) and BP_2-S_2-lPEI_1 (B) complexes (N/P = 12) with DNA (○) and siRNA (△; uncomplexed polymers: □) and the emission intensity was measured over the course of 4 h every 4 (A) or 5 min (B). The data were normalized against the intensity at the first time point and corrected for photobleaching. (Experimental details Section 4.2.1)

The cleavage rates are inversely proportional to the molecular weight of the polyplex components and increase in the following order: DNA/S_2-lPEI < DNA/lPEI < siRNA/S_2-lPEI < siRNA/lPEI. It is well established that to a large degree, the interactions between nucleic acids and most polycations depend on the number and density of charges.[32, 174] According to a simplified thermodynamic model conceived by Schaffer et al., which disregards the effects of competing ions, the probability for polyplex dissociation decreases with increasing polymer chain length.[175] Although not stated explicitly, their model similarly applies when the nucleic acid length is considered.[38] The most stable polyplexes would be those based on long polymers and large nucleic acids (DNA/S_2-lPEI). Conversely, polyplexes based on short polymers and small nucleic acids would be the least stable (siRNA/lPEI). Thus, the cleavage rate can serve as indirect measurement for polyplex stability.

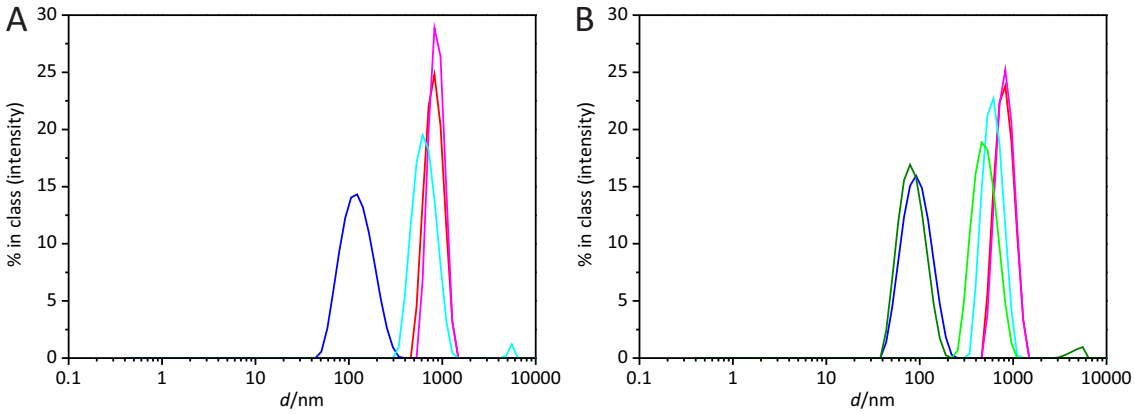

Figure 4.4: Particle size distributions by intensity of lPEI and S_2-lPEI_b/DNA polyplexes in different media

lPEI (A) and S_2-lPEI_b/DNA (B) polyplexes (N/P = 12) in PBS (red), 50 mM HEPES pH = 7.4 (blue), and 10 mM HEPES pH = 7.4 (olive green). Particle size measurements were also performed in media containing HAM's F12 (magenta, cyan, and green). (Experimental details Section 4.2.4)

Schaffer et al. have hypothesized that the effect of polymer length on the polyplex dissociation increases further in the presence of charged cellular compounds like chromatin, polyamines, and other nucleic acids, which may penetrate and competitively dissociate the complex.[175] In addition to the polymer's affinity to the nucleic acid, the presence of excess PEI – PEI which is not directly bound to the nucleic acid – plays an important role in the stability of PEI based polyplexes. Excess PEI is present whenever polyplexes are formed above the critical N/P ratio and forms a shell around the polyplex core.[162] An ionic competitor has to penetrate this outer layer first in order to destabilize the polyplex.[175] Complete destabilization will not take place if the free polymer's binding capacity exceeds the concentration of the competitor.[162]

The predicted polyplex stabilities were confirmed by dynamic light scattering measurements in media of different ionic strengths and the absence or presence of biological competitors. DNA and PEI formed complexes regardless of the ionic strength or the presence of serum (Figure 4.4). siRNA/PEI polyplexes, albeit irregular in size, were only formed with the higher molecular

weight polycation S_2-lPEI in a medium with a low concentration of competing cations (10 mM HEPES buffer; Figure 4.5).

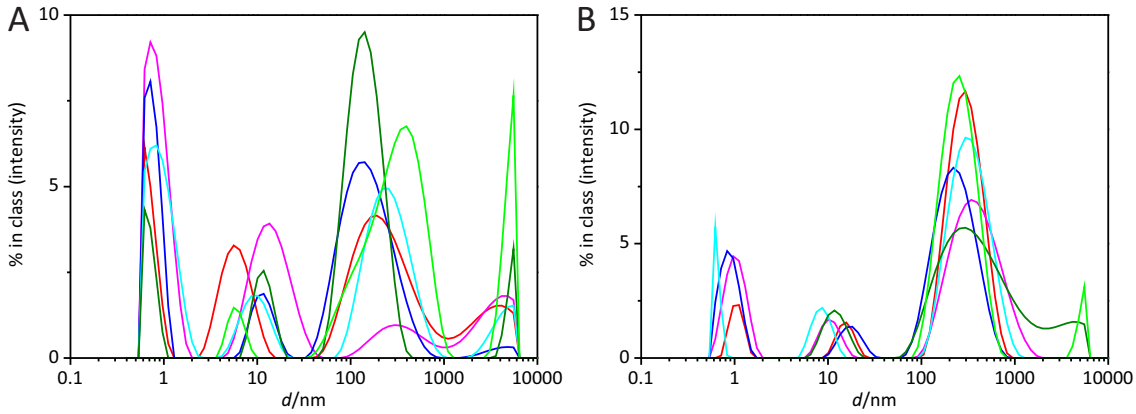

Figure 4.5: Particle size distributions by intensity of lPEI and S_2-lPEI_b/siRNA polyplexes in different media

lPEI (A) and S_2-lPEI_b/siRNA (B) polyplexes (N/P = 12) in PBS (red), 50 mM HEPES pH = 7.4 (blue), and 10 mM HEPES pH = 7.4 (olive green). Particle size measurements were also performed in media containing HAM's F12 (magenta, cyan, and green). (Experimental details Section 4.2.4)

Given the correlation between the predicted and measured polyplex stabilities and the measured disulfide cleavage rates, it seems obvious that the extent of polyplex shielding and disulfide cleavage are similarly related. In other words, the reductant's penetration ability governs the cleavage tempo. This ability cannot be very pronounced because the cleavage of the two most stable complexes S_2-lPEI_b/DNA and lPEI/DNA is very slow. The reductant's high sensitivity towards steric repulsion is further confirmed by the fact that even in cases where no ordered polyplexes were formed, the cleavage is significantly (S_2-lPEI_b/siRNA) or at least slightly (lPEI/siRNA) impeded. The transfection (Section 2.2.3) and quenching (see below) experiments indicate that in those cases, nucleic acid and polycation have to be at least weakly associated or are forming "monomolecular complexes" consisting of only one siRNA per PEI strand. Van Rompaey et al. have described such complexes for antisense oligonucleotides and diaminobutane-dendrimers.[176] The weak nucleic acid/polycation interaction is apparently already sufficient to exert steric hindrance on the relatively bulky reductant GSH. In view of these results, it appears unlikely that a disulfide cleavage alone would lead to an efficient intracellular release of the nucleic acid cargo. The cleavage would have stopped long before any significant polymer degradation occurred. Efficient decomplexation and full cargo release more likely requires the synergistic effect of ion exchange reactions and disulfide cleavage, where competing cellular polyions first loosen the polyplex, which gives reductants better access to inner polyplex layers. Conversely, the polymer's degradation makes the complex more susceptible towards ion exchange reactions.

4.3.2 Additional quenching experiments

In some instances where covalently bound fluorescent probes are used to investigate polymer/nucleic acid complexes, factors like self-quenching or energy transfers are taken into consideration. What is even more frequently overlooked, however, is the fact that nucleic acid bases can also have an effect on external fluorophores. The most prominent example is the nucleobase guanine, which can quench many fluorophores through an photoinduced photo electron transfer process.[171] In order to get a better understanding of the photophysical processes within polyplexes based on fluorescently labeled PEIs, different lPEI and S_2-lPEI derivatives were complexed with DNA or RNA and investigated in further detail.

In a first experiment, the emission intensity of BP_2-lPEI and TAMRA-lPEI_2, in complex with increasing amounts of plasmid DNA and siRNA was measured. In case of BP_2-lPEI, the emission intensity of the polyplexes generally exceeded that of the free polymer, regardless of the nucleic acid type and remained constant within the margin of error except at the lowest N/P tested (highest nucleic acid amount). At that point its emission intensity decreased markedly (Figure 4.6A). siRNA complexes always exhibited a weaker fluorescence than the corresponding DNA complexes.
In contrast, TAMRA-lPEI_2 based polyplexes were less fluorescent than the uncomplexed polycation and their emission intensity decreased with increasing nucleic acid amount until N/P = 4 (Figure 4.6B). Below that N/P, a further decrease was only seen for DNA but not siRNA complexes.

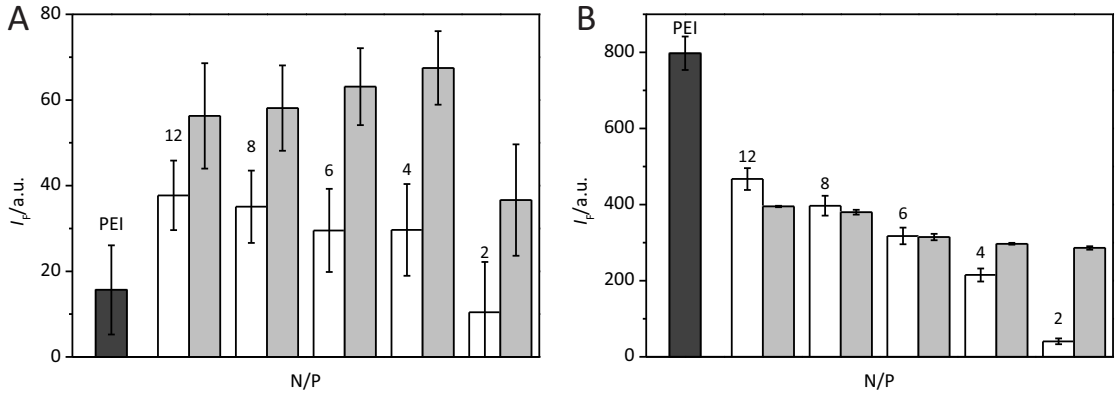

Figure 4.6: Fluorescence of BP_2-lPEI and TAMRA-lPEI_2 in complex with DNA and siRNA
The fluorescence intensity of a constant amount of BP_2-lPEI (A; λ_{ex} = 488 nm/λ_{em} = 512 nm) or TAMRA-lPEI_2 (B; λ_{ex} = 554 nm/λ_{em} = 582 nm) was measured (n = 3) in the presence of increasing amounts of DNA (white columns) and siRNA (gray columns). The dark gray columns represent the fluorescence intensity of the corresponding uncomplexed polymer. (Mean values ± sample standard deviation; experimental details Section 4.2.2)

The different trends of the emission intensity are related to the structural differences between the fluorescent probes. BP_2's dimeric structure strongly promotes the formation of non-fluo-

rescent H-aggregates, i.e., polymer bound BP_2 is already quenched to the maximum extent possible. Within nucleic acid complexes, however, the probe-probe self-quenching becomes less efficient as the spatial arrangement of the constituent BP monomers is disturbed due to steric constraints or changes in the local electronic environment. The emission of the monomeric fluorophore TAMRA, on the other hand, is unperturbed, unless the complex formation moves individual fluorophores or a fluorophore and a nucleobase close enough together for quenching. This hypothesis is substantiated by the fact that polyplexes labeled with the monomeric BODIPY variant (BP-lPEI_3/DNA; data not shown) exhibit a comparable, albeit less pronounced intensity decrease with increasing N/P. Independent of the fluorescent label, the emission intensity of pDNA complexes is lower than that of the corresponding siRNA complexes, though for TAMRA-lPEI_2 based polyplexes this is only apparent at lower N/Ps. This may indicate that pDNA is bound more tightly than siRNA, since quenching generally increases with decreasing interchromophoric distance.

Another interesting aspect is the course of the emission intensities at the highest nucleic acid concentrations. The emission of BP_2 labeled polyplexes, for instance, decreases abruptly at N/P = 2. Since that N/P is in the region of the critical ratio, the decrease could be related to a PEI redistribution between the DNA groove and backbone.[162] It is also possible that the BP_2 dequenching is here overcompensated due to an increased quenching because of the comparatively high nucleobase density. The emission intensity of TAMRA-PEI/pDNA polyplexes decreases steadily from N/P = 12 to 2, while the intensity for siRNA complexes remains almost constant below N/P = 8. It appears that at this point, no more siRNA is bound by the polymer, which again shows that the interaction between the polycation and a short nucleic acid is relatively weak.

It is remarkable that weak polymer-nucleic acid interactions (no ordered polyplexes were formed) could be detected with the fluorescence assay developed here. Polymer attached fluorophores are apparently highly sensitive towards such interactions. It is not surprising that fluorescently labeled nucleic acids would behave similarly. Vader et al. have complexed an Alexa Fluor 488 modified siRNA with a variety of transfection agents.[177] Regardless of the agent they used, they always observed a fluorescence decrease. However, the signal could be fully restored by disrupting the complexes through the addition of 2 % SDS.

Evidently, such quenching phenomena complicate the quantification of both polyplex components in in vivo and in vitro studies, and may lead to the misinterpretation of data. The quenching mechanism is generally thought to be a probe-probe self-quenching due to the close association of the fluorophores within the complex. The role of the nucleic acid has not been investigated in detail yet, even though nucleobases are well known quenchers. A better understanding of this aspect might provide additional information on the close interaction

between polycation and nucleic acid within polyplexes or smaller, less well defined molecular assemblies. Guanine is the only nucleobase efficiently able to quench rhodamines through a photoinduced electron transfer mechanism;[178] a PET interaction between guanine and BODIPY FL has also been reported.[129] In order to elucidate if PET is also a relevant quenching mechanism for polyplexes, model polyplexes based on TAMRA labeled PEIs and double stranded DNA oligomers were investigated with steady-state and time-resolved fluorescence measurements.

The steady-state measurements revealed an almost linear decrease in the polyplex' emission intensity with increasing oligomer concentration, similar to that observed for pDNA complexes (Figure 4.2B), regardless of the polymer type (TAMRA-lPEI_2 and TAMRA-S_2-lPEI) or the oligomer's base sequence (Figure 4.7A and B). Complexes with the $p(dCdG)_{14}$ oligomer consistently had a lower emission intensity than those with the $p(dAdT)_{14}$ oligomer; on average, the intensity was reduced by about 17 % and 28 % for TAMRA-lPEI_2 and TAMRA-S_2-lPEI, respectively. The effect of the presence of guanine strongly suggests that PET contributes significantly to the quenching in addition to the probe-probe self-quenching. In order to substantiate this hypothesis, the intensity data were complemented with fluorescence lifetime data obtained in additional time-correlated single photon counting measurements of TAMRA-lPEI_2/oligomer complexes (Figure 4.8A). The static and dynamic quenching constants $k_{q,s}$ and $k_{q,d}$ were determined with the help of Stern-Volmer plots. If PET indeed played a role as second quenching mechanism, one would see a base sequence related change in the quenching constants.

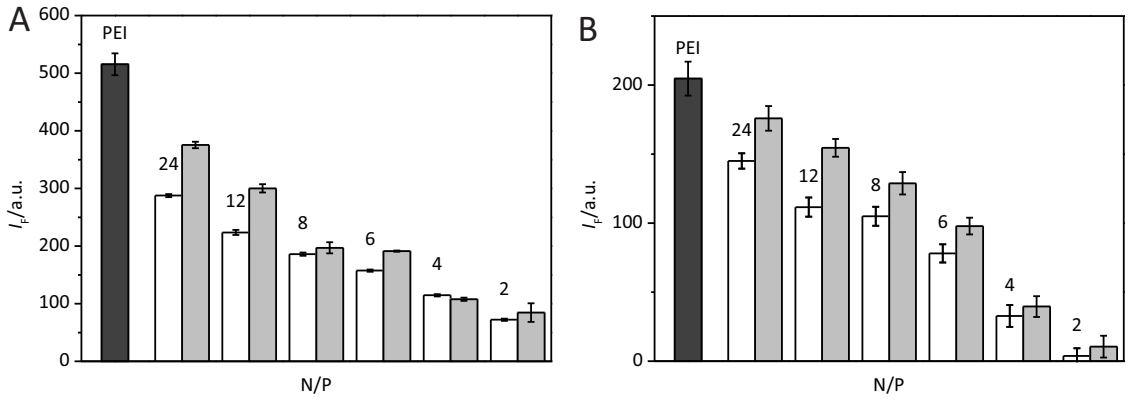

Figure 4.7: Fluorescence of TAMRA-lPEI_2 and TAMRA-S_2-lPEI/DNA polyplexes

The fluorescence intensity (λ_{ex} = 554 nm/λ_{em} = 582 nm) of a constant amount of TAMRA-lPEI_2 (A) or TAMRA-S_2-lPEI (B) was measured in the presence of increasing amounts of $p(dCdG)_{14}$ (white columns) and $p(dAdT)_{14}$ (gray columns). The dark gray columns represent the fluorescence intensity of the corresponding uncomplexed polymer. (Mean values ± sample standard deviation; experimental details Section 4.2.2)

The lifetime of lPEI_2 attached TAMRA (2.39 ns; data not shown) was in the same range as for the free dye (2.28 ns[179] and 2.41 ns[122]), so the polycation itself has no quenching effect. Complex formation with $p(dCdG)_{14}$, reduced the lifetime to between 2.28 ns (N/P = 24) and

0.99 ns (N/P = 2), while a moderate increase to between 2.71 ns and 3.15 ns was measured for p(dAdT)$_{14}$ complexes. An increasing lifetime of rhodamine derivatives with an increasing DNA concentration has been attributed to the formation of ground state complexes with DNA nucleotides.[172] The Stern-Volmer analysis of the lPEI_2/p(dCdG)$_{14}$ lifetime data (Figure 4.8A) revealed the dynamic quenching to be extremely efficient: With a value of 5.9 × 10^{13} M^{-1} s^{-1}, the dynamic bimolecular quenching constant is several magnitudes higher than that obtained for the quenching of TAMRA by 50 mM dGMP (1.81 × 10^{9} M^{-1} s^{-1})[172], and even higher than what is considered to be the largest possible value for diffusion-limited quenching in aqueous solution (1 × 10^{10} M^{-1} s^{-1})[79]. The bimolecular quenching constant k_q is related to the collisional frequency Z between fluorophore and quencher

$$Z = \frac{k_q}{f_Q}[Q] \tag{4.12}$$

where f_Q is quenching efficiency.[79] Thus, under the reasonable assumption that f_Q is constant under all experimental conditions, the collisional frequency between TAMRA and the DNA-quencher must be extraordinarily high. Apparently, molecular movement within polyplexes is so heavily restricted that fluorophore and quencher remain at van der Waals contact (≈0.4 nm) at all times. The Stern-Volmer analysis of the steady-state data further corroborated a close association between fluorophore and quencher (Figure 4.8B). The static bimolecular quenching constant for TAMRA-lPEI_2/p(dCdG)$_{14}$ (3.1 × 10^{14} M^{-1} s^{-1}) is about ten times higher than the dynamic quenching constant; $k_{q,s}$ for the complex with p(dAdT)$_{14}$ is 2.6 × 10^{14} M^{-1} s^{-1}.

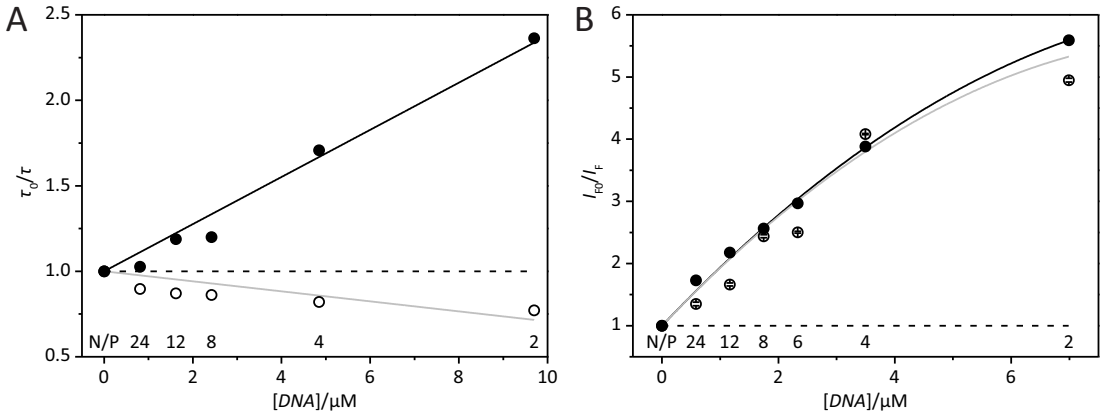

Figure 4.8: Stern-Volmer plots for TAMRA-lPEI_2 in complex with double stranded DNA oligomers

The fluorescence lifetime (A; λ_{ex} = 370 nm/λ_{em} = 582 nm) and fluorescence intensity (B; λ_{ex} = 554 nm/λ_{em} = 582 nm) of a constant amount of TAMRA-lPEI_2 were measured in the presence of increasing amounts of p(dCdG)$_{14}$ (●) and p(dAdT)$_{14}$ (○). The data were normalized against the data from the uncomplexed polymer; the dashed line corresponds to y = 1. A first (A) or second (B) degree polynomial was fitted to the data. (Experimental details Section 4.2.2)

Static quenching appears to be the main fluorescence quenching mechanism in the investigated polyplexes and the only mechanism in complexes based on oligomers that contain only adenine and thymidine. It is very likely that the static quenching originates from the formation of non-fluorescent ground state complexes between individual TAMRA molecules ("probe-probe self-quenching"), as the value of $k_{q,s}$ is basically unaffected by the oligomer's base sequence. It cannot be ruled out completely, that ground-state TAMRA/nucleotide complexes are also formed, but that seems unlikely at this point for steric reasons. Since dynamic quenching is only significant in TAMRA-lPEI_2/p(dCdG)$_{14}$ polyplexes, it is almost definitely caused by a PET from the highly efficient quencher guanine to TAMRA. Although the dynamic quenching is weaker than static quenching, its contribution to the overall reduction of the emission intensity cannot be neglected.

The Stern-Volmer analysis of the steady-state data (Figure 4.8B) might also reveal some information on the internal structure of the polyplexes. All plots display a slight downward curvature, which generally signifies the existence of more than one fluorophore population with different accessibilities to quenchers.[172] Quenchers could have better access to polymer bound fluorophores located at the periphery of the polyplex than to fluorophores in the polyplex core. In this case the less accessible fraction is relatively small (≈10 %), but it has to be pointed out that no ordered polyplexes were formed under the experimental conditions. It would be worthwhile to repeat these experiments with larger, CG rich nucleic acids to confirm this hypothesis.

4.4 Conclusions

The development of more efficient gene carriers is in part impeded by the lack of suitable analytical tools, especially fluorescence-based methods, to assess polycation/nucleic acid interactions.

In contrast to FRET or intercalator based methods, the single polymer-probe quenching assay developed here is able to provide information on short-range polycation/nucleic acid interactions and the polyplex structure above the critical N/P ratio. It relies on a TAMRA labeled polymer, whose emission is quenched upon the interaction with nucleic acids. With only one external probe, the labeling procedure and the data interpretation and validation are simplified. According to steady-state and time-resolved fluorescence data, the emission intensity decrease during complexation is mainly caused by probe-probe self-quenching. Apparently, the fluorophores are forced together very closely as the presence of the nucleic acid greatly reduces the polymer's electrostatic intra- and interstrand repulsion. A very short-ranged photoinduced electron transfer from guanine to TAMRA was also observed and significantly con-

tributes to the overall quenching. Based on additional data for BP-lPEI and TAMRA's structural and photophysical similarity to many other dyes, this may generally occur in fluorescently labeled polyplexes.

The assay was used to study polyplexes composed of PEIs and nucleic acids of varying size. Regardless of the components' molecular weight, fluorescence quenching, i.e., a close molecular interaction, was observed even in cases where no ordered complexes were formed. Thus, the assay may have a higher sensitivity than PCS or agarose gel electrophoresis based methods. Additional TCSPC measurements confirmed the very strong PEI/nucleic acid interaction. For lPEI/DNA oligomer complexes, the static and dynamic quenching constants were several magnitudes higher than what can be expected for diffusion limited quenching. The relevance of this unexpectedly high interaction strength for the cleavage and decomplexation of (reduction sensitive) polyplexes was investigated with the BP_2 dequenching assay.

Polyplexes become more resistant against ion exchange reactions with increasing polymer/nucleic acid interaction strength, which in turn increases with the components' molecular weight. The BP_2-assay helped to establish a similar relationship for disulfide cleavage reactions. With increasing molecular weight of the binding partners, the cleavage rates decreased rapidly and the reaction eventually stopped as in case of S_2-lPEI/pDNA. Most likely, the reductant progressively fails to penetrate into the complex. Based on this observation, it appears unlikely that polyplex cleavage alone is sufficient to allow for a complete cargo release inside cells. Full cargo release probably additionally requires cellular ionic competitors to concurrently displace the polyplex components. Uptake and intracellular cleavage of those reduction sensitive polyplexes were investigated more closely in the following chapter.

5 Intracellular uptake and cleavage studies

5.1 Introduction

Biodegradable polymers have extensively been studied for a long time and found many biomedical applications. Their use as drug delivery systems began in the 1960s with the development of fully synthetic poly(hydroxy acids) for surgical sutures[180, 181]. Shortly thereafter, these then novel polymers led to the development of numerous injectable microparticulate drug depots[180] and ultimately, degradable nanoparticulate gene carriers[181]. The most common degradation mechanism of polymer based gene delivery systems is hydrolysis. Systems based on alternative degradation mechanisms have received much less attention. Bioreducible polymers typically contain disulfide bonds and became the focus of interest as bioreducible polycations for gene delivery as late as the early 2000s.[35] Today, bioreducible polycations are the most widely investigated polymer class for biomedical applications, still, many fundamental questions concerning their mechanism of action are unresolved.[35]

It is generally agreed that on the most basic level, the frequently observed positive impact that bioreducible polycations have on gene delivery relies on their unique ability to combine high extracellular carrier stability and cargo protection with rapid intracellular cargo release, in many cases close to the sites of nucleic acid action.[35, 40, 182] Evidently, this view of the delivery process is too simplistic as it fails to explain many experimental observations. Relatively recently, for instance, the importance of the disulfide mediated nucleic acid cargo unpacking for the transfection efficacy of cross-linked linear PEIs was challenged, when Bonner et al. observed that the presence of uncomplexed polymer and not the carrier's reducibility turned out to be critical for the delivery success;[33] similar observations have been made for non-reducible delivery systems as well.[75] It is not clear if and how this finding translates to other redox-sensitive carriers, nevertheless, it impressively demonstrates how little of the delivery process is actually understood.

5.1.1 Cellular redox environment

Redox responsive carriers are unique in their ability to provide a quick transition from high extracellular stability to rapid intracellular carrier disintegration by exploiting the large redox gradient between extra- and intracellular space.[34] While the former environment is oxidizing, cellular organelles and the cytosol are mostly reducing.[40] The cellular redox environment regulates a number of basic cell functions, such as the activity of key enzymes and genes, as well as proliferation and apoptosis.[183, 184] It changes dynamically depending on external and internal factors like the cell cycle[35, 183] and was defined as the sum of the reduction potential and reducing capacity of a set of linked redox couples found in a cell or cellular organelle[183]. In general, such redox couples include oxidized and reduced pyridine nucleotides, and small molecular weight or protein bound thiols and disulfides.[184] One of their main functions is to mediate cellular disulfide reductions and isomerizations. Eukaryotes possess several redox systems, like the thioredoxin (Trx) and glutaredoxin (Grx) system to retain cytosolic protein thiols in the reduced state.[185] Overall, however, the cellular redox environment is determined by the glutathione-glutathione disulfide (GSH/GSSG) system.[34, 185] The reason why the GSSG/2·GSH system is considered to be the major cellular redox buffer is due to the fact that the GSH concentration exceeds that of most other redox active compounds by far.[183]

The majority of the GSH is normally located at its main synthesis site, the cytosol, where the GSH concentration reaches the millimolar range (1-11 mM)[183]. The GSH biosynthesis is a two-step enzymatic reaction. In the first, rate-limiting step, glutamate cysteine ligase (GCL; previously known as γ-glutamylcysteine synthetase, γ-GCS) catalyzes the formation of γ-glutamyl-L-cysteine from L-glutamate, L-cysteine, and ATP. Glutathione synthetase (GSS) subsequently catalyzes the condensation of γ-glutamyl-L-cysteine and glycine, to form GSH.[186] GSH participates in a number of cellular processes, including the glutathione-S-transferase mediated detoxification of xenobiotics, the glutathione peroxidase mediated detoxification of peroxides and the non-enzymatic regeneration of oxidized glutaredoxins.[185] The latter two processes result in the formation of GSSG. In order to maintain the high cytosolic GSH/GSSG (30:1 to 100:1) ratio, GSH is regenerated from GSSG by glutathione reductase (GR) in an NADPH dependent reaction.[183] High GSH concentrations are also found in the nucleus (up to 20 mM) and in mitochondria (5 mM).[35] Experiments conducted with the glutamate cysteine ligase inhibiting agent buthionine sulphoximine (BSO) suggest that these GSH pools are at least partially independent from the cytosolic pool.[187] Organelles topologically connected to the extracellular space are typically oxidizing. The endoplasmic reticulum, for example, has a GSH/GSSG ratio ranging from 1:1 to 3:1,[34] making it considerably more oxidizing than even the extracellular space.[35] A similar GSH redox ratio is found in the acidic environment of endosomes and lysosomes, nevertheless these organelles exhibit a limited GSH independent reduction capabil-

ity,[35, 188] mediated by cysteine in conjunction with gamma-interferon-inducible lysosomal thiol reductase (GILT). Since the low endolysosomal pH strongly disfavors the formation of thiolate anions,[40] the active nucleophile in disulfide exchange reactions (Figure 5.1),[34] a very high cysteine/cystine ratio has to be maintained through cysteine and cystine specific transporters in order for the reduction to be efficient. The cell membrane and its immediate vicinity are also known to be reducing due to the cellular GSH export as part of the γ-glutamyl cycle[186] and the presence of surface associated redox enzymes like reduced protein disulfide isomerase (PDI)[34]. PDI is a prototypical thiol-disulfide oxidoreductase that catalyzes cellular thiol-disulfide exchanges. The members of this enzyme family have a Cys-X-X-Cys active site motif in common with thioredoxin.[34, 35]

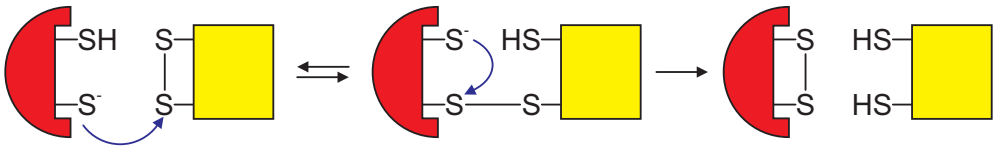

Figure 5.1: Thiol-disulfide exchange reactions catalyzed by oxidoreductases

A reduced thiol-disulfide oxidoreductase (e.g., PDI; red) contains a thiolate anion that is able to attack disulfide bonds (blue arrows) in a number of cellular compounds (e.g., proteins, peptides, and small molecules; yellow). Eventually, the enzyme is oxidized, while the substrate now contains two thiols.

Depending on the redox environment and substrate, PDI catalyzes disulfide formation, cleavage, or isomerization. In its reduced (thiol) form, PDI catalyzes disulfide reductions (Figure 5.1). The reaction mechanism involves the attack of PDI's thiolate anion on the oxidized molecule's disulfide bond to form a mixed disulfide. The mixed disulfide is then cleaved by PDI's remaining thiolate. Finally, oxidized PDI is regenerated with the help redox molecules like GSH.[35] Disulfide reductions mediated by small molecules involve a similar mechanism but usually lack the specificity and efficiency of the enzyme catalyzed mechanism.

5.1.2 Cellular uptake, trafficking, and processing

It is evident that the exact spatiotemporal point where the carrier enters a reducing cellular environment and is subsequently cleaved has a profound impact on the delivery success. If the nucleic acid cargo is released under degradative conditions, it will probably never reach its designated target in the cytosol or nucleus. Thus, a profound understanding of the carrier's uptake and cellular processing (Figure 5.2) is important to maximize the intended biological effect.

According to our current understanding, there are no major differences in the uptake and intracellular trafficking of "conventional" and redox-sensitive carriers.[35] Cell-surface proteoglycans, in particular heparan sulfate proteoglycans (HSPGs), are considered to be the primary

and probably only endocytic receptors for polyplexes and other cationic gene carrier systems.[189, 190] Considering their strong negative charge and the typically positive charge of polyplexes, it seems obvious to assume a charge mediated ligand-receptor interaction. However, while the significance of HSPGs for polyplex uptake and transgene expression is undisputed, their role in the actual cell surface binding is questioned in newer literature. There is some evidence that hydrophobic interactions play a much more prominent role than previously thought.[191] An increased hydrophobicity of the PEI (e.g., through conjugation with hydrophobic groups), for instance, often correlates with an improved transfection efficiency.[42] HSPGs could still enhance polyplex endocytosis and transgene expression by inducing lipid raft clustering and by promoting endosomal escape, but they do not appear necessary per se for successful gene delivery.[192]

As the outer plasma membrane surface contains oxidoreductases, such as PDI and redox-active thiols,[34] there is some controversy whether or not disulfide reductions already take place at this stage of the uptake. Multiple studies performed with viral proteins,[193] toxins,[34] macromolecular drug-polymer conjugates,[194, 195] and more recently redox-sensitive carriers[196-198] suggest that this may indeed be the case. Li et al., for instance, have compared the delivery properties of a series of bioreducible poly(amido amine)s (PAAs). They observed an increasing transfection efficiency and nucleic acid release for DNA-polyplexes with increasing disulfide content of the carrier.[196] When cells were pretreated with the membrane impermeant thiol blocking agent DTNB (5,5'-dithiobis-(2-nitrobenzoic acid)), the transfection efficiency was independent of the disulfide content. An increased release was also seen for antisense oligonucleotide (AON) polyplexes but that did not translate into a higher target knock-down, so apparently carrier disassembly is not a major barrier for AON-delivery. More importantly, the authors were unable to confirm the popular hypothesis that the superior transfection efficiency of reducible polycations is related to a higher DNA bioavailability due to a faster and more complete DNA-release. According to current models, an increased intracellular carrier disassembly rate would be reflected in altered DNA clearance rate, but for PAA/DNA polyplexes the clearance rate did not depend on the carrier's disulfide content. Thus, as with AONs, carrier disassembly cannot be a major barrier for DNA-delivery with PAAs. Instead, Li et al. identified thiol-disulfide exchange reactions on the cell membrane in combination with an increased uptake as key to the enhanced transfection properties of their reduction sensitive DNA polyplexes. Increased uptake has also been reported for reducible PEI polyplexes[198], which suggests that this might be a general property of reduction sensitive carriers. Brülisauer et al. have used a non-reduction sensitive third-generation PAMAM dendrimer, labeled with a reduction sensitive, monomeric BODIPY probe as model to investigate the cleavage mechanism and uptake enhancement of DNA polyplexes in more detail.[197] They concluded that most, if not all, of the carrier's reduction takes place in the extracellular space and is mediated

by cell-surface oxidoreductases. Shielded carriers, e.g., systems equipped with a PEG corona, are, however, more likely to be cleaved by small molecular reductants due to steric effects. The generally low concentration of those reductants in the vicinity of the cell membrane may explain the extracellular stability of shielded systems, compared to non-shielded ones. Furthermore, they did not observe an efficient bioreduction in endolysosomal compartments. The enhanced uptake was explained by the formation of mixed disulfides that anchors the carrier to cell surface.

Despite the growing evidence for an extracellular carrier cleavage, not all studies have found evidence for the involvement of cell surface thiols.[194, 195, 199, 200] Just to give one example, Saito et al. have developed a DNA carrier system based on protamine linked to the cytotoxic pore-forming protein listeriolysin O (LLO) via a disulfide bridge. The toxin is inactive unless the disulfide is cleaved.[199] The comparison of the cytotoxicity and LDH release of free and carrier bound LLO strongly suggested that the reduction process is more dominant after internalization, although, evidence was found for at least some reduction at an early endocytosis stage.

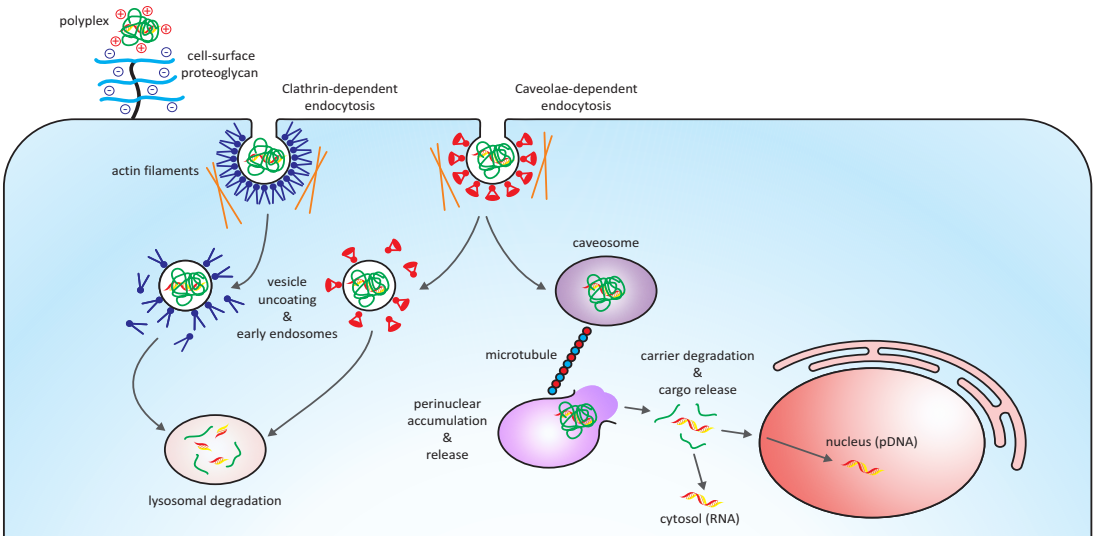

Figure 5.2: Simplified uptake and cellular trafficking scheme of (redox-sensitive) polyplexes

Cationic, non-targeted polyplexes bind to negatively charged cell-surface proteoglycans and are then internalized primarily via clathrin and caveolin-mediated endocytosis. The clathrin-coated and caveolar endocytic vesicles move along actin filaments to the cell interior where they are uncoated and fuse with early endosomes. After endosomal maturation, the fusion with lysosomes leads to the degradation of the nucleic acid cargo, unless the carrier is able to escape the endolysosomal compartment through the “proton sponge” mechanism. In case of a caveolin-mediated endocytosis, polyplexes are also directed to caveosomes, which do not develop into lysosomes. Caveosomes are actively transported along microtubule to the perinuclear region, where the carrier is released. Once exposed to the highly reducing environment of the cytoplasm, the redox-sensitive carrier is degraded and releases its nucleic acid cargo. The molecular target sites of RNAs, such as siRNA or mRNA are located in the cytosol, while pDNA still has to enter the nucleus for transgene expression. Note: Alternative reduction sites have been omitted for the sake of clarity.

Similar to the cell surface's role, the role of the endolysosomal compartment in the reduction of internalized material is disputed. Some studies found evidence for disulfide cleavage along endocytic pathways, while others did not. Yang et al. have demonstrated that the disulfide reduction machinery is active along the entire folate-receptor pathway in KB cells.[200] The cleavage of their FRET probe (folate-(BODIPY FL)-S_2-rhodamine) began in endosomes and did not significantly depend on a cell surface associated or lysosomal reduction. They proposed the involvement of an endosomal ferrireductase in the probe's reduction. Additional folate and transferrin receptor colocalization experiments led them to the conclusion that their findings may also apply to other endocytic pathways. In contrast, when Austin et al. treated SKBr3 cells with a self-quenched trastuzumab-S_2-(rhodamine red)$_{4.5}$ fluorescence probe, they observed no fluorescence increase, i.e., no disulfide linker cleavage upon internalization.[195] They investigated this phenomenon further and developed a method to measure the redox potential of endocytic compartments by expressing a redox-sensitive GFP variant (roGFP1), fused to various endocytic proteins. Surprisingly, recycling endosomes, late endosomes, and lysosomes were found to be oxidizing.

To complicate matters further, primary cultures and cell lines of the very same cell type have been shown to differ in their ability to process internalized reduction sensitive carriers.[40] Such cell type dependent variations could derive from a number of factors, including vesicular trafficking kinetics, expression levels of redox-active proteins, as well as cell proliferation and differentiation.[33, 201] Considering the currently available data, endolysosomal disulfide reduction does not appear to be a universal cellular ability but seems to be restricted to certain specialized cell types, such as antigen-presenting cells (APCs), including bone marrow-derived dendritic cells (BMDCs) and macrophages (BMMs), but also fibroblasts. Redox potential measurements, similar to the method used by Austin et al. have revealed that the endosomal compartments of those cells are reducing, albeit to different degrees.[201] Moreover, disulfide reduction was observed, beginning at early endosomes and continuing throughout the endolysosomal maturation. Endosomal reduction in APCs is mediated by GILT and is pivotal for antigen presentation as it facilitates the unfolding and optimal degradation of endocytosed proteins.[40] It is conceivable to exploit the unique reductive capability of APC for the development of genetic vaccines. This could be done by equipping the carrier with a reductively activated endosomal release function, such as listeriolysin O. Such a system could be quite similar to the LLO-S_2-bPEI 25 and S_2-lPEI 1.8/DNA carrier combination developed by Choi and Lee,[202] but would probably require a non-bioreducible polymer to avoid premature endolysosomal cargo degradation.

Another significant factor in the cellular processing of gene carriers is the uptake mechanism, as it determines the endocytic pathway the vehicles are delivered to and not all pathways re-

sult in a productive transfection. The trafficking pathway substantially depends on factors like the carrier type, the type of nucleic acid, the nature of the target cells, as well as the cell division cycle.[203-205] Interestingly, the presence of disulfide bonds within the carrier does not influence trafficking.[35] For PEI based carriers, several uptake mechanisms, including flotillin-dependent,[190] clathrin- and caveolin-dependent endocytosis,[206, 207] and macropinocytosis[208] have been described. The most commonly cited internalization mechanisms are clathrin- and caveolin-dependent endocytosis.

Clathrin-mediated endocytosis, which is thought to be the kinetically most effective endocytic uptake mechanism,[204] involves the formation of clathrin-coated pits. These pits are pinched off the plasma membrane in a dynamin dependent way to form clathrin-coated vesicles that move along actin filaments towards the cell's interior where they fuse with early endosomes.[209] Early endosomes then mature to late endosomes, which finally fuse with lysosomes. Lysosomes are acidic organelles (pH = 4.5-5.0)[210] with a high content of degradative enzymes, specialized on the breakdown of biomolecules. It is generally agreed that to avoid cargo degradation, any gene delivery system targeting this route must be capable of leaving the endolysosomal compartment at a relatively early endocytosis stage.[204] The most commonly cited escape mechanism for PEIs and comparable polycations with a sufficiently high buffering capacity at physiological conditions is the "proton sponge" effect. It was proposed by Behr[28, 29] and refers to PEI's ability to counteract lysosomal acidification by absorbing the protons that are being pumped into the vesicle by vacuolar-type H^+-ATPases. This process is accompanied by an increased influx of chloride and water, which causes an osmotic swelling.[28] The increased protonation of the polymer amines causes the polymer strands to expand due to electrostatic repulsion, which exerts a mechanical stress on the lysosomal membrane. Combined with direct polymer interactions with the inner lysosomal surface, the organelle eventually ruptures and releases its contents into the cytosol.[28, 204] PEI's endosomolytic property is related to the buffering capacity of its secondary and tertiary amines. Compared to primary amines, they have a relatively low pK_a, thus, are not fully protonated under physiological pH (2°: 50 %, 3°: <50 %).[67] Despite the popularity of the proton sponge hypothesis, more and more evidence has come to light in recent years that question the validity of this explanation or at least suggest that it cannot be the sole or most dominant endolysosomal escape mechanism.[204] Benjaminsen et al. as well as others, for instance, have been unable to confirm an increasing intralysosomal pH commonly associated with the proton sponge effect.[28] However, the significance of a possible pH increase itself is unclear and the hypothesis could still be valid even though no pH-change is observed. Other critics argue that the osmotic pressure built up during endolysosomal acidification would theoretically not be sufficient to cause lysosomes to burst. An increased membrane tension could, nonetheless, contribute to the polyplex release

through causing the formation of temporary membrane pores or by promoting the organelle's eventual disruption due to other factors.[28, 204] On a more fundamental level, in many cases there is a surprising lack of correlation between the vector buffering capacity and the transfection efficiency. There are numerous examples where PEI N-acylation, which decreases the number of protonable amines, has greatly increased the gene transfection efficiency.[75] The topology of PEI also influences the transfection efficiency in a way that cannot be simply explained by the proton sponge mechanism. For example, the transfection efficiency of long PEI chains is superior to that of short chains, although from a thermodynamic point of view the latter would generate a higher intravesicular osmotic pressure at the same polymer concentration.[75] Yue et al. have offered a different interpretation of PEI's role in the endosomal escape and the transfection process in general, where long free PEI are decisive.[75, 211, 212] According to their model, the PEI chains bound to DNA provide the charge neutrality needed to condense the nucleic acid into small, compact particles but otherwise contribute little to the overall transfection. A successful transfection in fact depends on the presence and length of free PEI chains. The ideal chain length with regards to the transfection efficiency and toxicity is about 15 to 20 nm. Interestingly, at this chain length the polymer topology is almost irrelevant for the transfection efficiency. In case of shorter chains, lPEIs are significantly more efficient than bPEIs.[75] They hypothesized that the long cationic polymer chains may embed themselves in anionic vesicular membranes and partially pass through them. The polymer residues present on the outer vesicular surface would interfere with anionic signaling (SNARE) proteins that mediate the fusion with lysosomes and eventually prevent the carrier's endolysosomal degradation. The actual endosomal escape may also be related to the membrane interaction of the polymer.[75] Incidentally, their model could also explain the enhanced efficiency of hydrophobically modified PEIs, since such modifications increase membrane interactions. The effects of the free polymer are not limited to reducing the lysosomal entrapment of polyplexes. According to a recent follow-up study, the free polymer also enhances the nuclear translocation of DNA, the transcription efficiency, and the mRNA's transfer to the cytosol. The cellular uptake, on the other, hand is hardly affected.[212]

Caveolin-dependent endocytosis begins with the engulfment of cargo molecules in caveolae, a subset of lipid rafts that appear as flask-shaped invaginations of the plasma membrane in the presence of caveolin-1.[209] The invaginations bud off the plasma membrane in a dynamin dependent way to form caveolar endocytic vesicles, which fuse with early endosomes and caveosomes. Although the caveolin-dependent endocytosis is slower than the clathrin mediated endocytosis, it is thought to be more efficient in terms of transfection as the pH neutral organelles do not develop into lysosomes, leaving more nucleic acid cargo intact.[204, 209] Caveolar endocytosis per se does not preclude the carriers' exposure to acidic conditions. In fact, acidi-

fication appears to be an essential step for successful gene delivery.[213] How acidification determines the delivery success in this case has seemingly not been investigated in detail, yet. It is, however, reasonable to assume the involvement of the proton sponge or a related mechanism.

The roles of the clathrin- and caveolin-dependent endocytosis in the uptake and transfection efficiency of PEI-based polyplexes have been studied by blocking the respective uptake routes with chemical inhibitors or an siRNA mediated depletion of endocytic proteins. One of the main questions is why the amount of internalized nucleic acid often correlates poorly with the transgene expression.[206, 207, 213, 214] Although the sometimes low specificity of especially chemical inhibitors can make data interpretation challenging,[215] there is general consensus that successful gene delivery particularly involves the caveolar pathway, as it at least partially circumvents cargo routing to lysosomes. Delivery systems specifically designed to take this uptake route, for instance, by having a diameter above the size limit for clathrin-dependent internalization (approx. 200 nm[206, 216]) or by carrying specific targeting ligands (e.g., folate[213]), regularly exhibit higher transfection efficiencies than non-optimized formulations. Inhibiting competing uptakes routes will not necessarily increase transfection efficiency. There is evidence for the existence of compensatory uptake mechanisms, which reroute cargo to non-productive pathways.[214]

The cytoskeleton plays a major role in polyplex uptake and intracellular trafficking.[217] Actin filaments are involved in the uptake itself and early phase trafficking, while in later stages polyplexes are actively transported along microtubules.[189] Depending on the uptake route, the microtubule associated movement includes transport from endosomes to lysosomes, as well as perinuclear accumulation. Based on colocalization experiments with fluid phase markers[189] and microtubule-depolymerizing agents[217], polyplexes are still almost entirely localized in vesicles when they reach the perinuclear region. Perinuclear accumulation seems to be essential for the transfection success, at least as far as the delivery of plasmid DNA is concerned. Cells treated with microtubule network disrupting agents show a dramatically reduced transfection efficiency, even though lysosomal cargo degradation is concurrently inhibited.[217] In other words, the chances for transgene expression increase with the amount of material delivered to the vicinity of the nucleus. This is understandable considering that the size restrictions imposed by the nuclear pore complex are a huge barrier for the nuclear entry of free and complexed DNA in postmitotic cells.[204, 218] Combined with the negligible cytoplasmic diffusional mobility of pDNA and other macromolecules[219], which also indirectly increases the risk for degradation by cytoplasmic nucleases, only a small fraction of the delivered material eventually enters the nucleus. The form in which DNA enters the nucleus, i.e., “free” or in complex with a synthetic polycation, is still a matter of debate. Both possibilities are supported by ex-

perimental data.[218, 220] Microtubule also play major a role in the transfection of dividing cells. Bausinger et al. were able to track the movement of polyplexes along the microtubule of the spindle apparatus and observed carrier accumulation at the site of the emerging daughter nuclei.[189]

Once the delivery system is released from the endolysosomal compartment, it is exposed to the highly reducing environment of the cytoplasm (or the nucleus). Here it faces another important barrier for efficient gene delivery: vector unpacking.[36, 221] Nucleic acids still in complex with a carrier are not or not sufficiently biologically active, so the delivery system must possess efficient means for their release. In polycationic carriers, the release is mediated by ion exchange reactions, i.e., charged cellular components competitively displace the nucleic acid cargo or the polymer. Huth et al. have suggested that mainly tRNA, the second most abundant cellular RNA class, is responsible for the extranuclear cargo displacement in polyamine gene vectors.[222] This conclusion is substantiated by Bertschinger et al., who have observed a higher affinity for RNA than for DNA in most PEI variants.[162] The polyplexes' susceptibility to ion exchange reactions is directly related to the interaction strength of the constituent polyions. As a rule of thumb, polyplex stability increases with polymer chain length and nucleic acid molecular weight (Section 4.3.1). For that reason, the reductive cleavage of the carrier polymer is generally thought to facilitate cargo release in comparison to non-cleavable systems. The validity of this hypothesis is supported by the results of fluorescence-labeling studies. Christensen et al. have observed a diffuse cytoplasmic distribution of fluorescently labeled DNA when a disulfide containing poly(amido ethylenimine) carrier was used. In contrast, an unmodified PEI carrier resulted in globular intracellular structures, interpreted as intact polyplexes.[60] Similar results have been obtained with labeled polymers.[36]

Several groups have investigated the role GSH in the biological activity of reduction sensitive carriers by modulating the cellular GSH concentration, either by using chemical agents like BSO or glutathione reduced ethyl ester (GSH-EE), or by using cell lines with different innate GSH levels.[35, 46, 47, 223] Artificially increasing the GSH level usually increases the transfection activity, albeit the observed differences are often small. Not all nucleic acid types benefit equally from a bioreducible delivery system. The group around David Oupický has used a panel of pancreatic cancer cell lines, with intracellular GSH levels ranging from 1.1 to 7.5 mM, to measure the relative transfection increase of pDNA, mRNA, siRNA, and AON complexes with bioreducible PAA (rPAA) compared to its non-reducible counterpart (PAA) of similar molecular mass.[47] Surprisingly, there was no consistent increase in the relative rPAA transfection efficiency with increasing GSH level. In some cases the transfection efficiency of rPAA polyplexes was even lower than that of the respective PAA-complexes. More importantly, only the high molecular weight nucleic acids (pDNA, mRNA) profited significantly from a rPAA delivery. For AON, the

transfection efficiency increased only marginally; siRNA/rPAA polyplexes demonstrated a similar or slightly lower relative transfection. mRNA was the only nucleic acid that benefited from a delivery with a redox-sensitive carrier across all GSH concentrations. It is worth noting that similar results have been obtained in an earlier study in which reducible and non-reducible PLL derivatives were used for the delivery into three breast cancer cell lines (*c*(GSH) = 2.2 to 3.7 mM).[46] The reason why short nucleic acids like AON and siRNA hardly profit from a delivery with bioreducible carriers probably lies in their already inherently low polycation affinity. Therefore, the polycation's breakdown will not substantially increase vector unpacking. This is different for pDNA and mRNA, however, rapid carrier disassembly does not automatically translate into higher relative transfection levels as other factors come into play as well. The lowest relative transfection efficiency by far, for example, was observed for pDNA polyplexes at the highest GSH concentration and suggests that an optimal unpacking rate exists. If unpacking is too fast, the DNA will be degraded by cytoplasmic nucleases before it is able to reach the nucleus. Slow unpacking, on the other hand, leaves the DNA inaccessible for transcription and might expose it longer to nucleases. The data were also interpreted as evidence for the minor role of nuclear GSH in carrier unpacking. Since the nucleus lacks nuclease activity under normal circumstances, an increased nuclear unpacking would never result in a lower transfection activity. All in all, taking the significantly lower relative transfection increases compared to mRNA polyplexes into account, vector unpacking is a much less critical barrier for the biological activity of pDNA polyplexes than for that of mRNA polyplexes.[196] DNA's lower affinity to polycations likely facilitates its displacement by cytosolic nucleic acids[222], proteins[224], and probably chromosomal DNA, while no similarly efficient mRNA release mechanism is known.

Given the number of open questions surrounding the cellular fate of redox-responsive carriers, there is an urgent need for better tools to investigate the processes outlined above. The fluorescently labeled, redox responsive carriers developed in this work have already demonstrated their usefulness in studying polyplex cleavage under artificial, reductive conditions (Chapter 4). The Chapter at hand seeks to investigate if these carriers can also be used to study polyplex uptake, trafficking and processing in cells. For that reason, CHO cells were treated with different reduction sensitive and non-reduction sensitive polycations in complex with pDNA and siRNA. Carrier cleavage was followed with flow cytometry, confocal laser scanning microscopy, and fluorescence spectroscopy. The cleavage was indeed dependent on cellular thiols and began relatively early after uptake. The majority of the carrier, however, appeared to be cleaved after it had reached the cytosol and the cleavage had a measurable impact on the cellular GSH content.

5.2 Materials and methods

5.2.1 Uptake and cellular processing

Chemicals

Glutathione reduced ethyl ester (GSH-EE), *N*-ethylmaleimide (NEM), and chloroquine diphosphate (CQ) were purchased from Sigma-Aldrich (Munich, Germany) in the highest available quality. Monochlorobimane (mBCl) was obtained from Invitrogen (Darmstadt, Germany). The suppliers of all other materials used are listed in the previous chapters.

MTT assay

The influence of polyplexes on the metabolic activity of CHO cells was assessed in an MTT (3-(4,5-dimethylthiazol-2-yl)-2,5-diphenyltetrazolium bromide) assay. For that, Chinese hamster ovary cells (CHO-K1; ATCC No. CCL-61) were seeded in 24-well plates at an initial density of 80,000 cells/well and grown overnight (37 °C, 5 % CO_2) in Ham's F-12 medium, supplemented with 10 % fetal calf serum (Biochrom AG, Berlin, Germany). Prior to the addition of polyplexes, the cells were washed with DPBS (w/o Ca^{2+}, Mg^{2+}, and phenol red; Invitrogen, Darmstadt, Germany) and the medium was replaced with 200 µL serum free Ham's F-12.
Polyplexes were formed at N/P = 8, in a total volume of 40 µL DPBS according to the general procedure outlined in Section 2.2.3 and were allowed to mature for 5 min. One microgram DNA was used per well (phRLTluc); each sample was prepared in triplicate. The cells were then incubated (37 °C, 5 % CO_2) with the polyplexes for between 15 min and 240 min. The polyplex additions were timed in a way that all incubations were completed at the same time. Reference cells were incubated with 200 µL serum free Ham's F-12 (100 % metabolic activity) or 216 µL serum free Ham's F-12 supplemented with 24 µL of a 10 g/L SDS solution (0 % metabolic activity) for 240 min. Following the incubation, the cells were washed with PBS and 1.2 mL of a MTT working solution (650 mg/L MTT in Ham's F-12 with 10 % fetal calf serum) was added to each well. After four hours of incubation at 37 °C, the solution was replaced with 1.5 mL of a 100 g/L SDS solution. The MTT formazan was solubilized overnight at room temperature and protected from light on an orbital shaker (70 rpm). Finally, sample absorbance at 570 nm was measured on an Uvikon 941 spectrometer upgraded with a UVS900 light kit (Goebel Instrumentelle Analytik, Au in der Hallertau, Germany). A 100 g/L SDS solution served as reference. The relative cellular metabolic activity was calculated by subtracting the absorbance of SDS

treated cells from the absorbance of polyplex treated cells. The result was normalized against the absorbance of untreated cells.

Flow cytometry

For the flow cytometric assays, Chinese hamster ovary cells (CHO-K1; ATCC No. CCL-61) were seeded in 24-well plates at an initial density of 80,000 cells/well and grown overnight (37 °C, 5 % CO_2) in Ham's F-12 medium, supplemented with 10 % fetal calf serum (Biochrom AG, Berlin, Germany). Prior to the addition of polyplexes, the cells were washed with DPBS (w/o Ca^{2+}, Mg^{2+}, and phenol red; Invitrogen, Darmstadt, Germany) and the medium was replaced with 200 µL serum free Ham's F-12.

Polyplexes were formed at N/P = 8, unless indicated otherwise, in a total volume of 40 µL DPBS according to the general procedure outlined in Section 2.2.3 and were allowed to mature for 5 min. Generally, 1 µg nucleic acid was used per well (DNA: pGL3-Enhancer or phRLTluc; siRNA: Bcl-2), unless stated otherwise; each sample was prepared in triplicate. The cells were then incubated (37 °C, 5 % CO_2) with the polyplexes for between 15 min and 240 min; where indicated, the cells were only incubated for 15 min. The polyplex additions were timed in a way that all incubations were completed at the same time. Then, the supernatant of each well, containing non-adherent cells was collected and combined with the detached cells after trypsinization with 250 µL trypsin. If necessary, the cells were carefully scraped off from the bottom of the wells. The cells were washed once or twice with ice-cold DPBS (200 g, 4 °C) and resuspended in 350 µL of the same buffer. The samples were kept on ice until they were measured with the flow cytometer.

In certain experiments the cells were incubated with additional reagents:

In cases where chloroquine was used, 10 µL of a 2.5 mM CQ stock solution (in DPBS) or pure DPBS was added to the serum free medium 20 min before the polyplex addition (c_{final}(CQ) = 100 µM).

For experiments where NEM was used, the maximum tolerable dose and incubation time were determined first by incubating the cells for 30 or 60 min with 240 µL Ham's F-12/10 % FCS, supplemented with either the appropriate volume of a 625 µM NEM stock solution (in DPBS) for final a NEM concentration ranging from 10 to 500 µM or 10 µL pure DPBS. Intact, whole cells were identified and gated in the SSC/FSC plot. Cell viability was evaluated with a PI-assay (see Section 2.2.3). Cells with increased green autofluorescence were identified by plotting their emission intensity in the green channel (530/30 nm) against the forward scattering intensity. The threshold for increased emission intensity was set, using the autofluorescence of untreated cells as reference. In the subsequent experiments with NEM, the cells were incubat-

ed for 1 h with 240 µL Ham's F-12/10 % FCS, supplemented with 10 µL of a 625 µM NEM stock solution (in DPBS; c_{final}(NEM) = 25 µM) or pure DPBS. Immediately prior to the polyplex addition, the cells were washed with DPBS and the medium was replaced with 200 µL Ham's F-12. The same protocol was applied for the GSH-EE incubation, however, the incubation time was 2 h and a 250 mM GSH-EE stock solution (in DPBS; c_{final}(GSH-EE) = 10 mM) or pure DPBS was used. When cell were treated with a combination of GSH-EE and CQ, GSH-EE was added 2 h before the start of the CQ incubation.
For the mBCl-based GSH assay, a 100 mM mBCl stock solution in DMSO was diluted to 4 mM with DPBS. After a two hour long polyplex incubation, followed by a GSH-EE or NEM treatment, the cells were washed with DPBS and 297 µL Ham's F-12, supplemented with 3 µL of the mBCl stock solution (c_{final}(mBCl) = 40 µM) was added to each well. After 20 min the cells were washed again and trypsinized for flow cytometry.

All flow cytometric measurements, with the exception of two experiments, were carried out on a BD FACSCalibur flow cytometer (Heidelberg, Germany), controlled by the software BD CellQuest Pro. The fluorophores were excited at 488 nm. The BODIPY and TAMRA emissions were collected in the FL1 (530/30 nm) and the FL2 (585/42 nm) channel, respectively. The measurements for the mBCl thiol determination and for one of the TAMRA-lPEI_2 uptake experiments were performed on a BD FACSCanto II (Heidelberg, Germany), at the Institute for Pathology of the University of Regensburg, with assistance from Prof. Gero Brockhoff. The mBCl-GSH adduct was excited at 405 nm and its emission was collected in the AmCyan channel (525/50 nm); TAMRA was excited at 488 nm and detected in the PE channel (585/42 nm).
In all cases, ten thousand events were collected per sample and the data analysis was performed with WinMDI 2.9 (J. Trotter, The Scripps Research Institute, La Jolla, CA, USA). First of all, the sideward scattering intensity was plotted against the forward scattering intensity and a gate was set on the events corresponding to intact, living cells. Next, the fluorescence intensity of the respective fluorescent label was plotted against the forward scattering intensity. Then a threshold for the emission intensity was set, using untreated cells as reference for cellular autofluorescence. Finally, the number and mean fluorescence intensity of all events with a fluorescence intensity above the autofluorescence level were assessed and the results were exported to MS Excel via MDI StatCon 2.6.

5.2.2 Confocal laser scanning microscopy

The intracellular distribution and processing of BP_2-labeled DNA polyplexes were studied with the help of a Zeiss Axiovert 200 M microscope (objective: Plan-Neofluar 40×/1.3 Oil) coupled to a Zeiss LSM 510 scanning device (Carl Zeiss Co. Ltd., Germany). The fluorophore was excited

at 488 nm (Ar^+-laser) and the emitted light was collected using a 505-530 nm bandpass filter in single track mode. The images were analyzed with ZEN 2012 (Carl Zeiss Microscopy GmbH, Jena, Germany).

On the day prior to the experiments, Chinese hamster ovary cells (CHO-K1; ATCC No. CCL-61) were seeded in 24-well glass bottom plates at an initial density of 80,000 cells/well in Ham's F-12 medium, supplemented with 10 % fetal calf serum (Biochrom AG, Berlin, Germany). The cells were grown overnight (37 °C, 5 % CO_2) and then washed with DPBS (w/o Ca^{2+}, Mg^{2+}, and phenol red; Invitrogen, Darmstadt, Germany), before changing to 200 µL serum free Ham's F-12 medium.

For experiments with chloroquine (CQ), the cells were preincubated for 10 min with either 10 µL of a chloroquine stock solution (2.5 mM in DPBS) or pure DPBS.

PEI/DNA polyplexes (DNA: pGL3-Enhancer; N/P = 12) were formed in a total volume of 40 µL DPBS according to the general procedure outlined in Section 2.2.3 and allowed to mature for 5 min. Generally, 1 or 2 µg DNA were used per well. After the addition of the polyplexes, the cells were incubated (37 °C, 5 % CO_2) for one, four, and six (only in CQ experiments) hours. Immediately prior to the measurements, the cells were washed twice with DPBS before changing to 240 µL Ham's F-12/10 % FCS, containing 20 mM HEPES to maintain a pH of 7.4 without CO_2 injection.

5.3 Results and discussion

5.3.1 Preliminary experiments

In order to study uptake, trafficking and intracellular processing of reduction sensitive polyplexes based on polycations labeled with the redox sensitive BP_2 probe, several general experimental variables, including incubation times, N/P ratios, and amounts of nucleic acids had to be established. It is important to carefully set those variables as some unspecific cellular responses can mimic the fluorescence intensity increase following the probe's cleavage. Cellular autofluorescence, for instance, can be an issue as it occurs in the same spectral range[225] as the emission of many dyes, including BODIPY. Autofluorescence is usually weak and, more importantly, of constant intensity, which allows it to be simply subtracted from the probe's fluorescence. The presence of cytotoxic agents like PEI, however, can alter autofluorescence drastically,[226] and interfere with intensity based assays. Similarly, externally induced changes in the metabolic activity of cells could interfere with the intracellular processing of the carrier.

Cellular metabolic activity

Initially, it was investigated if and how the presence of the cystine cross-linker and the fluorescent label influenced the metabolic activity of CHO-K1 cells. It is conceivable, for instance, that the uptake of large amounts of cleavable disulfides depleted the cellular thiol pool, which in turn could interfere with carrier processing and lead to unspecific toxicity due to the rise of reactive oxygen species. It would then be difficult to compare the data obtained for the processing of linear and disulfide cross-linked polycations.

The MTT-assay is widely used for assessing cellular metabolic activity. It is based on the NAD(P)H-dependent reduction of a tetrazolium dye. Since, NAD(P)H plays a key role in maintaining the cellular GSH/GSSG balance (see Section 5.1.1), the assay is indirectly sensitive to changes in the cellular thiol pool, i.e., any significant changes in the redox balance would also be reflected in changes in the cellular metabolic activity.

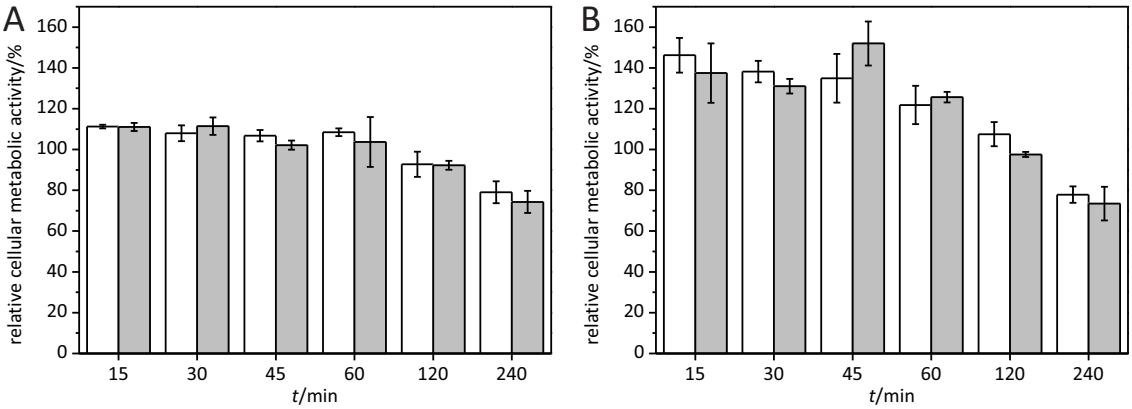

Figure 5.3: Time course of the relative metabolic activities of PEI/DNA-polyplex treated CHO cells

CHO cells were incubated for between 15 and 240 min with pDNA polyplexes based on (A) BP_2-lPEI (white bars) and S_2-lPEI_b (gray) or (B) S_2-lPEI_b (white) vs BP_2-S_2-lPEI_1 (gray). Per 80,000 cells, 1 µg of phRLTluc DNA was used (n = 3, N/P = 8). The cellular metabolic activity was determined with an MTT assay and the data were normalized against the activity of untreated cells; mean values ± sample standard deviation shown. (Experimental details Section 5.2.1)

CHO cells were treated with pDNA polyplexes based on BP_2-lPEI, S_2-lPEI_b, and BP_2-S_2-lPEI_1 under the same conditions used in the later uptake experiments. In all cases a slight (to approx. 110 %, Figure 5.3A) to moderate (to approx. 150 %, Figure 5.3B) increase in the metabolic activity was seen in the first hour of incubation, followed by a modest, steady decrease to about 80 % of the reference value. The assay appeared to be quite sensitive towards variations of the experimental conditions and only allowed for qualitative assessments, as the activity of S_2-lPEI_b/DNA treated cells varied by as much as about 35 % between two independent experiments. These variations are probably related to slightly different cell culture conditions. Adherent cells are known to be contact inhibited, i.e., their metabolism slows down when the culture approaches confluence.[227] Taking this into account, there were no significant differ-

ences between the polyplex types. Neither the presence of the cross-linker nor of the fluorescent label changed the metabolic activity noticeably.

As far as the time course of the metabolic activity itself is considered, the increase seen within the first hour could signify the beginning of the transgene expression, however, metabolic activities above 100 % upon exposure to low doses of cytotoxic agents are not uncommon[228] and the transgene expression for PEI based carriers has been reported to start only about 4.5-5.5 h posttransfection[229]. The decreased activity later on is a result of increasing cytotoxic effects due to the prolonged exposure to especially free PEI. This early stage toxic reaction is commonly referred to as Phase I or immediate cytotoxicity and is caused by binding of PEI molecules to plasma surface proteoglycans, resulting in membrane destabilization and phosphatidylserine exposure.[229, 230]

NEM-Toxicity

When investigating the intracellular processing of redox sensitive carriers, it is often necessary to modulate the cellular thiol or more specifically the GSH concentration. One of the most commonly used agents for thiol depletion is *N*-ethylmaleimide (NEM). In contrast to glutathione synthesis inhibitors like buthionine sulfoximine (BSO), it reacts nonspecifically with GSH and protein thiols and does not require overnight incubation. It is important to note, however, that about 20 % of protein thiols are resistant to NEM modification under native conditions.[231]

Typically, an almost complete GSH-depletion requires a 30 min incubation with 50-100 µM NEM[232, 233] but preliminary experiments revealed that those conditions were far too toxic for the CHO cells used here. In order to determine the maximum tolerable NEM dose, CHO cells were incubated with between 10 and 500 µM NEM for 30 and 60 min before assessing their integrity (Figure 5.4A), viability (Figure 5.4B), and autofluorescence in the spectral range of the BODIPY emission (Figure 5.4C). NEM-concentrations above 25 µM caused a steep decrease of the first two parameters and a steep increase of the latter, especially at the longer incubation time. After 60 min of incubation, practically no viable cells remained at an NEM concentration equal to or greater than 150 µM (Figure 5.4B). Based on these data, a one hour incubation with 25 µM NEM was considered tolerable. In order to verify that those conditions actually lead to a significant GSH depletion, the intracellular GSH concentration of suspended CHO cells, preincubated with 12.5 and 25 µM NEM or 100 µM BSO, was determined with an mBCl assay (data not shown). mBCl itself is non-fluorescent but in the presence of GSH the enzyme glutathione S-transferase catalyzes the formation of a highly fluorescent mBCl-GSH adduct.[234] Hence, the adduct's emission intensity correlates with the initial GSH level. An incubation with 25 µM NEM lowered the GSH content very significantly (18 % of the emission intensity of non-

treated cells), albeit to a lesser degree than the BSO treatment (7 %), probably because part of the NEM was also consumed in competing reactions with protein thiols. A treatment with only 12.5 µM NEM was inefficient (68 %).

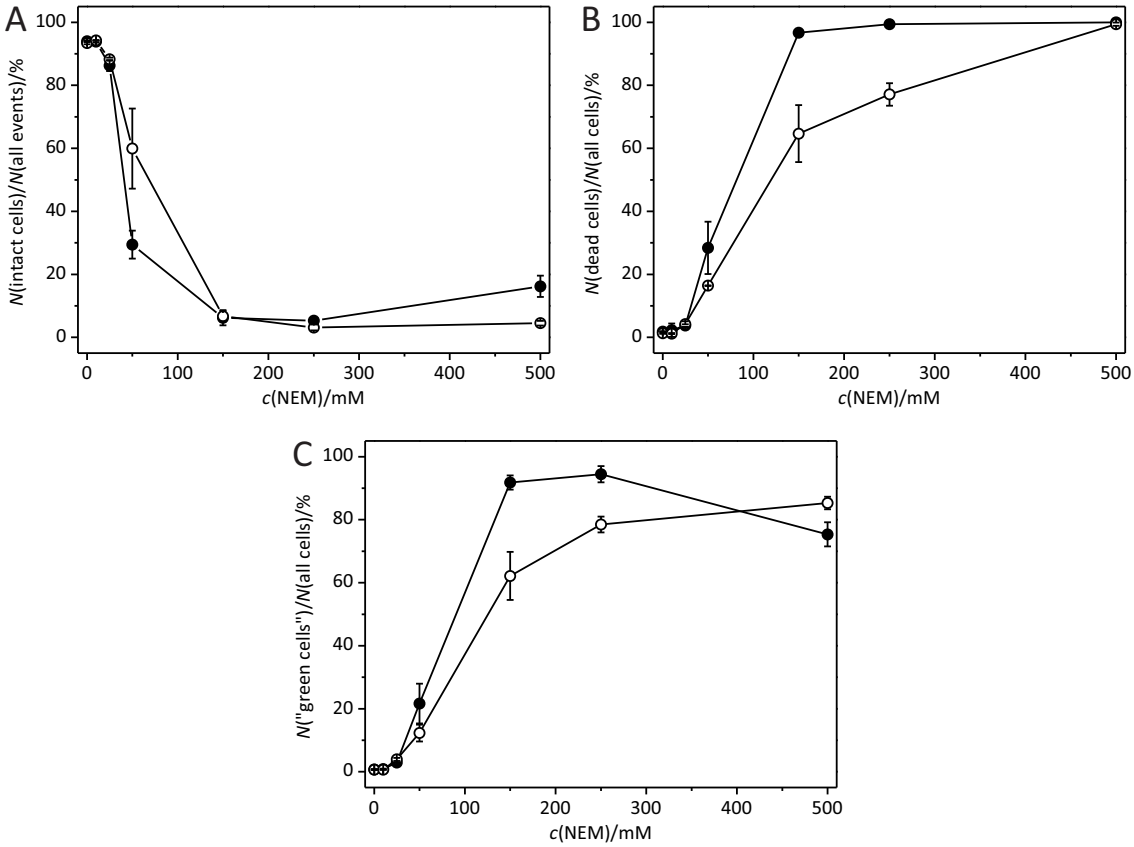

Figure 5.4: Determination of maximum tolerable NEM dose and incubation time

CHO cells were incubated with different NEM concentrations (10 to 500 µM) for 30 min (○) or 1 h (●). Cell integrity, viability, and cellular autofluorescence intensity was determined with flow cytometry (n = 3). A: Ratio of intact cells to all measured events. B: Ratio of non-viable cells (identified through PI uptake) to all intact cells. C: Ratio of cells with an increased autofluorescence (530/30 nm) in comparison with non-treated cells to all intact cells. (Mean values ± sample standard deviation; experimental details Section 5.2.1)

Taken together, a one hour incubation with 25 µM NEM was indeed enough to reduce the intracellular GSH concentration to a level suitable for subsequent experiments.

TAMRA-PEI/DNA uptake

Next, the basic experimental parameters for a flow cytometric investigation of the cellular processing of BODIPY-PEI based polyplexes (Section 5.3.2) were established. For that purpose, preliminary experiments were performed with TAMRA-PEIs. TAMRA is an ideal tool to establish a reference time course of the cellular emission intensity during polyplex uptake and processing as it is insensitive towards reactions with thiols and pH-changes.

In a first experiment, CHO cells were incubated for 15 min with TAMRA-lPEI_2/DNA polyplexes (Figure 5.5A, ●; N/P = 8) and non-complexed TAMRA-lPEI_2 (○). After the cells had been washed and the medium had been replaced, the TAMRA emission intensity was followed for up to 240 min. The initial 15 min incubation led to a rapid, about fourfold intensity increase compared to non-treated cells (data not shown), followed by a further, significantly slower increase after the medium replacement. The emission intensity of cells only treated with the polymer plateaued at about 45-60 min posttransfection (Figure 5.5A, ●), while that of polyplex treated cells steadily increased further (Figure 5.5A, ○). In both cases, the fluorescence intensity at the 4 h time point approximately corresponded to the intensity 24 h posttransfection (data not shown).

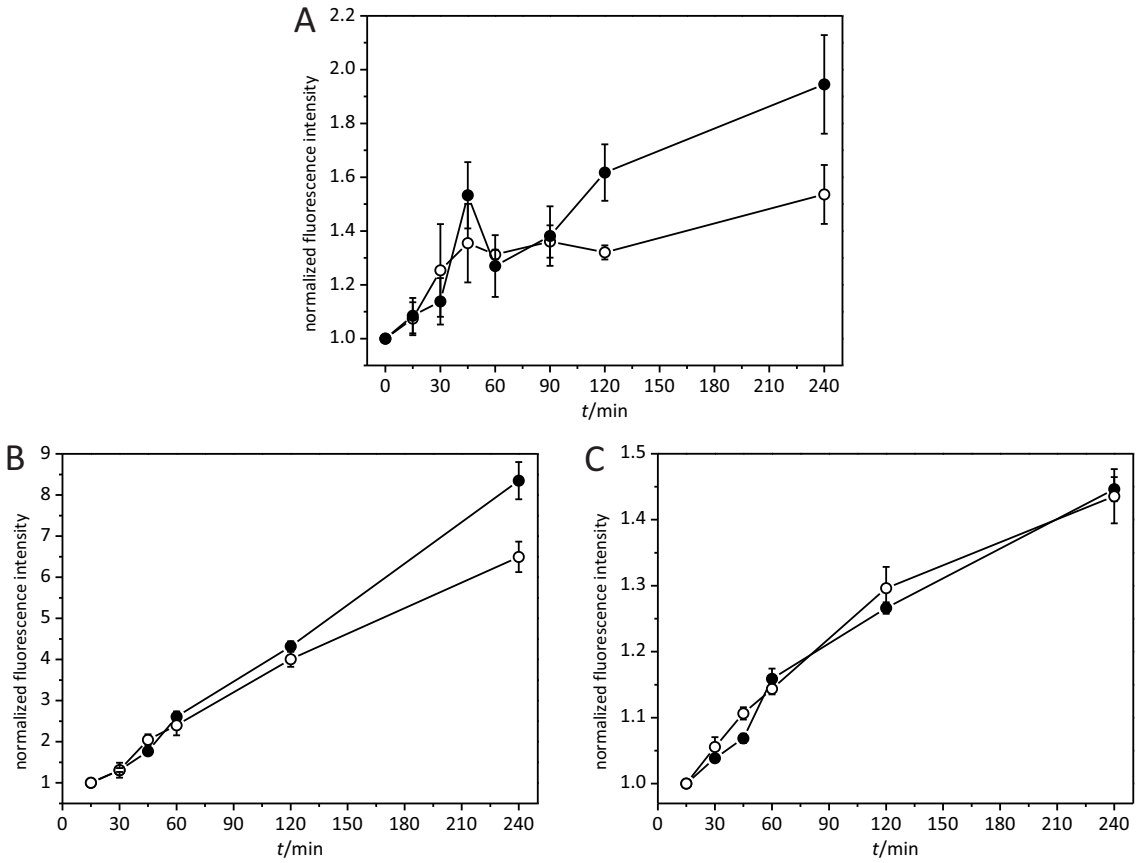

Figure 5.5: Fluorescence intensity of TAMRA-PEI/DNA treated CHO cells and the influence of CQ

A: CHO cells were incubated for 15 min with TAMRA-lPEI_2 alone (○) or in complex with pDNA (●) and then cultivated for up to 240 min. B and C: CHO cells were pretreated for 20 min with a 100 µM chloroquine solution (●; untreated cells: ○) before the addition of pDNA polyplexes based on TAMRA-lPEI_2 (B) or TAMRA-S_2-lPEI_b (C). The polyplex incubation times ranged from 15 to 240 min.

Per 80,000 cells, 2 µg of pGL3-Enhancer (A) or 1 µg of phRLTluc (B and C) DNA were used (n = 3, N/P = 8). The cellular TAMRA fluorescence intensity was determined with flow cytometry. (Mean values ± sample standard deviation; experimental details Section 5.2.1)

The fast and strong fluorescence intensity increase during the initial 15 min incubation period signifies a phase during which HSPGs and polyplexes bind to each other and are rapidly co-

internalized.[191] A surface attachment this rapid has been reported for other cell types as well.[189] Interestingly, the role of HSPGs in the polyplexes' cell surface binding itself is disputed. While it is commonly assumed that anionic HSPGs and cationic gene carriers interact electrostatically,[190] newer experimental data based on the transfection efficiency of alkylated PEI carriers and polyplex uptake in HSPG depleted cells highlight the role of hydrophobic interactions. Nevertheless, HSPGs appear to be important for efficient uptake and transfection, by inducing lipid raft clustering and by providing additional means for endosomal escape.[192] It is worth noting that disulfides are less hydrophobic than methylene groups[36] so their presence might potentially impede cell binding.

The initial fast HSPG dependent polyplex uptake is quickly saturated and the internalization rate becomes dependent on the HSPG recycling rate.[192] As the time frame of this first phase is short compared to the overall intracellular trafficking and processing, large differences in the emission intensity time courses of the polycationic carriers tested here cannot be expected. Thus, only the following, slower phase was investigated more closely (Figure 5.5A) in the subsequent experiments.

As all unbound carrier is removed during the washing step and medium replacement following the initial 15 min incubation, the fluorescence intensity increases in the second phase have to be related to the uptake and intracellular processing of already cell associated material. Considering the label's pH-insensitivity and the absence of any redox cleavable polymer functionality, the fluorescence dequenching is likely related to a decompaction of the carrier and non-complexed polymer. Polyplexes (Figure 5.6B) and free PEIs (Figure 5.6A) are known to accumulate in, presumably HSPG containing, lipid raft rich areas of the plasma membrane before uptake.[192, 220] This clustering should have little effect on the polyplexes' emission intensity, as TAMRA's fluorescence had already been quenched during polyplex formation (see Section 4.3.2). In case of the free polycation, however, the high local polymer concentration, combined with the near-neutral pH environment and the HSPGs' charge neutralizing effect, both of which lower the polymer's intra- and interstrand repulsion, allows individual probes to come into close enough contact with each other to allow for efficient fluorescence quenching. The label would later regain its emissive properties once the polymer has reached acidic organelles and the endocytic receptors have been recycled back to the plasma membrane. This hypothesis is supported by data from Payne et al. who have investigated vesicular polyplex trafficking in colocalization experiments.[190] The fast initial increase in the TAMRA-lPEI_2 emission observed here, for instance, coincides with the time at which Payne et al. saw a maximum polyplex colocalization with Rab5, a marker for early endosomes (pH = 5.9-6.8)[235]. At that stage, 15-20 min after uptake, most endocytic receptor recycling takes place. Later on they observed a steadily increasing colocalization with the late endosomal (pH = 4.9-6.0) marker Rab9 which

plateaued after about 40 min.[235] Since the TAMRA emission reaches a plateau at roughly the same time, this suggests that non-complexed TAMRA-lPEI_2 reaches the endolysosomal compartment in a fully dequenched state (Figure 5.5A, ○).

The slow and steady intensity increase in case of polyplexes, on the other hand (Figure 5.5A, ●), can be explained with the significant complex stability, demonstrated in the previous chapter. Probe-probe dequenching can only occur if the polyplex dissociates and the distance between individual TAMRA molecules increases sufficiently. In this case, however, ionic competitors are simply unable to quickly and fully penetrate the complex to destabilize it.

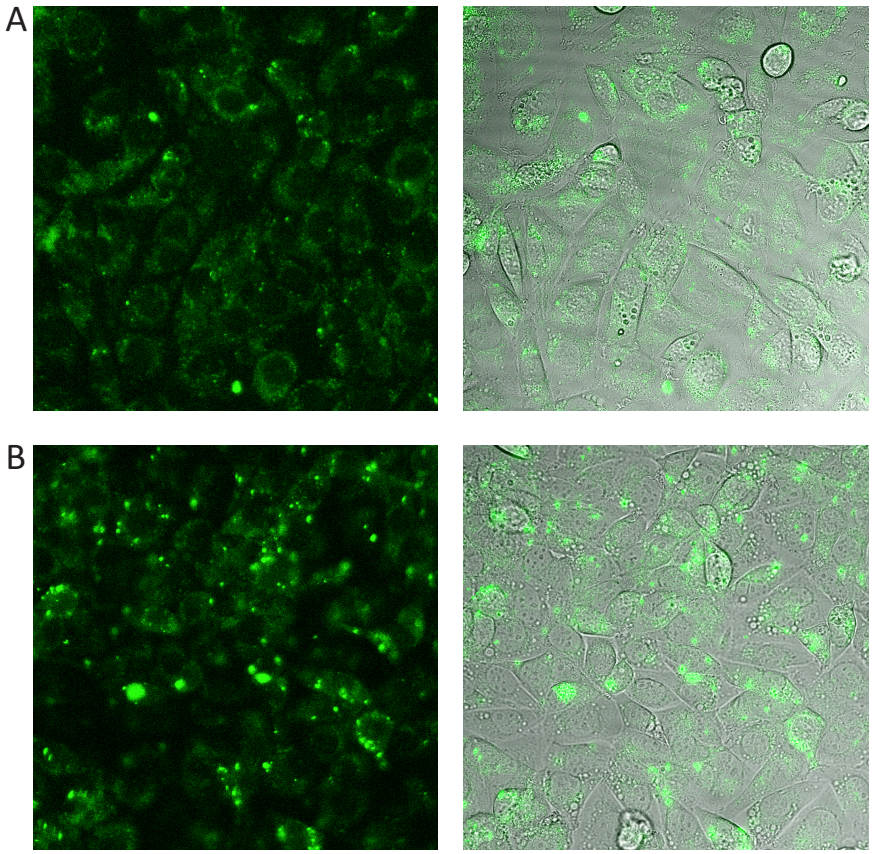

Figure 5.6: Representative confocal micrographs of BP_2-lPEI and BP_2-lPEI/DNA treated CHO cells

CHO cells were incubated for 1 h with either BP_2-lPEI (A) or BP_2-lPEI/DNA polyplexes (B). Per 80,000 cells, 1 µg pGL3-Enhancer pDNA was used (N/P = 12). All images were taken using identical measurement settings. Left column: BODIPY fluorescence images, right column: transmitted light images combined with the fluorescence images. Picture dimensions: 225 µm × 225 µm. (Experimental details Section 5.2.2)

In order to gain a more detailed insight into polyplex trafficking and processing, cells were treated with DNA polyplexes based on TAMRA-lPEI_2 (Figure 5.5B) and its disulfide cross-linked counterpart TAMRA-S_2-lPEI_b (Figure 5.5C) in combination with chloroquine. Chloroquine is a lysosomotropic agent known to enhance gene expression for certain polycationic gene delivery systems through a combination of at least three different mechanisms.[236] As weak base (pK_a = 8.1 and 10.2) it strongly accumulates in acidic cellular compartments, especially lysosomes. An only 30 min exposure to 100 µM CQ can lead to an intracellular concen-

tration of around 4 mM (12 mM after 4 h). Once located in late endosomes and lysosomes, CQ facilitates the release of the delivered nucleic acid by preventing vesicular acidification similar to PEI.[236] For that reason, mainly carriers lacking buffering capacity in the relevant pH-range, such as PLL, benefit from a CQ treatment. Low molecular weight PEIs, as the one used here, are also known to be insufficiently endosomolytically active and require the presence of external lysosomotropic agents in order to attain high transfection efficiencies[53, 237]. CQ is also a strong intercalator and appears to increase carrier destabilization, making more unpacked DNA available for transcription. There seems to be an optimal CQ concentration above which DNA accessibility is reduced again.[238] The direct CQ-DNA interaction has also been suggested to provide beneficial changes of the biophysical properties of the nucleic acid, for instance, by offering DNase protection.

This experiment with CQ and all subsequent uptake experiments used a simplified incubation protocol, where the polyplexes are not removed after 15 min, but remain on the cells for up to 4 h. Therefore, the intensity time course reflects a continuous cellular polyplex association as well as polyplex uptake and intracellular processing. In case of TAMRA-lPEI_2 (Figure 5.5B), the fluorescence intensity increased steadily over the course of 4 h. The presence of CQ resulted in a slightly higher intensity increase at the end of the incubation period. This is most probably an artifact as a complementary experiment performed under the same conditions with lPEI/DNA polyplexes labeled with monomeric (i.e., pH- and redox-insensitive) BODIPY revealed no differences (Figure 5.8B). An incubation with polyplexes based on TAMRA-S_2-lPEI_b (Figure 5.5C) also resulted in a steady intensity increase, unaffected by the presence of CQ. The fluorescence time course can be interpreted as further evidence for the extraordinary stability of PEI/DNA complexes, even with low molecular weight lPEI (see Section 4.3.1). If a significant carrier destabilization occurred, either through the direct action of CQ or indirectly by ion competition after the polyplex had been forced into the cytosol, the TAMRA probe would be dequenched, thus increasing the emission intensity. Moreover, the almost identical time courses for the redox-sensitive and the inert carrier system confirm that both are indeed processed similarly[35].

5.3.2 Processing of BODIPY-PEI based polyplexes

The uptake and intracellular processing of reduction sensitive polyplexes was investigated with the help of linear and disulfide cross-linked PEIs, labeled with either BP_2 or its non-thiol cleavable monomeric counterpart BP.

First, it had to be established if the BP_2 probe is indeed cleaved under the experimental conditions and if this cleavage is thiol dependent. For that, CHO cells were incubated with DNA polyplexes based on BP_2-lPEI (Figure 5.7A, ○) and BP-lPEI_3 (●) as non-cleavable reference. In

both cases, the BODIPY emission increased linearly over the whole observation period of four hours. In case of BP_2-lPEI, however, the intensity rose much faster right from the beginning. In order to verify that the increase was dependent on cellular thiols, the cells were pretreated with NEM before the addition of BP_2-lPEI/DNA and indeed, the presence of the thiol blocker (Figure 5.7B, ●) led to a decreased fluorescence intensity compared to non-pretreated cells (○). Again considering the carrier's inability to reach the cytosol on its own, both findings indicate that the carrier is exposed to reductive conditions at the cell membrane or right after uptake and during all its way through the endolysosomal compartment. In theory, the intensity increase for BP_2-lPEI polyplexes could also be caused by a cleavage in the thiol rich cytosol, if the polyplexes escaped the endolysosomal compartment due to some weak, residual endosomolytic activity. The resulting emission increase would be indistinguishable from an endolysosomal reduction. To verify that the intensity increase was unrelated to an endolysosomal escape, the cells were also incubated with BP_2-PLL/DNA polyplexes after a NEM pretreatment (Figure 5.13B). PLL is a non-buffering vector, well known to be incapable of inducing endosomal escape without additional modifications.[239] Again, the presence of NEM significantly lowered the fluorescence intensity compared to non-NEM treated cells and the overall emission followed a similar pattern as that of BP_2-lPEI/DNA/±NEM treated cells (Figure 5.7B), confirming that PEI (and PLL) based polyplexes are indeed exposed to reductive conditions in the endolysosomal compartment, and quite possibly already at the plasma membrane.

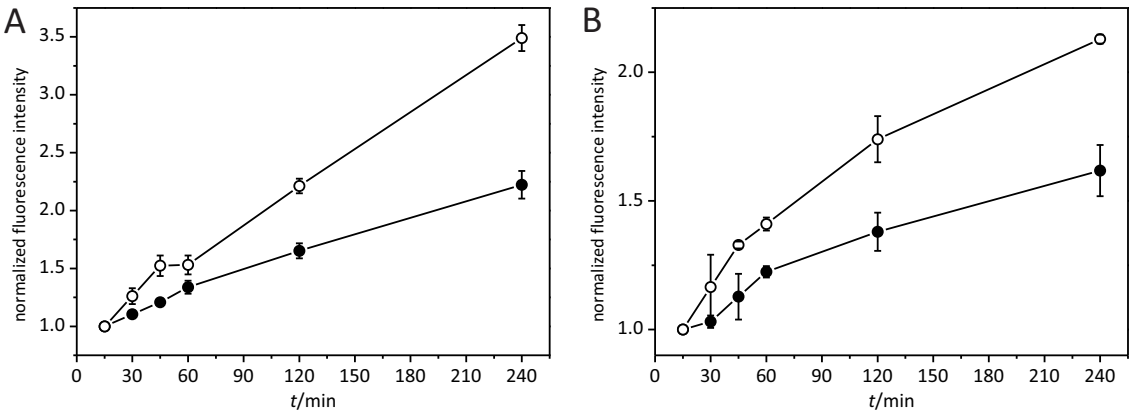

Figure 5.7: Fluorescence intensity of BODIPY-PEI/DNA treated CHO cells and the influence of NEM

A: CHO cells were incubated for between 15 and 240 min with BP_2-lPEI (○) or BP-lPEI_3 (●) in complex with pDNA. B: CHO cells were pretreated for 1 h with a 25 µM NEM solution (●; untreated cells: ○). After a washing step, the cells were incubated for between 15 and 240 min with BP_2-lPEI/pDNA polyplexes.

Per 80,000 cells, 1 µg of pGL3-Enhancer (A) or phRLTluc (B) DNA was used (n = 3, N/P = 8). The cellular BODIPY fluorescence intensity was determined with flow cytometry. (Mean values ± sample standard deviation; experimental details Section 5.2.1)

A long-lasting cleavage, starting immediately after exposing CHO-cells to a polymeric reduction sensitive probe has also been observed by Feener et al.[240] With the help of their probe con-

sisting of radioiodinated tyramine linked through a disulfide bond to a non-proteolytically degradable poly-D-lysine ([^{125}I]-tyn-SS-PDL), they were able to identify two distinct cleavage phases. The first phase was cell surface related and could be blocked by membrane impermeant sulfhydryl inhibiting agents. The second, intracellular phase began about 30 min after incubation and by using subcellular fractionation and kinetic analysis, they identified the Golgi apparatus as the most probable reduction site. Neither endosomes nor lysosomes appeared to be involved in the probe's cleavage. The relevance of this finding for the processing of polyplexes is, however, questionable. The Golgi apparatus is usually not regarded as a major player in the reduction of internalized gene carriers in more recent literature, nor do unmodified polyplexes seem to reach it to a significant degree[241]. The fundamentally different conclusion of Feener et al. may be explained by considering the limitations of their analytical method as well as the characteristics of their probe. Subcellular fractionation is notorious for cross-contamination of components from various compartments. The identity of each individual fraction must, therefore, be verified by checking for the presence of compartment specific protein markers. In their case this had only been done for the lysosomal but not for the Golgi fraction. More importantly, their polymeric probe has demonstrated a strong adherence to cell membranes and it is highly likely that this binding persists after uptake and during trafficking.[240] As a result, the probe would be subjected to membrane recycling and may reach pH-neutral intracellular sites where the initially observed membrane associated reduction could continue.[240] Polyplexes at the other hand, would have been released from the endolysosomal compartment at this time point.

The previous experiments alone did not reveal the extent of probe cleavage during uptake and at the early trafficking stage, compared to the cleavage during the entire intracellular processing. Considering the high cytosolic GSH content, most of the carrier may actually only be cleaved after having reached this compartment. In order to assess the role of cytosolic cleavage, cells were pretreated with CQ before the addition of BP_2-lPEI/DNA. The pretreatment resulted in a considerable intensity increase after sixty minutes of incubation (Figure 5.8A, ●) compared to the non-pretreated control. Similar to TAMRA-lPEI_2/DNA, this was not the case when BP-lPEI_3/DNA polyplexes were used (Figure 5.8B, ●). Confocal microscopy revealed that the fluorescence intensity increase was not evenly distributed within cells, but mainly concentrated in large perinuclear structures (Figure 5.9B). It should be noted that the observed fluorescence intensity changes cannot be the result of some non-specific side effect related to CQ. The agent is not known to significantly affect polyplex uptake,[236] does not absorb or emit in the wavelength range ($\lambda_{abs\ max}$ = 342 nm, $\lambda_{em\ max}$ = 380 nm) relevant for this experiment and has an exceptionally low fluorescence quantum yield[242]. The emission intensity increase coincides with the time polyplexes approximately need to reach late endosomes and lysosomes[190, 243],

from where the polyplexes would be released into the cytosol in the presence of CQ. Thus, it is reasonable to assume that the measured intensity increase originates from the cleavage of the redox sensitive probe in the cytosol. This hypothesis is supported by corresponding confocal micrographs, where in non-CQ treated cells (Figure 5.9A), the fluorescence is concentrated in small, circular, mainly perinuclear spots, which is commonly interpreted as polyplexes localized in vesicles[30, 243]. Upon endosomal release in the presence of CQ, however (Figure 5.9B), the fluorescence appears as large, strongly emitting irregular patches. Considering the experiments with TAMRA-PEIs (Figure 5.5) and the fact that the addition of CQ had no similar effect on the emission of BP-lPEI_3/DNA treated cells (Figure 5.8B, ●), the fluorescent patches most likely consist of intact polyplexes and dequenched BP monomers, released from a dangling configuration (Section 3.5.3). Apparently, polyplex stability and with it, the pDNA cargo release rate is unaffected by the endosomal escape, which again confirms the considerable complex stability found in the earlier in vitro experiments (Section 4.3.1).

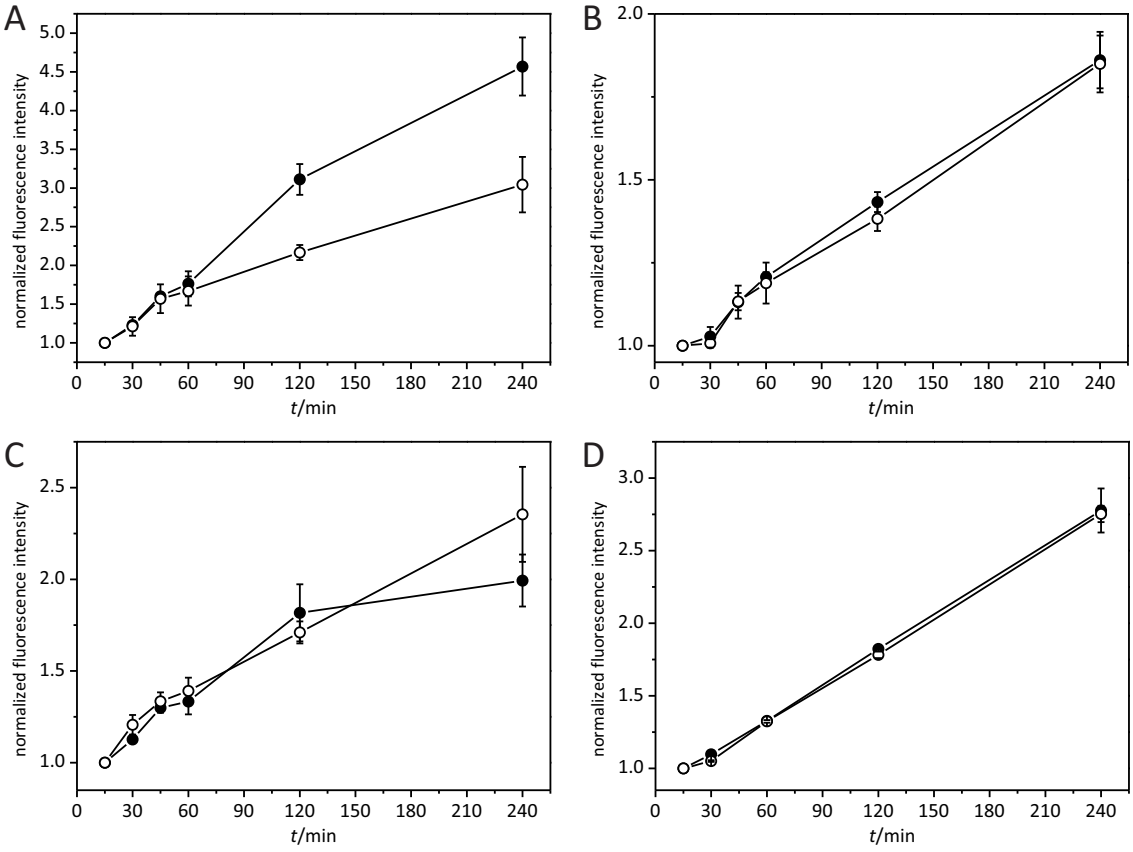

Figure 5.8: Fluorescence intensity of BODIPY-PEI/DNA treated CHO cells and the influence of CQ/GSH-EE

CHO cells were incubated for between 15 and 240 min with either BP_2-lPEI (A) or BP-lPEI_3 (B) based DNA polyplexes after a 20 min pretreatment with 100 µM chloroquine (●; untreated cells: ○). Additionally, cells were treated with BP_2-lPEI/DNA polyplexes after a 2 h pretreatment with 10 mM glutathione ethyl ester (●; untreated cells: ○) alone (C) or in combination (D) with 100 µM chloroquine.

Per 80,000 cells, 1 µg of pGL3-Enhancer (A and B) or phRLTluc (C and D) DNA was used (n = 3, N/P = 8). The cellular BODIPY fluorescence intensity was determined with flow cytometry. (Mean values ± sample standard deviation; experimental details Section 5.2.1)

The contribution of the cytosolic cleavage to the overall cellular cleavage was estimated based on the relative fluorescence intensity increases at 240 min. Cells treated with only BP_2-lPEI/DNA (i.e., cellular association, non-cytosolic cleavage) displayed a 2.1 to 3.4-fold intensity increase. The additional treatment with NEM (i.e., only cellular association, no cleavage) and CQ (i.e., cellular association, cytosolic and non-cytosolic cleavage) resulted in a 1.6 and 4.5-fold increase, respectively. Thus, the non-cytosolic cleavage alone would amount to a 0.5 to 1.9-fold increase. The probe's reduction only in the cytosol, however, would increase the emission intensity 1.1 to 2.4-fold, which suggests that the cytosol is the main reduction site for polyplexes capable of endosomal escape.

In an additional experiment to elucidate the role of cytosolic GSH in the cleavage of the redox probe, cells were incubated with GSH-EE to increase the cellular and especially the cytosolic GSH level. Surprisingly, the GSH-EE pretreatment did not increase the cleavage rate (Figure 5.8C), even if the cells were additionally treated with CQ (Figure 5.8D). As the experiments with NEM have clearly demonstrated that the probe's cleavage is definitely dependent on cellular thiols, this raises the question if and to what degree a physiological cellular GSH level is actually limiting for the cleavage. In order to get a clearer picture of the relationship between GSH level and probe (and carrier) cleavage, the intracellular GSH content was measured with a GSH specific mBCl assay. It must be pointed out, however, that an mBCl assay is susceptible to relatively small changes in the experimental conditions and, therefore, only allows for a qualitative or semi-quantitative GSH determination. mBCl itself, for instance, has been suspected to stimulate the GSH resynthesis[244] and the mBCl-GSH adduct is known to be degraded and exported[234, 244], resulting in lower apparent GSH levels. This susceptibility is in fact reflected in the data of a first experiment where CHO cells were treated with increasing amounts of uncomplexed lPEI (Figure 5.10A, white bars) or S_2-lPEI_b (Figure 5.10B, white bars) and their corresponding complexes with DNA (Figure 5.10, gray bars). At the lowest N/P (6, lPEI) the mBCl-GSH fluorescence intensity corresponded to a GSH level above that of non-polymer treated cells. Conversely, at the highest N/P (24, S_2-lPEI_b) the apparent GSH-concentration was lower than that of NEM treated cells. Moreover, the adduct's emission intensity always decreased with increasing N/P, i.e., polymer dose, even with the lPEI (and bPEI 25; data not shown) – a reference polymer devoid of any thiol reactive functionality. It is obviously difficult to compare the absolute fluorescence intensities of cells treated with different PEI variants, due to the non-specific, most probably toxic polymer effects that interfere with the assay. It may still be useful to at least assess the general trend for each individual polymer.

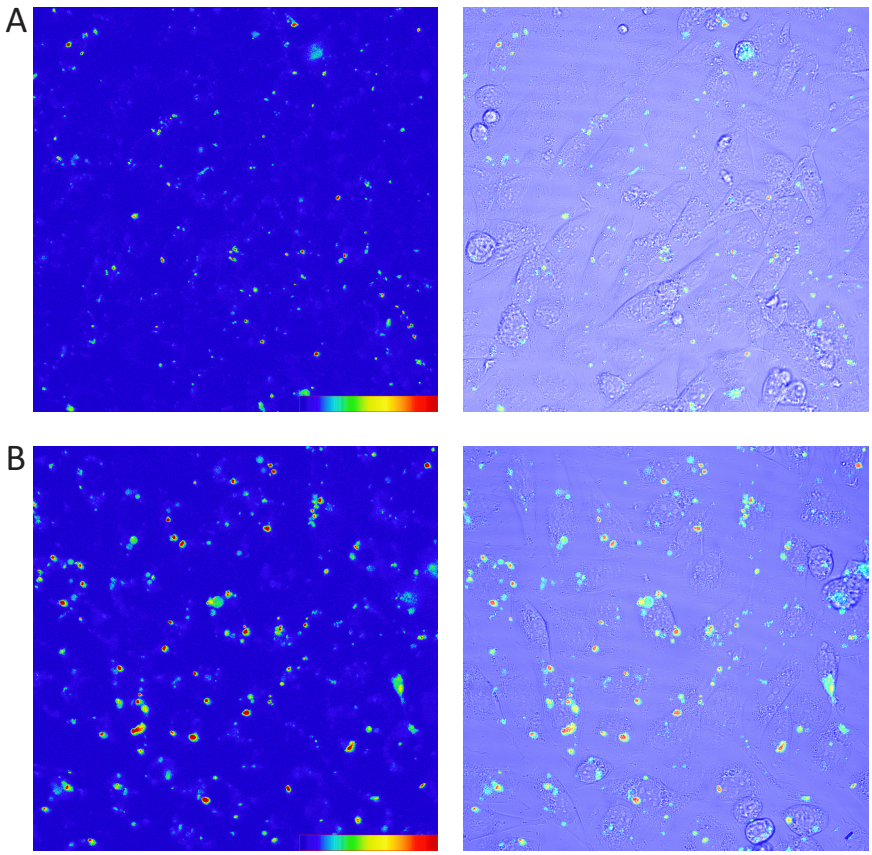

Figure 5.9: Representative confocal micrographs of BP_2-lPEI/DNA treated CHO cells in combination with CQ
CHO cells were incubated for 6 h with BP_2-lPEI/DNA polyplexes after a 15 min pretreatment with 100 µM CQ (B; untreated cells: A). Per 80,000 cells, 1 µg pGL3-Enhancer pDNA was used (N/P = 12). All images were taken using identical measurement settings. Left column: color coded BODIPY fluorescence images (dark blue: lowest fluorescence intensity, dark red: highest intensity), right column: transmitted light images combined with the fluorescence images. Picture dimensions: 225 µm × 225 µm. (Experimental details Section 5.2.2)

In case of the lPEI reference, the fluorescence intensity was independent of a DNA complexation, regardless of the N/P (Figure 5.10A). A polyplex formation apparently did not have any unspecific effect on the mBCl-assay. Cells treated with S_2-lPEI_b based polyplexes, on the other hand, exhibited a higher intensity, i.e., possessed a higher apparent GSH level than those treated with the cross-linked polymer alone, especially at moderate N/P ratios (Figure 5.10B). The signal intensity followed the same general trend as for lPEI treated cells. Reduction sensitive and insensitive polyplexes were also directly compared in a single experiment (Figure 5.11). Here, a treatment with S_2-lPEI_b/DNA (darker bars) always resulted in lower intensities than a treatment with lPEI/DNA (lighter bars). Admittedly, this direct comparison of the emission intensity values might be problematic for the reasons outlined above. Still, the consistently lower values for the S_2-lPEI_b treated cells suggest that the mBCl assay is indeed able to measure the GSH consumption during polymer cleavage, at least to some degree. This conclusion is further substantiated when the difference in the GSH consumption for the cleavage of free and DNA complexed S_2-lPEI_b (Figure 5.10B) is compared to the data for the in vitro GSH

cleavage in the absence of cells (Section 4.3.2). In these earlier experiments, PEIs complexed with nucleic acids were cleaved significantly slower due to steric restrictions than the corresponding uncomplexed polymers (Figure 4.3). The cleavage was particularly slow when both polyplex components were of high molecular weight (BP_2-S_2-lPEI_1/pDNA; Figure 4.3B). Understandably, the cleavage of those polyplexes would require less GSH than the cleavage of the free polycation and this was exactly observed in the current mBCl assay. Moreover, in accordance with the data for TAMRA-PEIs (Figure 5.5), polyplexes seem to maintain their high stability at least up through the non-cytosolic stage of the delivery. If cellular polyionic competitors were able to sufficiently destabilize the polyplexes at this stage to allow for a complete polymer cleavage, there would be no difference in the GSH consumption.

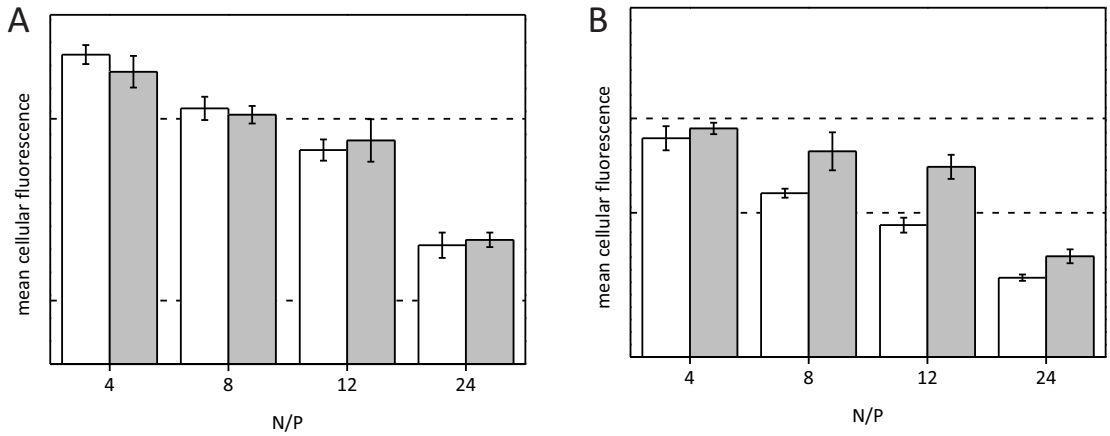

Figure 5.10: mBCl-GSH fluorescence intensity of lPEI/DNA and S_2-lPEI_b/DNA treated CHO cells

CHO cells were treated for 4 h with either lPEI (A) and S_2-lPEI_b (B) based pDNA complexes (gray bars) or the corresponding amount of uncomplexed polymer (white bars); per 80,000 cells, 1 µg pDNA was used (n = 3). Following a washing step, the cells were treated with a 40 µM mBCl-solution for 1 h and after an additional washing step were then transferred to a 96-well plate. The fluorescence intensity of the mBCl-GSH adduct was determined with a fluorescence spectrometer (λ_{ex} = 420 nm, λ_{em} = 483 nm). Higher intensity values signify a higher apparent cellular GSH level. The upper dashed line refers to the fluorescence intensity of non-polymer treated cells; the lower dashed line refers to non-polymer treated cells, additionally treated with 25 µM NEM for 1 h. (Mean values ± sample standard deviation; experimental details Section 5.2.1)

Once the polyplexes reach the cytosol, however, the presence of RNA and particularly tRNA should induce cargo displacement and thus make the carrier polymer more accessible to GSH, i.e., more GSH would be consumed. To test this hypothesis, cells were treated with lPEI/DNA and S_2-lPEI_b/DNA in the presence (Figure 5.11, darker bars) and absence of CQ (lighter bars). The addition of the endosomolytic agent CQ did indeed decrease the apparent cellular GSH level, even for the reduction insensitive polyplex variant. Evidently, the agent must have an unspecific effect on either the GSH level or the mBCl-assay itself. A closer look at the data reveals that the measured decrease in the cellular GSH concentration cannot be attributed solely to an effect of CQ. At the lowest N/P, for instance, the presence of CQ significantly lowered the mBCl-GSH signal intensity of cells incubated with S_2-lPEI_b/DNA compared to non-CQ treated

cells. In case of the reduction insensitive polyplexes the signal was unaffected. At the higher N/P ratios the differences were less pronounced, but a CQ treatment still led to higher relative intensity decreases for S_2-lPEI_b/DNA (minus 20-24 %) than for lPEI/DNA (minus 14-17 %). The overall differences were admittedly small and could indicate that the polymer is still not accessible enough for an efficient cleavage.

Taken together, the data suggests that the carrier's reduction depends on GSH at both the endolysosomal and the cytosolic stage of the delivery. The exact reduction mechanism is likely different at each stage. Under the conditions found in the cytosol, GSH is capable of reducing the carrier polymer directly. The conditions in the endolysosomal pathway, on the other hand, disfavor a reduction mechanism involving GSH directly (Section 5.1.1). GSH could thus be a cofactor in an enzymatic reduction, but this was not explored in more detail in this work.

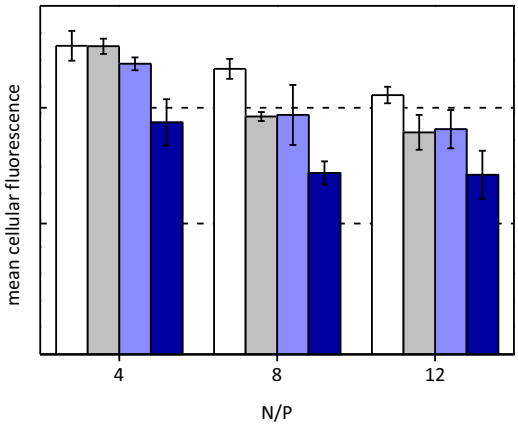

Figure 5.11: mBCl-GSH fluorescence intensity of lPEI/DNA and S_2-lPEI_b/DNA treated CHO cells and the influence of CQ

CHO cells were incubated for 4 h with lPEI (white bars) and S_2-lPEI_b (light blue bars) based pDNA complexes. In addition, cells were pretreated for 20 min with a 100 µM chloroquine solution before the addition of the polyplexes (gray and dark blue bars). Per 80,000 cells, 1 µg pDNA was used (n = 3). Following a washing step, the cells were treated with a 40 µM mBCl-solution for 1 h and after an additional washing step, the fluorescence intensity of the mBCl-GSH adduct was determined with flow cytometry. Higher intensity values signify a higher apparent cellular GSH level. The upper and lower dashed line refers to the fluorescence intensity of non-polymer treated cells and non-polymer treated cells, treated with 25 µM NEM for 1 h, respectively. (Mean values ± sample standard deviation; experimental details Section 5.2.1)

The question whether or not a physiological GSH level limits carrier degradation could not be answered satisfactorily but there is some evidence that it is not the case. For one, an elevated cellular GSH concentration did not increase the extent of disulfide cleavage (Figure 5.8C and D). Admittedly, these experiments were performed with BP_2-labeled model polyplexes based on lPEI, and not S_2-lPEI. That means that GSH would only be consumed in the cleavage of the fluorescent probe and not the polymer. Thus, even with a CQ pretreatment to maximize the cytosolic polyplex concentration, the overall disulfide concentration may still be too low to have a significant impact on the cellular GSH level. The cleavage of carriers based on disulfide

cross-linker polymer could still be limited by the amount of intracellular GSH. Considering the indirect evidence from the MTT-assay, however, this may actually not be the case. S_2-lPEI_b did not appear to perturb the GSH/GSSG homeostasis to a higher degree than BP_2-lPEI (Figure 5.3A).

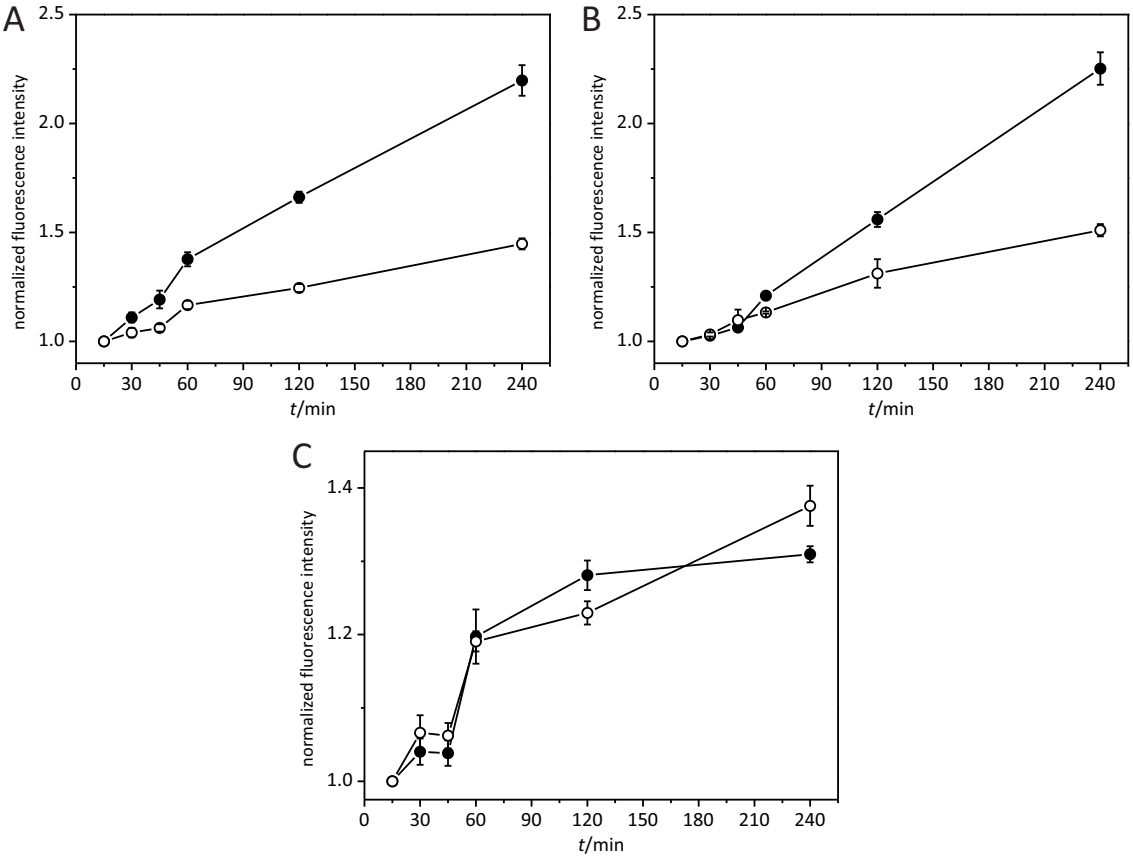

Figure 5.12: Fluorescence intensity of BODIPY-PEI/siRNA and DNA treated CHO cells and the influence of CQ

A: CHO cells were incubated for between 15 and 240 min with BP_2-lPEI/siRNA (○) or BP_2-lPEI/DNA (●) polyplexes. B: CHO cells were pretreated for 20 min with a 100 µM chloroquine solution (●; untreated cells: ○) before the addition of BP_2-lPEI/siRNA polyplexes. The polyplex incubation times ranged from 15 to 240 min. C: CHO cells were incubated for between 15 and 240 min with siRNA polyplexes based on BP_2-lPEI (○) or BP-lPEI_3 (●).

Per 80,000 cells, 1 µg of either phRLTluc DNA or Bcl-2 siRNA was used (n = 3, N/P = 8). The cellular BODIPY fluorescence intensity was determined with flow cytometry. (Mean values ± sample standard deviation; experimental details Section 5.2.1)

It was also investigated how the nucleic acid type influences the intracellular polyplex processing. The in vitro, cell free dequenching experiments in the previous chapter revealed the cleavage rate to be inversely proportional to the molecular weight of the nucleic acid, which in most part can be attributed to an increasing steric hindrance. DNA polyplexes are generally cleaved very slowly, while polyplexes with siRNA demonstrate very high or intermediate cleavage rates depending on the polymer's molecular weight (Figure 4.3). Surprisingly, the opposite trend was seen in experiments involving cells. Here the fluorescence intensity for BP_2-lPEI/DNA complexes increased significantly and almost linearly over the whole observation period

(Figure 5.12A, ●). For siRNA polyplexes (○), on the other hand, the intensity rose only slowly after about 60 to 90 min and the total intensity increase was much lower. In the presence of CQ, the fluorescence time course was similar to that of BP_2-lPEI/DNA (Figure 5.12B, ●). This sensitivity towards CQ and the fact that the shape of the time course resembles a saturation curve (Figure 5.12C, ○) are strong indicators that siRNA polyplexes accumulate in acidic organelles. Such an accumulation is in line with earlier experiments where a low molecular weight lPEI failed to facilitate the intracellular release of siRNA compared to bPEI and S_2-lPEI.[61] Ultimately, this resulted in a low gene silencing efficiency. siRNA complexes based on BP_2-lPEI (Figure 5.12C, ○) and its non-cleavable counterpart BP-lPEI_3 (●) were also compared and their time courses were almost identical. lPEI/siRNA complexes are apparently not exposed to reductive conditions, as otherwise the intensity of BP_2-lPEI/siRNA would have risen more strongly than that of BP-lPEI_3/siRNA.

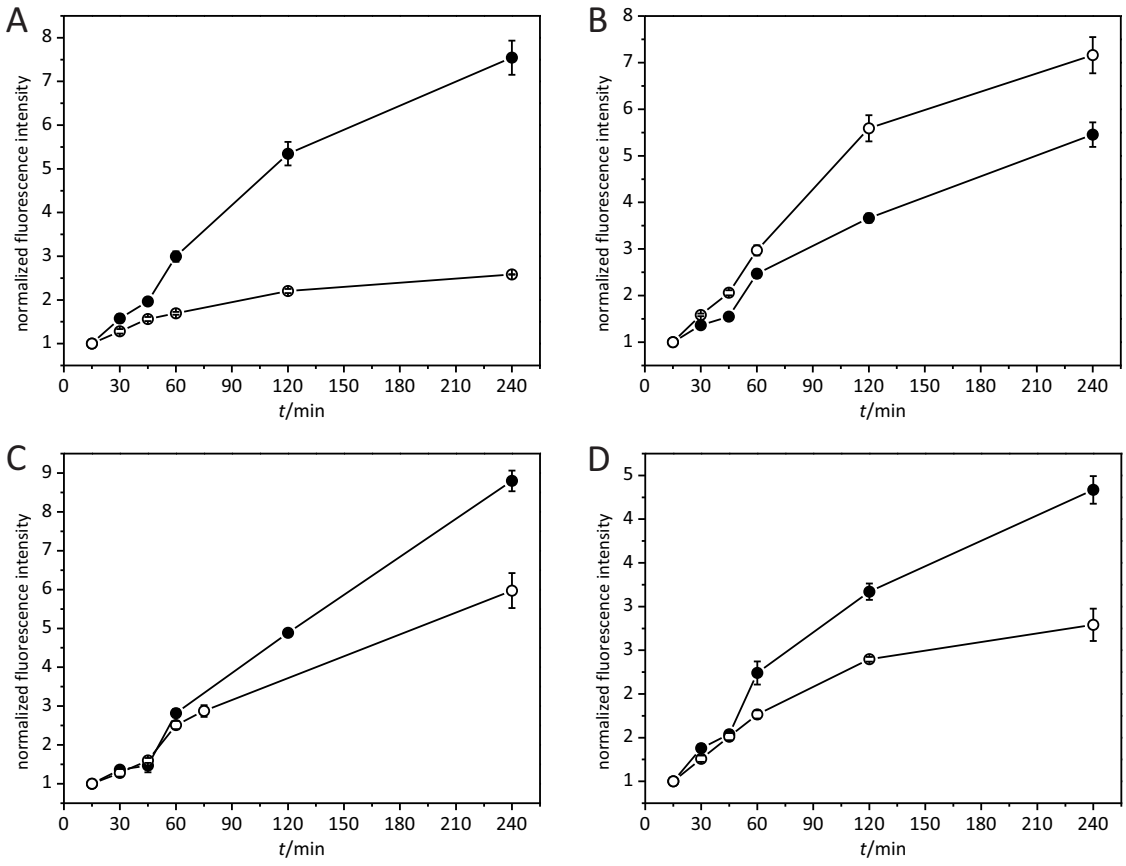

Figure 5.13: Fluorescence intensity of BP_2-PLL/siRNA and DNA treated CHO cells and the influence of CQ

A: CHO cells were incubated for between 15 and 240 min with of BP_2-PLL/siRNA (○) or BP_2-PLL/DNA (●) polyplexes. B: CHO cells were pretreated for 1 h with a 25 µM NEM solution (●; untreated cells: ○). After a washing step, the cells were incubated for between 15 and 240 min with BP_2-PLL/pDNA polyplexes. C and D: CHO cells were pretreated for 20 min with a 100 µM chloroquine solution (●; untreated cells: ○) before the addition of BP_2-PLL/pDNA (C) or BP_2-PLL/siRNA (D) polyplexes. The polyplex incubation times ranged from 15 to 240 min.

Per 80,000 cells, 1 µg of either phRLTluc DNA or Bcl-2 siRNA was used (n = 3, N/P = 8). The cellular BODIPY fluorescence intensity was determined with flow cytometry. (Mean values ± sample standard deviation; experimental details Section 5.2.1)

Finally, the uptake and intracellular processing of BP_2-PLL based DNA and siRNA polyplexes were investigated. The emission intensity time courses (Figure 5.13) showed a remarkable resemblance to those of the corresponding lPEI based polyplexes, which could imply that nucleic acid complexes with low molecular weight linear polycations are all processed similarly. BP_2-PLL/siRNA polyplexes, for instance, demonstrated the same uptake saturation (Figure 5.13A) and sensitivity towards CQ (Figure 5.13D) as BP_2-lPEI/siRNA complexes.

The question remains why siRNA and pDNA polyplexes based on the very same low molecular weight linear polycation appear to be processed so differently. Endocytosis is a complex and highly regulated process.[245] Which endocytic pathway internalized macromolecules, and by extension nanoparticles, are going to take depends very much on the nature of the cargo and physical properties of the carrier, like size and surface charge. The lPEI used here as model was unable to form ordered and well-defined complexes with siRNA (see Section 4.3.1). Thus, it is not far-fetched to assume that siRNA/lPEI and pDNA/lPEI polyplexes are internalized and trafficked differently. This assumption is substantiated by the fact that PEI complexes with short, single stranded nucleic acids and pDNA utilize different internalization pathways.[73] Although identifying the exact siRNA/lPEI endocytosis mechanism is beyond the scope of this work, several of its properties can be deduced from the available experimental data. Measured by the effect of CQ (Figure 5.12B) and the identical fluorescence intensity time courses for BP-lPEI_3 and BP_2-lPEI based siRNA polyplexes, the vesicles are non-reducing, albeit acidic and, therefore, cannot be identical to the vesicles involved in pDNA/lPEI trafficking. Considering how quickly the siRNA/lPEI uptake is saturated, the overall cellular uptake capacity of this pathway has to be relatively low (Figure 5.12C). This limited capacity combined with the carrier's accumulation in acidic vesicles make the siRNA delivery with low molecular weight PEI very inefficient; the delivery with other low molecular weight polycations such as PLL may be affected similarly. Indeed, lPEI (M_n = 15 kDa, M_w = 18 kDa) delivered a lower amount of siRNA per cell (Figure 2.6B) than its disulfide cross-linked counterpart S_2-lPEI_b (M_n = 49 kDa, M_w = 57 kDa). The data of Breunig et al., who have compared the siRNA delivery ability of lPEI 5 kDa, a disulfide cross-linked PEI based on lPEI 2.6 kDa, and bPEI 25 kDa, suggests that the effect may be even more pronounced with shorter lPEIs.[61] The short lPEI delivered the smallest amount of nucleic acid by far and in contrast to the other PEIs tested, an increase in the N/P ratio hardly increased the amount of internalized nucleic acid. Again, these observations would be consistent with an overall low uptake capacity combined with a quickly saturated uptake.

Since the uptake and processing mechanisms of siRNA polyplexes based on low molecular weight, unmodified linear PEIs have not been studied in great detail so far, it is difficult to deduce their concrete nature from only the data available here. There is, however, a mechanistic study from Ming et al., who have investigated the internalization of a backbone modified antisense oligonucleotide (AON) via lipo- and polyplexes.[73] Their 20 base splice-switching AON

was complexed with JetPEI, a linear PEI variant whose exact molecular weight (distribution) is not disclosed by the manufacturer but generally described as “low molecular weight”[246] or 22 kDa[247] polymer. In contrast to pDNA/PEI polyplexes, AON polyplexes were internalized through unconventional, noncaveolar, and clathrin-independent endocytosis processes and it was speculated that this is related to the lower mean particle size of the latter (336 nm; pDNA/PEI: approx. 1000 nm). The delivery was functional as after 24 h the oligonucleotides were found in the nucleus and the expression of a reporter gene was seen. Quite conceivably, the siRNA/lPEI (and siRNA/pLL) polyplexes examined here in this work utilize comparable or even the same pathways. It can be argued that this is contradicted by the accumulation of these carriers in endocytic vesicles, which was not observed by Ming et al. However, this apparent accumulation may actually be the result of the relatively short, four hour observation period in combination with a very slow endosomal release. Breunig et al., for instance, have used a very similar experimental setup like the one used here and were able to demonstrate a functional siRNA delivery in CHO-K1 cells with lPEI 5 kDa after 48 h, although the intracellular release was inefficient compared to bPEI 25 kDa and especially disulfide cross-linked lPEI.[61] At any rate, the relative inability of siRNA/lPEI complexes to escape from endocytic vesicles likely increases the chances for cargo degradation. Thus, the delivery becomes even less efficient, unless the nucleic acid is chemically stabilized as in the study of Ming et al. Ultimately, the question whether or not the polyplexes examined here are actually routed to unconventional, noncaveolar, and clathrin-independent pathways cannot be answered satisfactorily at this point without further studies that include endocytosis inhibitors.

5.4 Conclusions

The cellular uptake and processing of polymeric gene carriers is a complex process, making it very hard to pinpoint the exact biological and non-biological factors that contribute to the delivery success. The use of bioresponsive carriers adds another layer of complexity as carrier cleavage and subsequent cargo release have to be considered as well. For that reason it was investigated if the underlying processes could be studied with polyplexes labeled with a reduction sensitive fluorescent dye.

The fluorescence intensity of polyplexes based on DNA and both redox sensitive and insensitive PEI followed the same time course, suggesting that their uptake and early stage processing are identical. Overall, the time courses are consistent with a HSPG dependent polyplex uptake, followed by a transfer from early to late endosomes.

The carriers are exposed to reductive conditions from very early on during uptake and intracellular trafficking but more importantly, there are hints that the endolysosomal compartment is

involved in carrier reduction. This is very surprising, since so far the capability for endolysosomal reduction has only been ascribed to specialized cell types. The reduction is inhibited by NEM, indicating that it is mediated by cellular thiols. While the exact nature of the reductant remains elusive, the results of an mBCl-assay imply that GSH might be involved directly or indirectly. The main reduction site, however, seems to be the cytosol where at least an estimated two-thirds of the overall reduction takes place. According to indirect evidence provided by an MTT-assay, the reduction itself does not seem to perturb the cellular redox homeostasis to a notable degree.

While lowering the cellular thiol concentration significantly inhibits carrier cleavage, an artificial increase of the GSH level interestingly does not have the opposite effect. A physiological GSH level is apparently not a limiting factor for the carrier's reduction per se. Incomplete vector unpacking could, however, limit carrier reduction. The DNA/PEI polyplexes used in this work have demonstrated a remarkable resistance against a GSH mediated cleavage in cell free vitro assays (see Section 4.2.1), likely related to a strong steric hindrance. It has been speculated that the presence of polyionic cellular competitors, such as tRNA and polyamines, could completely dissociate the polyplexes to allow for a more efficient cleavage. The experiments here, however, found no evidence that this is actually the case.

A comparison of PEI based siRNA and pDNA polyplexes revealed notable differences in their trafficking. While the latter are directed to acidic, reducing vesicles, the former accumulate in non-reducing vesicles that also happen to be acidic; similar observations were made with PLL based polyplexes. Although it is not entirely clear how these differences come about, they may be related to physical differences between the polyplex variants that result in an uptake through a different route. The uptake mechanism for siRNA/lPEI appears to possess a comparatively low capacity combined with a slow release to the cytosol. As consequence, only a relatively low amount of siRNA reaches the cytosol. This uptake mechanism could thus offer an additional explanation for the low gene silencing efficiency of low molecular weight linear PEI based carriers.

6 Summary, conclusions and outlook

6.1 Overview

Gene therapy has long fascinated scientist, authors, and the general public alike since it holds the potential to treat the very root cause of hereditary disorders. The road from therapeutic concepts to clinical applications was paved with setbacks and disappointing results, but substantial clinical progress has been made in the last decade.[2] Today, multiple gene therapies are available on the market and many more are in development.[7-9] The current progress is to some extent driven by the advent of gene editing, which could lead to completely new therapeutic approaches.

"Classic" gene therapies are based on the permanent integration of genes into the host cell genome in order to express a therapeutic protein. Other approaches, which are not regarded as gene therapies in the strictest sense, use oligonucleotides, such as siRNA, mRNA, and AON to target processes downstream of the gene transcription. Since nucleic acids are generally susceptible to enzymatic degradation and are unable to enter cells on their own, therapeutic success very much depends on the efficiency and efficacy of a gene delivery system. Most current therapies use viral vectors.[2, 10] Viruses are highly efficient transfection agents, but their potential immunogenicity and genotoxicity are great concerns and their industrial production is expensive. For that reason, there is a growing interest in non-viral delivery systems,[4] among which the polycation PEI is considered to be the gold standard.[30] Nucleic acid complexes based on PEI are termed polyplexes. Their transfection efficiency and cytotoxicity increases concurrently with the polymer's molecular weight and degree of branching. One strategy to break up this correlation is to cross-link low molecular weight linear PEIs (lPEI) with biodegradable, reduction sensitive disulfide linkers.[27] These linkers are exceptionally stable in the oxidizing extracellular environment, but are thought to be cleaved rapidly under the thiol rich conditions found within cells. In essence, the efficiency of high molecular weight branched PEI would be combined with the low toxicity of low molecular weight lPEI.[31, 36] In reality the situation is, however, more complex and in some cases the presence of disulfides has even been

shown to be detrimental to the delivery success.[35] In fact, an insufficient understanding of many aspects of the delivery process impedes the development of better redox sensitive carriers. This is in part related to the lack of suitable analytical tools to investigate polycation/nucleic acid interactions, polyplex uptake, trafficking, and processing. For that reason, the main objective of this work was the development of new fluorescence-based analytical tools to gain better insights into those processes. This was achieved, among other things, by (1) developing a novel, straightforward method for labeling polyamines with a wide variety of fluorescent probes, including a redox sensitive dye, (2) thoroughly investigating the photophysical and chemical properties of polymer bound fluorophores and fluorescently labeled polycations in complex with nucleic acids, and (3) by using these polycations to study polymer/nucleic acid interactions and (4) the cleavage and intracellular trafficking of reduction sensitive polyplexes.

6.2 Summary

Earlier studies have suggested that the transfection efficiency of reduction sensitive polyplexes increases with the linker content.[31, 37] The amount of linker, however, cannot be increased indefinitely due to the formation of insoluble polymer gels at higher cross-linking ratios, even though most polymer strands remain unmodified.[31] Thus, it was first evaluated if an existing process for cross-linking low molecular weight lPEIs with L-cystine[31] could be improved to allow for higher cross-linking ratios (Chapter 2).

By carefully optimizing the reaction conditions, it was indeed possible to synthesize a S_2-lPEI derivative with a higher percentage of cross-linked polymer strands (about one third) and narrower molecular weight distribution (from M_n = 15 kDa, M_w = 18 kDa, *PDI* = 1.18 to M_n = 49 kDa, M_w = 57 kDa, *PDI* = 1.15) than previously thought possible. There was no indication for an overstabilization, as the S_2-lPEI was still cleaved completely within three hours after exposure to a physiological GSH concentration. The new derivative's transfection efficacy was comparable (50 % at N/P = 12) or, under some experimental conditions, even higher than those of the S_2-lPEIs developed in the preceding work[31]. Unfortunately, its cytotoxicity was relatively high (cell viability between 84 % and 31 % at N/P = 6 and N/P = 30, respectively), probably due to the comparatively high molecular weight of the linear starting material. Cross-linking interestingly increased the amount of siRNA (by about 100 %), but not the amount of pDNA delivered per cell and this has previously been attributed to an improved cellular uptake of siRNA polyplexes.[61] A closer look at the experimental setup in conjunction with additional data suggested, however, that this observation could in fact be the result of an experimental artifact. Linear PLL (M_n = 4.3 kDa, M_w = 6.4 kDa, *PDI* = 1.49) was also cross-linked, but that resulted in a

product (M_n = 4.9 kDa, M_w = 9.5 kDa, *PDI* = 1.95) that had neither an increased transfection efficacy nor a reasonable cytotoxicity.

The focus of this work was to study polymer cleavage, nucleic acid/polycation interactions, and intracellular processing of polyplexes with fluorescently labeled polymers. Conventional labeling procedures often involve dyes with a pre-activated carboxylic group. Those dyes are expensive and only a limited range is available. Since the cross-linking method combined the carboxylic acid activation and the reaction with a polymer amine in a simple, inexpensive one-pot reaction, the process was adapted for polycation labeling (Chapter 3). The general synthesis parameters were established by labeling various PEI variants with two representative members of the immensely popular family of xanthene dyes, FAM and TAMRA. The reaction with lPEI and S_2-lPEI only had minimal impact on the photophysical properties of the dyes. Only minor bathochromic shifts (10-27 nm) of the absorption and emission maxima were observed. The reaction of TAMRA with bPEI, however, resulted in a product with drastically altered properties. This finding was unexpected as the structures of lPEI and bPEI are closely related. The photophysical changes could be traced back to the formation of non-emitting H-dimers ($\lambda_{abs\ max}$ = 526-529 nm), whose probable structure was elucidated based on the relative position of their absorption band. The labeling also affected the dye's chemical properties, i.e., TAMRA had become pH-sensitive and was irreversibly discolored under alkaline conditions, likely due to the reaction with primary PEI amines. Both the photophysical and chemical changes were unrelated to the novel labeling method, because "conventional" labeling with TAMRA-SE yielded similar results.

The newly established procedure was then used to label PEIs with the redox sensitive probe BP_2. BP_2 is non-fluorescent, but turns brightly fluorescent in the presence of thiols like GSH. The dye was specifically chosen for its close structural similarity to the cross-linker L-cystine. This similarity ensures that the disulfide cleavage rates for probe and cross-linker are in the same range. Again, profound photophysical changes, related to the presence of multiple aggregate species (H-dimers/trimers, higher order H-aggregates, and strongly emissive J-dimers) were observed. While there was no obvious connection between aggregate formation and labeling conditions (e.g., probe density) or labeling procedure, the lower interchromophoric distance within H-dimers on bPEI (R = 0.43 nm) compared to those on the other PEIs (R = 0.47 and 0.49 nm) suggested that the aggregation tendency is related to the host polymer structure. In view of bPEI's relatively compact structure, steric effects apparently play a major in the aggregation. However, since no aggregation was observed with S_2-lPEI, factors such as the charge density of the polycation probably contribute significantly to the aggregation process. The highest aggregation tendency was observed with BP_2-S_2-PLL, so the ability to promote H-dimerization may be a general feature of polycations. Overall, it is very surprising that although

the observed photophysical and chemical changes greatly affect the validity of any fluorescence based assays, this is apparently the first time that they have been reported in conjunction with polycationic gene carriers. The cleavage of the BP_2 probe itself was not affected by the labeling. When exposed to a physiological GSH concentration, BP_2-PEIs became highly fluorescent and can, therefore, be used to investigate polymer cleavage.

The strong impact of steric factors on the emissive properties of the fluorescent probes was confirmed during polyplex formation and cleavage (Chapter 4). In general, polyplex formation dequenched the emission of BP_2-lPEI (up to 4-fold intensity increase), while it quenched that of TAMRA-lPEI (around 50-75 % intensity decrease). The absolute value of the intensity change depended on the polymer/nucleic acid ratio and the type of nucleic acid (pDNA or siRNA). The high packing density within polyplexes probably interfered with the formation of BP_2 H-aggregates, but at the same time forced neighboring TAMRA fluorophores close enough together for an efficient probe-probe quenching. When cleaved, BP_2-lPEI/DNA polyplexes unexpectedly became less emissive, while the fluorescence in their vicinity increased. Obviously, highly fluorescent BP monomers are being released during cleavage, but the remaining polymer bound monomers stay quenched due to continued dye aggregation. Interestingly, polyplex cleavage also affected the TAMRA-lPEI initially used as internal emission intensity standard. Although TAMRA is redox insensitive and no efficient energy transfer from BODIPY is possible, the cleavage increased its fluorescence intensity and impressively demonstrated how important it is to thoroughly evaluate the suitability of reference dyes when investigating polyplexes. Polyplex cleavage was investigated in more detail by measuring the cleavage rates of siRNA and DNA polyplexes based on BP_2-lPEI and BP_2-S_2-lPEI. BP_2-lPEI/siRNA was cleaved almost as fast as non-complexed BP_2-lPEI ($t_{½}$ ≈ 100 min), while the cleavage of BP_2-S_2-lPEI/DNA came to a complete standstill within 60 min. All in all, the cleavage rates were inversely proportional to the molecular weights of the polyplex constituents (DNA/S_2-lPEI < DNA/lPEI < siRNA/S_2-lPEI < siRNA/lPEI), i.e., the thermodynamic stability of the polyplex. In tightly bound complexes such as BP_2-S_2-lPEI/DNA, the reductant is unable to fully penetrate the polyplex core. In fact, full intracellular disintegration of such polyplexes may not be possible unless additional factors like ion exchange reactions are involved.

Interestingly, the cleavage rate seemed to be sensitive towards weak PEI/nucleic acid interactions, as it was reduced even in cases where no ordered complexes were formed. This finding, in combination with the previous observations, led to the development of another fluorescence-based assay for investigating polymer/nucleic acid interactions. It is based on nucleobase-specific quenching interactions between the nucleic acid and the fluorescent probe on the polymer. Such interactions have never been investigated in conjunction with polyplexes. Static and time-resolved fluorescence measurements with model complexes revealed the pre-

dominant quenching mechanism to be static quenching ($k_{q,s} \approx 10^{14}$ M^{-1} s^{-1}), likely through the formation of non-emissive ground state complexes. There was also a significant contribution from dynamic quenching caused by a very short-ranged photoinduced electron transfer (PET) from the nucleobase guanine to the fluorophore. The unusually high dynamic bimolecular quenching constant of 5.9×10^{13} M^{-1} s^{-1} indicated that probe and quencher remain at van der Waals contact (≈0.4 nm) at all times and again argues for very strong steric restrictions within polyplexes. This conclusion was substantiated by data that may evidence that fluorophores located in the core and on the surface of polyplexes are accessible to quenchers to different degrees. In view of the direct quencher/fluorophore contact, the method developed here may in fact be better suited for investigating polyplexes than methods like FRET, which rely on relatively long-ranged fluorophore interactions. More importantly, FRET requires fluorophores with unaltered photophysical properties, which apparently is rarely the case with polyplexes.

Finally, uptake, trafficking, and processing of the labeled polyplexes were studied in CHO-K1 cells (Chapter 5). Once again, the high stability of some polyplex variants became apparent in first experiments with TAMRA-PEI/DNA, where no evidence for an efficient cargo release was found, regardless of whether the polyplexes were located in the endolysosomal compartment or the cytosol. Cellular (poly)ionic competitors were probably unable to efficiently destabilize the complexes due to steric hindrance.

Intracellular disulfide cleavage itself was investigated with the help of BP_2 labeled DNA polyplexes. Cells incubated with redox sensitive polyplexes showed a stronger fluorescence intensity increase than those treated with inert polyplexes. According to this result and taking into consideration that the intensity increase was prevented in the presence of the thiol depleting agent NEM, probe cleavage is dependent on cellular thiols. The emission intensity time courses corresponded to those of DNA polyplexes based on BP_2-PLL, a polymer without endosomolytic activity. All in all, the data suggest that polyplexes are already exposed to reductive conditions during or immediately after uptake and this exposure continues throughout endolysosomal trafficking. This early reduction contributes significantly to the total cellular disulfide reduction, with the cytosol still being the main reduction site. Early and cytosolic reduction appears to be GSH-dependent to some extent, but a normal physiological GSH level seemingly had no limiting effect. To find evidence for a reduction in the endolysosomal compartment is particularly interesting, since it is commonly believed that this ability is mainly restricted to cells derived from hematopoietic bone marrow progenitor cells. The data may additionally suggest that DNA polyplexes are too stable to be completely cleaved intracellularly and could explain earlier results where an increase of the cellular GSH level was not always accompanied with an increase of the transfection efficiency.[35]

Although complex stability apparently played a pivotal role in polyplex reduction, other factors

played an important role as well. The presumably less thermodynamically stable siRNA/PEI complexes, for instance, were not exposed to reductive conditions unless the endosomolytic agent chloroquine was present. In that case, their fluorescence intensity profiles matched those of siRNA/PLL polyplexes and indicated that the uptake is quickly saturated. Taken together, the data may suggest that siRNA/PEI and DNA/PEI polyplexes are trafficked differently. siRNA/PEI polyplexes appear to accumulate in acidic, non-reducing organelles with limited storage capacity. This observation is in line with earlier results showing that siRNA polyplexes based on low molecular weight lPEIs have a low delivery efficiency.[61]

6.3 Conclusions and outlook

Whenever fluorescent labels are attached polymer carriers to study non-viral gene delivery systems, it is almost always implicitly assumed that their properties match those of their parent fluorophores. In fact, many analytical methods such as FRET are based on this very assumption. This thesis clearly showed, however, that polycation labeling and polyplex formation can drastically alter the photophysical and chemical properties of fluorescent probes. Neither the polymer nor the nucleic acid can be considered as “inert” with respect to the probe. Not taking this into account can very easily lead to the misinterpretation of data. Therefore, it would be very useful to further investigate these complex photophysical and chemical changes with more sophisticated spectroscopic methods than were possible within the scope of this work. Data for a larger set of polymers and fluorophores could help to identify the factors contributing to the observed changes more precisely.

The main objective of this work, the development of a fluorescence based method to study the thiol dependent cleavage of reduction sensitive polymers and polyplexes, was successfully implemented by using a self-quenched fluorescent label. The new method was used to investigate carrier cleavage in cell-free experiments, as well as in experiments involving CHO-K1 cells. The data from those experiments could help to improve the design of future redox sensitive delivery systems. Polyplexes appear to be exposed to reductive conditions surprisingly early in the delivery process, but the polyplex dissociation itself seems to be impeded due to steric restrictions, especially with DNA polyplexes. For that reason, cargo release may be an important issue that needs to be addressed in the design of future delivery systems. The experiments also identified an issue specific to siRNA-polyplexes. Some siRNA-polyplex variants appear to be routed to a non-transfection productive pathway. Future siRNA carriers should be designed to bypass this pathway altogether (e.g., through targeting) or be able to efficiently escape the organelles involved.

Appendix

References

[1] Kumar S R, Markusic D M, Biswas M et al. (2016) Clinical development of gene therapy: results and lessons from recent successes. *Mol Ther Methods Clin Dev*, 3(16034), 10.1038/mtm.2016.34

[2] Dunbar C E, High K A, Joung J K et al. (2018) Gene therapy comes of age. *Science*, 359(6372):eaan4672, 10.1126/science.aan4672

[3] Keeler A M, ElMallah M K, and Flotte T R (2017) Gene Therapy 2017: Progress and Future Directions. *Clin Transl Sci*, 10(4):242-248, 10.1111/cts.12466

[4] Foldvari M, Chen D W, Nafissi N et al. (2016) Non-viral gene therapy: Gains and challenges of non-invasive administration methods. *J Control Release*, 240:165-190, 10.1016/j.jconrel.2015.12.012

[5] Mullin E (2018-04-21) The World's Most Expensive Medicine Is Being Pulled from the Market. *MIT Technology Review*, https://www.technologyreview.com/s/601165/the-worlds-most-expensive-medicine-is-a-bust/amp/

[6] Regalado A (2018-05-04) The World's Most Expensive Medicine Is a Bust. *MIT Technology Review*, https://www.technologyreview.com/s/601165/the-worlds-most-expensive-medicine-is-a-bust/amp/

[7] Fernández C R (2017-10-25) The UK Recommends the use of GSK's €594,000 Gene Therapy. *Labiotech.eu*, https://labiotech.eu/medical/gsk-strimvelis-uk-nice/

[8] Curran K (2018-08-15) The gene therapy sector is experiencing an acceleration. *Rising Tide Biology*, https://www.risingtidebio.com/what-is-gene-therapy-uses/

[9] Dall'Osso C, Saini A (2018-03-26) The Gene Therapy Pipeline — And The Biggest Challenges Facing Developers. *Bioprocess Online*, https://www.bioprocessonline.com/doc/the-gene-therapy-pipeline-and-the-biggest-challenges-facing-developers-0001

[10] Naldini L (2015) Gene therapy returns to centre stage. *Nature*, 526(7573):351-360, 10.1038/nature15818

[11] George L A, Sullivan S K, Giermasz A et al. (2017) Hemophilia B Gene Therapy with a High-Specific-Activity Factor IX Variant. *N Engl J Med*, 377(23):2215-2227, 10.1056/NEJMoa1708538

[12] Pardi N, Hogan M J, Porter F W et al. (2018) mRNA vaccines – a new era in vaccinology. *Nat Rev Drug Discov*, 17:261-279, 10.1038/nrd.2017.243

[13] Ryther R C C, Flynt A S, Phillips III J A et al. (2004) siRNA therapeutics: big potential from small RNAs. *Gene Ther*, 12:5-11, 10.1038/sj.gt.3302356

[14] Juliano R L (2016) The delivery of therapeutic oligonucleotides. *Nucleic Acids Res*, 44(14):6518-6548, 10.1093/nar/gkw236

[15] Wu S Y, Lopez-Berestein G, Calin G A et al. (2014) RNAi Therapies: Drugging the Undruggable. *Sci Transl Med*, 6(240):240ps7, 10.1126/scitranslmed.3008362

[16] USFDA (2018-08-10) FDA approves first-of-its kind targeted RNA-based therapy to treat a rare disease. *U.S. Food and Drug Administration - Press Announcements*, https://www.fda.gov/NewsEvents/Newsroom/PressAnnouncements/ucm616518.htm

[17] European Medicines Agency (2018-08-27) Human medicine European public assessment report (EPAR): Onpattro. *Public Assessment Report*, https://www.ema.europa.eu/en/medicines/human/EPAR/onpattro

[18] Lino C A, Harper J C, Carney J P et al. (2018) Delivering CRISPR: a review of the challenges and approaches. *Drug Deliv*, 25(1):1234-1257, 10.1080/10717544.2018.1474964

[19] Olden B R, Cheng Y, Yu J L et al. (2018) Cationic polymers for non-viral gene delivery to human T cells. *J Control Release*, 282:140-147, 10.1016/j.jconrel.2018.02.043

[20] Galibert L, Merten O W (2011) Latest developments in the large-scale production of adeno-associated virus vectors in insect cells toward the treatment of neuromuscular diseases. *J Invertebr Pathol*, 107:S80-S93, 10.1016/j.jip.2011.05.008

[21] Ramamoorth M, Narvekar A (2015) Non viral vectors in gene therapy - an overview. *J Clin Diagn Res*, 9(1):GE01-GE06, 10.7860/JCDR/2015/10443.5394

[22] Wu L, Xie J, Li T et al. (2017) Gene delivery ability of polyethylenimine and polyethylene glycol dual-functionalized nanographene oxide in 11 different cell lines. *R Soc Open Sci*, 4(10):170822-170822, 10.1098/rsos.170822

[23] Bhise N S, Shmueli R B, Gonzalez J et al. (2012) A novel assay for quantifying the number of plasmids encapsulated by polymer nanoparticles. *Small*, 8(3):367-373, 10.1002/smll.201101718

[24] Ma B, Zhang S, Jiang H et al. (2007) Lipoplex morphologies and their influences on transfection efficiency in gene delivery. *J Control Release*, 123(3):184-194, 10.1016/j.jconrel.2007.08.022

[25] Cullis P R, Hope M J (2017) Lipid Nanoparticle Systems for Enabling Gene Therapies. *Mol Ther*, 25(7):1467-1475, 10.1016/j.ymthe.2017.03.013

[26] Zatsepin T S, Kotelevtsev Y V, and Koteliansky V (2016) Lipid nanoparticles for targeted siRNA delivery - going from bench to bedside. *Int J Nanomedicine*, 11:3077-3086, 10.2147/IJN.S106625

[27] Patnaik S, Gupta K C (2013) Novel polyethylenimine-derived nanoparticles for in vivo gene delivery. *Expert Opin Drug Deliv*, 10(2):215-228, 10.1517/17425247.2013.744964

[28] Benjaminsen R V, Mattebjerg M A, Henriksen J R et al. (2013) The Possible "Proton Sponge" Effect of Polyethylenimine (PEI) Does Not Include Change in Lysosomal pH. *Mol Ther*, 21(1):149-157, 10.1038/mt.2012.185

[29] Behr J P (1997) The Proton Sponge: a Trick to Enter Cells the Viruses Did Not Exploit. *Chimia (Aarau)*, 51(1-2):34-36

[30] Breunig M (2005) Polyethylenimine-based nucleic acid delivery, *PhD thesis*, University of Regensburg, Regensburg, Germany, URN: urn:nbn:de:bvb:355-opus-5911

[31] Lungwitz U (2006) Polyethylenimine-derived gene carriers and their complexes with plasmid DNA. Design, synthesis and characterization, *PhD thesis*, University of Regensburg, Regensburg, Germany, URN: urn:nbn:de:bvb:355-opus-7445

[32] Luten J, van Nostrum C F, De Smedt S C et al. (2008) Biodegradable polymers as non-viral carriers for plasmid DNA delivery. *J Control Release*, 126(2):97-110, 10.1016/j.jconrel.2007.10.028

[33] Bonner D K, Zhao X, Buss H et al. (2013) Crosslinked linear polyethylenimine enhances delivery of DNA to the cytoplasm. *J Control Release*, 167(1):101-107, 10.1016/j.jconrel.2012.09.004

[34] Saito G, Swanson J A, and Lee K D (2003) Drug delivery strategy utilizing conjugation via reversible disulfide linkages: role and site of cellular reducing activities. *Adv Drug Deliv Rev*, 55(2):199-215, 10.1016/S0169-409X(02)00179-5

[35] Oupický D, Li J (2014) Bioreducible Polycations in Nucleic Acid Delivery: Past, Present, and Future Trends. *Macromol Biosci*, 14(7):908-922, 10.1002/mabi.201400061

[36] Lin C, Engbersen J F (2009) The role of the disulfide group in disulfide-based polymeric gene carriers. *Expert Opin Drug Deliv*, 6(4):421-439, 10.1517/17425240902878010

[37] Gosselin M A, Guo W, and Lee R J (2001) Efficient Gene Transfer Using Reversibly Cross-Linked Low Molecular Weight Polyethylenimine. *Bioconjug Chem*, 12(6):989-994, 10.1021/bc0100455

[38] Gary D J, Puri N, and Won Y Y (2007) Polymer-based siRNA delivery: Perspectives on the fundamental and phenomenological distinctions from polymer-based DNA delivery. *J Control Release*, 121(1-2):64-73, 10.1016/j.jconrel.2007.05.021

[39] Zheng M, Librizzi D, Ayse Kiliç et al. (2012) Enhancing in-vivo circulation and siRNA delivery with biodegradable polyethylenimine-graft-polycaprolactone-block-poly(ethylene glycol) copolymers. *Biomaterials*, 33(27):6551-6558, 10.1016/j.biomaterials.2012.05.055

[40] Bauhuber S, Hozsa C, Breunig M et al. (2009) Delivery of Nucleic Acids via Disulfide-Based Carrier Systems. *Adv Mater*, 21(32-33):3286-3306, 10.1002/adma.200802453

[41] Ren K, Ji J, and Shen J (2005) Construction of Polycation-Based Non-Viral DNA Nanoparticles and Polyanion Multilayers via Layer-by-Layer Self-Assembly. *Macromol Rapid Commun*, 26(20):1633-1638, 10.1002/marc.200500482

[42] Mintzer M A, Simanek E E (2008) Nonviral Vectors for Gene Delivery. *Chem Rev*, 109(2):259-302, 10.1021/cr800409e

[43] Sauer A M, Schlossbauer A, Ruthardt N et al. (2010) Role of Endosomal Escape for Disulfide-Based Drug Delivery from Colloidal Mesoporous Silica Evaluated by Live-Cell Imaging. *Nano Lett*, 10(9):3684-3691, 10.1021/nl102180s

[44] Morille M, Passirani C, Vonarbourg A et al. (2008) Progress in developing cationic vectors for non-viral systemic gene therapy against cancer. *Biomaterials*, 29(24-25):3477-3496, 10.1016/j.biomaterials.2008.04.036

[45] Miyata K, Kakizawa Y, Nishiyama N et al. (2004) Block Catiomer Polyplexes with Regulated Densities of Charge and Disulfide Cross-Linking Directed To Enhance Gene Expression. *J Am Chem Soc*, 126(8):2355-2361, 10.1021/ja0379666

[46] Manickam D S, Hirata A, Putt D A et al. (2008) Overexpression of Bcl-2 as a proxy redox stimulus to enhance activity of non-viral redox-responsive delivery vectors. *Biomaterials*, 29(17):2680-2688, 10.1016/j.biomaterials.2008.03.009

[47] Manickam D S, Li J, Putt D A et al. (2010) Effect of innate glutathione levels on activity of redox-responsive gene delivery vectors. *J Control Release*, 141(1):77-84, 10.1016/j.jconrel.2009.08.022

[48] Godbey W T, Wu K K, and Mikos A G (1999) Size matters: Molecular weight affects the efficiency of poly(ethylenimine) as a gene delivery vehicle. *J Biomed Mater Res*, 45(3):268-275, 10.1002/(SICI)1097-4636(19990605)45:3<268::AID-JBM15>3.0.CO;2-Q

[49] Fischer D, von Harpe A, Kunath K et al. (2002) Copolymers of Ethylene Imine and N-(2-Hydroxyethyl)-ethylene Imine as Tools To Study Effects of Polymer Structure on Physicochemical and Biological Properties of DNA Complexes. *Bioconjug Chem*, 13(5):1124-1133, 10.1021/bc025550w

[50] Lungwitz U, Breunig M, Blunk T et al. (2005) Polyethylenimine-based non-viral gene delivery systems. *Eur J Pharm Biopharm*, 60(2):247-266, 10.1016/j.ejpb.2004.11.011

[51] Neu M, Fischer D, and Kissel T (2005) Recent advances in rational gene transfer vector design based on poly(ethylene imine) and its derivatives. *J Gene Med*, 7(8):992-1009, 10.1002/jgm.773

[52] Wagner E, Kloeckner J (2006) Gene Delivery Using Polymer Therapeutics. In: Satchi-Fainaro R, Duncan R, Advances in Polymer Science: Polymer Therapeutics I, Springer, Berlin/Heidelberg, 10.1007/12_023

[53] Breunig M, Lungwitz U, Liebl R et al. (2005) Gene delivery with low molecular weight linear polyethylenimines. *J Gene Med*, 7(10):1287-1298, 10.1002/jgm.775

[54] Ganta S, Devalapally H, Shahiwala A et al. (2008) A review of stimuli-responsive nanocarriers for drug and gene delivery. *J Control Release*, 126(3):187-204, 10.1016/j.jconrel.2007.12.017

[55] Lee Y, Mo H, Koo H et al. (2007) Visualization of the Degradation of a Disulfide Polymer, Linear Poly(ethylenimine sulfide), for Gene Delivery. *Bioconjug Chem*, 18(1):13-18, 10.1021/bc060113t

[56] Oster C G, Wittmar M, Unger F et al. (2004) Design of Amine-Modified Graft Polyesters for Effective Gene Delivery Using DNA-Loaded Nanoparticles. *Pharm Res*, 21(6):927-931, 10.1023/B:PHAM.0000029279.50733.55

[57] Meng F, Hennink W E, and Zhong Z (2009) Reduction-sensitive polymers and bioconjugates for biomedical applications. *Biomaterials*, 30(12):2180-2198, 10.1016/j.biomaterials.2009.01.026

[58] Bauhuber S, Liebl R, Tomasetti L et al. (2012) A library of strictly linear poly(ethylene glycol)–poly(ethylene imine) diblock copolymers to perform structure–function relationship of non-viral gene carriers. *J Control Release*, 162(2):446-455, 10.1016/j.jconrel.2012.07.017

[59] Oupický D, Parker A L, and Seymour L W (2001) Laterally Stabilized Complexes of DNA with Linear Reducible Polycations: Strategy for Triggered Intracellular Activation of DNA Delivery Vectors. *J Am Chem Soc*, 124(1):8-9, 10.1021/ja016440n

[60] Christensen L V, Chang C W, Kim W J et al. (2006) Reducible Poly(amido ethylenimine)s Designed for Triggered Intracellular Gene Delivery. *Bioconjug Chem*, 17(5):1233-1240, 10.1021/bc0602026

[61] Breunig M, Hozsa C, Lungwitz U et al. (2008) Mechanistic investigation of poly(ethylene imine)-based siRNA delivery: Disulfide bonds boost intracellular release of the cargo. *J Control Release*, 130(1):57-63, 10.1016/j.jconrel.2008.05.016

[62] Huang S Y, Pooyan S, Wang J et al. (1998) A Polyethylene Glycol Copolymer for Carrying and Releasing Multiple Copies of Cysteine-Containing Peptides. *Bioconjug Chem*, 9(5):612-617, 10.1021/bc980038p

[63] Bacalocostantis I, Mane V P, Kang M S et al. (2012) Effect of Thiol Pendant Conjugates on Plasmid DNA Binding, Release, and Stability of Polymeric Delivery Vectors. *Biomacromolecules*, 13(5):1331-1339, 10.1021/bm3004786

[64] Breunig M, Lungwitz U, Klar J et al. (2004) Polyplexes of Polyethylenimine and per-N-methylated Polyethylenimine-Cytotoxicity and Transfection Efficiency. *J Nanosci Nanotechnol*, 4(5):512-520, 10.1166/jnn.2004.080

[65] Gebben B, van den Berg H W A, Bargeman D et al. (1985) Intramolecular crosslinking of poly(vinyl alcohol). *Polymer (Guildf)*, 26(11):1737-1740, 10.1016/0032-3861(85)90295-2

[66] Kim Y H, Park J H, Lee M et al. (2005) Polyethylenimine with acid-labile linkages as a biodegradable gene carrier. *J Control Release*, 103(1):209-219, 10.1016/j.jconrel.2004.11.008

[67] Ketola T M, Hanzlíková M, Leppänen L et al. (2013) Independent versus Cooperative Binding in Polyethylenimine–DNA and Poly(l-lysine)-DNA Polyplexes. *J Phys Chem B*, 117(36):10405-10413, 10.1021/jp404812a

[68] Mädler S, Bich C, Touboul D et al. (2009) Chemical cross-linking with NHS esters: a systematic study on amino acid reactivities. *J Mass Spectrom*, 44(5):694-706, 10.1002/jms.1544

[69] Fahrmeir J, Gunther M, Tietze N et al. (2007) Electrophoretic purification of tumor-targeted polyethylenimine-based polyplexes reduces toxic side effects in vivo. *J Control Release*, 122(3):236-245, 10.1016/j.jconrel.2007.05.013

[70] von Harpe A, Petersen H, Li Y et al. (2000) Characterization of commercially available and synthesized polyethylenimines for gene delivery. *J Control Release*, 69(2):309-322, 10.1016/S0168-3659(00)00317-5

[71] Grotzky A, Manaka Y, Fornera S et al. (2010) Quantification of α-polylysine: a comparison of four UV/Vis spectrophotometric methods. *Anal Methods*, 2(10):1448-1455, 10.1039/C0AY00116C

[72] Ferruti P, Knobloch S, Ranucci E et al. (1998) A novel modification of poly(L-lysine) leading to a soluble cationic polymer with reduced toxicity and with potential as a transfection agent. *Macromol Chem Phys*, 199(11):2565-2575, 10.1002/(SICI)1521-3935(19981101)199:11<2565::AID-MACP2565>3.0.CO;2-G

[73] Ming X, Sato K, and Juliano R L (2011) Unconventional internalization mechanisms underlying functional delivery of antisense oligonucleotides via cationic lipoplexes and polyplexes. *J Control Release*, 153(1):83-92, 10.1016/j.jconrel.2011.04.029

[74] Akinc A, Langer R (2002) Measuring the pH environment of DNA delivered using nonviral vectors: Implications for lysosomal trafficking. *Biotechnol Bioeng*, 78(5):503-508, 10.1002/bit.20215

[75] Yue Y (2013) Springer Theses: How Free Cationic Polymer Chains Promote Gene Transfection, *PhD thesis*, Springer International Publishing, Cham, Heidelberg, New York, Dordrecht, London, 10.1007/978-3-319-00336-8

[76] Lakowicz J R (2006) Introduction to Fluorescence. In: Lakowicz J R, Principles of Fluorescence Spectroscopy, 3rd edn., Springer, Berlin, Germany

[77] Haugland R P (2005) The Handbook - A Guide to Fluorescent Probes and Labeling Technologies, tenth edn. Invitrogen Corp, Carlsbad, CA, USA

[78] Greulich K O (2005) Single-Molecule Studies on DNA and RNA. *ChemPhysChem*, 6(12):2458-2471, 10.1002/cphc.200500038

[79] Lakowicz J R (2006) Quenching of Fluorescence. In: Lakowicz J R, Principles of Fluorescence Spectroscopy, 3rd edn., Springer, Berlin, Germany

[80] Piston D W, Kremers G J (2007) Fluorescent protein FRET: the good, the bad and the ugly. *Trends Biochem Sci*, 32(9):407-414, 10.1016/j.tibs.2007.08.003

[81] Meyer B H, Martinez K L, Segura J M et al. (2006) Covalent labeling of cell-surface proteins for in-vivo FRET studies. *FEBS Lett*, 580(6):1654-1658, 10.1016/j.febslet.2006.02.007

[82] Rost F W D (1991) Microfluorometry: errors, standardization and data processing. In: Quantitative Fluorescence Microscopy, 1st edn., Cambridge University Press, Cambridge, Great Britain

[83] Valdes-Aguilera O, Neckers D C (1989) Aggregation phenomena in xanthene dyes. *Acc Chem Res*, 22(5):171-177, 10.1021/ar00161a002

[84] Lakowicz J R (2006) Instrumentation for Fluorescence Spectroscopy. In: Lakowicz J R, Principles of Fluorescence Spectroscopy, 3rd edn., Springer, Berlin, Germany

[85] Schäfer F P (1977) Principles of dye laser operation. In: Schäfer F.P., Topics in applied physics: Dye lasers, 2nd revised edn., Springer, Berlin

[86] Sauer M, Hofkens J, Enderlein J (2011) Basic Principles of Fluorescence Spectroscopy. In: Handbook of Fluorescence Spectroscopy and Imaging: From Single Molecules to Ensembles, 1st edn., Wiley-VCH Verlag GmbH & Co. KGaA, Weinheim, 10.1002/9783527633500.ch1

[87] Kuhn H (1958) The electron gas theory of the color of natural and artificial dyes: problems and principles. In: Zechmeister L, Fortschritte der Chemie organischer Naturstoffe: 16 edn., Springer, Wien

[88] Drexhage K H (1977) Structure and Properties of Laser Dyes. In: Schäfer F.P., Topics in applied physics: Dye lasers, 2nd revised edn., Springer, Berlin

[89] Atkins P W (1996) Quantentheorie: Methoden und Anwendungen. In: Höpfner Arno, Physikalische Chemie, 2nd edn., VCH Verlagsgesellschaft mbH, Weinheim

[90] Atkins P W (1996) Spektroskopie 1: Rotations- und Schwingungsübergänge. In: Höpfner Arno, Physikalische Chemie, 2nd edn., VCH Verlagsgesellschaft mbH, Weinheim

[91] Born M, Oppenheimer R (1927) Zur Quantentheorie der Molekeln. *Ann Phys*, 389(20):457-484, 10.1002/andp.19273892002

[92] Franck J, Dymond E G (1926) Elementary processes of photochemical reactions. *Trans Faraday Soc*, 21(February):536-542, 10.1039/TF9262100536

[93] Condon E (1926) A Theory of Intensity Distribution in Band Systems. *Phys Rev*, 28(6):1182-1201, 10.1103/PhysRev.28.1182

[94] Kasha M (1950) Characterization of electronic transitions in complex molecules. *Discuss Faraday Soc*, 9:14-19, 10.1039/DF9500900014

[95] Strickler S J, Berg R A (1962) Relationship between Absorption Intensity and Fluorescence Lifetime of Molecules. *J Chem Phys*, 37(4):814-822, 10.1063/1.1733166

[96] Kasha M, Rawls H R, and El-Bayoumi A (1965) The exciton model in molecular spectroscopy. *Pure Appl Chem*, 11(3-4):371-392, 10.1351/pac196511030371

[97] Jelley E E (1936) Spectral Absorption and Fluorescence of Dyes in the Molecular State. *Nature*, 138:1009-1010, 10.1038/1381009a0

[98] Scheibe G (1936) Über die Veränderlichkeit des Absorptionsspektrums einiger Sensibilisierungsfarbstoffe und deren Ursache. *Angew Chem*, 49(31):563, 10.1002/ange.19360493110

[99] Scheibe G (1937) Über die Veränderlichkeit der Absorptionsspektren in Lösungen und die Nebenvalenzen als ihre Ursache. *Angew Chem*, 50(11):212-219, 10.1002/ange.19370501103

[100] Daré-Doyen S, Doizi D, Guilbaud P et al. (2003) Dimerization of Xanthene Dyes in Water: Experimental Studies and Molecular Dynamic Simulations. *J Phys Chem B*, 107(50):13803-13812, 10.1021/jp034845j

[101] Penzkofer A, Leupacher W (1987) Fluorescence behaviour of highly concentrated rhodamine 6G solutions. *J Lumin*, 37(2):61-72, 10.1016/0022-2313(87)90167-0

[102] Ogawa M, Kosaka N, Choyke P L et al. (2009) H-Type Dimer Formation of Fluorophores: A Mechanism for Activatable, in Vivo Optical Molecular Imaging. *ACS Chem Biol*, 4(7):535-546, 10.1021/cb900089j

[103] Packard B Z, Toptygin D D, Komoriya A et al. (1996) Profluorescent protease substrates: intramolecular dimers described by the exciton model. *Proc Natl Acad Sci U S A*, 93(21):11640-11645, 10.1073/pnas.93.21.11640

[104] Karolin J, Johansson L B A, Strandberg L et al. (1994) Fluorescence and Absorption Spectroscopic Properties of Dipyrrometheneboron Difluoride (BODIPY) Derivatives in Liquids, Lipid Membranes, and Proteins. *J Am Chem Soc*, 116(17):7801-7806, 10.1021/ja00096a042

[105] Baeyer A (1871) Ueber eine neue Klasse von Farbstoffen. *Ber Dtsch Chem Ges*, 4(2):555-558, 10.1002/cber.18710040209

[106] Hermanson G T (2008) Fluorescent Probes. In: Bioconjugate Techniques, second edn., Academic Press, London

[107] van Dam G M, Themelis G, Crane L M A et al. (2011) Intraoperative tumor-specific fluorescence imaging in ovarian cancer by folate receptor-α targeting: first in-human results. *Nat Med*, 17(10):1315-1319, 10.1038/nm.2472

[108] Klonis N, Sawyer W H (1996) Spectral properties of the prototropic forms of fluorescein in aqueous solution. *J Fluoresc*, 6(3):147-157, 10.1007/BF00732054

[109] Lavis L D, Rutkoski T J, and Raines R T (2007) Tuning the pK_a of Fluorescein to Optimize Binding Assays. *Anal Chem*, 79(17):6775-6782, 10.1021/ac070907g

[110] Han J, Burgess K (2009) Fluorescent Indicators for Intracellular pH. *Chem Rev*, 110(5):2709-2728, 10.1021/cr900249z

[111] Treibs A, Kreuzer F H (1968) Difluorboryl-Komplexe von Di- und Tripyrrylmethenen. *Justus Liebigs Ann Chem*, 718(1):208-223, 10.1002/jlac.19687180119

[112] Dahim M, Mizuno N K, Li X M et al. (2002) Physical and Photophysical Characterization of a BODIPY Phosphatidylcholine as a Membrane Probe. *Biophys J*, 83(3):1511-1524, 10.1016/S0006-3495(02)73921-0

[113] Loudet A, Burgess K (2007) BODIPY Dyes and Their Derivatives: Syntheses and Spectroscopic Properties. *Chem Rev*, 107(11):4891-4932, 10.1021/cr078381n

[114] Bergström F, Mikhalyov I, Hägglöf P et al. (2001) Dimers of Dipyrrometheneboron Difluoride (BODIPY) with Light Spectroscopic Applications in Chemistry and Biology. *J Am Chem Soc*, 124(2):196-204, 10.1021/ja010983f

[115] Mikhalyov I, Gretskaya N, Bergström F et al. (2002) Electronic ground and excited state properties of dipyrrometheneboron difluoride (BODIPY): Dimers with application to biosciences. *Phys Chem Chem Phys*, 4(22):5663-5670, 10.1039/B206357N

[116] Zhu S, Zhang J, Vegesna G et al. (2010) Highly Water-Soluble Neutral BODIPY Dyes with Controllable Fluorescence Quantum Yields. *Org Lett*, 13(3):438-441, 10.1021/ol102758z

[117] Tleugabulova D, Zhang Z, and Brennan J D (2002) Characterization of Bodipy Dimers Formed in a Molecularly Confined Environment. *J Phys Chem B*, 106(51):13133-13138, 10.1021/jp027126y

[118] Saki N, Dinc T, and Akkaya E U (2006) Excimer emission and energy transfer in cofacial boradiazaindacene (BODIPY) dimers built on a xanthene scaffold. *Tetrahedron*, 62(11):2721-2725, 10.1016/j.tet.2005.12.021

[119] Alamiry M A H, Benniston A C, Copley G et al. (2011) Intramolecular Excimer Formation for Covalently Linked Boron Dipyrromethene Dyes. *J Phys Chem A*, 115(44):12111-12119, 10.1021/jp2070419

[120] Da Poian A T, Gomes O, and Coelho-Sampaio T (1998) Kinetics of intracellular viral disassembly and processing probed by Bodipy fluorescence dequenching. *J Virol Methods*, 70(1):45-58, 10.1016/S0166-0934(97)00166-3

[121] Marks D, Bittman R, and Pagano R (2008) Use of Bodipy-labeled sphingolipid and cholesterol analogs to examine membrane microdomains in cells. *Histochem Cell Biol*, 130(5):819-832, 10.1007/s00418-008-0509-5

[122] Vámosi G, Gohlke C, and Clegg R M (1996) Fluorescence characteristics of 5-carboxytetramethylrhodamine linked covalently to the 5' end of oligonucleotides: multiple conformers of single-stranded and double-stranded dye-DNA complexes. *Biophys J*, 71(2):972-994, 10.1016/S0006-3495(96)79300-1

[123] Kolmakov K, Belov V, Bierwagen J et al. (2010) Red-Emitting Rhodamine Dyes for Fluorescence Microscopy and Nanoscopy. *Chemistry*, 16(1):158-166, 10.1002/chem.200902309

[124] Toprak M, Arik M (2010) An investigation of energy transfer between coumarin 35 and xanthene derivatives in liquid medium. *Turk J Chem*, 34:285-293, 10.3906/kim-0808-40

[125] Arden-Jacob J, Frantzeskos J, Kemnitzer N U et al. (2001) New fluorescent markers for the red region. *Spectrochim Acta A Mol Biomol Spectrosc*, 57(11):2271-2283, 10.1016/S1386-1425(01)00476-0

[126] Czerney P, Grane G, Birckner E et al. (1995) Molecular engineering of cyanine-type fluorescent and laser dyes. *J Photochem Photobiol A Chem*, 89(1):31-36, 10.1016/1010-6030(94)04018-W

[127] del Monte F, Levy D (1998) Formation of Fluorescent Rhodamine B J-Dimers in Sol–Gel Glasses Induced by the Adsorption Geometry on the Silica Surface. *J Phys Chem B*, 102(41):8036-8041, 10.1021/jp982396v

[128] Christie R J, Tadiello C J, Chamberlain L M et al. (2009) Optical Properties and Application of a Reactive and Bioreducible Thiol-Containing Tetramethylrhodamine Dimer. *Bioconjug Chem*, 20(3):476-480, 10.1021/bc800367e

[129] Li X, Zhu R, Yu A et al. (2011) Ultrafast Photoinduced Electron Transfer between Tetramethylrhodamine and Guanosine in Aqueous Solution. *J Phys Chem B*, 115(19):6265-6271, 10.1021/jp200455b

[130] Kurata S, Kanagawa T, Yamada K et al. (2001) Fluorescent quenching-based quantitative detection of specific DNA/RNA using a BODIPY© FL-labeled probe or primer. *Nucleic Acids Res*, 29(6):e34-e34, 10.1093/nar/29.6.e34

[131] Wightman L, Kircheis R, Rössler V et al. (2001) Different behavior of branched and linear polyethylenimine for gene delivery in vitro and in vivo. *J Gene Med*, 3(4):362-372, 10.1002/jgm.187

[132] Seib F P, Jones A T, and Duncan R (2007) Comparison of the endocytic properties of linear and branched PEIs, and cationic PAMAM dendrimers in B16f10 melanoma cells. *J Control Release*, 117(3):291-300, 10.1016/j.jconrel.2006.10.020

[133] Kunishima M, Kawachi C, Monta J et al. (1999) 4-(4,6-dimethoxy-1,3,5-triazin-2-yl)-4-methyl-morpholinium chloride: an efficient condensing agent leading to the formation of amides and esters. *Tetrahedron*, 55(46):13159-13170, 10.1016/S0040-4020(99)00809-1

[134] Hungerford G, Benesch J, Mano J F et al. (2007) Effect of the labelling ratio on the photophysics of fluorescein isothiocyanate (FITC) conjugated to bovine serum albumin. *Photochem Photobiol Sci*, 6(2):152-158, 10.1039/B612870J

[135] Sauer M, Hofkens J, Enderlein J (2011) Fluorophores and Fluorescent Labels. In: Handbook of Fluorescence Spectroscopy and Imaging: From Single Molecules to Ensembles, 1st edn., Wiley-VCH Verlag GmbH & Co. KGaA, Weinheim, Germany, 10.1002/9783527633500.ch2

[136] Zhang W, Tang B, Liu X et al. (2009) A highly sensitive acidic pH fluorescent probe and its application to HepG2 cells. *Analyst*, 134(2):367-371, 10.1039/B807581F

[137] Yuan L, Lin W, and Feng Y (2011) A rational approach to tuning the pKa values of rhodamines for living cell fluorescence imaging. *Org Biomol Chem*, 9(6):1723-1726, 10.1039/C0OB01045F

[138] Sjöback R, Nygren J, and Kubista M (1995) Absorption and fluorescence properties of fluorescein. *Spectrochim Acta A Mol Biomol Spectrosc*, 51(6):L7-L21, 10.1016/0584-8539(95)01421-P

[139] Kunishima M, Kawachi C, Hioki K et al. (2001) Formation of carboxamides by direct condensation of carboxylic acids and amines in alcohols using a new alcohol- and

water-soluble condensing agent: DMT-MM. *Tetrahedron*, 57(8):1551-1558, 10.1016/S0040-4020(00)01137-6

[140] Murphy R F, Powers S, and Cantor C R (1984) Endosome pH measured in single cells by dual fluorescence flow cytometry: rapid acidification of insulin to pH 6. *J Cell Biol*, 98(5):1757-1762, 10.1083/jcb.98.5.1757

[141] Bradley D F, Wolf M K (1959) Aggregation of Dyes Bound to Polyanions. *Proc Natl Acad Sci U S A*, 45(7):944-952, 10.1073/pnas.45.7.944

[142] Van der Auweraer M, Verschuere B, and De Schryver F C (1988) Absorption and fluorescence properties of Rhodamine B derivatives forming Langmuir-Blodgett films. *Langmuir*, 4(3):583-588, 10.1021/la00081a016

[143] Hernando J, van der Schaaf M, van Dijk E M H P et al. (2002) Excitonic Behavior of Rhodamine Dimers: A Single-Molecule Study. *J Phys Chem A*, 107(1):43-52, 10.1021/jp0218995

[144] Bernacchi S, Mély Y (2001) Exciton interaction in molecular beacons: a sensitive sensor for short range modifications of the nucleic acid structure. *Nucleic Acids Res*, 29(13):e62-e62, 10.1093/nar/29.13.e62

[145] Simpson W T, Peterson D L (1957) Coupling Strength for Resonance Force Transfer of Electronic Energy in Van der Waals Solids. *J Chem Phys*, 26(3):588-593, 10.1063/1.1743351

[146] Packard B Z, Toptygin D D, Komoriya A et al. (1998) Intramolecular Resonance Dipole–Dipole Interactions in a Profluorescent Protease Substrate. *J Phys Chem B*, 102(4):752-758, 10.1021/jp972845b

[147] Hasegawa T, Kondo Y, Koizumi Y et al. (2009) A highly sensitive probe detecting low pH area of HeLa cells based on rhodamine B modified β-cyclodextrins. *Bioorg Med Chem*, 17(16):6015-6019, 10.1016/j.bmc.2009.06.046

[148] El Baraka M, Deumié M, Viallet P et al. (1991) Fluorimetric studies of solutions of pyronin dyes: equilibrium constants in water and partition coefficients in organic-solvent-water systems. *J Photochem Photobiol A Chem*, 56(2–3):295-311, 10.1016/1010-6030(91)80030-L

[149] Zhan X Q, Qian Z H, Zheng H et al. (2008) Rhodamine thiospirolactone. Highly selective and sensitive reversible sensing of Hg(ii). *Chem Commun*,(16):1859-1861, 10.1039/B719473K

[150] Brotzel F, Chu Y C, and Mayr H (2007) Nucleophilicities of Primary and Secondary Amines in Water. *J Org Chem*, 72(10):3679-3688, 10.1021/jo062586z

[151] Kong H J, Liu J, Riddle K et al. (2005) Non-viral gene delivery regulated by stiffness of cell adhesion substrates. *Nat Mater*, 4(6):460-464, 10.1038/nmat1392

[152] Hermanson G T (2008) Functional Targets. In: Bioconjugate Techniques, second edn., Academic Press, London

[153] Marushchak D, Kalinin S, Mikhalyov I et al. (2006) Pyrromethene dyes (BODIPY) can form ground state homo and hetero dimers: Photophysics and spectral properties. *Spectrochim Acta A Mol Biomol Spectrosc*, 65(1):113-122, 10.1016/j.saa.2005.09.035

[154] Martínez Martínez V, López Arbeloa F, Bañuelos Prieto J et al. (2005) Characterization of Rhodamine 6G Aggregates Intercalated in Solid Thin Films of Laponite Clay. 2 Fluorescence Spectroscopy. *J Phys Chem B*, 109(15):7443-7450, 10.1021/jp050440i

[155] Martínez Martínez V, López Arbeloa F, Bañuelos Prieto J et al. (2004) Characterization of Rhodamine 6G Aggregates Intercalated in Solid Thin Films of Laponite Clay. 1. Absorption Spectroscopy. *J Phys Chem B*, 108(52):20030-20037, 10.1021/jp047552e

[156] Makrigiorgos M (1997) Detection of lipid peroxidation on erythrocytes using the excimer-forming property of a lipophilic BODIPY fluorescent dye. *J Biochem Biophys Methods*, 35(1):23-35, 10.1016/S0165-022X(97)00020-1

[157] Boldyrev I A, Zhai X, Momsen M M et al. (2007) New BODIPY lipid probes for fluorescence studies of membranes. *J Lipid Res*, 48(7):1518-1532, 10.1194/jlr.M600459-JLR200

[158] Utsuno K, Uludag H (2010) Thermodynamics of Polyethylenimine-DNA Binding and DNA Condensation. *Biophys J*, 99(1):201-207, 10.1016/j.bpj.2010.04.016

[159] Sun C, Tang T, Uludag H et al. (2011) Molecular Dynamics Simulations of DNA/PEI Complexes: Effect of PEI Branching and Protonation State. *Biophys J*, 100(11):2754-2763, 10.1016/j.bpj.2011.04.045

[160] Prevette L E, Kodger T E, Reineke T M et al. (2007) Deciphering the Role of Hydrogen Bonding in Enhancing pDNA–Polycation Interactions. *Langmuir*, 23(19):9773-9784, 10.1021/la7009995

[161] Bloomfield V A (1997) DNA condensation by multivalent cations. *Biopolymers*, 44(3):269-282, 10.1002/(SICI)1097-0282(1997)44:3<269::AID-BIP6>3.0.CO;2-T

[162] Bertschinger M, Backliwal G, Schertenleib A et al. (2006) Disassembly of polyethylenimine-DNA particles in vitro: Implications for polyethylenimine-mediated DNA delivery. *J Control Release*, 116(1):96-104, 10.1016/j.jconrel.2006.09.006

[163] Budker V, Trubetskoy V, and Wolff J A (2006) Condensation of nonstochiometric DNA/polycation complexes by divalent cations. *Biopolymers*, 83(6):646-657, 10.1002/bip.20602

[164] Boeckle S, von Gersdorff K, van der Piepen S et al. (2004) Purification of polyethylenimine polyplexes highlights the role of free polycations in gene transfer. *J Gene Med*, 6(10):1102-1111, 10.1002/jgm.598

[165] Trubetskoy V S, Slattum P M, Hagstrom J E et al. (1999) Quantitative Assessment of DNA Condensation. *Anal Biochem*, 267(2):309-313, 10.1006/abio.1998.3032

[166] Breunig M, Lungwitz U, Liebl R et al. (2006) Fluorescence resonance energy transfer: Evaluation of the intracellular stability of polyplexes. *Eur J Pharm Biopharm*, 63(2):156-165, 10.1016/j.ejpb.2006.01.012

[167] Ko Y T, Bickel U, and Huang J (2011) Polyethylenimine/Oligonucleotide Polyplexes Investigated by Fluorescence Resonance Energy Transfer and Fluorescence Anisotropy. *Oligonucleotides*, 21(2):109-114, 10.1089/oli.2010.0271

[168] Itaka K, Harada A, Nakamura K et al. (2002) Evaluation by Fluorescence Resonance Energy Transfer of the Stability of Nonviral Gene Delivery Vectors under Physiological Conditions. *Biomacromolecules*, 3(4):841-845, 10.1021/bm025527d

[169] Olmsted J, Kearns D R (1977) Mechanism of ethidium bromide fluorescence enhancement on binding to nucleic acids. *Biochemistry*, 16(16):3647-3654, 10.1021/bi00635a022

[170] Kautsky H (1939) Quenching of luminescence by oxygen. *Trans Faraday Soc*, 35:216-219, 10.1039/TF9393500216

[171] Lakowicz J R (2006) Mechanisms and Dynamics of Fluorescence Quenching. In: Lakowicz J R, Principles of Fluorescence Spectroscopy, 3rd edn., Springer, Berlin, Germany

[172] Heinlein T, Knemeyer J P, Piestert O et al. (2003) Photoinduced Electron Transfer between Fluorescent Dyes and Guanosine Residues in DNA-Hairpins. *J Phys Chem B*, 107(31):7957-7964, 10.1021/jp0348068

[173] Xiao W, Stern D, Jain M et al. (2001) Multiplex capillary denaturing high-performance liquid chromatography with laser-induced fluorescence detection. *BioTechniques*, 30(6):1332-1338, 10.2144/01306rr01

[174] Gabrielson N P, Pack D W (2006) Acetylation of Polyethylenimine Enhances Gene Delivery via Weakened Polymer/DNA Interactions. *Biomacromolecules*, 7(8):2427-2435, 10.1021/bm060300u

[175] Schaffer D V, Fidelman N A, Dan N et al. (2000) Vector unpacking as a potential barrier for receptor-mediated polyplex gene delivery. *Biotechnol Bioeng*, 67(5):598-606, 10.1002/(SICI)1097-0290(20000305)67:5<598::AID-BIT10>3.0.CO;2-G

[176] Van Rompaey E, Engelborghs Y, Sanders N et al. (2001) Interactions Between Oligonucleotides and Cationic Polymers Investigated by fluorescence Correlation Spectroscopy. *Pharm Res*, 18(7):928-936, 10.1023/A:1010975908915

[177] Vader P, van der Aa L J, Engbersen J F J et al. (2010) A method for quantifying cellular uptake of fluorescently labeled siRNA. *J Control Release*, 148(1):106-109, 10.1016/j.jconrel.2010.06.019

[178] Doose S, Neuweiler H, and Sauer M (2009) Fluorescence Quenching by Photoinduced Electron Transfer: A Reporter for Conformational Dynamics of Macromolecules. *ChemPhysChem*, 10(9-10):1389-1398, 10.1002/cphc.200900238

[179] Unruh J R, Gokulrangan G, Wilson G S et al. (2005) Fluorescence Properties of Fluorescein, Tetramethylrhodamine and Texas Red Linked to a DNA Aptamer. *Photochem Photobiol*, 81(3):682-690, 10.1111/j.1751-1097.2005.tb00244.x

[180] Wright J C, Hoffman A S (2012) Historical Overview of Long Acting Injections and Implants. In: Wright J C, Burgess D J, Long Acting Injections and Implants, Springer US, Boston, MA

[181] Phua K K L, Roberts E R H, Leong K W (2011) 1.123 - Degradable Polymers A2 - Ducheyne, Paul. In: Comprehensive Biomaterials, Elsevier, Oxford, 10.1016/B978-0-08-055294-1.00253-1

[182] Oupický D, Carlisle R C, and Seymour L W (2001) Triggered intracellular activation of disulfide crosslinked polyelectrolyte gene delivery complexes with extended systemic circulation in vivo. *Gene Ther*, 8(9):713-724, 10.1038/sj.gt.3301446

[183] Schafer F Q, Buettner G R (2001) Redox environment of the cell as viewed through the redox state of the glutathione disulfide/glutathione couple. *Free Radic Biol Med*, 30(11):1191-1212, 10.1016/S0891-5849(01)00480-4

[184] May J M, Qu Z c, and Nelson D J (2006) Cellular disulfide-reducing capacity: An integrated measure of cell redox capacity. *Biochem Biophys Res Commun*, 344(4):1352-1359, 10.1016/j.bbrc.2006.04.065

[185] López-Mirabal H R, Winther J R (2008) Redox characteristics of the eukaryotic cytosol. *Biochim Biophys Acta Mol Cell Res*, 1783(4):629-640, 10.1016/j.bbamcr.2007.10.013

[186] Sastre J, Pallardo F V, Viña J (2005) Glutathione. In: The Handbook of Environmental Chemistry: Reactions, Processes, Springer, Berlin/Heidelberg, 10.1007/b101148

[187] Green R, Graham M, O'Donovan M et al. (2006) Subcellular compartmentalization of glutathione: Correlations with parameters of oxidative stress related to genotoxicity. *Mutagenesis*, 21(6):383-390, 10.1093/mutage/gel043

[188] Cheng R, Feng F, Meng F et al. (2011) Glutathione-responsive nano-vehicles as a promising platform for targeted intracellular drug and gene delivery. *J Control Release*, 152(1):2-12, 10.1016/j.jconrel.2011.01.030

[189] Bausinger R, von Gersdorff K, Braeckmans K et al. (2006) The Transport of Nanosized Gene Carriers Unraveled by Live-Cell Imaging. *Angew Chem Int Ed Engl*, 45(10):1568-1572, 10.1002/anie.200503021

[190] Payne C K, Jones S A, Chen C et al. (2007) Internalization and Trafficking of Cell Surface Proteoglycans and Proteoglycan-Binding Ligands. *Traffic*, 8(4):389-401, 10.1111/j.1600-0854.2007.00540.x

[191] Mozley O L, Thompson B C, Fernandez-Martell A et al. (2014) A mechanistic dissection of polyethylenimine mediated transfection of CHO cells: To enhance the efficiency of

recombinant DNA utilization. *Biotechnol Progress*, 30(5):1161-1170, 10.1002/btpr.1932

[192] Mozley O L (2013) A Mechanistic Dissection of Polyethylenimine Mediated Transfection of Chinese Hamster Ovary Cells, *PhD thesis*, University of Sheffield, Sheffield, UK, uk.bl.ethos.595228

[193] Fenouillet E, Barbouche R, and Jones I M (2007) Cell Entry by Enveloped Viruses: Redox Considerations for HIV and SARS-Coronavirus. *Antioxid Redox Signal*, 9(8):1009-1034, 10.1089/ars.2007.1639

[194] Shen W C, Ryser H J, and LaManna L (1985) Disulfide spacer between methotrexate and poly(D-lysine). A probe for exploring the reductive process in endocytosis. *J Biol Chem*, 260(20):10905-10908

[195] Austin C D, Wen X, Gazzard L et al. (2005) Oxidizing potential of endosomes and lysosomes limits intracellular cleavage of disulfide-based antibody–drug conjugates. *Proc Natl Acad Sci U S A*, 102(50):17987-17992, 10.1073/pnas.0509035102

[196] Li J, Manickam D S, Chen J et al. (2012) Effect of cell membrane thiols and reduction-triggered disassembly on transfection activity of bioreducible polyplexes. *Eur J Pharm Sci*, 46(3):173-180, 10.1016/j.ejps.2012.02.020

[197] Brülisauer L, Kathriner N, Prenrecaj M et al. (2012) Tracking the Bioreduction of Disulfide-Containing Cationic Dendrimers. *Angew Chem Int Ed Engl*, 51(50):12454-12458, 10.1002/anie.201207070

[198] Kang H C, Kang H J, and Bae Y H (2011) A reducible polycationic gene vector derived from thiolated low molecular weight branched polyethyleneimine linked by 2-iminothiolane. *Biomaterials*, 32(4):1193-1203, 10.1016/j.biomaterials.2010.08.079

[199] Saito G, Amidon G L, and Lee K D (2003) Enhanced cytosolic delivery of plasmid DNA by a sulfhydryl-activatable listeriolysin O/protamine conjugate utilizing cellular reducing potential. *Gene Ther*, 10(1):72-83, 10.1038/sj.gt.3301859

[200] Yang J, Chen H, Vlahov I R et al. (2006) Evaluation of disulfide reduction during receptor-mediated endocytosis by using FRET imaging. *Proc Natl Acad Sci U S A*, 103(37):13872-13877, 10.1073/pnas.0601455103

[201] Lee J (2012) Localization and Dynamics of Disulfide Reduction and Their Key Redox Regulators during Internalization in Endolysosomal Compartments, *PhD thesis*, University of Michigan, Ann Arbor, Michigan, USA

[202] Choi S, Lee K D (2008) Enhanced gene delivery using disulfide-crosslinked low molecular weight polyethylenimine with listeriolysin o-polyethylenimine disulfide conjugate. *J Control Release*, 131(1):70-76, 10.1016/j.jconrel.2008.07.007

[203] Vercauteren D, Piest M, van der Aa L J et al. (2011) Flotillin-dependent endocytosis and a phagocytosis-like mechanism for cellular internalization of disulfide-based poly(amido amine)/DNA polyplexes. *Biomaterials*, 32(11):3072-3084, 10.1016/j.biomaterials.2010.12.045

[204] Won Y Y, Sharma R, and Konieczny S F (2009) Missing pieces in understanding the intracellular trafficking of polycation/DNA complexes. *J Control Release*, 139(2):88-93, 10.1016/j.jconrel.2009.06.031

[205] Poon G M K, Gariépy J (2007) Cell-surface proteoglycans as molecular portals for cationic peptide and polymer entry into cells. *Biochem Soc Trans*, 35(4):788-793, 10.1042/BST0350788

[206] Rejman J, Bragonzi A, and Conese M (2005) Role of Clathrin- and Caveolae-Mediated Endocytosis in Gene Transfer Mediated by Lipo- and Polyplexes. *Mol Ther*, 12(3):468-474, 10.1016/j.ymthe.2005.03.038

[207] van der Aa M A E M, Huth U S, Häfele S Y et al. (2007) Cellular Uptake of Cationic Polymer-DNA Complexes Via Caveolae Plays a Pivotal Role in Gene Transfection in COS-7 Cells. *Pharm Res*, 24(8):1590-1598, 10.1007/s11095-007-9287-3

[208] Hufnagel H, Hakim P, Lima A et al. (2009) Fluid Phase Endocytosis Contributes to Transfection of DNA by PEI-25. *Mol Ther*, 17(8):1411-1417, 10.1038/mt.2009.121

[209] Sahay G, Alakhova D Y, and Kabanov A V (2010) Endocytosis of nanomedicines. *J Control Release*, 145(3):182-195, 10.1016/j.jconrel.2010.01.036

[210] Mindell J A (2012) Lysosomal acidification mechanisms. *Annu Rev Physiol*, 74:69-86, 10.1146/annurev-physiol-012110-142317

[211] Yue Y, Jin F, Deng R et al. (2011) Revisit complexation between DNA and polyethylenimine - Effect of length of free polycationic chains on gene transfection. *J Control Release*, 152(1):143-151, 10.1016/j.jconrel.2011.03.020

[212] Cai J, Yue Y, Wang Y et al. (2016) Quantitative study of effects of free cationic chains on gene transfection in different intracellular stages. *J Control Release*, 238:71-79, 10.1016/j.jconrel.2016.07.031

[213] Gabrielson N P, Pack D W (2009) Efficient polyethylenimine-mediated gene delivery proceeds via a caveolar pathway in HeLa cells. *J Control Release*, 136(1):54-61, 10.1016/j.jconrel.2009.02.003

[214] Hwang M E, Keswani R K, and Pack D W (2015) Dependence of PEI and PAMAM Gene Delivery on Clathrin- and Caveolin-Dependent Trafficking Pathways. *Pharm Res*, 32(6):2051-2059, 10.1007/s11095-014-1598-6

[215] Vercauteren D, Vandenbroucke R E, Jones A T et al. (2010) The Use of Inhibitors to Study Endocytic Pathways of Gene Carriers: Optimization and Pitfalls. *Mol Ther*, 18(3):561-569, 10.1038/mt.2009.281

[216] Rejman J, Oberle V, ZUHORN I S et al. (2004) Size-dependent internalization of particles via the pathways of clathrin- and caveolae-mediated endocytosis. *Biochem J*, 377(1):159-169, 10.1042/bj20031253

[217] Grosse S, Aron Y, Thévenot G et al. (2007) Cytoskeletal involvement in the cellular trafficking of plasmid/PEI derivative complexes. *J Control Release*, 122(1):111-117, 10.1016/j.jconrel.2007.06.015

[218] Dean D A, Strong D D, and Zimmer W E (2005) Nuclear entry of nonviral vectors. *Gene Ther*, 12(11):881-890, 10.1038/sj.gt.3302534

[219] Lechardeur D, Verkman A S, and Lukacs G L (2005) Intracellular routing of plasmid DNA during non-viral gene transfer. *Adv Drug Deliv Rev*, 57(5):755-767, 10.1016/j.addr.2004.12.008

[220] Godbey W T, Wu K K, and Mikos A G (1999) Tracking the intracellular path of poly(ethylenimine)/DNA complexes for gene delivery. *Proc Natl Acad Sci U S A*, 96(9):5177-5181, 10.1073/pnas.96.9.5177

[221] Wolff J A, Rozema D B (2008) Breaking the Bonds: Non-viral Vectors Become Chemically Dynamic. *Mol Ther*, 16(1):8-15, 10.1038/sj.mt.6300326

[222] Huth S, Hoffmann F, von Gersdorff K et al. (2006) Interaction of polyamine gene vectors with RNA leads to the dissociation of plasmid DNA-carrier complexes. *J Gene Med*, 8(12):1416-1424, 10.1002/jgm.975

[223] Carlisle R C, Etrych T, Briggs S S et al. (2004) Polymer-coated polyethylenimine/DNA complexes designed for triggered activation by intracellular reduction. *J Gene Med*, 6(3):337-344, 10.1002/jgm.525

[224] Iida T, Mori T, Katayama Y et al. (2007) Overall interaction of cytosolic proteins with the PEI/DNA complex. *J Control Release*, 118(3):364-369, 10.1016/j.jconrel.2006.12.027

[225] Croce A C, Bottiroli G (2014) Autofluorescence Spectroscopy and Imaging: A Tool for Biomedical Research and Diagnosis. *Eur J Histochem*, 58(4):2461, 10.4081/ejh.2014.2461

[226] Fritzsche M, Mandenius C F (2010) Fluorescent cell-based sensing approaches for toxicity testing. *Anal Bioanal Chem*, 398(1):181-191, 10.1007/s00216-010-3651-6

[227] Riss T L, Moravec R A, Niles A L et al (2013) Cell Viability Assays. In: Sittampalam S G, Coussens N P, Brimacombe K, Grossman A, Arkin M, Auld D, Austin C, Baell J, Bejcek B, Chung T D Y, Dahlin J L, Devanaryan V, and Foley T L, Assay Guidance Manual, Eli Lilly & Company and the National Center for Advancing Translational Sciences, Bethesda, MD, USA

[228] Weyermann J, Lochmann D, and Zimmer A (2005) A practical note on the use of cytotoxicity assays. *Int J Pharm*, 288(2):369-376, 10.1016/j.ijpharm.2004.09.018

[229] Moghimi S M, Symonds P, Murray J C et al. (2005) A two-stage poly(ethylenimine)-mediated cytotoxicity: implications for gene transfer/therapy. *Mol Ther*, 11(6):990-995, 10.1016/j.ymthe.2005.02.010

[230] Taranejoo S, Liu J, Verma P et al. (2015) A review of the developments of characteristics of PEI derivatives for gene delivery applications. *J Appl Polym Sci*, 132(25):42096 (1)-42096 (8), 10.1002/APP.42096

[231] Winther J R, Thorpe C (2014) Quantification of thiols and disulfides. *Biochim Biophys Acta Gen Subj*, 1840(2):838-846, 10.1016/j.bbagen.2013.03.031

[232] Pires M M, Chmielewski J (2008) Fluorescence Imaging of Cellular Glutathione Using a Latent Rhodamine. *Org Lett*, 10(5):837-840, 10.1021/ol702769n

[233] Hedley D W, Chow S (1994) Evaluation of methods for measuring cellular glutathione content using flow cytometry. *Cytometry*, 15(4):349-358, 10.1002/cyto.990150411

[234] Chatterjee S, Noack H, Possel H et al. (1999) Glutathione levels in primary glial cultures: Monochlorobimane provides evidence of cell type-specific distribution. *Glia*, 27(2):152-161, 10.1002/(SICI)1098-1136(199908)27:2<152::AID-GLIA5>3.0.CO;2-Q

[235] Huotari J, Helenius A (2011) Endosome maturation. *EMBO J*, 30(17):3481-3500, 10.1038/emboj.2011.286

[236] Cheng J, Zeidan R, Mishra S et al. (2006) Structure–Function Correlation of Chloroquine and Analogues as Transgene Expression Enhancers in Nonviral Gene Delivery. *J Med Chem*, 49(22):6522-6531, 10.1021/jm060736s

[237] Bettinger T, Read M L (2001) Recent developments in RNA-based strategies for cancer gene therapy. *Curr Opin Mol Ther*, 3(2):116-124

[238] Yang S, Coles D J, Esposito A et al. (2009) Cellular uptake of self-assembled cationic peptide-DNA complexes: Multifunctional role of the enhancer chloroquine. *J Control Release*, 135(2):159-165, 10.1016/j.jconrel.2008.12.015

[239] Cervia L D, Chang C C, Wang L et al. (2017) Distinct effects of endosomal escape and inhibition of endosomal trafficking on gene delivery via electrotransfection. *PLoS One*, 12(2):e0171699, 10.1371/journal.pone.0171699

[240] Feener E P, Shen W C, and Ryser H J (1990) Cleavage of disulfide bonds in endocytosed macromolecules. A processing not associated with lysosomes or endosomes. *J Biol Chem*, 265(31):18780-18785

[241] Ross N L, Munsell E V, Sabanayagam C et al. (2015) Histone-targeted Polyplexes Avoid Endosomal Escape and Enter the Nucleus During Postmitotic Redistribution of ER Membranes. *Mol Ther Nucleic Acids*, 4(E226), 10.1038/mtna.2015.2

[242] Viola G, Salvador A, Cecconet L et al. (2007) Photophysical Properties and Photobiological Behavior of Amodiaquine, Primaquine and Chloroquine. *Photochem Photobiol*, 83(6):1415-1427, 10.1111/j.1751-1097.2007.00181.x

[243] Suh J, An Y, Tang B C et al. (2012) Real-time gene delivery vector tracking in the endo-lysosomal pathway of live cells. *Microsc Res Tech*, 75(5):691-697, 10.1002/jemt.21113

[244] Hedley D W, Hallahan A R, and Tripp E H (1990) Flow cytometric measurement of glutathione content of human cancer biopsies. *Br J Cancer*, 61(1):65-68, 10.1038/bjc.1990.14

[245] Conner S D, Schmid S L (2003) Regulated portals of entry into the cell. *Nature*, 422(6927):37-44, 10.1038/nature01451

[246] Di Gioia S, Conese M (2008) Polyethylenimine-mediated gene delivery to the lung and therapeutic applications. *Drug Des Devel Ther*, 2:163-188, 10.2147/DDDT.S2708

[247] Breunig M, Lungwitz U, Liebl R et al. (2007) Breaking up the correlation between efficacy and toxicity for nonviral gene delivery. *Proc Natl Acad Sci U S A*, 104(36):14454-14459, 10.1073/pnas.0703882104

Abbreviations

(Boc-Cys-OH)$_2$.....N^{α},$N^{\alpha'}$-di-Boc-L-cystine
2-ME.....2-mercaptoethanol
A.....adenine (9*H*-purin-6-amine)
AAV .....adeno-associated virus
AON.....antisense oligonucleotide
APC.....antigen-presenting cell
ATCC .....American Type Culture Collection
b-BACH bis-BODIPY-FL-propionyl-1,2-*cis*-diaminocyclohexane
BMDCs .....bone marrow-derived dendritic cells
BMMs.....bone marrow-derived macrophages
BODIPY FL, BP .....4,4-difluoro-5,7-dimethyl-4-bora-3a,4a-diaza-s-indacene-3-propionic acid
BP SE .....*N*-succinimidyl ester activated BODIPY FL
BP_2.....L-cystine cross-linked BODIPY FL
bPEI .....branched poly(ethyleneimine)
BP-SH .....BODIPY FL L-cysteine or “cleaved” BODIPY FL
BSO.....buthionine sulphoximine
C .....cytosine (4-aminopyrimidin-2(1*H*)-one)
CAR.....chimeric antigen receptor
Cas9.....CRISPR associated protein 9
CD.....cluster of differentiation
CHO .....Chinese hamster ovary cell
CLSM .....confocal laser scanning microscopy
CQ .....chloroquine ((*RS*)-*N'*-(7-chloroquinolin-4-yl)-*N*,*N*-diethyl-pentane-1,4-di-amine)
CRISPR.....clustered regularly interspaced short palindromic repeats
DAEM .....donor-acceptor energy migration
DDEM.....donor-donor energy migration
DMSO.....dimethyl sulfoxide
DMTMM.....4-(4,6-Dimethoxy-1,3,5-triazin-2-yl)-4-methylmorpholinium chloride
DNA.....deoxyribonucleic acid
DOTAP .....1,2-dioleoyl-3-trimethylammonium propane
DOTMA.....1,2-di-O-octadecenyl-3-trimethylammonium propane
DPBS.....Dulbecco's phosphate buffered saline

DSB .....double-strand break
DSP .....dithiobis(succinimidyl propionate), Lomant's reagent
DTNB .....5,5'-dithiobis-(2-nitrobenzoic acid), Ellman's reagent
EGFP .....enhanced green fluorescent protein
EMA.....European Medicines Agency
EtBr.....ethidium bromide
F.....fluorescence
FAM .....carboxyfluorescein
FCS.....fetal calf serum
FDA.....Food and Drug Administration
FITC.....fluorescein isothiocyanate
FRET.....Förster resonance energy transfer
FWHM .....full width at half maximum
G .....guanine (2-amino-9*H*-purin-6(1*H*)-one)
GCL .....glutamate cysteine ligase
GFC .....gel-filtration chromatography
GILT.....gamma-interferon-inducible lysosomal thiol reductase
Grx.....glutaredoxin
GSH.....L-glutathione (γ-L-glutamyl-L-cysteinyl-glycine)
GSH-EE .....glutathione ethyl ester (γ-Glu-Cys-Gly-OEt)
GSS .....glutathione synthetase
GSSG.....glutathione disulfide
HCl .....hydrochloric acid
HDR .....homology directed repair
HEPES .....4-(2-Hydroxyethyl)piperazine-1-ethanesulfonic acid
HOMO .....highest occupied molecular orbital
HPLC .....high-performance liquid chromatography
HSC .....hematopoietic stem cell
HSPG.....heparan sulfate proteoglycan
IC .....internal conversion
ISC .....intersystem crossing
LB.....lysogeny broth
LLO.....listeriolysin O
LNP .....lipid nanoparticle
lPEI.....linear poly(ethyleneimine)
LUMO .....lowest unoccupied molecular orbital
mBCl .....monochlorobimane

MES ..... 2-(*N*-morpholino)ethanesulfonic acid
miRNA ..... micro RNA
mRNA ..... messenger RNA
MTT ..... 3-(4,5-dimethylthiazol-2-yl)-2,5-diphenyl¬tetrazolium bromide
MTX ..... methotrexate
N/P ..... quotient of nitrogen atoms to nucleic acid phosphorous atoms
NaOAc/HOAc ..... sodium acetate/acetic acid
NEM ..... *N*-ethylmaleimide
NHEJ ..... non-homologous end joining
NMR ..... nuclear magnetic resonance
NMWL ..... nominal molecular weight limit
P ..... phosphorescence
PAA ..... poly(amido amine)
PAMAM ..... poly(amidoamine)
PCS ..... photon correlation spectroscopy (dynamic light scattering)
PDEAEMA ..... poly(*N*,*N*-diethylamino-2-ethylmethacrylate)
PDI ..... protein disulfide isomerase
pDNA ..... plasmid DNA
PHPMA ..... poly(*N*-(2-hydroxypropyl)methacrylamide)
PI ..... propidium iodide
PLGA ..... poly(lactic-co-glycolic acid)
PLL ..... poly(L-lysine)
PMT ..... photomultiplier
PS ..... polystyrene
RC ..... regenerated cellulose
RISC ..... RNA-induced silencing complex
RNA ..... ribonucleic acid
RNAi ..... RNA interference
SDS ..... sodium dodecyl sulfate
SE ..... succinimidyl ester
siRNA ..... small interfering RNA
SNARE ..... soluble NSF(*N*-ethylmaleimide-sensitive factor) attachment protein) receptor
T ..... thymidine (5-Methylpyrimidine-2,4(1*H*,3*H*)-dione)
TALEN ..... transcription activator-like effector nuclease
TAMRA SE ..... *N*-succinimidyl ester activated TAMRA
TAMRA ..... tetramethylrhodamine

TCSPC .....time-correlated single photon counting
TICT .....twisted internal charge transfer
TLC.....thin layer chromatography
TRIS .....tris(hydroxymethyl)aminomethane
Trx.....thioredoxin
UV-Vis.....ultraviolet-visible
w/o .....without
YOYO-1 .....1,1'-(4,4,8,8-tetramethyl-4,8-diazaundecamethylene)bis[4-[(3-methyl-benzo-1,3-oxazol-2-yl)methylidene]-l,4-dihydroquinolinium] tetraiodide
ZFN .....zinc finger nuclease
γ-GCS.....γ-glutamylcysteine synthetase

Symbols

$\tilde{\nu}$ ..... wavenumber

°C ..... degree Celsius

µg ..... microgram

µL ..... microliter

µmol ..... micromole

A ..... absorbance

a.u. ..... arbitrary units

bp ..... base pairs

c ..... amount of substance concentration

C ..... coulomb

c_0 ..... speed of light in vacuum

cm^{-1} ..... wavenumber

Da ..... dalton

DP_n ..... degree of polymerization

E ..... energy

eV ..... electronvolt

f ..... oscillator strength

f_Q ..... quenching efficiency

g ..... g-force

g ..... gram

h ..... hour

h ..... Planck constant

I, I_F ..... intensity, fluorescence intensity

J ..... Joule

k ..... Boltzmann constant

K ..... Kelvin

kDa ..... kilodalton

k_{nr} ..... rate constant for nonradiative transitions

k_r ..... rate constant for radiative transitions

l ..... length

L ..... liter

m ..... mass

M ..... $mol \cdot L^{-1}$

M ..... molar mass

MDa.....megadalton

mg .....milligram

min .....minute

mL.....milliliter

mm .....millimeter

mM.....mmol·L^{-1}

mmol .....millimole

M_n.....number average molecular weight

mol .....mole

M_p.....peak molecular weight

M_w .....weight average molecular weight

MWCO .....molecular weight cutoff

n .....amount of substance, quantum number, refractive index

n, N .....number of entities

nm .....nanometer

ns.....nanosecond

PDI .....polydispersity index

pH.....pH value

pK_a .....logarithmic acid dissociation constant

pK_a' .....apparent logarithmic acid dissociation constant

ps.....picosecond

R .....dipole-dipole distance

r .....molar ratio

R_0 .....Förster radius

s.....second

T .....absolute temperature

t .....temperature in °C

t .....time

$t_{½}$ .....half-life

t_R.....retention time

U.....exciton coupling interaction energy

V .....volume

Z.....collisional frequency

γ.....mass concentration

ε.....molar absorption coefficient

$ε_0$ .....vacuum permittivity

ζ .....mass ratio

κ .....orientation factor

λ .....wavelength

$\lambda_{abs\ max}$ .....wavelength of maximum absorbance

$\lambda_{em\ max}$ .....wavelength of maximum emission

λ_{em} .....emission wavelength

λ_{ex} .....excitation wavelength

μ_{GE} .....transition dipole moment

ν .....frequency

ρ .....electrical resistivity

τ.....lifetime; volume element

τ_n .....natural lifetime

ϕ.....volume fraction

Φ_f .....quantum yield of fluorescence

ψ .....wave function

ω .....mass fraction

Mathematical formulae

Calculation of N/P values

The N/P value is defined as the ratio of the molar amount of polymer amine nitrogen atoms *n*(N) to the molar amount of phosphorous atoms *n*(P) in the nucleic acid backbone phosphates:

$$N/P = \frac{n(\mathrm{N})}{n(\mathrm{P})} \tag{6.1}$$

n(P) in a given mass of double-stranded nucleic acid is calculated according to:

$$n(\mathrm{P}) = 2 \cdot n(\mathrm{bp}) \cdot \frac{m(\mathrm{DNA})}{M(\mathrm{DNA})} \tag{6.2}$$

The amount of nitrogen atoms in a given quantity of PEI hydrochloride is determined by:

$$n(\mathrm{N})_{\mathrm{PEI{\cdot}HCl}} = \frac{m(\mathrm{PEI{\cdot}HCl}) \cdot \omega(\mathrm{N})}{M(\mathrm{N})} \tag{6.3}$$

ω is the mass fraction of nitrogen of a PEI sample as measured with elemental analysis; *M*(N) is the molar mass of nitrogen (14.0067 g/mol).

The amount of nitrogen atoms in PLL hydrochloride is calculated from the molar amount of PLL·HCl multiplied by the number of lysine residues (*N*(Lys residues)) plus the N-terminus:

$$n(\mathrm{N})_{\mathrm{PLL{\cdot}HCl}} = \frac{m(\mathrm{PLL{\cdot}HCl})}{M(\mathrm{PLL{\cdot}HCl})} \cdot (N(\text{Lys residues}) + 1) \tag{6.4}$$

In order to calculate $n(\mathrm{N})_{\mathrm{PLL{\cdot}HCl}}$ the molecular mass *M*(PLL·HCl) is derived from:

$$M(\mathrm{PLL} \cdot \mathrm{HCl}) = 18.05\ \mathrm{g/mol} + N(\text{Lys residues}) \cdot 164.62\,\mathrm{g/mol} \tag{6.5}$$

164.62 g/mol is the molecular mass of one lysine hydrochloride unit.

Estimation of the apparent pK_a value

The pK_a' of FAM attached to lPEI was estimated from the dye's fluorescence intensity at different pH-values. Its value differs from the thermodynamic constant because the fluorescence intensity is proportional to the concentration of the investigated species and not to their chemical activities.

Fluorescein exhibits a complex acid-base equilibrium between up to seven prototropic forms.[109] At near neutral pH the dianionic (phenolate, FAM-O^-) and the monoanionic (phenol, FAM-OH) form contribute most to the fluorescence.[108, 138]

$$\text{FAM-OH} \rightleftarrows \text{FAM-O}^- + \text{H}^+$$

Consequently, the overall fluorescence intensity is the sum of their respective fluorescence intensities multiplied by their fraction *f*:

$$I_\text{F} = f(\text{OH})I_\text{F}(\text{OH}) + f(\text{O}^-)I_\text{F}(\text{O}^-) \tag{6.6}$$

From this relationship and the Henderson-Hasselbalch equation the fitting equation is derived:[109]

$$I_\text{F} = I_\text{F}(\text{OH}) + \frac{I_\text{F}(\text{O}^-) - I_\text{F}(\text{OH})}{1 + 10^{\text{p}K_a' - \text{pH}}} \tag{6.7}$$

A far better fit and a more reliable determination of the inflection point (pK_a') could be achieved with a similar Boltzmann function:

$$I_\text{F} = I_\text{F}(\text{OH}) + \frac{I_\text{F}(\text{O}^-) - I_\text{F}(\text{OH})}{1 + e^{\frac{\text{p}K_a' - \text{pH}}{\text{dpH}}}} \tag{6.8}$$

dpH is the width parameter. It describes the change in pH corresponding to the most significant change in I_F.

List of publications

Scientific journals/book chapters

In preparation — V. Durán, E. Grabski, B. Bošnjak, **C. Hozsa**, J. Becker, H. Yasar, B. Costa, N. Koller, Y. Lueder, O. Danov, B. Wiegmann, G. Brandes, V. Kaever, C-M. Lehr, R. K. Gieseler, M. Furch, R. Förster, T. Graalmann, U. Kalinke: Fucosylated lipid nanocarriers loaded with antibiotics efficiently inhibit mycobacterial propagation in human macrophages.

2015 — T. Frenz, E. Grabski, V. Durán, **C. Hozsa**, A. Stępczyńska, M. Furch, R. Gieseler and U. Kalinke: Antigen presenting cell-selective drug delivery by glycan-decorated nanocarriers. *European Journal of Pharmaceutics and Biopharmaceutics* 95 (Pt A), 13-17

2013 — **C. Hozsa**, M. Breunig and A. Göpferich: Monitoring the Degradation of Reduction Sensitive Gene Carriers with Fluorescence Spectroscopy and Flow Cytometry. In: *Cellular and Subcellular Nanotechnology: Methods and Protocols,* Series: Methods in Molecular Biology, Vol. 991, Eds. V. Weissig, T. Elbayoumi, M. Olsen, Humana Press Inc., New York

2010 — M. Spoerner, **C. Hozsa**, J. A. Poetzl, K. Reiss, P. Ganser, M. Geyer and H. R. Kalbitzer: Conformational States of Human Rat Sarcoma (Ras) Protein Complexed with Its Natural Ligand GTP and Their Role for Effector Interaction and GTP Hydrolysis. *The Journal of Biological Chemistry* 285 (51), 39768–39778

2009 — H. R. Kalbitzer, M. Spoerner, P. Ganser, **C. Hozsa**, W. Kremer: A fundamental Link Between Folding States and Functional States of Proteins. *Journal of the American Chemical Society* 131 (46), 16714-16719

S. Bauhuber, **C. Hozsa**, M. Breunig, A. Göpferich: Delivery of Nucleic Acids via Disulfide-Based Carrier Systems. *Advanced Materials* 21, 3286-3306

M. Breunig, **C. Hozsa**, U. Lungwitz, K. Watanabe, U. Isao, K. Hiroyuki, A. Goepferich: Enhancing the Intracellular Release of siRNA with Biodegradable Poly(ethylene imine) as a Carrier System. *CRS Newsletter* 26 (2), 4-5

2008 — M. Breunig, **C. Hozsa**, U. Lungwitz, K. Watanabe, I. Umeda, H. Kato and A. Goepferich: Mechanistic Investigation of Poly(ethylene imine)-based

siRNA Delivery: Disulfide Bonds Boost Intracellular Release of the Cargo. *Journal of Controlled Release* 130 (1), 57-63

Patents

2017 M. J. Scolaro, S. M. Sullivan, R. K. Gieseler, **C. Hozsa**, M. Furch: Immunotherapies for malignant, neurodegenerative and demyelinating diseases by the use of targeted nanocarriers. WO2017017148 A1

Conferences (presentations)

2017 V. Durán, E. Grabski, T. Frenz, **C. Hozsa**, R. Gieseler, U. Kalinke: Glycan-functionalized liposomes as a cell-selective drug delivery approach for the treatment of Tuberculosis. International Conference on Nanomedicine and Nanobiotechnology (ICONAN), Barcelona

2010 **C. Hozsa**, M. Breunig, A. Göpferich: Shedding Light on the Intracellular Processing of Reduction Sensitive Poly(Ethylene Imine) Gene Carriers. *Jahrestagung der Deutschen Pharmazeutischen Gesellschaft (DPhG),* Braunschweig

Conferences (posters)

2010 **C. Hozsa**, M. Breunig, A. Göpferich: Investigating the Intracellular Fate of Reduction Sensitive Poly(ethylene imine) Based Gene Carriers. *7th World Meeting on Pharmaceutics, Biopharmaceutics and Pharmaceutical Technology,* Valetta (Malta).

2008 M. Breunig, **C. Hozsa**, U. Lungwitz, C. Russ, A. Göpferich: Disulfide-based Carriers Boost Intracellular Release of siRNA. *6th World Meeting on Pharmaceutics, Biopharmaceutics and Pharmaceutical Technology,* Barcelona

M. Breunig, **C. Hozsa**, U. Lungwitz, A. Goepferich: Enhancing the Intracellular Release of siRNA with Biodegradable Poly(ethylene imine) as Carrier System. *Controlled Release Society,* New York

Acknowledgements

Vorbei sind nun die Zeiten da ich – frei nach Poe – um eine Mittnacht graulich, trübe sann und traulich, müde über manchem alten Folio lang vergess'ner Lehr'. Obschon ich diese Arbeit alleine geschrieben habe, haben viele Menschen auf ganz unterschiedliche Weise zu ihrem Gelingen beigetragen. Ihnen gilt mein herzlichster Dank.

Mein besonderer Dank gilt Herrn Prof. Dr. Achim Göpferich für die Überlassung dieses spannenden und herausfordernden Themas, die vielen wertvollen Diskussionen, die Möglichkeit eigene Ideen und Ansätze zu verfolgen, die Gelegenheit meine Ergebnisse auf Konferenzen vorzustellen und das gute, freundschaftliche Arbeitsklima am Lehrstuhl. Ganz besonders möchte ich mich für seine sehr Geduld bedanken. Ohne seine fortwährende Unterstützung wäre diese Arbeit nie fertiggestellt worden.

Mein besonderer Dank gilt auch Frau apl. Prof. Dr. Miriam Breunig für die Betreuung meiner Arbeit und die Durchsicht meiner Manuskripte. Die Diskussionen mit ihr haben mich oft in die richtige Richtung gelenkt und sie hat meine Ideen und Ansätze stets gefördert. Auch ihr möchte ich für ihre große Geduld danken, ohne die diese Arbeit nie vollendet worden wäre.

Herrn Dr. Jörg Teßmar danke ich für sein stets offenes Ohr, seine zahlreichen fachlichen und technischen Ratschläge sowie konstruktiven Hinweise. Mein Dank gilt auch für seine Hilfe bei der Durchführung und Auswertung der Größenausschluss-Chromatographie.

Frau Dr. Uta Lungwitz möchte ich für die Synthese und Zurverfügungstellung der lPEIs sowie ihre Vorarbeiten danken, die diese Arbeit erst möglich gemacht haben.

Herrn Dr. Roger-Jan Kutta und Herrn Dr. Uwe Kensy (†) danke ich für die Möglichkeit zeitkorrelierte Einzelphotonenzählungen durchzuführen, für ihre Hilfe bei den Messungen, dem Auswerten der Rohdaten und ihre Ratschläge zur weiteren Datenanalyse.

Frau Renate Liebl danke ich für ihre Unterstützung bei den Zellkulturexperimenten und ihre zahlreichen hilfreichen Tipps und Kniffe beim Umgang mit den Zellen.

Ich danke Herrn Dr. Stefan Rothschenk für seine wertvolle Unterstützung im Umgang mit der oft widerspenstigen HPLC-Anlage, seine Einführung in die Geheimnisse des Praktikums Pharmazeutische Technologie und die Überlassung seiner Skripte. Nicht vergessen möchte ich auch seine angenehme musikalische Untermalung langer Freitagabende vor der HPLC. Ich danke ebenso Herrn Dr. Matthias Henke für seine Unterstützung bei HPLC-Problemen, den gemein-

samen Kampf gegen die Computerprobleme des Lehrstuhls, die Organisation unserer Zockerabende und das gemeinsame Entdecken immer absurderer B-Movies.

Meinem „Mitinsassen“ Herrn PD Dr. Ferdinand Brandl danke ich für unsere heitere Laborgemeinschaft, sein stets offenes Ohr, die sorgfältige Durchsicht dieses Manuskripts und seine langjährige Freundschaft. Ebenso danke ich Herrn PD Dr. Michael Spörner für die sorgfältige Durchsicht dieses Manuskripts, die angenehmen Abende im Kneitinger und seine langjährige Freundschaft.

Meinen Forschungspraktikanten Johannes Schönberger und Nicole Hübner danke ich für die engagierte Mitarbeit im Projekt.

Meiner Freundin Maren danke ich von ganzen Herzen, dass sie mich auf diesem langen, oft nicht einfachen Weg begleitet hat und mir stets eine Stütze war. Ohne sie wäre ich ihn wohl nie zu Ende gegangen. Meiner Tochter Helena danke ich, weil sie mir deutlich gemacht hat, wie wichtig Abschlüsse und Neuanfänge im Leben sind und ich ihr ein Vorbild sein darf.

Abschließend gilt mein tiefster Dank meinen Eltern, die mir diesen Weg nicht nur ermöglicht haben, sondern mich immer darin unterstützt und bestärkt haben ihn weiter zu gehen.

"It was the best of times, it was the worst of times, it was the age of wisdom, it was the age of foolishness, it was the epoch of belief, it was the epoch of incredulity, it was the season of Light, it was the season of Darkness, it was the spring of hope, it was the winter of despair, we had everything before us, we had nothing before us, we were all going direct to Heaven, we were all going direct the other way (...)"

Charles Dickens, "A Tale of Two Cities"